GENERALIZED THIN SHEET APPROXIMATION FOR MAGNETOTELLURIC MODELLING

by

RAMBABU POTHIREDDY RANGANAYAKI

B. Sc., Osmania University, India
(1962)

M. Sc., Osmania University, India
(1964)

M. S., University of Hawaii, Honolulu
(1972)

SUBMITTED IN PARTIAL FULFILLMENT OF THE REQUIREMENTS FOR THE DEGREE OF DOCTOR OF PHILOSOPHY

at the

MASSACHUSETTS INSTITUTE OF TECHNOLOGY

April, 1978

Signature of Author: .....
Department of Earth and Planetary Sciences
April 3, 1978

Certified by: ..
Thesis Supervisor

Accepted by: .....
Chairman, Departmental Committee on Graduate Students

WITHDRAWN
MAY 9 1978
LIBRARIES

GENERALIZED THIN SHEET APPROXIMATION FOR MAGNETOTELLURIC MODELLING

by

RAMBABU POTHIREDDY RANGANAYAKI

Submitted to the Department of Earth and Planetary Sciences on April 3, 1978, in partial fulfillment of the requirements for the degree of Doctor of Philosophy.

ABSTRACT

Crustal variations in the conductivity and resistivity of the earth cause great complications in the surface distribution of electric currents and fields. It is therefore necessary to take these variations into consideration while interpreting the magnetotelluric measurements made on an island or near a coast or in a region where the local geology is complicated. At low frequencies the crust can be treated as a thin sheet and the crustal conductivity variations can be incorporated into the thin sheet conductance variation. The theory of electromagnetic induction in thin sheets was first given by Price (1949). In this model the layer below the thin sheet is assumed to be a perfect insulator, which restricts the possible modes of solutions in the thin sheet. In general, the layer below the thin sheet, though very resistive compared to the surface sheet, is not a perfect insulator. Hence in the first model developed in this thesis, the perfectly insulating layer is replaced by a layer of finite conductivity. Thus the thin sheet model consists of a thin conducting sheet of variable conductivity over a general layered medium. In the earth the resistive layer below the surface conductive sheet is represented by the lower crust. The resistivity of the lower crust underneath the ocean is expected to be different from the resistivity of the lower crust below the continents. This difference in the lower crust resistivity value is taken into account in the second model called the Generalized Thin Sheet model. In the Generalized Thin Sheet model, the thin sheet is treated as an anisotropic thin sheet with different (parallel) conductivity and(perpendicular) resistivity variations.

Specific examples in which conductivity and resistivity vary only in one direction were studied. It was found that in a crustal environment, upon certain approximation it is possible to get simple analytical solutions for E variations perpendicular to the strike direction. In this case a new distance parameter appears which is the adjustment

distance for the surface telluric field to re-equilibrate itself with respect to the mantle current fields. This distance is given by the square root of the layer conductivity thickness product times the layer resistivity thickness product and can amount to hundreds of kilometers.

Electric fields measured at a point are influenced not only by the conductivity and the resistivity of the medium at the point of measurement, but also by the electrical properties of the medium considerable distance away. Therefore a new method called the 'method of imbedding' was developed in which fields close to the point of measurement are computed at close spacings, while fields farther away are determined at larger spacings. These methods were applied to modelling magnetotelluric measurements on the island of Oahu, Hawaii, in order to evaluate the procedures used by J. C. Larsen to interpret his magnetotelluric data.

Thesis Supervisor: Theodore R. Madden

Title: Professor of Geophysics

ACKNOWLEDGEMENTS

First I would like to thank my advisor, Prof. T. R. Madden, for his invaluable advice and guidance throughout the preparation of this thesis. The models developed and the 'imbedding' technique employed in the solution were suggested by Professor Madden.

Professor Madden's interest in the topic was first aroused by discussions with Professor A. Kuckes. Professor Kuckes also pointed out the adjustment distance parameter.

I am grateful to Dr. J. C. Larsen for providing me with the impedence data.

I benefited from discussions with Paul Kasameyer, Yed Angoran, Adolfo Vinas, Dale Morgan, Earle Williams, Jerry LaTorraca, and Olu Egagunloye.

My thanks are also due to Mrs. Delphine Radcliffe, who typed the thesis, for being always obliging and helpful.

I would like to thank especially my husband, Rambabu Pothireddy, for his cooperation and encouragement throughout my stay at M. I. T.

I am grateful to my parents for getting me interested in science when I was young.

Finally I would like to thank the Department for supporting me with Research and Teaching Assistantships. The research was supported by an ONR contract, N00014-76-C-0087, and an ERDA contract, EG-77-S-02-4342.

TABLE OF CONTENTS

TABLE OF CONTENTS (continued)

LIST OF FIGURES

LIST OF FIGURES (continued)

LIST OF FIGURES (continued)

LIST OF FIGURES (continued)

LIST OF FIGURES (continued)

LIST OF TABLES

CHAPTER I

INTRODUCTION

Naturally occurring electromagnetic fields induce currents within the earth which in turn cause changes in these primary fields. A study of these fields yields information about the conductivity variations within the earth. Longer period waves penetrate greater depths and so the conductivity structure of deeper layers can be learned.

Crustal conductivity variations are essentially controlled by the free water content of the rock mass (Madden, 1971), while the conductivity variations within the deep layers of the earth are associated with temperature variations (Tozer, 1959) and the physical state of the layer, e.g. the presence of highly conducting rock melt in amounts of only a few percent can increase the electrical conductivity of the region by more than an order of magnitude (Waff, 1974). Such relationships are useful in aiding an understanding of the earth and the processes that go on within it. For instance, analysis of motions in the upper mantle require a knowledge of the temperature distribution at least in the upper mantle (Elsasser, 1965).

The surface layer (crust) of the earth has an extremely complicated conductivity structure which complicates the distribution of induced currents. When the surface layer consists of oceans, the currents induced in the ocean appreciably reduce the fluctuations in the magnetic field with periods of the order of a day or less, and

hence an allowance has to be made for these currents in all such cases. If the oceans were a uniform shell covering the entire earth, this correction could easily be effected, but the presence of land masses (continents) lying by the side of the oceans makes this correction difficult, as the currents induced in the oceans are obstructed by the continents. Kasameyer (1974), in his study of low frequency magnetotelluric data of New England, found that electric field variations perpendicular to the strike directions were strongly enhanced and apparent resistivities were as high as 8000 ohm-m for 10^{-4} Hz, and signals with a period of 5 days on one line indicated an apparent resistivity of 700 ohm-m. He felt that large E-fields could be produced by crustal conductivity variations which channelled the electrical currents induced in the ocean, even for frequencies so low that the skin depth of waves is 100 times the thickness of the crust. Another problem that requires knowledge of induced currents in the ocean is the interpretation of anomalies of magnetic field variations observed on land near oceans and on islands. Measurements made on shore, along lines at right angles to the coast, show that the amplitude of the vertical component of the magnetic field variations depends on the distance from the coast or, more precisely, on the distance from the continent shelf edge. Horizontal variations are also affected but to a much smaller extent. These are known as coastal effects.

Schmucker (1964) studied coastal effects in considerable detail. Rikitake and his group studied coastal effects in Japan in great detail (Rikitake et al. 1952, 1953, 1958, 1959, 1962). The

vertical component of the magnetic field tends to be in opposite senses on opposite sides of an island. This "island effect" has been studied by Mason (1963), Klein (1972, 1976), Hermance and Grillot (1970), and others. Detailed calculations that take into account the real topography of land and ocean are necessary to determine whether these anomalies are entirely due to currents flowing in the ocean or are also due to currents in the upper mantle. Interpretation of measurements on islands requires the topography to be taken into account, because the oceanic currents are deflected by an island.

For low frequency inducing fields when the surface layer thickness is small compared with the skin depth and the horizontal wavelength, the surface layer can be treated as a thin sheet. The theory of electromagnetic induction in thin sheets and shells was first given by A. T. Price (1949). A detailed account of induction in thin sheets can also be found in Rikitake's "Electromagnetism and earth's interior". Price's model consists of an infinitesimally thin sheet of variable conductivity embedded in a non-conducting medium. Price's model does not include the effect of mantle conductivity. Mantle currents tend to suppress the fields induced in thin sheet. Roden (1964), Larsen (1968) and Bullard and Parker (1971) accounted for this effect by replacing the highly conducting part of the mantle by a perfectly conducting body and the fields due to currents in this perfect conductor were determined using an image technique. The effect of currents in the mantle is contained in the self-induction portion of the thin sheet equation.

It was pointed out by Bullard and Parker (1970) that it is not necessary to make the approximation of a perfectly conducting mantle and that any conducting body with conductivity a function of radius alone could be used. In this model the currents induced in the thin sheet are sealed off from the mantle and, similarly, currents induced in the mantle are sealed off from the ocean by the layer of perfect insulator between them. Only horizontal E mode is therefore possible in the thin sheet. The conductive (thin) sheet on the surface and the conductive mantle below are therefore coupled together by only inductive coupling. At very low frequencies, when self-induction becomes unimportant, the two conductors are decoupled, i.e. surface measurements are no longer influenced by mantle currents.

Price's method has been applied in the interpretation of measurements on islands to predict the electrical conductivity structure beneath them by several authors (Klein 1972; Sasai 1968; Honkura 1971, 1973; Honkura et al. 1974). In all these models mutual induction between the ocean and the mantle was ignored by assuming the disturbance field to be static. The disturbance fields in the ocean were estimated using numerical models based on the conductivity distribution defined by bathymetric maps. Larsen (1975) presented a new approach in that the disturbance field was not determined by direct modelling. Instead he defined certain parameters of disturbance, all except one of which were known. The unknown quantity was included as a parameter in the iterative

scheme to determine mantle conductivity. A similar technique was also applied by Klein (1976) in his interpretation of magnetic field data obtained on Hawaii island. Even in this study the layer below the thin sheet was assumed to be a perfect insulator and the mutual induction effect was neglected. However, the selection of the part of the response spectrum used in the interpretation of deep conductivity by a layered medium was based on the inequality conditions to be satisfied if the conductivity profile was to be a function of depth only (Weidelt, 1972).

In general the layer below the surface (thin) sheet, though very resistive compared to the thin sheet, is not a perfect insulator. To take this into account, the models used in this thesis replace the perfectly insulating layer by a layer that can assume any conductivity value and includes it as part of the thin sheet. The presence of conductive zones at the surface and resistive zones below makes the thin sheet anisotropic. Both horizontal E and horizontal B polarizations of the electromagnetic fields are now possible in the thin sheet. With this change, the surface sheet and the mantle below are coupled together by resistive coupling and so the electric currents in the mantle are influenced by surface electric currents, and vice versa, even at such low frequencies that the disturbance fields can be assumed static. The resistivity thickness product (ρ_s) of the layer now plays an impo[illegible] is found that the distance over which a discontinuity in surface conductivity value affects the surface electric field and current distribution depends on both the

conductivity thickness product and the resistivity thickness product of the layer. This effect arises for electric fields polarized perpendicular to strike. Examples studied show this distance to be of the order of hundreds of kilometers. In the case of land-ocean boundaries these effects are even more dramatic. It is found that variation in E fields perpendicular to a coastline is controlled not only by σ_s and ρ_s of the medium at the point of measurement but also by σ_s and ρ_s values hundreds of kilometers away. Thus surface electric field and current distribution are affected by σ and ρ properties of the medium considerable distance away.

The resistive layer below the thin sheet in the earth is usually represented by the lower crust. The crustal resistivity variation under continents has been studied with large-scale resistivity measurements which estimate the resistivity thickness product (see Madden 1971, Keller et al. 1966, Zijl 1969; also Brace 1971, Madden et al. 1962). But we do not have any information about resistivity properties in the oceanic lithosphere. Only a few measurements have been made at sea (Filloux 1967, Cox et al. 1970, Richards 1970). Conductivity structure of the ocean floor based on these measurements requires that the ocean floor should have high conductivity at shallow depths. At present we do not know if these are representative of ocean lithosphere conductivity values or if they only refer to values at the points of measurement (Cox 1971). These measurements could not tell anything about the resistivity of most resistive layers, although they may have been

influenced by the boundary adjustment effects. Appropriate magnetotelluric measurements made in the ocean at varying distances from continental margin should in fact be able to provide information about the oceanic lithospheric resistivity thickness product as this product has a profound effect on electric fields perpendicular to the coastline.

1.1 Thesis Organization

In Chapter II the theory of electromagnetic induction in thin sheets is discussed. First we briefly discuss Price's theory of electromagnetic induction in thin sheets. Second, the limitations of Price's theory and the theory of induction in a more realistic model consisting of a thin conductive sheet over a general layered medium are given. Finally we discuss the theory of the generalized thin sheet in which the thin sheet has both (parallel) conductivity and (perpendicular) resistivity variations.

Chapter III refers to specific examples in which the surface conductivity and resistivity variations are restricted to only one direction. First, model calculations are checked by comparing them with those obtained using network technique. Next we discuss the variation of electric fields perpendicular to strike in a crustal environment. Dependence of coastal magnetotelluric fields on σ and ρ properties in the ocean is discussed with the help of a land-ocean-land model. A one-dimensional model of the Hawaiian rise studied to find the anisotropy in apparent resistivity of the rise and the dependence of anisotropy on resistivity thickness product of the rise and the ocean.

In Chapter IV we present a detailed description of a new method called the 'method of imbedding', of computing model solutions for one-dimensional problems. In this method fields close to the point of measurement are determined at close spacings, while fields farther away are determined at larger spacings. Computational method is described for thin sheet model and

generalized thin sheet model for quasi-uniform source field and for source field with variations in the x and y directions. Imbedding solutions are checked by comparing them with those obtained using uniform spacing throughout .

In Chapter V we first check the two-dimensional computation. Next the method of imbedding for two-dimensional conductivity variation in the thin sheet is described. Finally these methods were applied to modelling magnetotelluric measurements on the island of Oahu to evaluate Larsen's procedure.

CHAPTER II

THEORY OF ELECTROMAGNETIC INDUCTION IN THIN SHEETS

In this chapter we briefly review Price's original analysis of the effect of a thin conducting layer. This analysis assumes the thin sheet is underlain by a perfect insulator, which assumption restricts the modes of possible solutions. In the second section we show how replacing the insulating layer by an arbitrary layered medium forces us to use vector equations instead of a scalar equation, but also allows us to include terms that were dropped in Price's original analysis. When the layered medium below the thin sheet has a poorly conducting layer on the top we find this layer has a profound effect on the resulting solutions. Such a layer can be incorporated into the thin sheet, which allows us to model variations in this layer as well as variations in the conducting layer above it. Such a combination is anisotropic. The analysis of an anisotropic thin sheet we call the generalized thin sheet analysis and this is developed in the third section.

2.1 Price's Theory of Electromagnetic Induction in Non-Uniform Thin Sheets

Since we are concerned mainly with the effect of local, as opposed to global, conductivity variations on the magnetotelluric fields, and also since the frequencies of field variations considered are such that the skin depths are only a small fraction of the radius of the earth (for a typical continental area with a resistive crust

skin depth would be about 700 km for a frequency of 0.1 cpd), we can ignore the sphericity of the earth and treat it as a plane-surfaced infinitely large conductor with a non-uniform distribution of conductivity. While the skin depths of variations are small compared with the radius of the earth, they are large compared to the crustal thickness, which allows the uppermost surface (crust) of the earth to be treated as a non-uniform thin sheet. The theory of electromagnetic induction in thin sheets and shells was first developed by A. T. Price (1949).

Imagine a non-uniform thin sheet distribution of conducting material in free space. The magnetic permeability (μ) is assumed to be the same everywhere and is set equal to the free space value. It is also assumed that the rate of time variation of magnetic and electric fields is so small that displacement currents can be neglected. ($\frac{\omega\epsilon}{\sigma} << 1$)

$$\begin{array}{c} (1)\,\sigma = 0 \\ \hline \sigma = \sigma(x, y) \\ \hline (2)\,\sigma = 0 \end{array}$$

From Maxwell's equations we have:

$$\nabla \times \vec{E} = i\mu\omega\vec{H} \qquad (2.1.1)$$

$$\nabla \times \vec{H} = \sigma\vec{E} \qquad (2.1.2)$$

In the air layer above the thin sheet we have, from (2.1.2),

$$\nabla \times \vec{H} = 0$$

$$\therefore \quad \vec{H} = -\vec{\nabla}\Omega$$

where Ω satisfies Laplace's Equation.

Since μ is everywhere the same,

$$\nabla \cdot \vec{H} = 0$$

i.e. on passing from the air-layer into the conducting material, the normal component $\vec{H}_z$ of $\vec{H}$ is continuous. If 'd', the thickness of the thin sheet, is infinitesimal, the normal component $\vec{H}_z$ will have the same value at corresponding points on opposite sides of the sheet. Similarly for an infinitesimally thin sheet, the parallel components $\vec{E}_x$ and $\vec{E}_y$ of $\vec{E}$ will have the same magnitude and direction at corresponding points on opposite sides of the sheet. Defining

$$J_s = \int_o^d J \, dz = \int_o^d \sigma E_s \, dz = \sigma_s E_s$$

where

$$\sigma_s = \int_o^d \sigma \, dz$$

we get an Ohm's Law for the thin sheet as:

$$\vec{E}_s = \rho_s \vec{J}_s \qquad (2.1.3)$$

where $\rho_s = [\sigma_s]^{-1}$ and E_s is the surface or horizontal component of E.

Applying (2.1.2) to a small rectangular circuit that has two sides of length parallel to the sheet with one on each side of the sheet, we obtain:

$$H_s^+ \delta_s - H_s^- \delta_s = J_s \delta_s \sin\theta$$

where the + and - suffixes indicate values at the positive and negative faces of the thin sheet and θ is the angle between δ_s and J_s.

Since this relation is true for any direction of δ_s tangential to the sheet we can write

$$\begin{aligned} \vec{J}_s &= + \vec{i}_z \times (\vec{H}_s^+ - \vec{H}_s^-) \\ &= - \vec{i}_z \times \vec{\nabla}_s (\Omega^+ - \Omega^-) \\ &= - \vec{i}_z \times \vec{\nabla}_s \psi \end{aligned} \qquad (2.1.4)$$

where $\vec{i}_z$ is a unit vector normal to the sheet, Ω^+ and Ω^- are the magnetic potentials on the positive and negative sides of the thin sheet (positive down), and ψ is a stream line function for currents flowing in the thin sheet.

From (2.1.1),

$$\text{curl } \vec{E}_s = i\mu\omega\vec{H}_z$$

Eliminating $\vec{E}_s$, using (2.1.3) and (2.1.4), we get

$$\begin{aligned} \rho_s \vec{\nabla}_s \cdot \vec{\nabla}_s \psi + \vec{\nabla}_s \rho_s \cdot \vec{\nabla}_s \psi &= i\mu\omega H_z \\ &= i\mu\omega (H_z^e + H_z^i) \end{aligned} \qquad (2.1.5)$$

where H_z^e (known) is the normal component of magnetic field due to external sources and H_z^i is due to the internal part. $\vec{\nabla}_s$ is the horizontal gradient operator.

H_z^i can be determined from the stream potential using Biot-Savart's law (Larsen 1968) as:

$$B_z^i = \frac{\mu}{4\pi} \iint \frac{\nabla\psi(x', y')}{d} \cdot \vec{K}\, dx'\, dy'$$

where

$$\vec{K} = \int \frac{\vec{\gamma}}{\gamma^3}\, dz'$$

$$\vec{\gamma} = (x - x')\vec{i}_x + (y - y')\vec{i}_y + (z - z')\vec{i}_z$$

Substituting for H_z^i from above in (2.1.5), we get

$$\rho_s \vec{\nabla}_s \cdot \vec{\nabla}_s \psi + \vec{\nabla}_s \rho_s \cdot \vec{\nabla}_s \psi = i\mu\omega \left\{ H_z^e + \frac{1}{4\pi} \iint \frac{\nabla\psi(x'y')}{d} \vec{K}\, dx'\, dy' \right\} \tag{2.1.6}$$

From this integro-differential equation ψ is determined. Equation (2.1.6) applies to a thin sheet embedded in free space and therefore cannot be applied to earth, in which mantle conductivity plays an important role. Currents induced in the mantle tend to suppress the fields produced by the currents in the ocean. A simple way this is accounted for is by replacing the highly conducting part of the mantle with a perfectly conducting body and then using the image technique to find the fields produced by currents in the perfect conductor (Roden 1964, Bullard and Parker 1971, Larsen 1968). Since B_z must vanish at the interface of the superconducting mantle (at a depth H_a), we imagine at a depth $2H_a$ a thin layer of electric currents which are the negative image of the thin sheet (surface) currents. Then, because of symmetry, B_z vanishes

at the interface of the superconducting mantle, and the magnetic field due to mantle currents can now be expressed as a function of currents in the surface thin sheet, i.e. in terms of the stream function ψ. On doing this we get one more surface integral. That is, in equation (2.1.6) now we would have two terms in the integral. The effect of the mantle currents is contained in the self-induction portion of the equation.

Thus in this model currents induced in the conducting layer are sealed off from the mantle and, similarly, currents induced in the mantle are sealed off from the conducting layer by the layer of perfect insulator between them. Hence there is no resistive coupling between the two conductors and they are coupled together by inductive coupling. At very low frequencies, when the disturbance fields behave like static fields, self-induction becomes unimportant and the two conductors are decoupled.

2.2 Theory of Electromagnetic Induction in Thin Sheet Overlying a Layered Medium

In general the layer below the surface (thin) sheet, though very resistive compared to the thin sheet, is not a perfect insulator. To take this into account, we replace the perfectly insulating layer below the thin sheet by a general horizontally layered medium. Therefore both horizontal E and horizontal B polarizations of the electromagnetic fields are now possible in the thin sheet. With this change the surface sheet and the mantle below are coupled together by resistive coupling and so the electric currents in the mantle are influenced by surface electric currents, and vice versa, even at such low frequencies that the disturbance fields can be assumed static.

Consider a thin conducting sheet with conductivity variations both in x and y directions. Beneath this sheet lies a medium with conductivity varying only in the z direction. This model is shown in Fig. 2.2-1. A varying magnetic field outside would induce electric current in the thin sheet and in the medium below. As before, if the magnetic field variations are sufficiently slow, displacement current can be neglected.

At the top of the layered medium we can find an impedance $[Z^z]$ (refer to Appendix 1) such that we have the relationship between electric fields (E_s^+) and magnetic fields (H_s^+) below the thin sheet as

$$E_s^+ = [Z^z] H_s^+ \qquad (2.2.1)$$

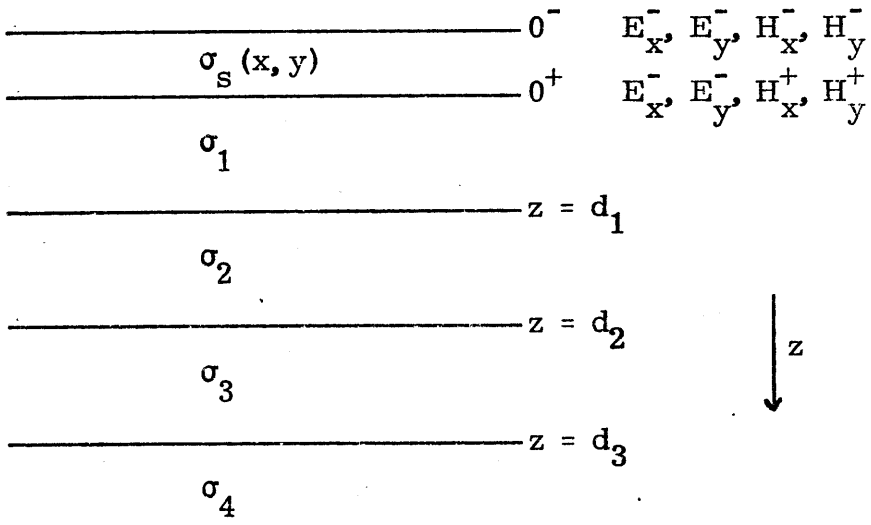
0^-
$E_x^-, E_y^-, H_x^-, H_y^-$
$\sigma_s(x, y)$
0^+
$E_x^-, E_y^-, H_x^+, H_y^+$
σ_1
$z = d_1$
σ_2
$z = d_2$
z
σ_3
$z = d_3$
σ_4

Fig. 2.2-1

Within the thin sheet we have from Maxwell's equations (neglecting displacement currents):

$$\nabla \times \vec{E} = i\mu\omega\vec{H} \qquad (2.2.2a)$$

$$\nabla \times \vec{H} = \sigma\vec{E} \qquad (2.2.2b)$$

From (2.2.2a) we get

$$\frac{\partial \vec{E}_s}{\partial z} = \vec{\nabla}_s (\vec{E}_s \cdot \vec{i}_z) - i\mu\omega\vec{i}_z \times \vec{H}_s$$

In the thin sheet model we assume that the tangential electric field at the top of the thin sheet ($\vec{E}_s^-$) is the same as the electric field at the bottom ($\vec{E}_s^+$). This assumption is valid if

$$\Delta E_s = \frac{\partial E_s}{\partial z}(\Delta Z)_1 \ll E_s$$

Assuming σ to be constant we can find E_s from (2.2.2a) and (2.2.2b) as

$$E_s = A\, e^{\sqrt{k_x^2 + k_y^2 - i\sigma\mu\omega}\, z}$$

Therefore $\Delta E_s \ll E_s$ if the thickness of the thin sheet $(\Delta Z)_1 \ll \frac{1}{k_x}$ and $\frac{1}{k_y}$, and $(\Delta Z)_1 \ll$ skin depth in the medium of which the thin sheet is composed.

With these assumptions we can set $\Delta E_s = 0$ across the thin sheet, i.e.

$$E_s^- = E_s^+ = E_s$$

From (2.2.2) we get

$$\frac{\partial \vec{H}_s}{\partial z} = \frac{\vec{\nabla}_s}{i\mu\omega}((\vec{\nabla}_s \times \vec{E}_s) \cdot \vec{i}_z) - \vec{i}_z \times \sigma\vec{E}_s \qquad (2.2.3)$$

$\nabla_s \times$ is vertical component of curl operator.

With the thin sheet assumption (2.2.3) can be written as:

$$\vec{H}_s^+ - \vec{H}_s^- = \frac{(\Delta Z)_1}{i\mu\omega}\vec{\nabla}_s((\vec{\nabla}_s \times \vec{E}_s) \cdot \vec{i}_z) - \vec{i}_z \times \sigma_s\vec{E}_s \qquad (2.2.4)$$

where H^- and H^+ are the magnetic fields at the top and bottom of the thin sheet, respectively, and

$$\sigma_s(x, y) = \int_0^{(\Delta Z)_1} \sigma(x, y)\, dz$$

Equation (2.2.4) is essentially the same as equation (2.1.4) in Price's theory. The important difference between the two is that in the present model H^+ cannot be derived from a scalar potential. However, with proper choice of conductivity for the layer below the thin sheet we can use this model to simulate Price's model (refer to section 2.3). If we set

$$[Y^+] = [Z^z]^{-1}$$

we have from (2.2.1)

$$H_s^+ = [Y^+]\, E_s \qquad (2.2.5)$$

Now, in the medium above the thin sheet, that is in the air layer, only for waves with $k = k_{source}$, do we have both incoming and outgoing waves. All other wavelengths are due to the currents in the thin sheet and the underlying half space, and are therefore

only outgoing waves.

Therefore, in the air layer $\frac{\partial}{\partial z}$ can be replaced by ik_{zo} for waves characterized by $k \neq$ source. From $\nabla \times \vec{E} = i\mu\omega\vec{H}^-$ we get $H_z = \frac{1}{i\mu\omega} \vec{\nabla}_s \times \vec{E}_s$. From $\vec{\nabla} \times \vec{H}^- = 0$ (assuming $\sigma_{aie} = 0$):

$$\vec{H}_s^- = \frac{-\vec{\nabla}_s}{\mu\omega k_{zo}} ((\vec{\nabla}_s \times \vec{E}_s) \cdot \vec{i}_z)$$

where $k_{zo} = -i\sqrt{k_x^2 + k_y^2}$.

H_s^- can be expressed in terms of E_s as:

$$H_s^- = [Y'^-] E_s \quad \text{for all outgoing waves}$$

$$= H_s^o \quad \text{for the source wavelength}$$

or simply

$$H_s^- = [Y'^-] E_s^- + H_s^o \tag{2.2.6}$$

where Y'^- is Y^- with the $k = 0$ wavelength excluded.

Substituting for H_s^- and H_s^+ from (2.2.5) and (2.2.6) into (2.2.4) we get

$$\vec{i}_s [Y^+_{mn} - Y'^-_{mn}](E_s)_{mn} - \frac{(\Delta Z)_1}{i\mu\omega} \vec{\nabla}_s ((\vec{\nabla}_s \times \vec{E}_s) \cdot \vec{i}_z) + \vec{i}_z \times \vec{J}_s = \vec{H}_s^o \tag{2.2.7}$$

where $\vec{i}_s$ is $\vec{i}_x + \vec{i}_y$ and $\vec{H}_s^o$ is the total tangential field at the source wavelength, $J_s = \sigma_s * E_s$. * stands for convolution, m, n refer to harmonic numbers in the x and y directions, respectively. (2.2.7) constitutes a system of $2(m \times n + 1)$ equations with $2(m \times n + 1)$ unknown. Solving these equations in the (k_x, k_y) domain involves

convolutions of σ_s and E_x and E_y, while solving in the (x, y) domain involves convolutions of Y_{xx}, Y_{xy}, etc. and E_x and E_y, both of which result in almost full coefficient matrix. In this case we have twice as many unknowns and twice as many equations as in Price's model (with or without mantle effect).

2.3 Theory of Electromagnetic Induction in a Generalized Thin Sheet Overlying a Layered Medium

In the thin sheet model the layer below the thin sheet is assumed to have a constant conductivity (or resistivity) value. While studying coastal or island effects, part of the sheet would represent land and part ocean. Resistivity below the thin sheet is therefore expected to be different under different parts of the thin sheet. The model in this section takes this difference beneath the thin sheet into account by incorporating into the thin sheet both conductivity and resistivity variations. This is done by treating the thin sheet as anisotropic with parallel conductivity different from perpendicular conductivity. ΔE across this anisotropic thin sheet would be very different from that across an isotropic thin sheet.

Assume σ (parallel conductivity) and ρ (perpendicular resistivity) are constants. From Maxwell's equations we can derive

$$\frac{\partial^2}{\partial z^2}\begin{bmatrix} E_x \\ E_y \end{bmatrix} = \begin{bmatrix} \sigma\rho k_x^2 + k_y^2 - i\mu\omega\sigma & \rho\sigma k_x k_y - k_x k_y \\ \rho\sigma k_x k_y - k_x k_y & k_x^2 + \sigma\rho k_y^2 - i\mu\omega\sigma \end{bmatrix} \begin{bmatrix} E_x \\ E_y \end{bmatrix}$$

Variation of E in the z-direction in the isotropic case depends on k_x, k_y and skin depth, while in the anisotropic case it is controlled by $k_x\sqrt{\sigma\rho}$ (or $k_y\sqrt{\sigma\rho}$), k_y (or k_x) and skin depth. If $\sqrt{\sigma\rho} > 1$, E changes in the z-direction more rapidly than in the isotropic case. If $\sqrt{\sigma\rho} < 1$, E changes in the z-direction less rapidly than in the isotropic case. If the anisotropy is due to layering with each layer

being isotropic, $\sigma\rho \geq 1$.

In the case of earth the surface layer (upper crust) is much more conductive than the lower crust, i.e. $\sigma_{\parallel}$ is much higher than $\frac{1}{\rho_{\perp}}$. Usually $\sigma_{\parallel}\rho_{\perp}$ is of the order of 100. Therefore ΔE cannot be set equal to zero in this case. In our model the anisotropic thin sheet is assumed to be actually made up of two thin isotropic sheets, one conductive and one resistive, the conductive thin sheet lying on top of the resistive thin sheet. This assumption is made because it represents the usual situation, but one could equally well handle models with a more general anisotropy. Including the resistive zone into the thin layer allows us to vary both conductivity and resistivity in the crust. The double thin sheet model called the Generalized Thin Sheet Model is shown in Fig. 2.3-1.

Since we consider the good conductor to lie on top of the poor conductor, most of the currents would flow in the top conductive zone and therefore most of $\frac{\partial H}{\partial z}$ would occur across the top zone. Because of the high conductivity, E_z in the top zone would be very small. If, in addition, we have $(\Delta Z)_1 \ll \frac{1}{k_x}$ or $\frac{1}{k_y}$ and $(\Delta Z)_1 \ll$ skin depth in the medium of which the conductive zone is composed, we can set $\frac{\partial E}{\partial z} \approx 0$ across the top zone. The lower zone is resistive; therefore the tangential current density in the lower resistive zone would be very small. This, together with $(\Delta Z)_2 \ll \frac{1}{k_x}$ or $\frac{1}{k_y}$, and $(\Delta Z)_2 \ll$ skin depth in the medium that makes up the resistive zone would make $\frac{\partial H}{\partial z} \approx 0$ across the lower zone.

Because of the poor conductivity of the lower zone E_z becomes

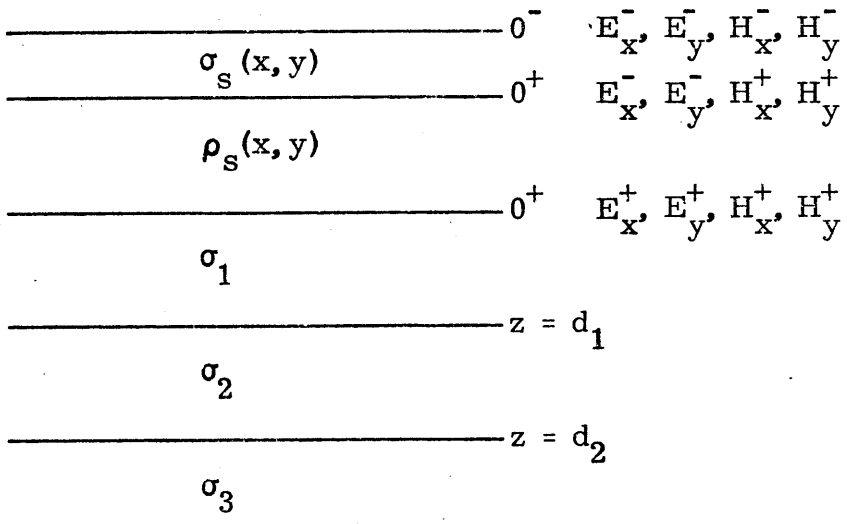
0^-
$E_x^-, E_y^-, H_x^-, H_y^-$
$\sigma_s(x,y)$
0^+
$E_x^-, E_y^-, H_x^+, H_y^+$
$\rho_s(x,y)$
0^+
$E_x^+, E_y^+, H_x^+, H_y^+$
σ_1
$z = d_1$
σ_2
$z = d_2$
σ_3

Fig. 2.3-1

important there and contributes to $\frac{\partial E_s}{\partial z}$ which occurs mainly across the lower resistive zone. As long as the linear dimensions of the generalized thin sheet are large, even quite thick zones can be treated as thin resistive sheet if the frequencies are low enough to make the skin depth large compared to the thickness.

Generalized Thin Sheet Solution

Within the generalized thin sheet we have from Maxwell's Equations (neglecting displacement currents):

$$\vec{\nabla} \times \vec{E} = i\mu\omega\vec{H} \qquad (2.3.1)$$

$$\vec{\nabla} \times \vec{H} = \sigma\vec{E} \qquad (2.3.2)$$

From (2.3.1) and (2.3.2) we get:

$$\frac{\partial \vec{E}_s}{\partial z} = \vec{\nabla}_s (\rho((\vec{\nabla}_s \times \vec{H}_s) \cdot \vec{i}_z)) - i\mu\omega\vec{i}_z \times \vec{H}_s \qquad (2.3.3)$$

$$\frac{\partial \vec{H}_s}{\partial z} = \frac{\vec{\nabla}_s}{i\mu\omega}((\vec{\nabla}_s \times \vec{E}_s) \cdot \vec{i}_z) - \vec{i}_z \times \sigma\vec{E}_s \qquad (2.3.4)$$

Assuming $\Delta E_s = 0$ across the top conductive thin sheet and $\Delta H_s = 0$ across the lower resistive thin sheet (with thin sheet approximations) (2.3.3) and (2.3.4) can be written

$$\vec{E}_s^+ - \vec{E}_s^- = \vec{\nabla}_s (\rho_s ((\vec{\nabla}_s \times \vec{H}_s^+) \cdot \vec{i}_z)) - i\mu\omega(\Delta Z)_2 \vec{i}_z \times \vec{H}_s^+ \qquad (2.3.5)$$

$$\vec{H}_s^+ - \vec{H}_s^- = \frac{(\Delta Z)_1}{i\mu\omega} \vec{\nabla}_s ((\vec{\nabla}_s \times \vec{E}_s^-) \cdot \vec{i}_z) - \vec{i}_z \times \sigma\vec{E}_s^- \qquad (2.3.6)$$

using the notations

$$\sigma_s(x,y) = \int_0^{(\Delta Z)_1} \sigma(x,y)\, dz$$

$$\rho_s(x,y) = \int_0^{(\Delta Z)_2} \rho(x,y)\, dz$$

Substituting for H^+ from (2.3.6) in (2.3.5) we get:

$$\begin{aligned} E_s^- &= (Z^z * + i\mu\omega (\Delta Z)_2 R)\, H_s^o \\ &+ (Z^z * Y'^- * + i\mu\omega(\Delta Z)_2\, Y'^- * R)\, E_s^- \\ &+ \frac{(\Delta Z)_1}{i\mu\omega} Z^z * \vec{\nabla}_s ((\vec{\nabla}_s \times \vec{E}_s) \cdot \vec{i}_z) \\ &+ (\Delta Z)_1 (\Delta Z)_2 (\vec{\nabla}_s \times (\vec{\nabla}_s \times \vec{E}_s)) \cdot \vec{i}_z \\ &- (Z^z * R - i\mu\omega(\Delta Z)_2)\sigma_s E_s^- \\ &+ \nabla_s (\rho_s (\nabla_s \sigma_s E_s) \end{aligned} \qquad (2.3.7)$$

where R is an operator such that

$$RA_x = -A_y$$

$$RA_y = A_x$$

∇_s is the scalar gradient operator, and use is made of the relationships

$$E_s^- = [Z^z] H_s^+$$

and

$$\bar{H}_s = H_s^o + [\bar{Y}'] * \bar{E}_s$$

and

$$\frac{\partial \bar{H}_y}{\partial x} - \frac{\partial \bar{H}_x}{\partial y} \approx 0$$

because the vertical air-earth current density is negligible.

* stands for convolution.

As in section 2.2, the H field at the source wavelength is used as a source term, while all other H fields are replaced by $\bar{E}_x$ and $\bar{E}_y$. With these substitutions (2.3.7) forms a completely deterministic set of equations with the electric fields $\bar{E}_x$ and $\bar{E}_y$ at each point of the grid surface of the thin sheet as unknowns.

In the case of one-dimensional conductivity and resistivity variation in the thin sheet (with quasi-uniform H incidence field) for E perpendicular to the strike direction, second, third and fourth terms on the right-hand side of equation (2.3.7) representing the secondary H contributions will drop out (as H in this case is uniform and equal to twice the incident amplitude). Equation (2.3.7) can therefore be written as (y represents the strike direction):

$$\frac{\partial}{\partial x}\left(\rho_s \frac{\partial \sigma_s E_x}{\partial x}\right) = E_x + Z' * \sigma_s E_x - Z' * H_y^o$$

where

$$Z' = Z_{xy}^z - i\mu\omega(\Delta Z)_2$$

If ρ_s is high, which is true for crustal environment, the solution to the above equation can be given as (assuming σ_s and ρ_s

constant):

$$J_x = A\, e^{\pm \frac{x}{\sqrt{\rho_s \sigma_s}}} + S$$

where A is a constant and S represents the layered medium solution. $\sqrt{\sigma_s \rho_s}$ therefore represents a horizontal distance (called here 'adjustment distance') at which about two-thirds of any excess tangential current leaks into the medium below the thin sheet or it is the distance required for the tangential currents from underneath to rise to the top. The more resistive the layer below the thin sheet, the greater the adjustment distance. In Price's model the layer below the thin sheet has a conductivity of zero or an infinite resistivity, and therefore the adjustment distance is infinity, which prevents the currents in the thin sheet from leaking into the medium below and vice versa. Typical values for σ_s and ρ_s show this distance to be of the order of hundreds of kilometers, and since this distance is smaller than the dimensions of large features on the earth, resistive coupling between the mantle and the surface is important. On the other hand, this distance is large enough that in most situations we would not expect the surface current levels to be in equilibrium with the local conductivity structure.

CHAPTER III

ONE-DIMENSIONAL SURFACE VARIATIONS

In this chapter we discuss cases in which conductivity and resistivity in the surface sheet vary only in one direction. One-dimensional solutions are often misleading because the uniformity along the strike direction should extend further than the adjustment distance. On continents the lower crust is often very resistive and in the oceans the surface conductivity is very high, both of which result in the adjustment distance being of the order of hundreds of kilometers. Nevertheless one-dimensional models are useful in illustrating certain aspects of thin layer effects.

We first investigate the accuracy of thin sheet model calculations by comparing the solutions obtained using the thin sheet model with those obtained using network analysis. The latter are two-dimensional calculations, while the thin sheet calculations of the same model are only one-dimensional but are restricted to low frequencies when the crust can be treated as a thin sheet. Generalized thin sheet calculations are checked by comparing the generalized thin sheet solution with the thin sheet solution when ρ_s (resistivity thickness product) is constant. Next we examine the effect of variable crustal resistivities on magnetotelluric fields. We shall see that these fields rather than being blind to high resistivity zone resistivity value are greatly affected by them. Finally we study the magnetotelluric fields induced in a one-dimensional model of the Hawaiian rise. These solutions will illustrate some of the thin layer effects of an actual geologic feature.

3.1 Comparison of Thin Sheet Model Solution with Network Solution

Thin sheet model solutions were compared with those obtained using network analysis (Kasameyer, 1974) for both E perpendicular to the strike and E parallel to the strike modes. These comparisons are shown in Figs. 3.1-1 and 3.1-2. Agreement between the two solutions is quite satisfactory.

If ρ_s is constant, the generalized thin sheet solution should be the same as the thin sheet solution when the resistive layer of the generalized thin sheet is made the top layer of the media underlaying a thin sheet. From Figs. 3.1-3 and 3.1-4 we see that the two solutions match perfectly.

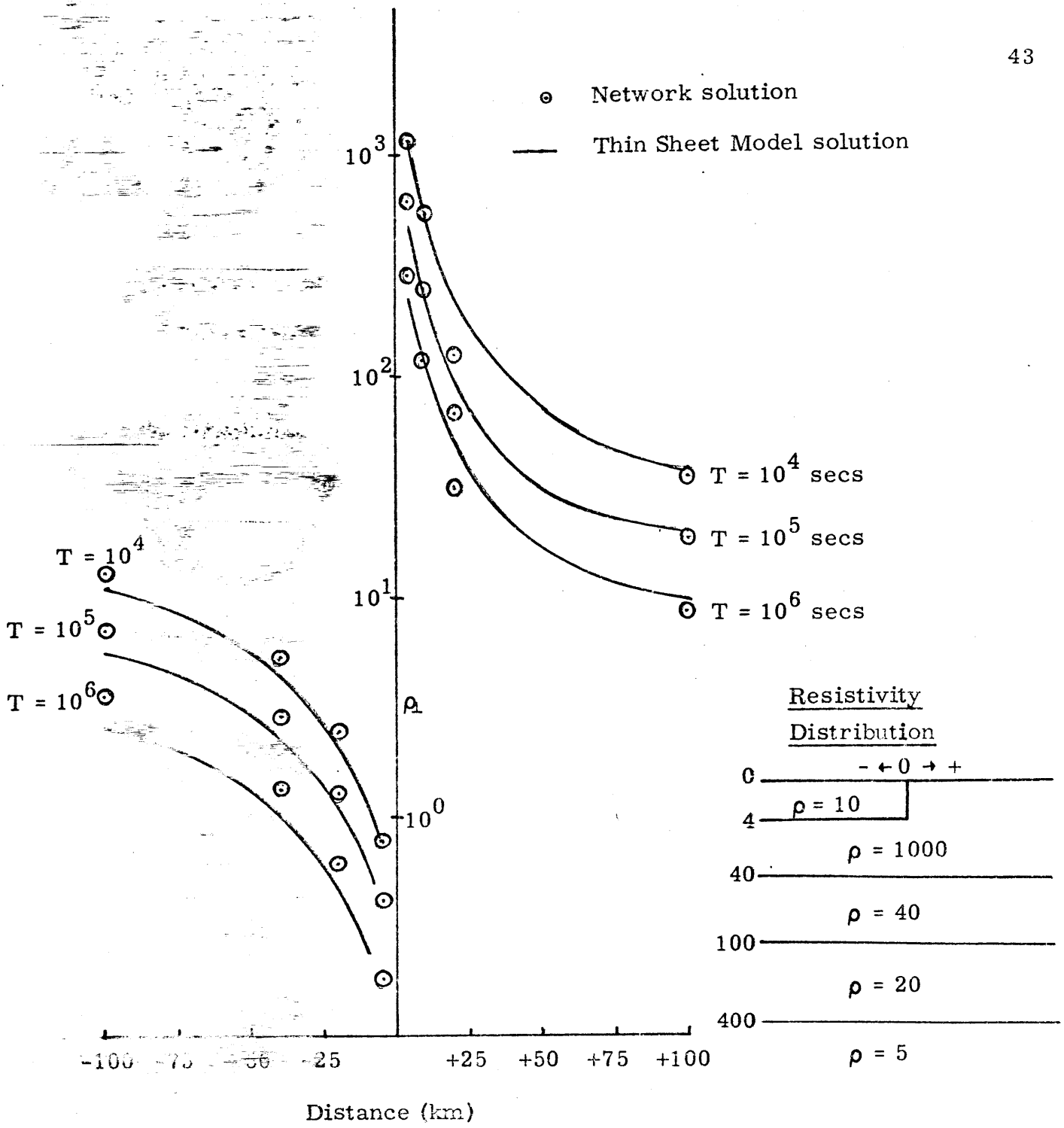

Fig. 3.4-1 Comparison of apparent resistivities (perpendicular to the strike) calculated by network solution (Kasameyer, 1974) and thin sheet model solution. T is period in seconds.

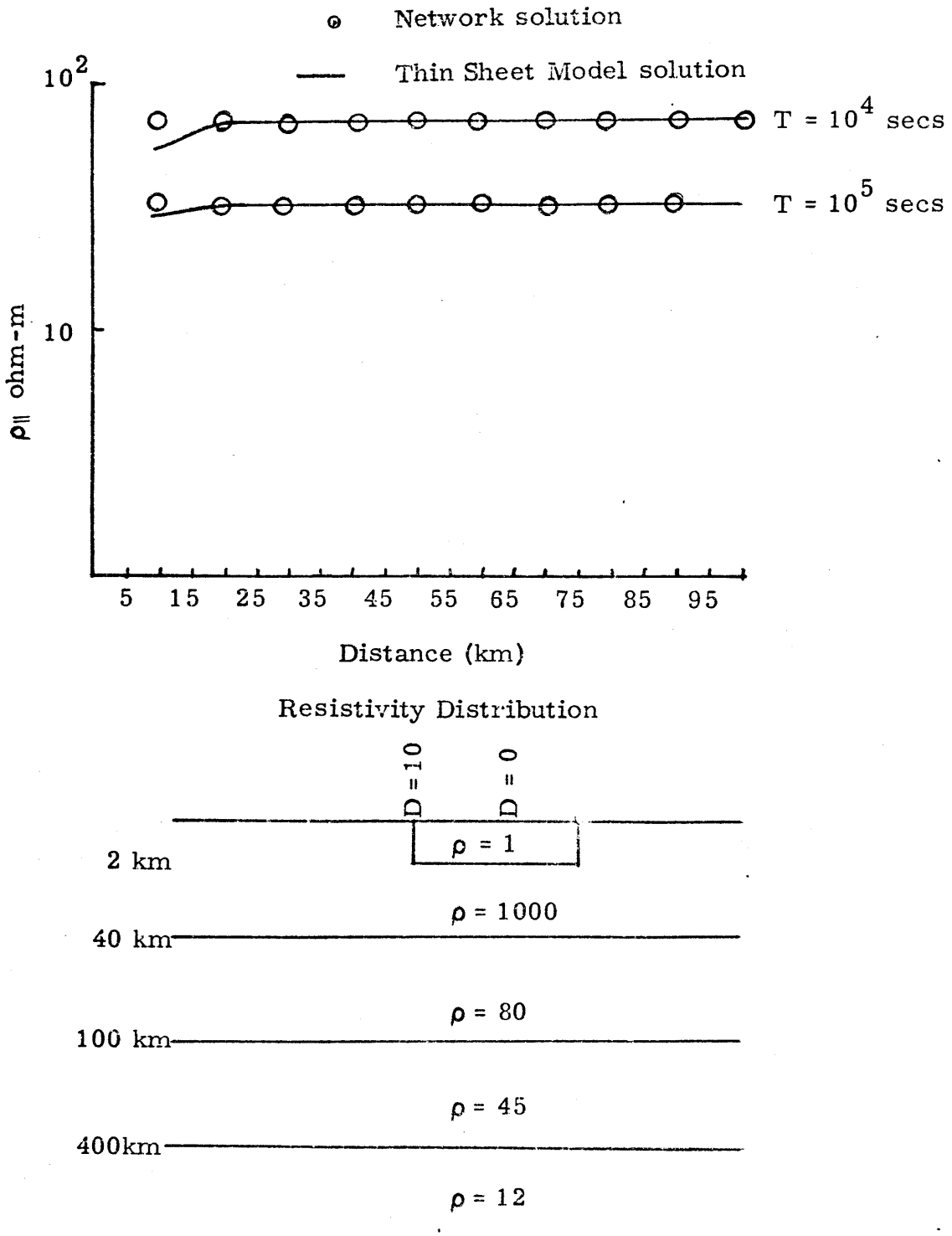

Fig. 3.1-2 Comparison of apparent resistivities (parallel to the strike) calculated by network solution (Kasameyer, 1974) and thin sheet model solution.

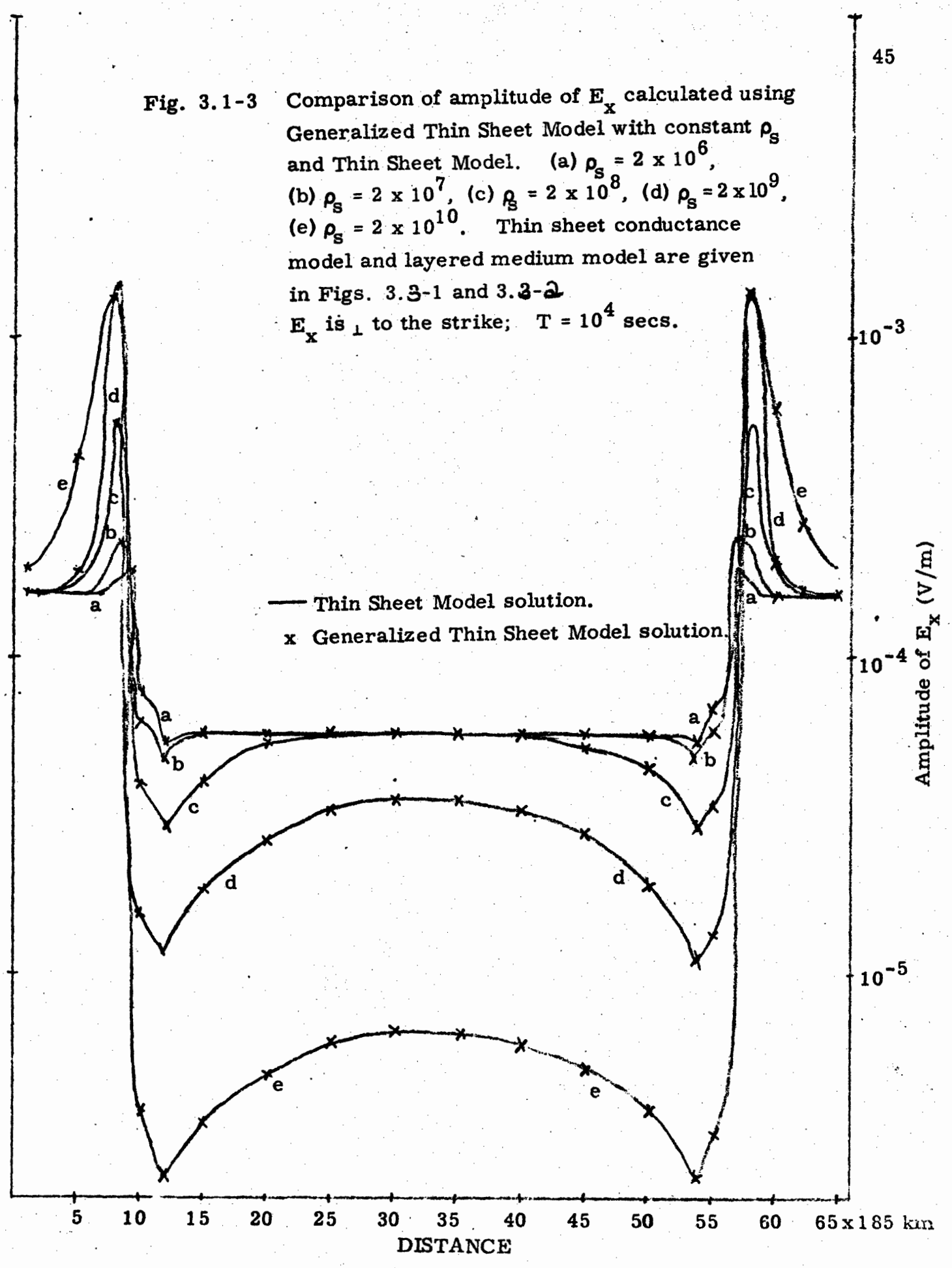

Fig. 3.1-3 Comparison of amplitude of E_x calculated using Generalized Thin Sheet Model with constant ρ_s and Thin Sheet Model. (a) $\rho_s = 2 \times 10^6$, (b) $\rho_s = 2 \times 10^7$, (c) $\rho_s = 2 \times 10^8$, (d) $\rho_s = 2 \times 10^9$, (e) $\rho_s = 2 \times 10^{10}$. Thin sheet conductance model and layered medium model are given in Figs. 3.3-1 and 3.3-2. E_x is $\perp$ to the strike; $T = 10^4$ secs.

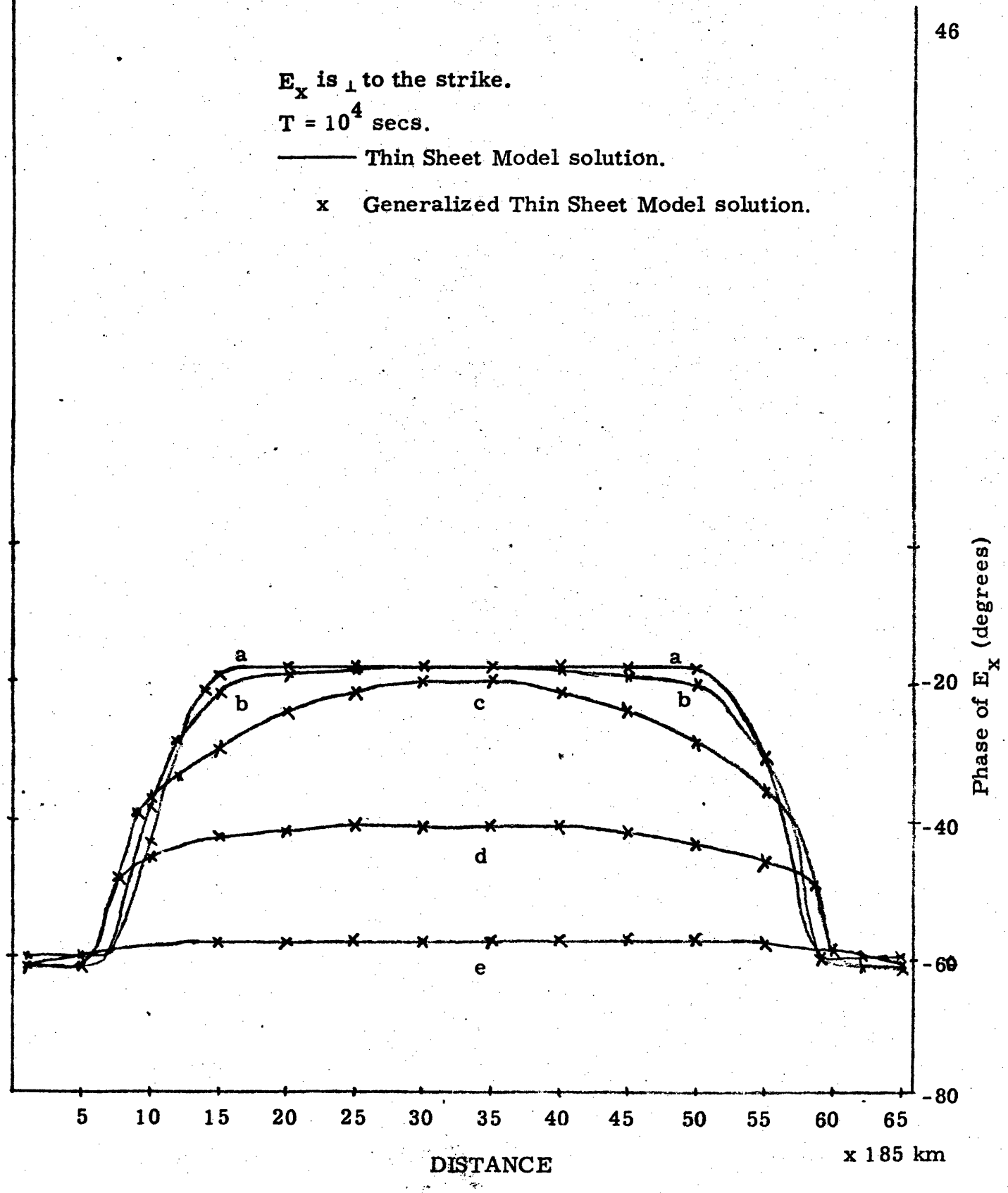

Fig. 3.1-4 Comparison of phase of E_x calculated using Generalized Thin Sheet Model with constant ρ_s and Thin Sheet Model. (a) $\rho_s = 2 \times 10^6$, (b) $\rho_s = 2 \times 10^7$, (c) $\rho_s = 2 \times 10^8$, (d) $\rho_s = 2 \times 10^9$, (e) $\rho_s = 2 \times 10^{10}$.

3.2 Electric Field Variations Perpendicular to the Strike Direction in a Crustal Environment

When the conductivity and the resistivity in the surface layer are constant in one direction over a distance large compared with the skin depth and adjustment distance in the medium, the surface variations of conductivity and resistivity can be represented by a one-dimensional model of the thin sheet. For such a model with quasi-uniform incidence field, the Maxwell equations decouple into two sets of equations, one for E perpendicular to the strike mode and the other for E parallel to the strike as follows:

E perpendicular to the strike

$$\frac{\partial H_y}{\partial z} = -\sigma E_x$$

$$\frac{\partial E_x}{\partial z} = \frac{\partial E_z}{\partial x} + i\mu\omega H_y$$

E parallel to the strike

$$\frac{\partial H_x}{\partial z} = \frac{1}{i\mu\omega}\frac{\partial H_z}{\partial x} + \sigma E_y$$

$$\frac{\partial E_y}{\partial z} = -i\mu\omega H_x$$

Therefore the Thin Sheet Model and Generalized Thin Sheet Model Equations are:

E perpendicular to the strike

$$H_y^+ - H_y^- = -\sigma_s E_x^- \qquad \text{Thin Sheet Model} \qquad (3.2.1)$$
$$E_x^- = E_x^+$$

$$H_y^+ - H_y^- = -\sigma_s E_x^- \qquad \text{Generalized Thin Sheet Model}$$

$$E_x^+ = E_x^- + \frac{\partial}{\partial x}\left(\rho_s \frac{\partial H_y^+}{\partial x}\right) + i\mu\omega(\Delta Z)_2 H_y^+ \qquad (3.2.2)$$

E parallel to the strike

$$H_x^+ = H_x^- + \frac{1}{i\mu\omega}\frac{\partial^2 E_y^-}{\partial x^2} + \sigma_s E_y^- \qquad \text{Thin Sheet Model}$$

$$E_y^+ = E_y^-$$

$$(3.2.3)$$

$$H_x^+ = H_x^- + \frac{1}{i\mu\omega}\frac{\partial^2 E_y^-}{\partial x^2} + \sigma_s E_y^- \qquad \text{Generalized Thin Sheet Model}$$

$$E_y^+ = E_y^- + i\mu\omega(\Delta Z)_2 H_x^+$$

$$(3.2.4)$$

Admittance above the thin sheet for the E perpendicular mode is zero because of the assumptions of quasi-uniform incidence field and absence of variation in σ and ρ along the y direction. For the same reasons ΔE_y in the E parallel mode does not depend on ρ and depends only on the thickness of the (generalized) thin sheet.

Equation (3.2.2) can be written as:

$$\rho_s \frac{\partial^2 \sigma_s E_x}{\partial x^2} = E_x + Z' \sigma_s E_x + Z' H_y^o \qquad (3.2.5)$$

where ρ_s is assumed constant and

$$Z' = Z_{xy}^* - i\mu\omega(\Delta Z)_2$$

* stands for convolution. The operator Z_{xy} is shown in 3.2-0.

When the conductivity contrasts in the thin sheet are high and ρ_s is small the Z_{xy} operator becomes very important. In a crustal environment, however, ρ_s is usually high. Under these conditions we can drop the $Z'\sigma_s E_x$ term in the above equation as a first approximation. We can, therefore, rewrite (3.2.5) as

$$\rho_s \sigma_s \frac{\partial^2 E_x}{\partial x^2} = E_x + Z' H_y^o$$

for a homogeneous quarter space. This differential equation would have a solution of the form

$$E_x = A e^{\pm \frac{x}{\sqrt{\sigma_s \rho_s}}} + S$$

where S is the layered medium solution. The amplitude A can be determined from the boundary conditions at the discontinuity. $\sqrt{\sigma_s \rho_s}$, which has the dimension of distance, was defined as the adjustment distance (Chapter II), the horizontal distance at which (1 - 1/e) of the excess surface current leaks into the mantle. Far away from the discontinuity ($x \to \infty$) the solution is the same as the Cagniard solution for the medium.

Let us consider two homogeneous quarter spaces (in a crustal environment) with a vertical contact at x = 0, y represents the strike direction. A_1, S_1, σ_1, ρ_1 are, respectively, the amplitude of the disturbed E_x field, undisturbed E_x field, conductivity thickness product and resistivity thickness product for side 1. A_2, S_2, σ_2, ρ_2 are the same quantities for side 2. From the continuity of H_y and E_z at x = 0 we can derive, using the relationships

$$H_y^+ = H_y^- - \sigma_s E_x$$

$$E_z^+ = \rho_s \frac{\partial H_y^+}{\partial x}$$

$$A_2 = \frac{\frac{S_1\sigma_1}{\sigma_2} - S_2}{\sqrt{\frac{\sigma_1\rho_2}{\sigma_2\rho_1}} + 1} \qquad (3.2.6a)$$

$$A_1 = -A_2 \sqrt{\frac{\sigma_2\rho_2}{\sigma_1\rho_1}} \qquad (3.2.6b)$$

From these we see that the amplitudes of the disturbed E_x fields depend on the σ and ρ properties on both sides of the discontinuity and that A_1 and A_2 have opposite signs. Let us suppose $\sigma_2 > \sigma_1$, then A_2 is negative and A_1 is positive (S_1 and S_2 will not be too different because the conductivity contrast is assumed to be modest and frequency is low). As σ_2 increases or ρ_2 decreases (for the same σ_1 and ρ_1), the magnitude of A_2 increases. But the magnitude of A_1 behaves slightly differently. It increases as σ_2 and ρ_2 increase. If $\sigma_2\rho_2 = \sigma_1\rho_1$, the two amplitudes A_1 and A_2 will be equal but of opposite sign. Also the adjustment distance in both cases would be the same.

Typical values of σ_s and ρ_s in a crustal environment suggest the adjustment distance to be of the order of hundreds of kilometers. We now study a few examples of continental conductivity and resistivity variations to show the effect of ρ_s variation on the distribution of surface fields and also to see the agreement between the solution calculated according to the simple formula and the actual solution. These results are summarized in Figs. 3.2-1 to 3.2-6. The same layered medium model was used for all the cases and it is shown in Fig. 3.2-1. From these figures we see that the agreement between the two solutions is very good.

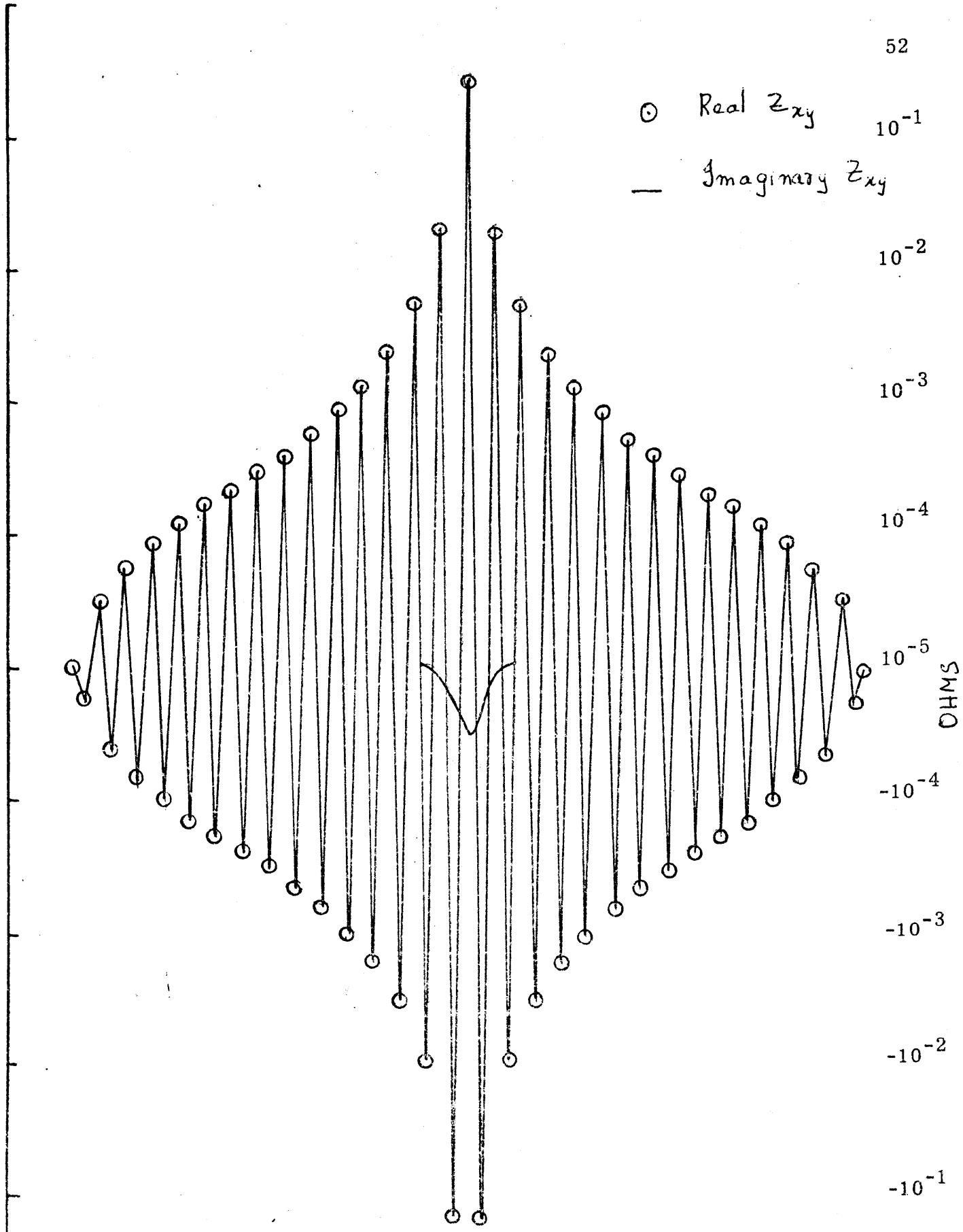

Fig. 3.2-0 Spatial Z_{xy} operator for layered medium shown in Fig. 3.2-1.

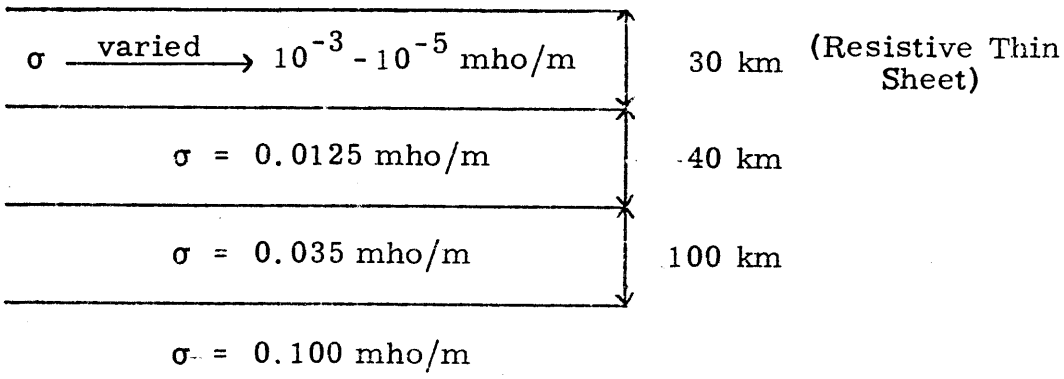

Fig. 3.2-1 Model of layered medium below the thin sheet.

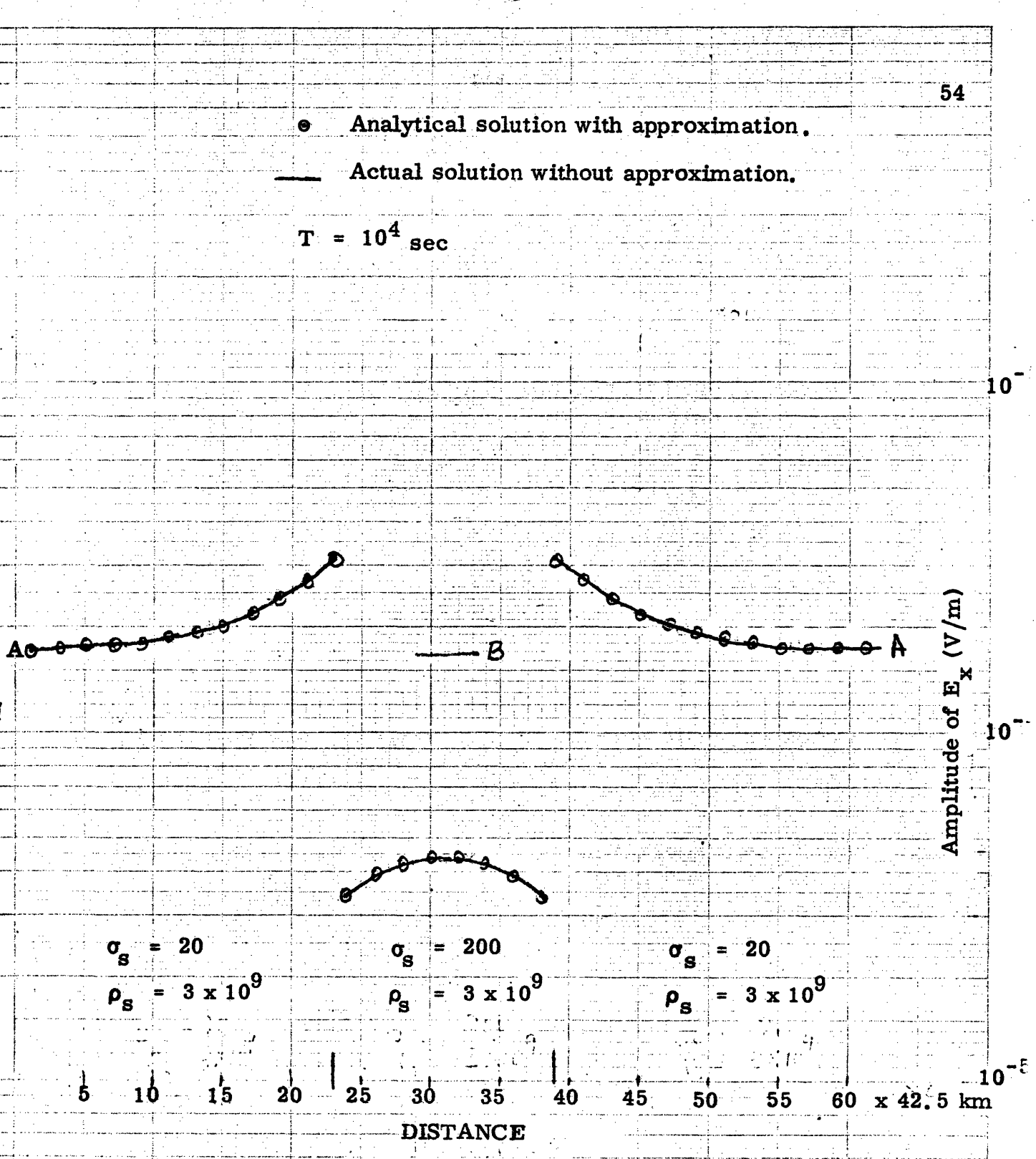

Fig. 3.2-2 Comparison of amplitudes of E_x (perpendicular to the strike) for σ_s and ρ_s shown. Layered medium model is shown in Fig. 3.2-1. A, B represent Cagniard field levels on resistive and conductive sides respectively.

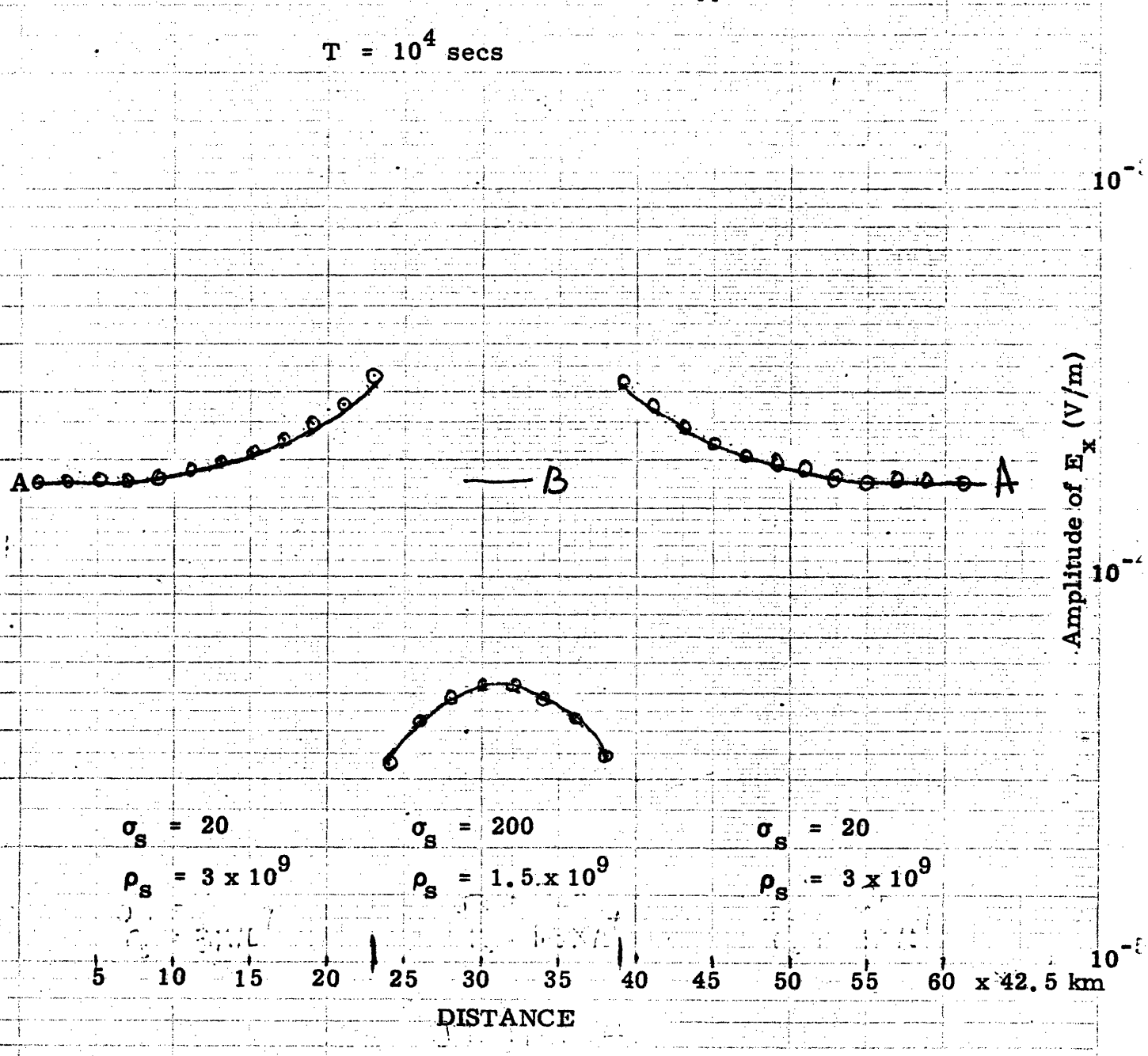

Fig. 3.2-3 Comparison of the amplitude of E_x (perpendicular to the strike) for σ_s and ρ_s variation shown. Layered medium model is given in Fig. 3.2-1. A, B represent Cagniard field levels on the resistive and conductive sides respectively.

Fig. 3.2-4 Comparison of the amplitudes of E_x (perpendicular to the strike) for σ_s and ρ_s variation shown. Layered medium model in Fig. 3.2-1. A, B represent Cagniard field levels on resistive and conductive sides respectively.

$T = 10^4$ secs.

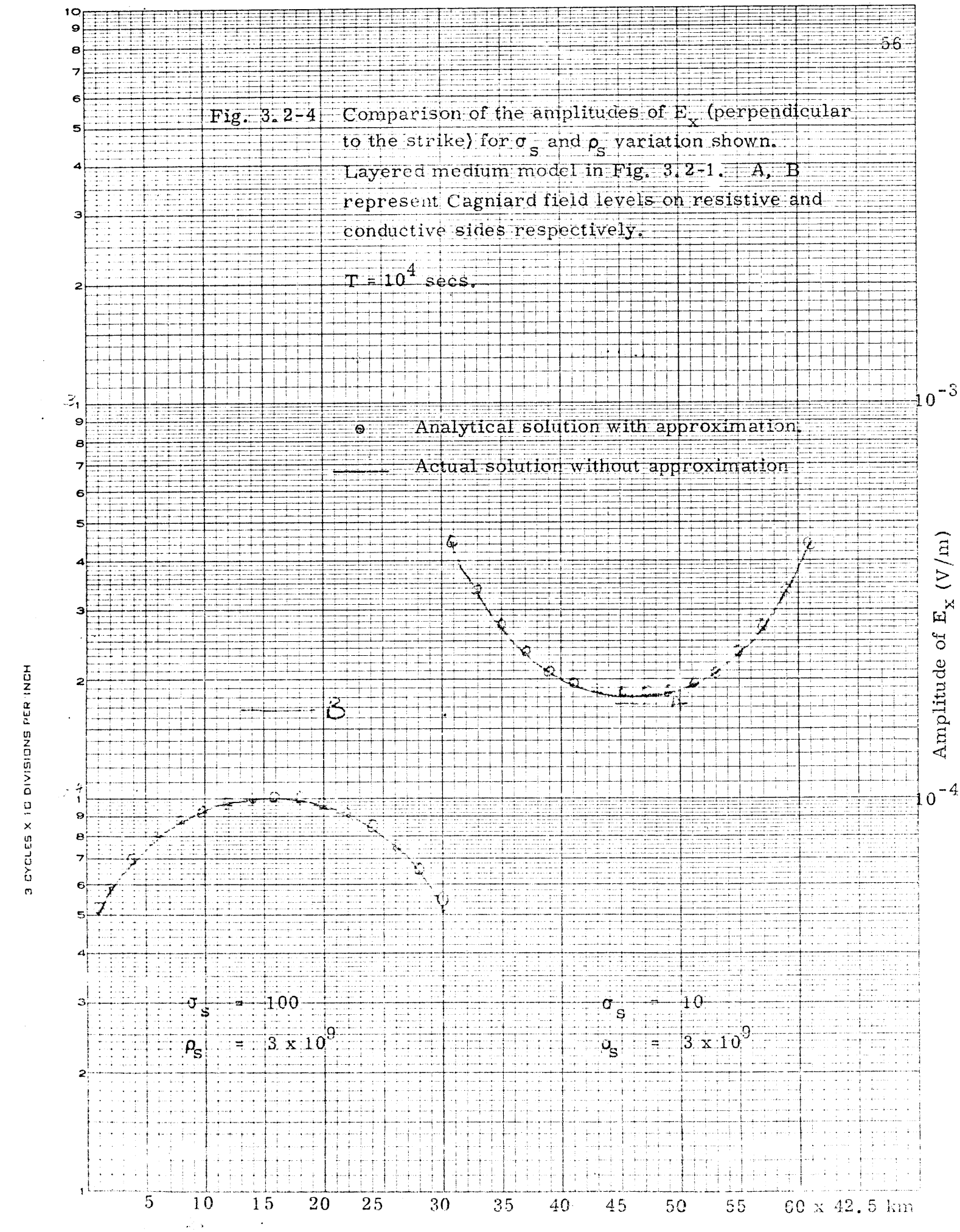

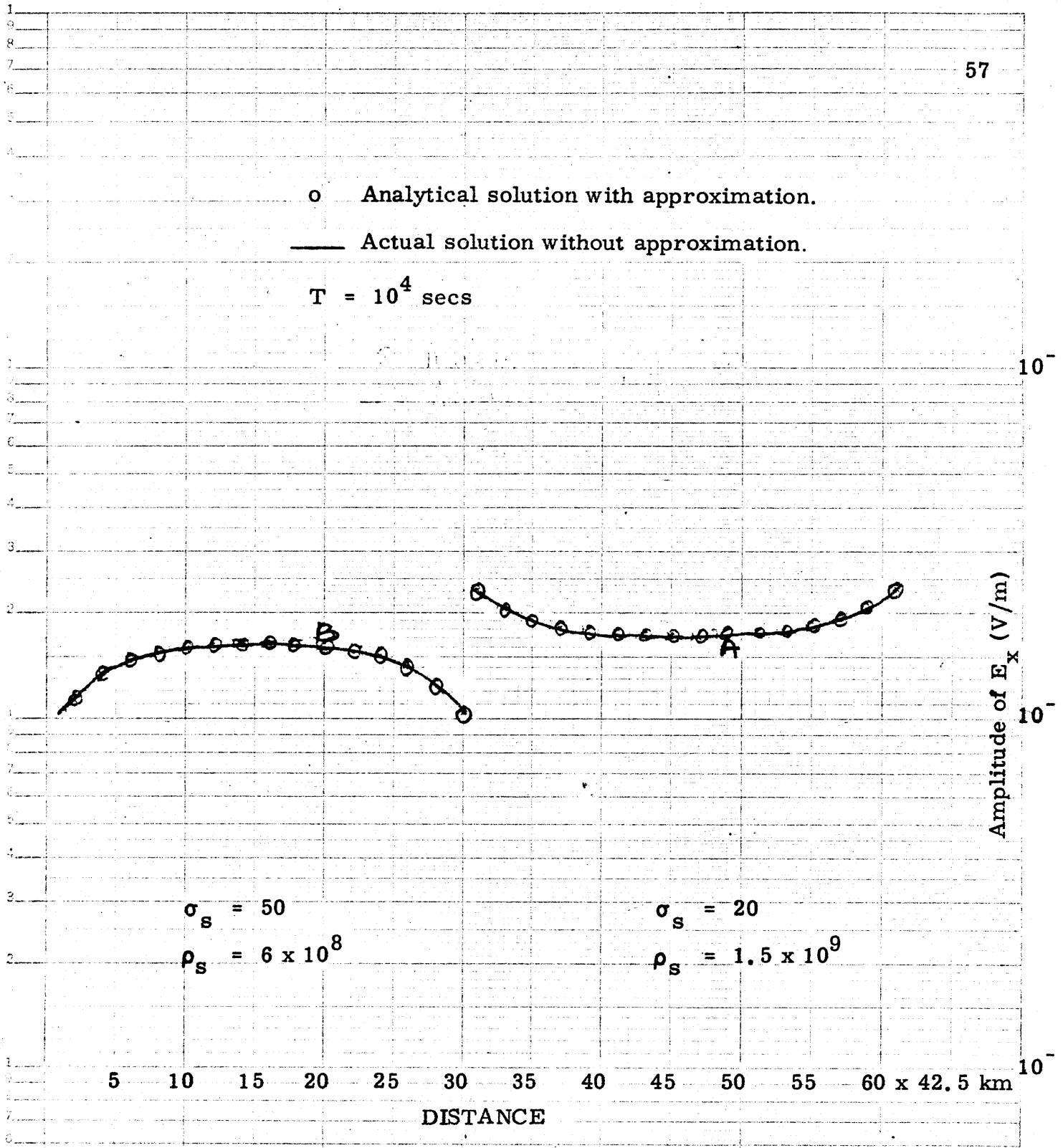

Fig. 3.2-5 Comparisons of the amplitudes of E_x (perpendicular to the strike direction). σ_s, ρ_s and T are as shown. Layered medium model in Fig. 3.2-1. A, B represent Cagniard field levels on the resistive and conductive sides respectively.

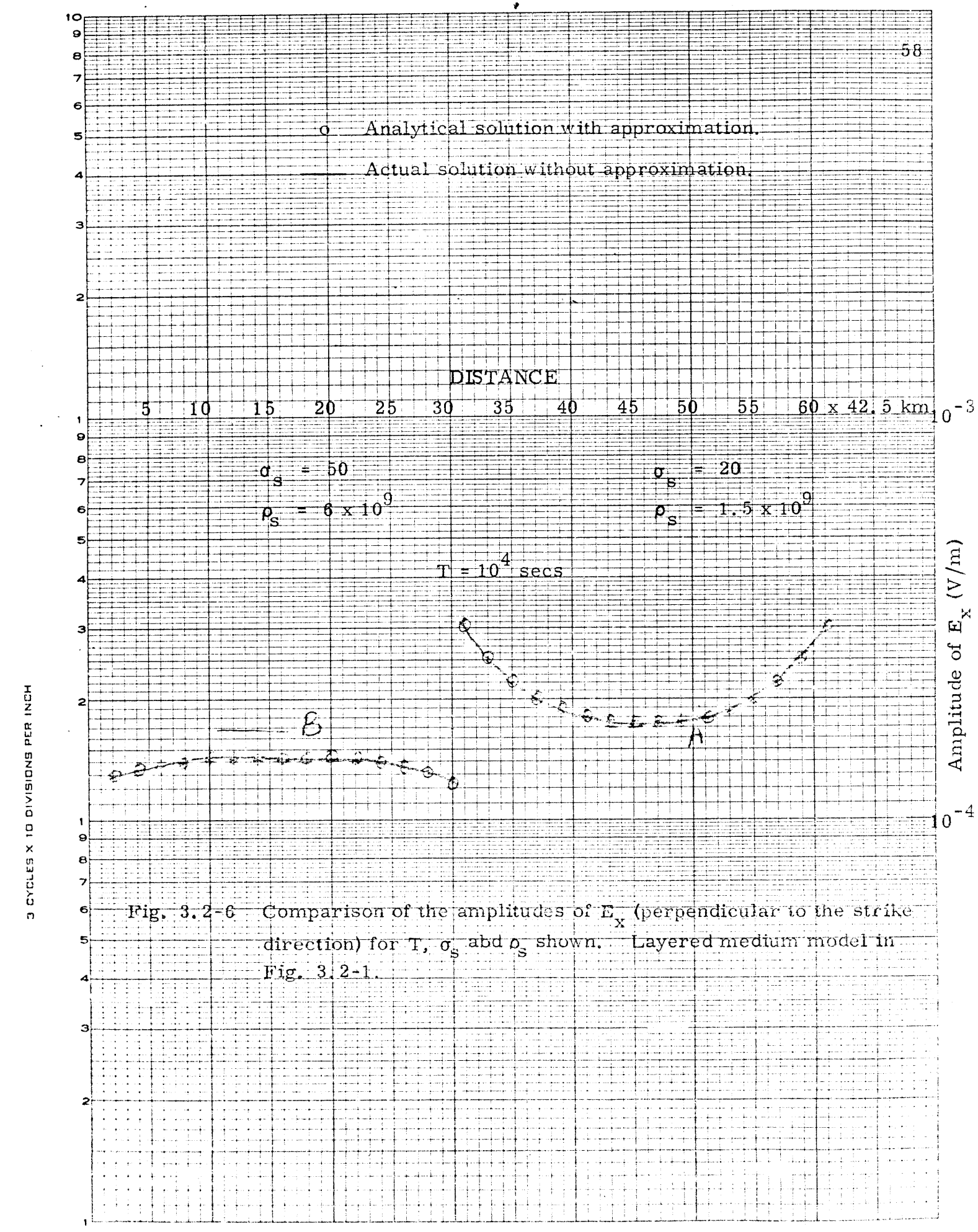

Fig. 3.2-6 Comparison of the amplitudes of E_x (perpendicular to the strike direction) for T, σ_s abd ρ_s shown. Layered medium model in Fig. 3.2-1.

3.3 Land-Ocean-Land Model Solutions

The Land-Ocean-Land model of the thin sheet is shown in Fig. 3.3-1. Here we study this model in great detail to show the dependence of local magnetotelluric measurements on σ and ρ properties considerable distances away.

The thin sheet was assumed to have a thickness of 4.2 km. The land portion of the thin sheet was given a conductivity of 0.95×10^{-3} mho/m. The ocean depth was 4 km, the conductivity of sea water was assumed to be 3.3 mho/m, and ocean sediment thickness was 200 m and a conductivity of 1 mho/m. The source field was uniform $\vec{H}_y$ ($\vec{H}_y$ being parallel to the strike direction). The resistivity of the layer below the thin sheet varied from 10^2 to 10^6 (the layered medium is shown in Fig. 3.3-2). Surface variations of the fields for these five models of the layered medium below the thin sheet are plotted in Figs. 3.3-3 to 3.3-5. In this case the $Z'\sigma_s E_x$ term cannot be neglected and field variations would not have the simple dependence on $\sqrt{\sigma_s \rho_s}$ alone.

Far away from the discontinuity, the fields should be constant and equal to the Cagniard solution. Close to the discontinuity, the E field on the land side would be above the Cagniard field value, while on the conductive side the E field would be below the Cagniard field value. Cagniard solutions for ocean (A) and land (B) are also marked on the figures. From Fig. 3.3.3 it can be seen that as the resistivity of the layer (or more correctly ρ_s) below the thin sheet increases, the adjustment distances in land and ocean increase. Secondly, the adjustment distance in land is now much greater than

the $\sqrt{\sigma_s \rho_s}$ value for the land. (For example, when $\rho = 10^5$, $\sqrt{\sigma_s \rho_s} \approx$ 45 km, but the E field remains above the one-third peak disturbance value for more than 200 km.) In other words, adjustment distance and field levels on land are controlled not only by the σ and ρ properties of the land at the point of measurement, but also by the σ and ρ properties in the ocean. Figures 3.3-6 to 3.3-8 show the same results for a much lower period ($T = 10^5$) of the field, thereby showing that near surface conductivity variations affect electric field and current distribution on the surface even at low frequencies. A comparison of figures 3.3-3 and 3.3-6 shows that for the same ρ_s the distance over which the E value is different from the Cagniard solution is greater for $T = 10^5$ secs on the ocean side and is about the same on the continent side.

Measurements of the magnetotelluric fields on the surface of the thin sheet are thus greatly influenced by ρ_s below the thin sheet. In the thin sheet model ρ_s below the ocean and the land are assumed to have the same value. Resistivities below ocean and land are expected to be different. In the generalized thin sheet model we take this difference in ρ_s below ocean and land into account by treating the thin sheet to be anisotropic with different parallel and perpendicular conductivities. Actually the generalized thin sheet is assumed to be made of two thin sheets, the top one being conductive and the bottom one resistive. The E field is assumed to remain constant across the top conductive thin sheet and the H field is assumed to remain constant across the lower resistive thin sheet. The lower resistive thin sheet represents the lower crust.

Generalized thin sheet solutions are given in Figs. 3.3-9 to 3.3.11. As expected, varying $\rho_s(x)$ below the thin sheet gives very different results compared to uniform $\rho_s(x)$. For example, comparing Fig. 3.3-9 (where ρ_s below the land is $2 \times 10^4 \times 10^5$ and ρ_s below the ocean is $2 \times 10^4 \times 10^4$) with Figs. 3.3-3d ($\rho_s$ = constant = $2 \times 10^4 \times 10^5$), we find that in the former the distance over which the E value is different from the Cagniard solution is smaller and the increase in the amplitude of E_x at the discontinuity is much smaller. On the ocean side the E field dips much lower in Fig. 3.3-9 than in Fig. 3.3-3c (where ρ_s = constant = $2 \times 10^4 \times 10^4$). The distance in the ocean over which the solution is different from the Cagniard solution for ocean is much greater now than when ρ_s below the thin sheet had a constant value of 2×10^8. This again goes to prove the importance of considering σ and ρ properties of the surrounding region while interpreting magnetotelluric data.

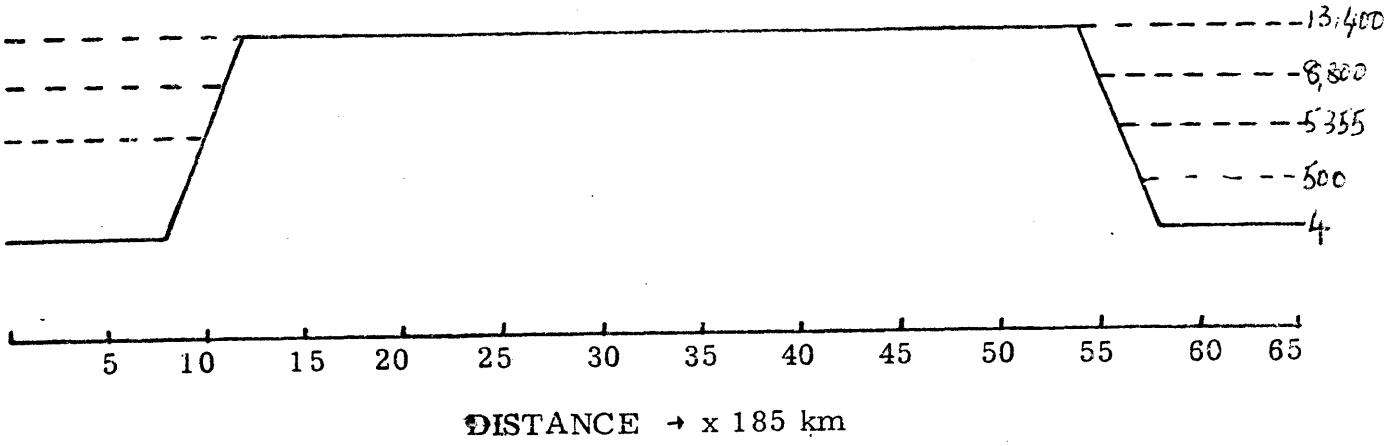

Fig. 3.3-1 Conductance of the thin sheet for Land-Ocean-Land Model (y-axes not to scale).

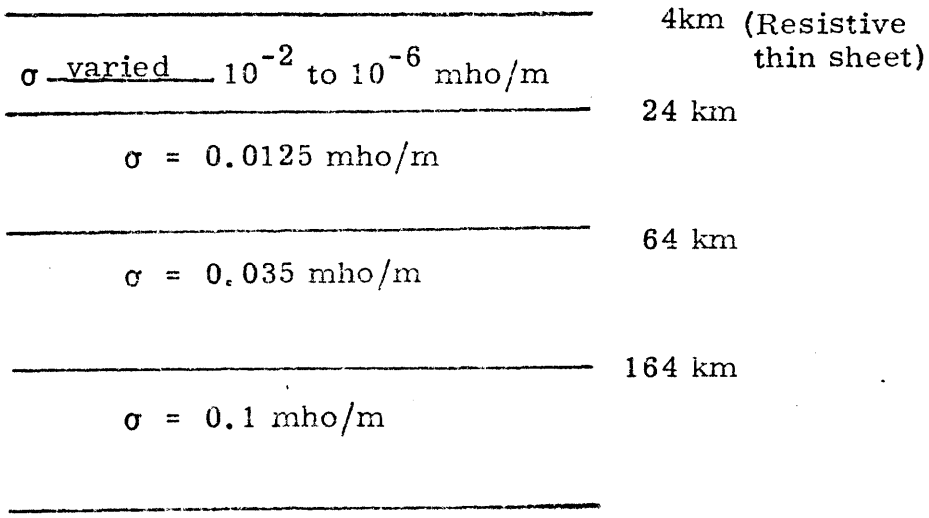

Fig. 3.3-2 Layered medium below the thin sheet for Land-Ocean-Land model.

Fig. 3.3-3 Amplitude of E_x for different values of ρ_s below the thin sheet. (a) $\rho_s = 2 \times 10^6$, (b) $\rho_s = 2 \times 10^7$, (c) $\rho_s = 2 \times 10^8$, (d) $\rho_s = 2 \times 10^9$, (e) $\rho_s = 2 \times 10^{10}$. Layered medium below the thin sheet is given in Fig. 3.3-2.

A - Amplitude of Cagniard solution for ocean.

B - Amplitude of Cagniard solution for land.

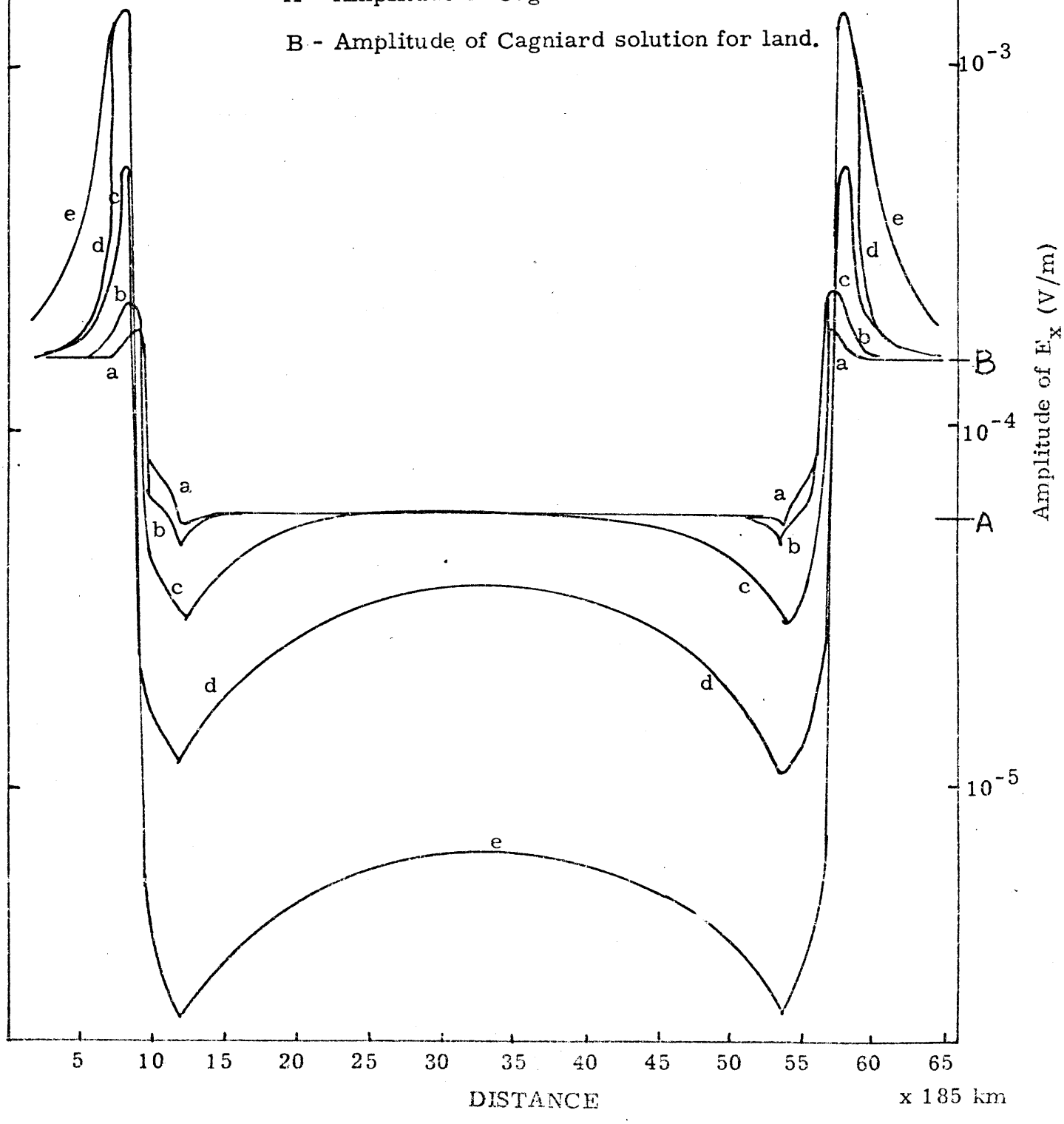

Fig. 3.3-4 Amplitude of current density J_x for different values of ρ_s below the thin sheet.

(a) $\rho_s = 2 \times 10^6$, (b) $\rho_s = 2 \times 10^7$, (c) $\rho_s = 2 \times 10^8$

(d) $\rho_s = 2 \times 10^9$, (e) $\rho_s = 2 \times 10^{10}$. Refer to Fig. 3.4-3 for details.

$T = 10^4$ secs.

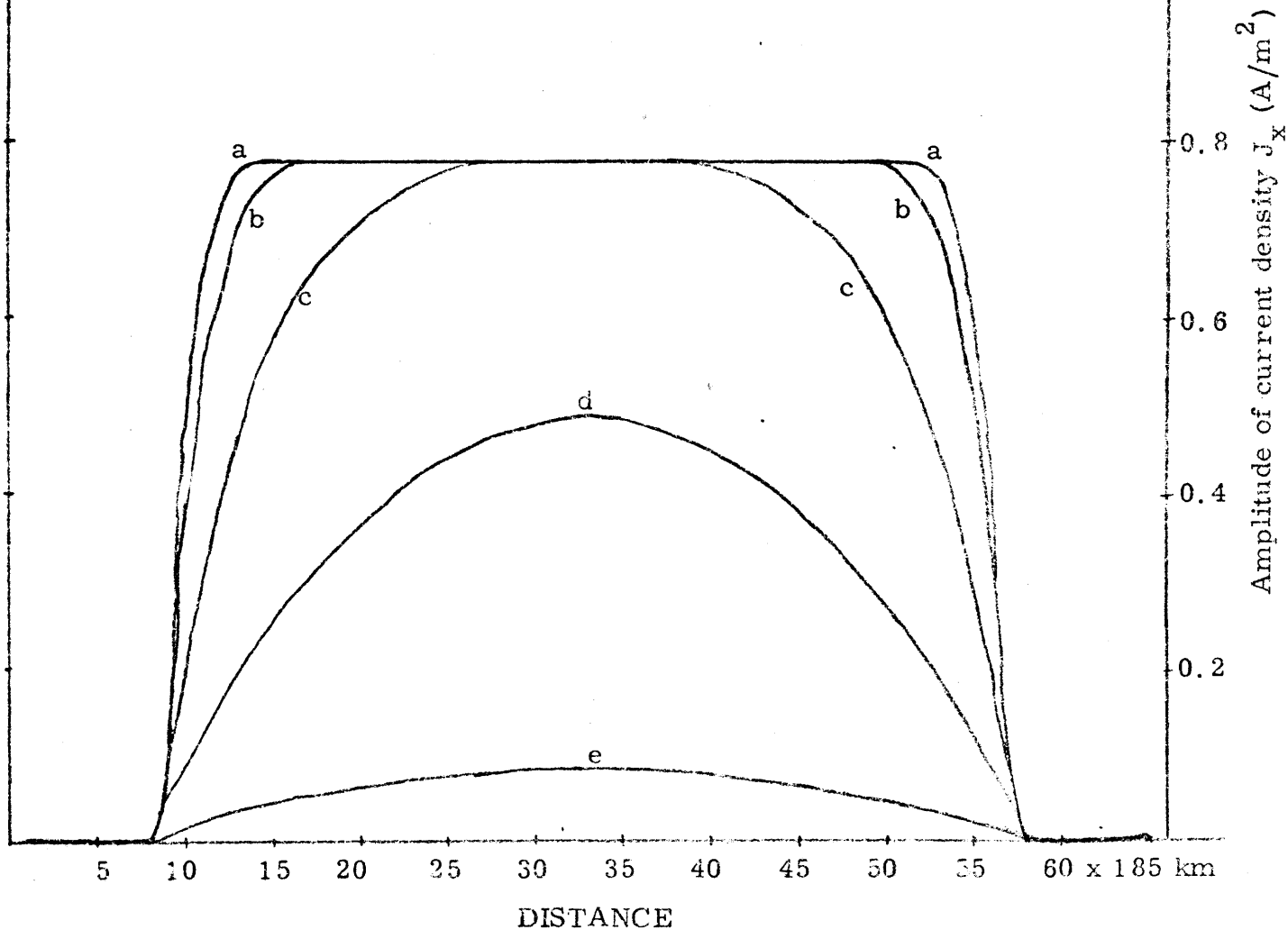

Fig. 3.3-5 Phase of E_x for different values of ρ_s below the thin sheet. (a) $\rho_s = 2 \times 10^6$, (b) $\rho_s = 2 \times 10^7$, (c) $\rho_s = 2 \times 10^8$, (d) $\rho_s = 2 \times 10^9$, (e) $\rho_s = 2 \times 10^{10}$. Refer to Fig. 3.4-3 for details.

$T = 10^4$ secs.

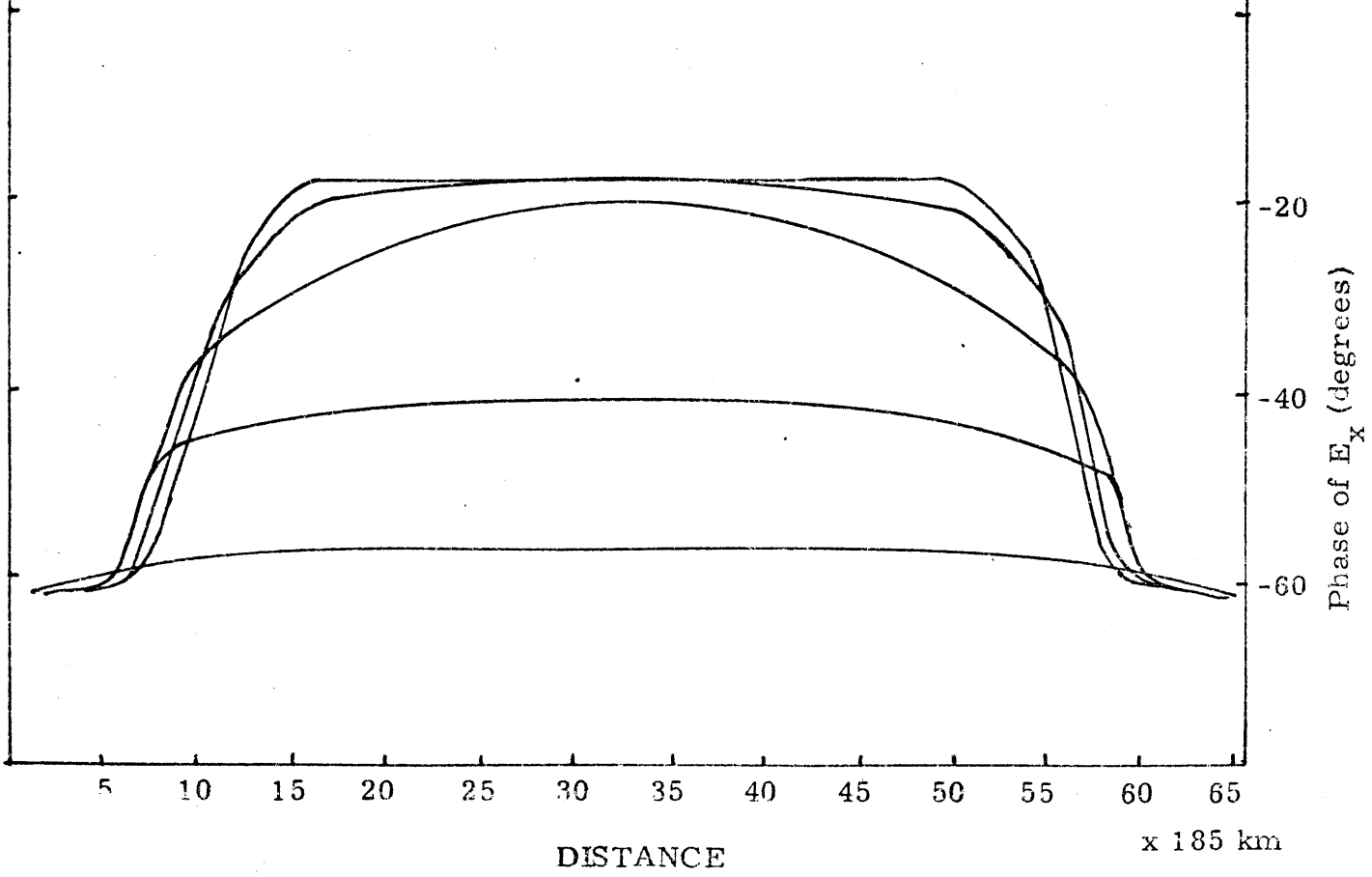

Fig. 3.3-6 Amplitude of E_x for different values of ρ_s below the thin sheet. (a) $\rho_s = 2 \times 10^6$, (b) $\rho_s = 2 \times 10^7$, (c) $\rho_s = 2 \times 10^8$, (d) $\rho_s = 2 \times 10^9$, (e) $\rho_s = 2 \times 10^{10}$. Refer to Fig. 3.2-3 for details.

A - amplitude of Cagniard solution for ocean.

B - amplitude of Cagniard solution for land.

$T = 10^5$ secs.

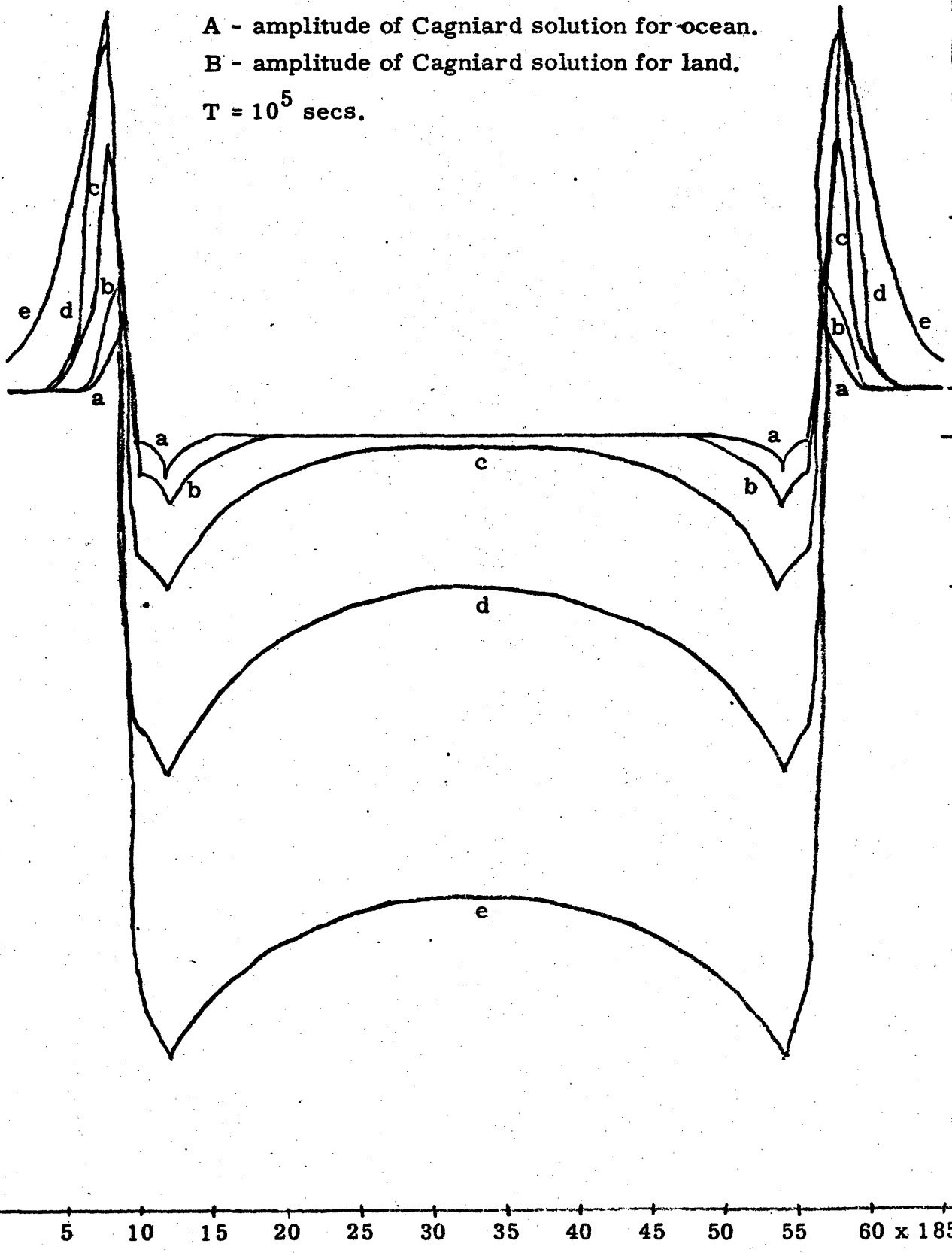

Fig. 3.3-7 Phase of E_x for different values of ρ_s below the thin sheet. (a) $\rho_s = 2 \times 10^6$, (b) $\rho_s = 2 \times 10^7$, (c) $\rho_s = 2 \times 10^8$, (d) $\rho_s = 2 \times 10^9$, (e) $\rho_s = 2 \times 10^{10}$. Refer to Fig. 3.2-3 for details.

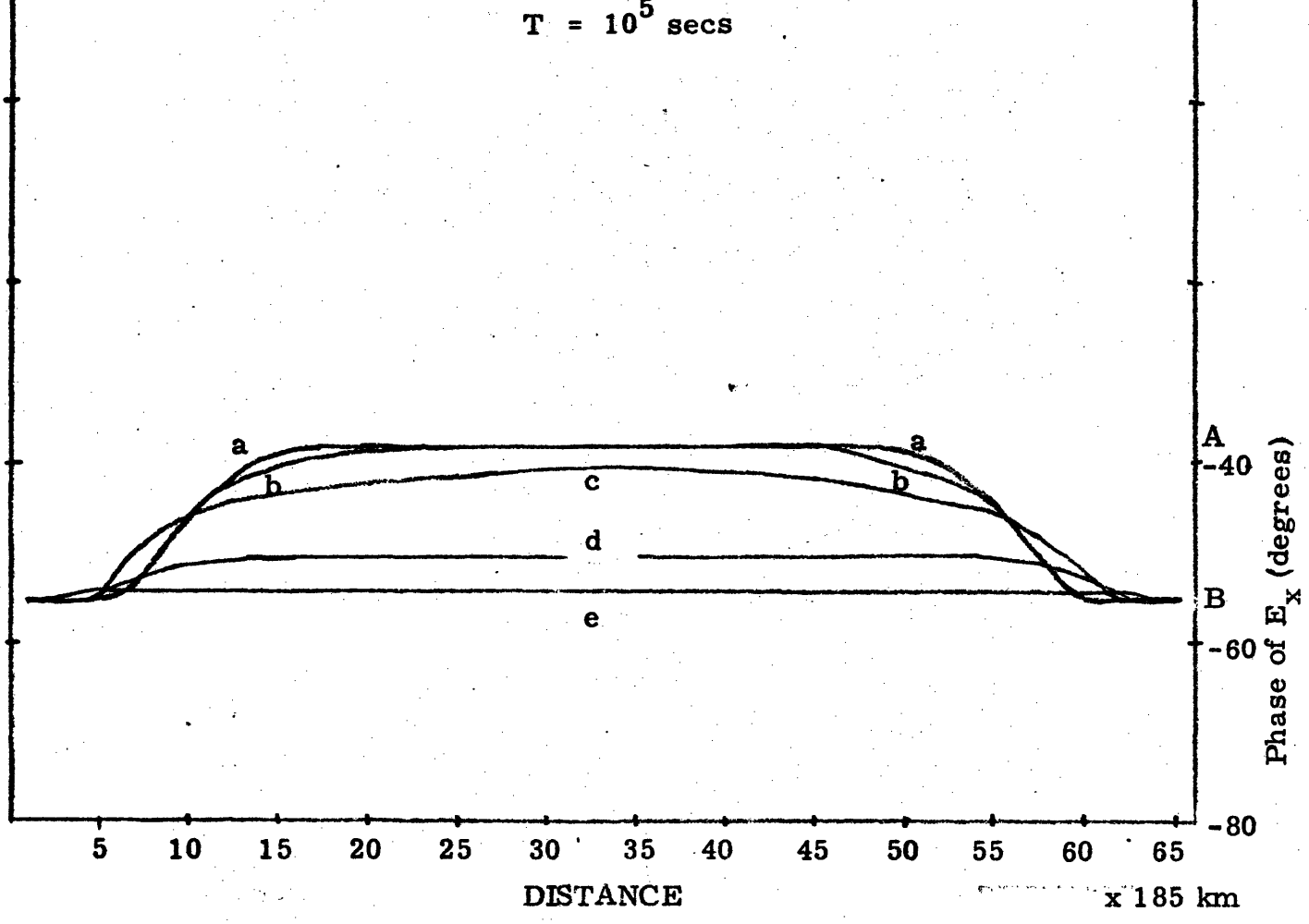

Fig. 3.3-8 Amplitude of current density J_x for different values of ρ_s below the thin sheet. (a) $\rho_s = 2 \times 10^6$, (b) $\rho_s = 2 \times 10^7$, (c) $\rho_s = 2 \times 10^8$, (d) $\rho_s = 2 \times 10^9$, (e) $\rho_s = 2 \times 10^{10}$. Refer to Fig. 3.2-3 for details.

$T = 10^5$ secs

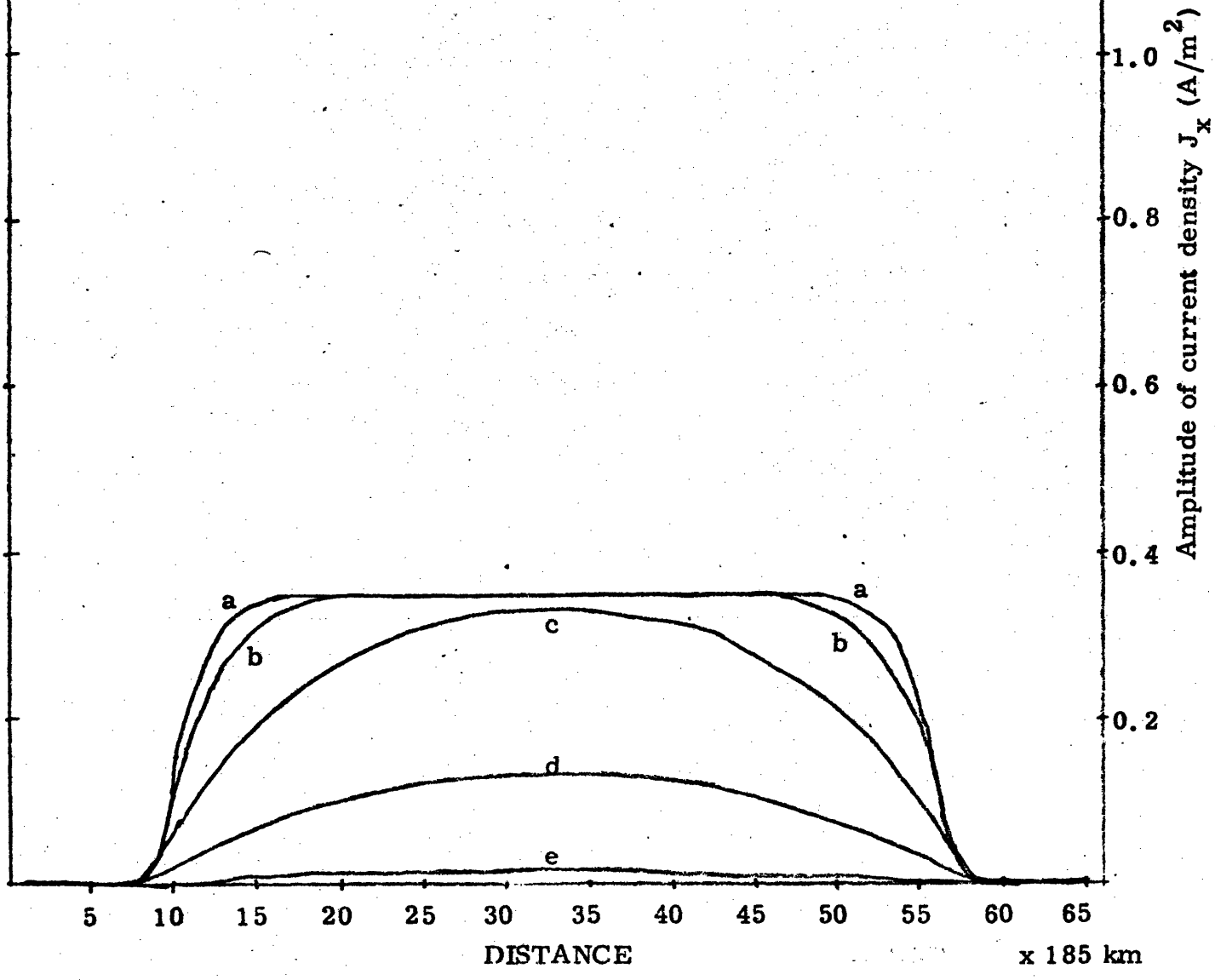

Fig. 3.3-9 Amplitude of E_x (perpendicular to strike for ρ_s variation shown). Thin sheet conductance is shown in Fig. 3.4-1 and layered medium model is shown in Fig. 3.4-2.

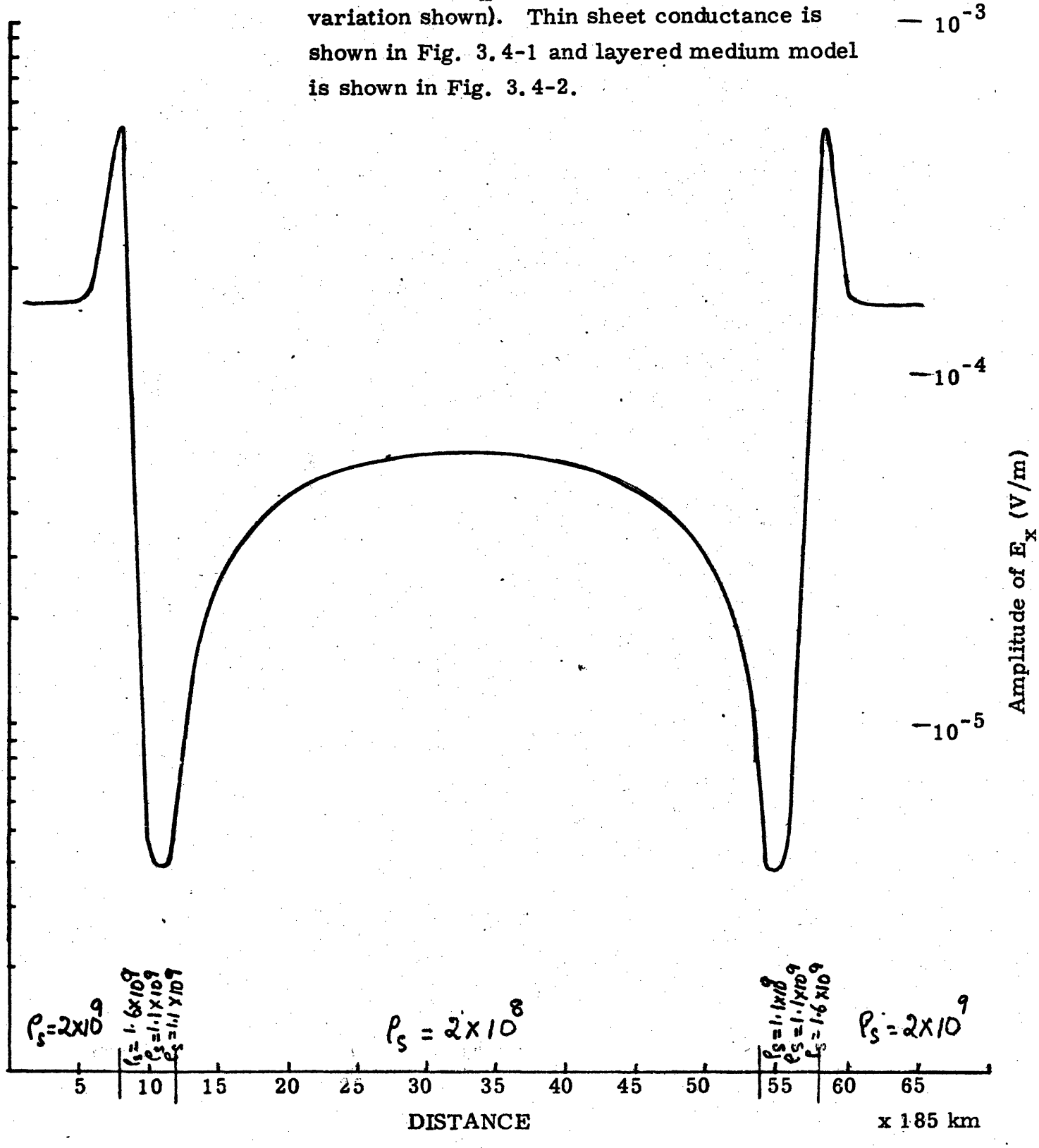

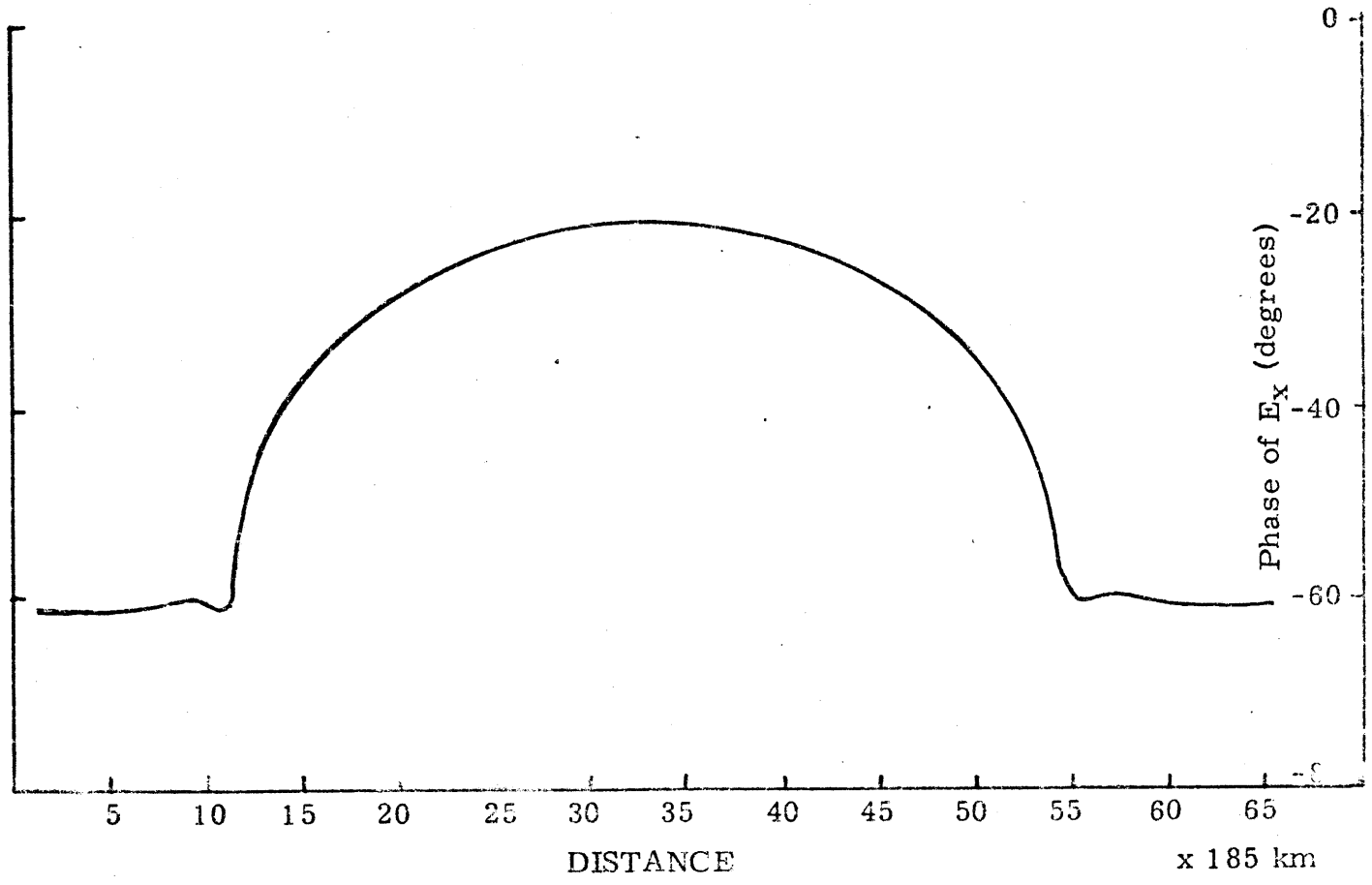

Fig. 3.3-10 Phase of E_x. For details refer to Fig. 3.4-9.

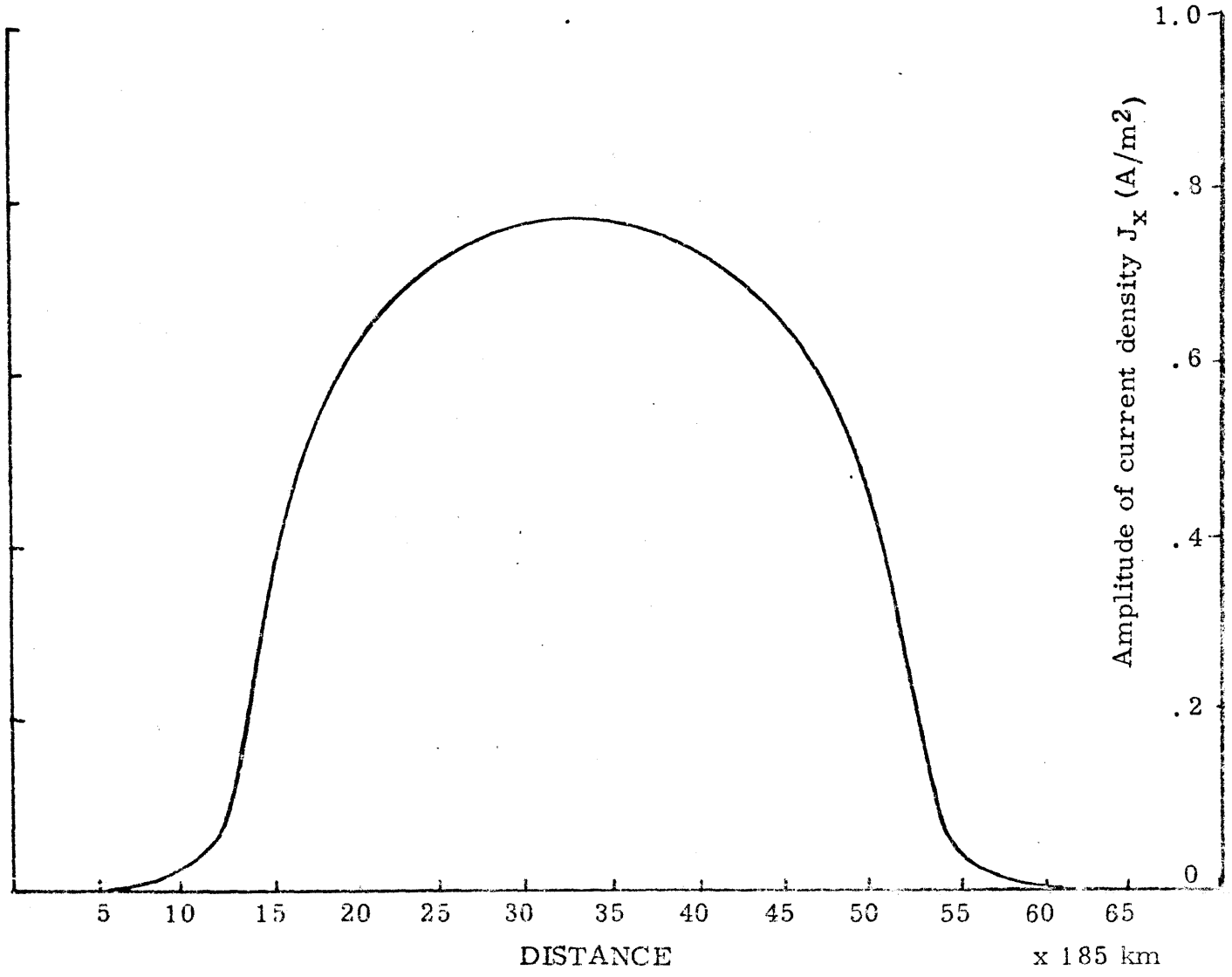

Fig. 3.3-11 Amplitude of current density J_x (perpendicular to strike). For details refer to Fig. 3.4-9.

3.4 One-Dimensional Modelling of an Island Chain

A long island-ridge like the one in the Pacific Ocean of which the Hawaiian chain is a part can be approximated by a one-dimensional thin sheet or a one-dimensional generalized thin sheet model. The thin sheet conductance model of the mid-oceanic rise is shown in Fig. 3.4-1. The ocean was assumed to have an average depth of 2900 fathoms (5458 m) and the conductivity of the oceanic water was taken as 3.32 mho/m. The ocean sediment thickness was taken as 200 m and the conductivity of the ocean sediment was set at 1 mho/m. The deep ocean and its sediments therefore have a conductance of 17,810 mhos. Average depth of the rise was 1000 fathoms (1882 m) which gives a conductivity thickness product of 6100 mhos for the rise. Other values in the conductance profile reflect the average bathymetry across the rise. The source field was aasumed to be quasi-uniform. Hence we would get two sets of solutions, one for E parallel to the strike and one for E perpendicular to the strike.

The model of the layered medium below the thin sheet is similar to that given by Larsen (1975) for the Hawaiian islands, the difference being that in our model the top layer (20 km thick) has a much lower conductivity value. Solutions were obtained for different values of conductivity for the top layer. These results are summarized in Figs. 3.4-1 to 3.4-6 for the E perpendicular mode. It can be seen that the amplitude of the E_x field on the rise is about two to three times higher than that for the ocean.

In Figs. 3.4-7 to 3.4-9 are shown the results of E_y parallel to

the strike. ρ_s in this case was given a constant value of 2×10^7. Apparent resistivity across the rise in this case is different from that for E perpendicular to the strike. The anisotropy is shown clearly in Table 3.4-1 where $\rho_\perp$ and $\rho_\parallel$ are tabulated side by side for each case.

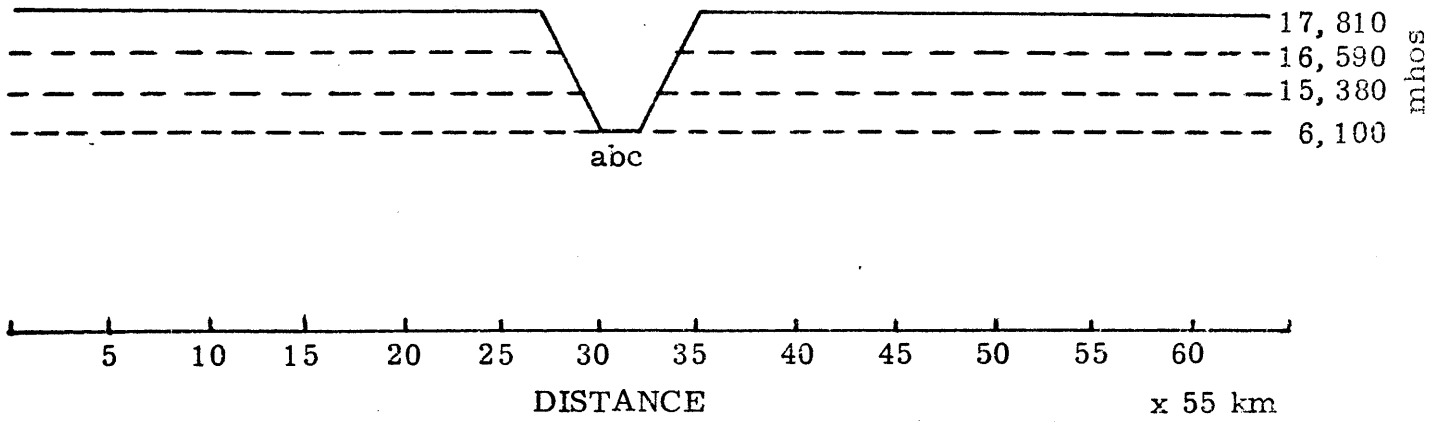

Fig. 3.4-1 Conductance of the thin sheet for Hawaiian Rise (y-axis not to scale).

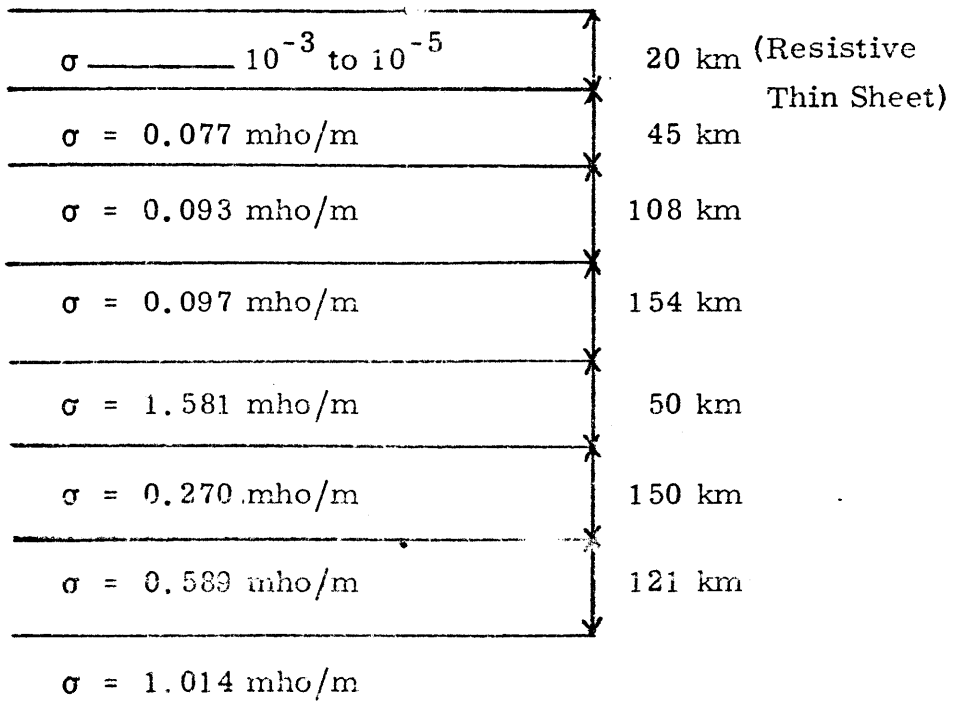

Fig. 3.4-2 Model of Layered Medium below the thin sheet for Hawaiian Rise.

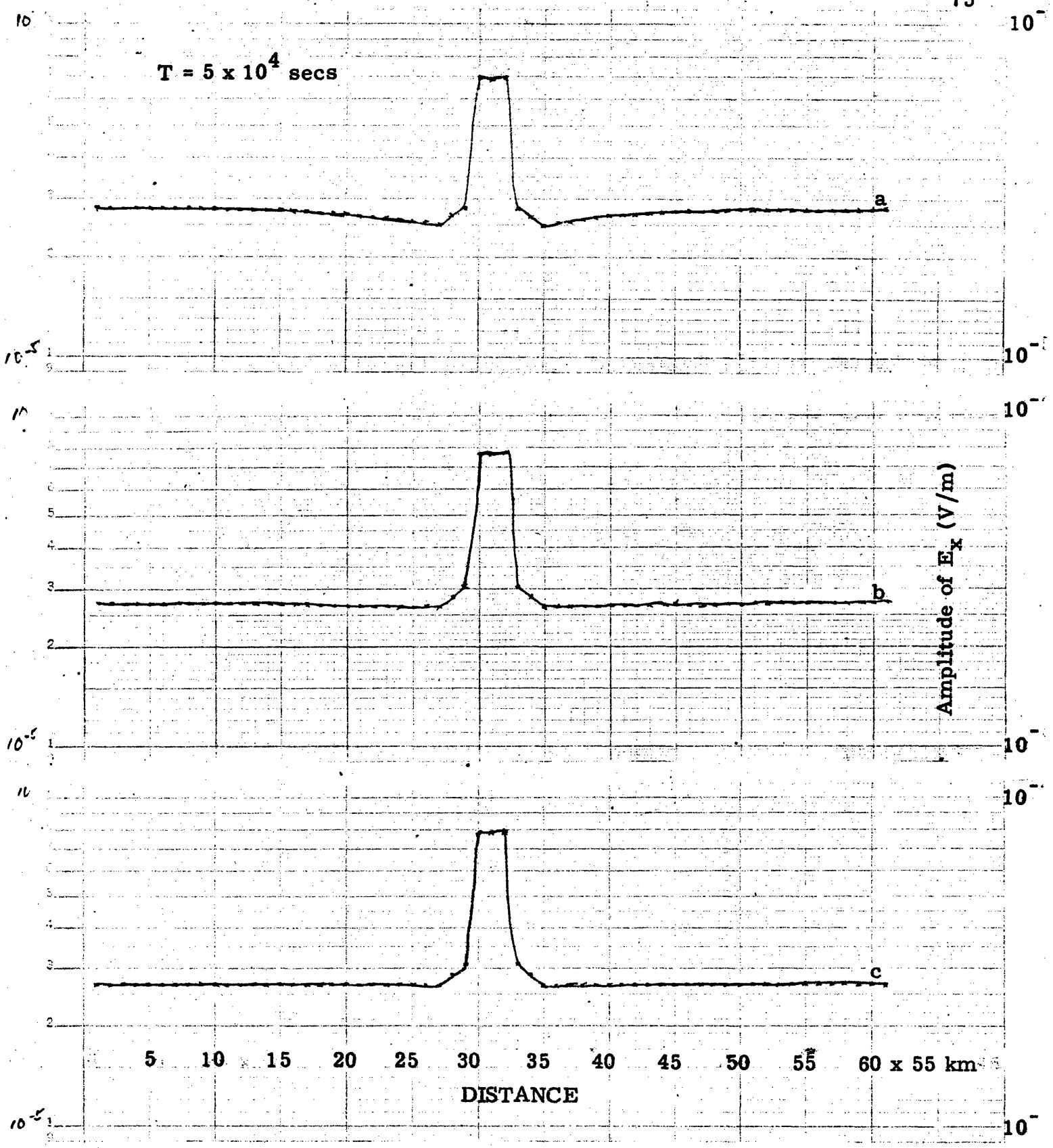

Fig. 3.4-3 Amplitude of E_x (perpendicular to the strike) for different values of ρ_s below the thin sheet: (a) $\rho_s = 2 \times 10^7$, (b) $\rho_s = 2 \times 10^8$, (c) $\rho_s = 2 \times 10^9$. Thin sheet conductance is shown in Fig. 3.4-1 and layered medium model is given in Fig. 3.4-2.

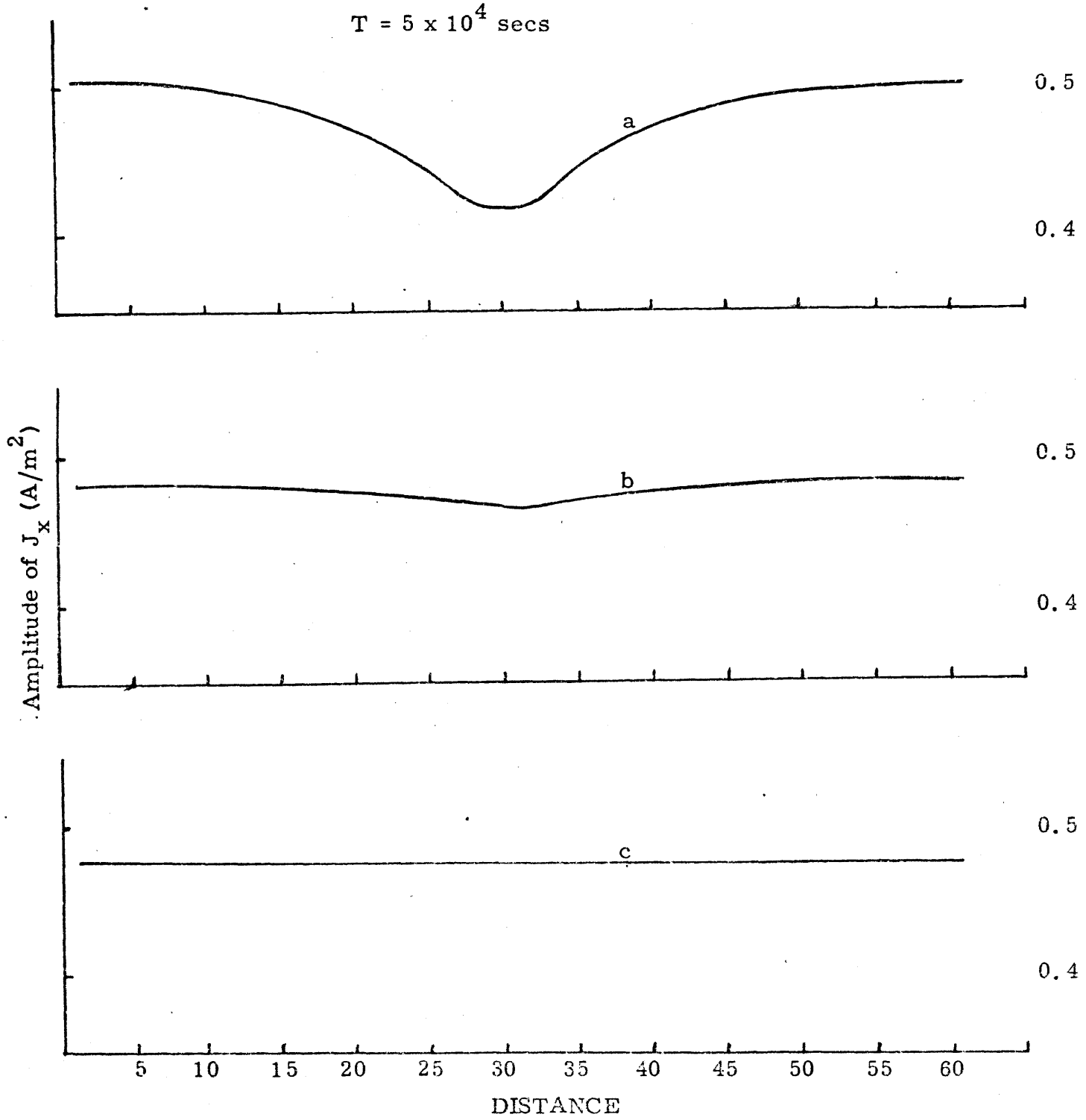

Fig. 3.4-4 Amplitude of J_x (perpendicular to strike) for different values of ρ_s. (a) $\rho_s = 2 \times 10^7$, (b) $\rho_s = 2 \times 10^8$, (c) $\rho_s = 2 \times 10^9$. Thin sheet conductance is shown in Fig. 3.4-1 and layered medium model is given in Fig. 3.4-2.

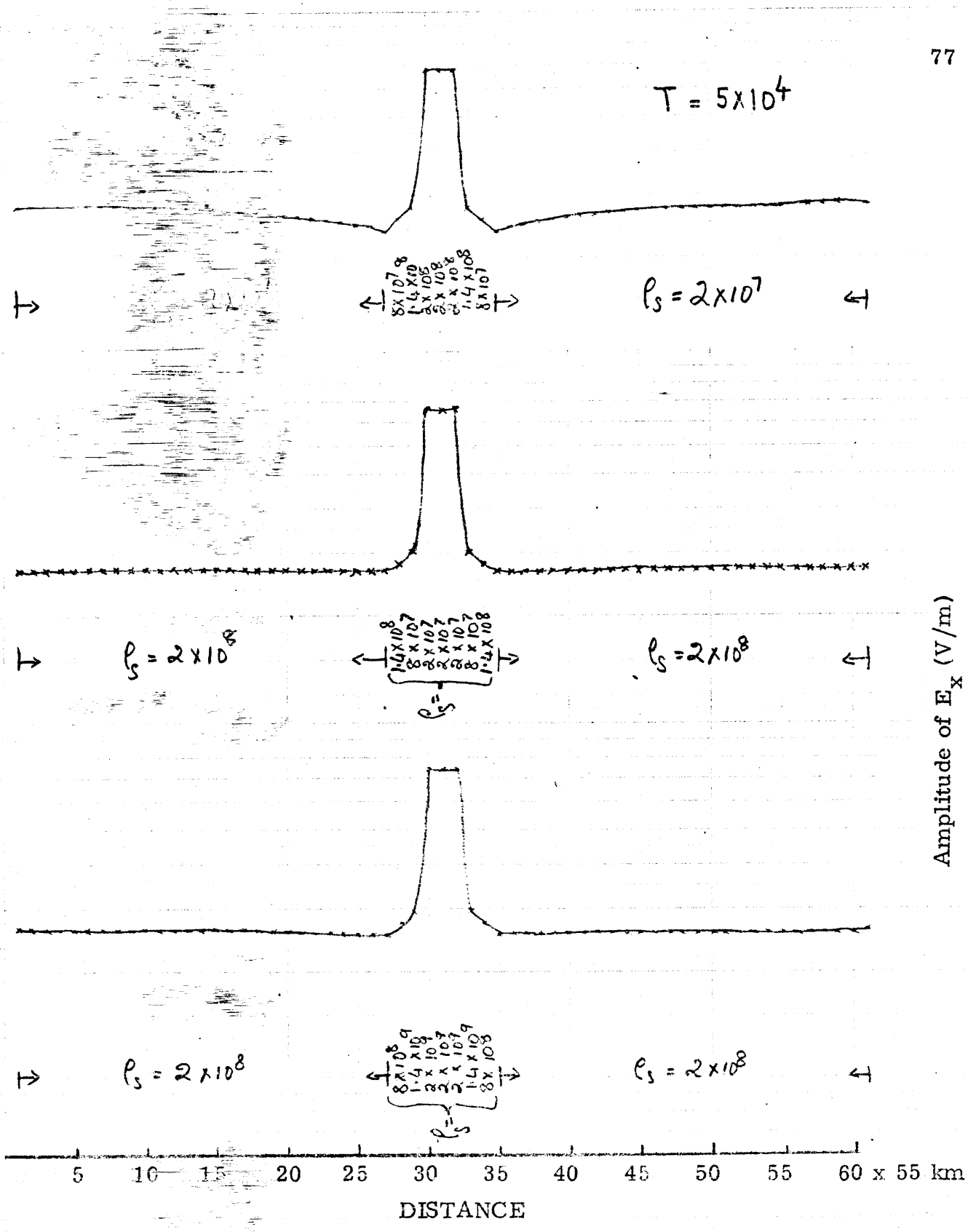

Fig. 3.4-5 Amplitude of E_x (perpendicular to strike) for ρ_s variations shown. [illegible] sheet conductance model is shown in Fig. 3.4-1 and [illegible] layered medium model is shown in Fig. 3.4-2.

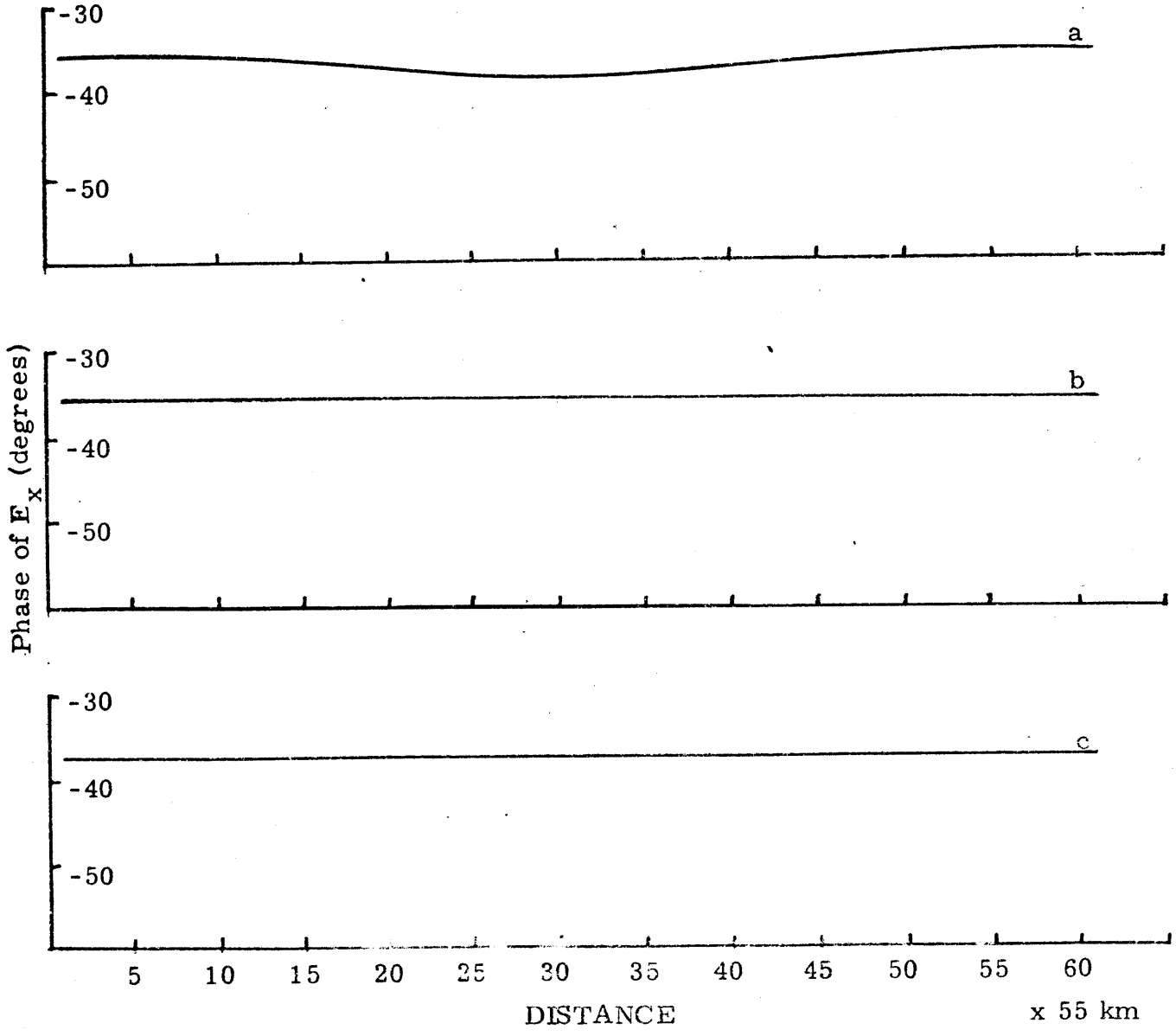

Fig. 3.4-6 Phase of E_x (perpendicular to strike) for ρ_s variations shown. Thin sheet conductance model is shown in Fig. 3.4-1 and layered medium model is shown in Fig. 3.4-2.

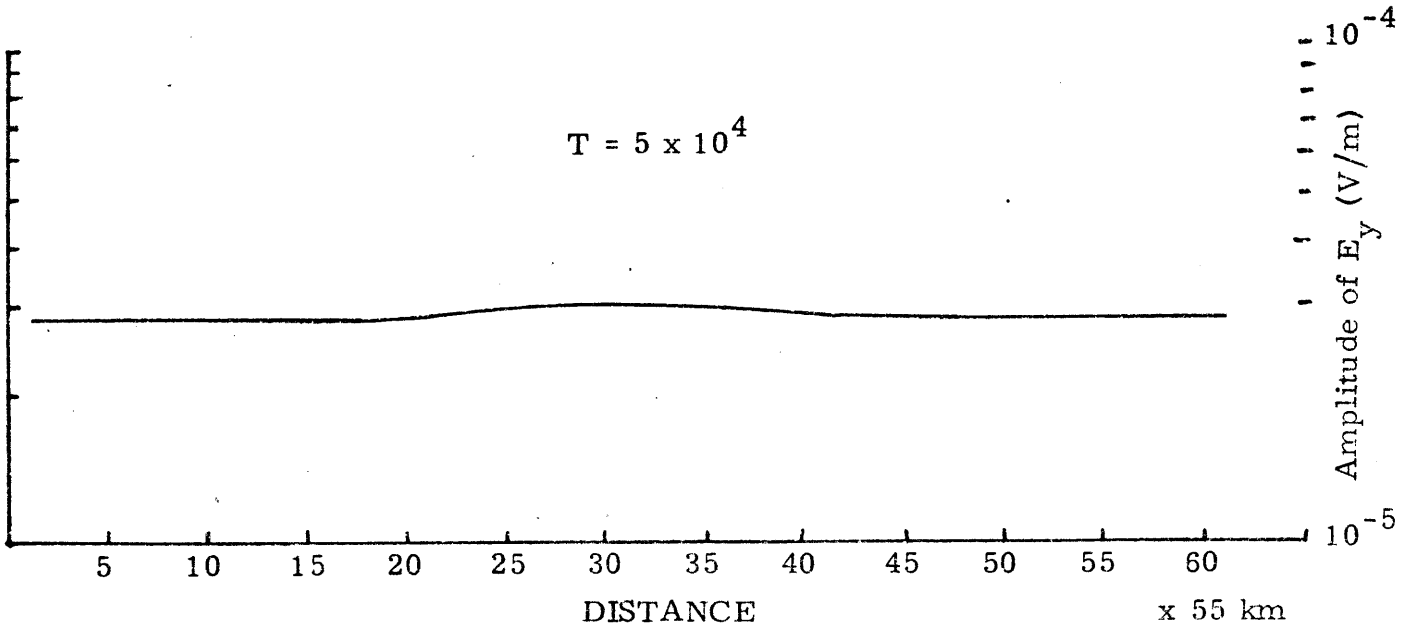

Fig. 3.4-7 Amplitude of E_y (parallel to the strike). Conductance of the thin sheet is given in Fig. 3.4-1. Layered medium below the thin sheet is shown in Fig. 3.4-2. ρ_s below the thin sheet had a constant value of 2×10^7.

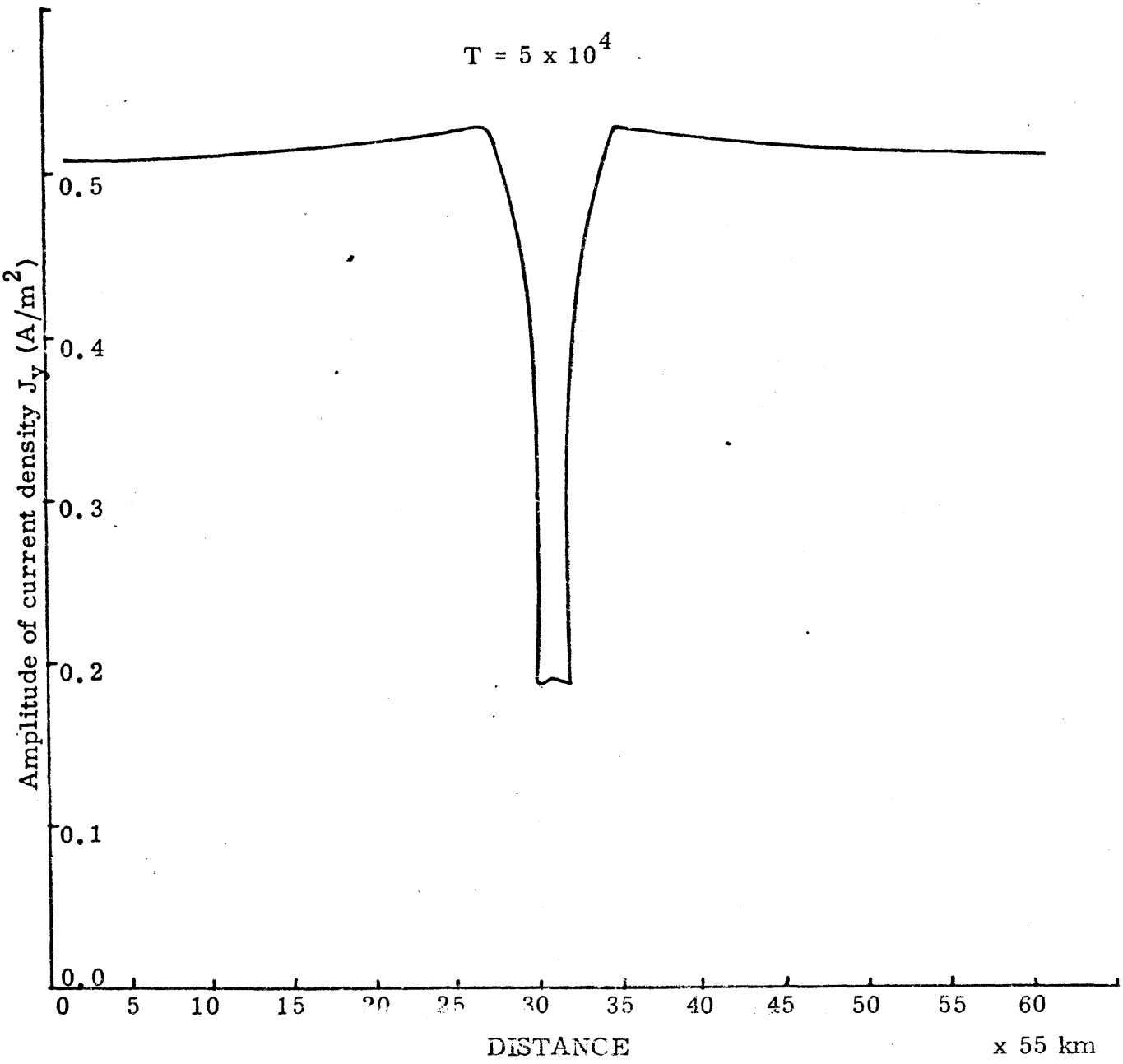

Fig. 3.4-8 Amplitude of current density J_y (parallel to the strike). Conductance of the thin sheet is given in Fig. 3.4-1. Layered medium below the thin sheet is shown in Fig. 3.4-2. ρ_s below the thin sheet had a constant value of 2 x 10^7.

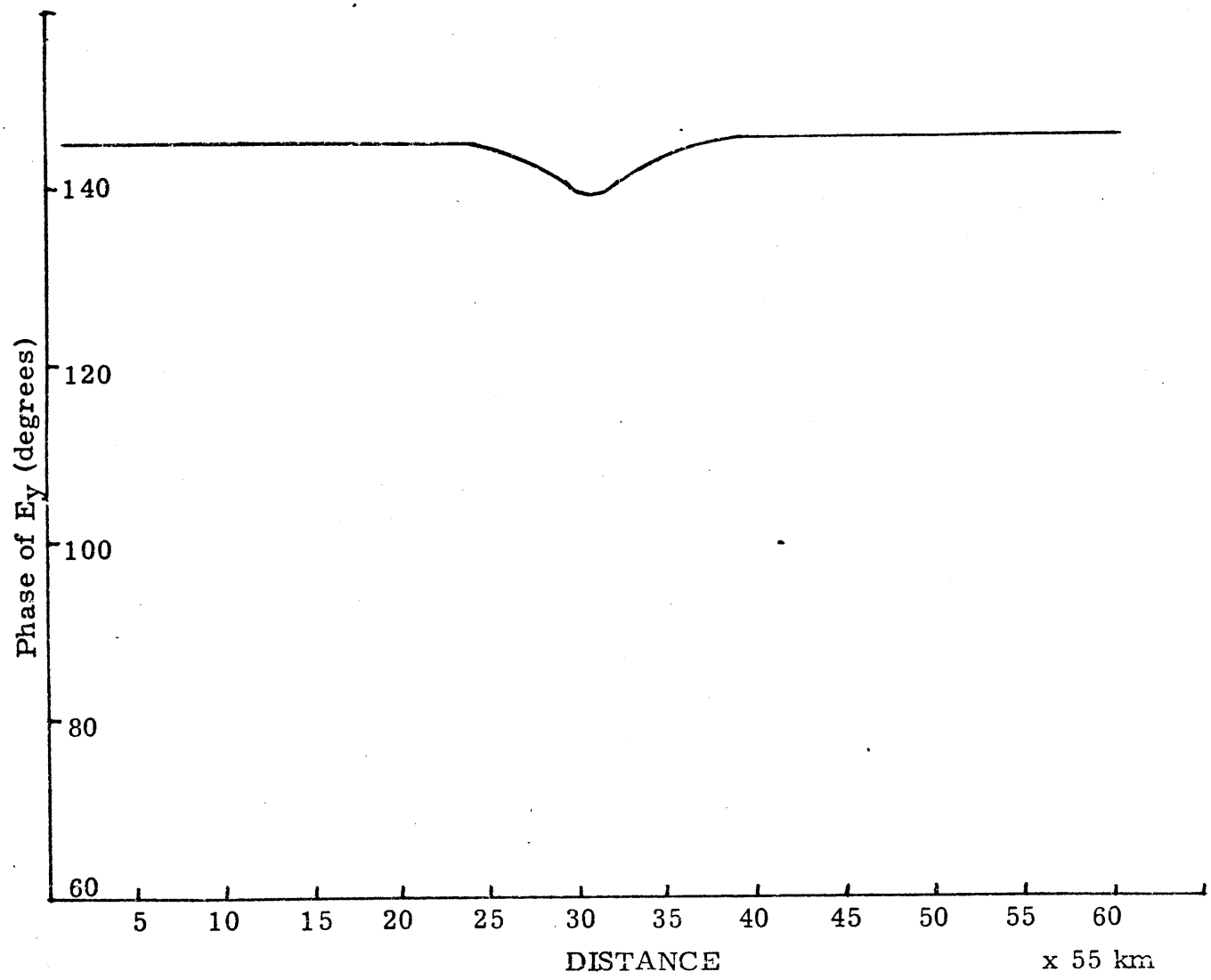

Fig. 3.4-9 Phase of E_y (parallel to the strike). Conductance of the thin sheet is given in Fig. 3.4-1. Layered medium below the thin sheet is shown in Fig. 3.4-2. ρ_s below the thin sheet had a constant value of 2×10^7.

Table 3.4-1

Position	Apparent Resistivity $\rho_\perp = \frac{1}{\mu\omega}\left(\frac{\lvert E_x\rvert}{\lvert H_y\rvert}\right)^2$ (ohm-m)	Apparent Resistivity $\rho_\parallel = \frac{1}{\mu\omega}\left(\frac{\lvert E_y\rvert}{\lvert H_x\rvert}\right)^2$ (ohm-m)	ρ_s below land	ρ_s below ocean
a	30.8	7.4	2×10^7	2×10^7
b	30.4	7.5		
c	30.8	7.4		
a	37.5	7.4	2×10^8	2×10^8
b	37.5	7.5		
c	37.5	7.4		
a	38.9	7.4	2×10^9	2×10^9
b	38.9	7.5		
c	38.9	7.4		
a	30.0	7.4	2×10^8	2×10^7
b	30.0	7.5		
c	30.0	7.4		
a	34.9	7.4	2×10^9	2×10^8
b	34.9	7.5		
c	34.9	7.4		
a	37.0	7.4	2×10^7	2×10^8
b	36.5	7.5		
c	37.0	7.4		

Parallel and perpendicular apparent resistivities across the Hawaiian rise (positions a, b, c) for different ρ_s variations. Positions a, b, c are marked on the conductance profile in Fig. 3.4-1. They are characterized by a conductance value of 6100 mhos. The layered medium model below the thin sheet is shown in Fig. 3.4-2.

CHAPTER IV

METHOD OF IMBEDDING

The model solution is determined by solving the simultaneous equations given by (2.2.7) or (2.3.7). For two-dimensional variation of conductivity and/or resistivity, we have, at each grid point on the surface, two unknowns, namely E_x and E_y. A small number of 9 by 9 grid points on the surface therefore results in a system of 162 simultaneous equations in complex variables (E_x and E_y are functions of temporal frequency and spatial coordinates). Because of the convolutions in equations (2.2.7) and (2.3.7), the coefficient matrix of the simultaneous equations would be a full (or almost full) matrix. The computing cost for even the small 9 x 9 grid is therefore not modest. To get a detailed distribution of the induced fields, certainly a much larger number of grid points would have to be considered.

The fields measured at a point are affected not only by the properties of the medium immediately surrounding it but also by σ and ρ properties considerable distances away (refer to Chapter III). While the solution is influenced by small scale variations of the medium immediately surrounding it, it is mainly sensitive to large scale variations or average properties at distances farther away from the point of measurement. Based on this physical behaviour of fields a new method called the method of imbedding is developed to compute the solution which enormously reduces the storage requirements and the number of computations involved and therefore the

computational cost.

"This method involves an approximate model, rather than an approximate solution of the true model" (Madden, 1976). The model is shown in Fig. 4.0 and is similar to the model used in embedded network analysis by Madden (1976). The entire region of interest (surrounding the point of measurement) is divided into an odd number of zones. Each zone has the average properties of the region it represents. The zone that contains the measurement point and its adjacent zones are further subdivided. The adjacent zones act as buffer zones to absorb the differences created by approximation and improve the accuracy in the middle. These subdivided zones can now show smaller scale fluctuations. This process is continued until that stage at which the subdivided zones represent the true variations in the properties of the medium.

In order to calculate the average properties of the medium, we start at the lowest level and work upwards. Starting at the lowest level, where the true variations in the properties are represented, average properties of the zones for the next level are computed and the process is continued until the average properties of all the zones at the highest level are computed. After the average properties of all the zones at all levels are calculated, the fields are computed from the highest to the lowest level. Using the average properties, the fields are calculated at each of the zones in the highest level. We are interested in determining the fields at much closer spacing than represented by the highest level zones. We therefore re-determine the field values at closer spacings for

the middle zones using the average properties of the medium at that level (calculated earlier) and assuming the fields in the outer zones to be the averages for the zones they subdivide into at the next level. The field values in the inner zones are recalculated again until the lowest level at which they represent the true variations in the properties of the medium is reached.

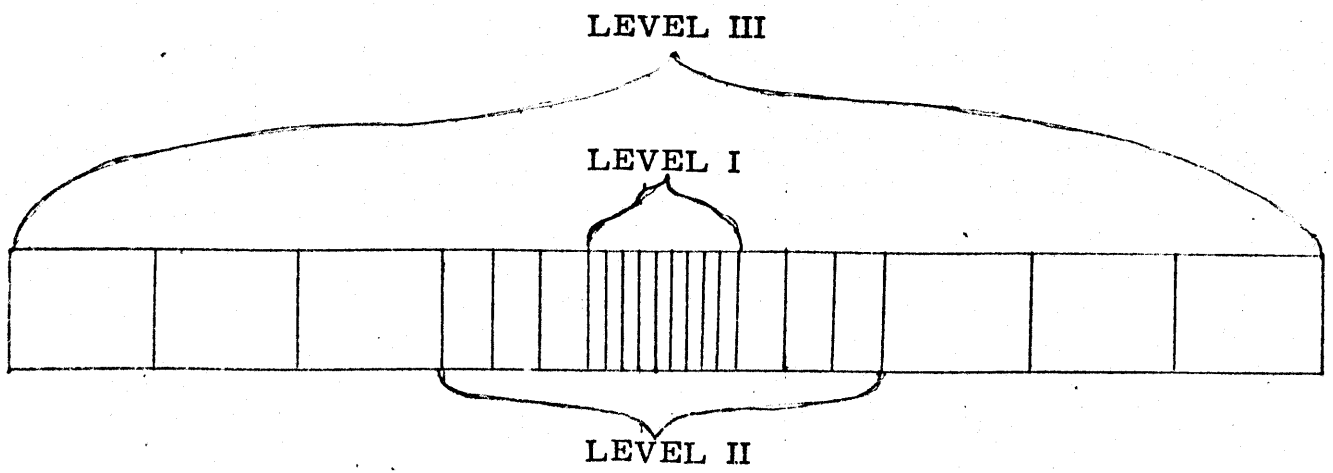

Fig. 4.0

4.1 Application to One-Dimensional Thin Sheet

The accuracy of the method can be tested fairly easily and elaborately in the case of conductivity varying only in one direction in the surface sheet, as 'true model' solutions, using a uniform spacing throughout equal to the spacing in the lowest level of the 'imbedding' method, can be computed with relative ease in this case. The method is tested for two types of source field variations: (1) quasi-uniform source fields; (2) a source field varying in both the x and y directions. The reason for using the second type of source field will be made clear a little later.

Consider a two-level zoning with conductivities as shown in Fig. 4.1-1 (step 1). We are interested in finding the fields at the point having conductivity σ_5. The measurement point (having conductivity σ_5) is placed in the middle of the zone that represents the true variations in the properties of the medium. There are two spacing distances corresponding to the two levels. d_1, the spacing for the lower level, is one-third the spacing for the higher level d_2. At the second level, the inner region can be replaced by three equivalent zones of length d_2. Therefore each of the three zones in level 1 has to be replaced by a single zone of level 2. This equivalent zone in the second level will be a tensor - in this case a diagonal tensor with different parallel conductivity (σ_{yy}) and perpendicular conductivity (σ_{xx}).

Therefore the first step is to calculate the average properties (σ_{xx}, σ_{yy}) for each of the three equivalent zones. These are determined by solving equations (2.2.7) for each of these and calculating

$\sigma_{xx} = \left| \sum_{i=1}^{3} J_{xi} / \sum_{i=1}^{3} E_{xi} \right|$ and $\sigma_{yy} = \left| \sum_{i=1}^{3} J_{yi} / \sum_{i=1}^{3} E_{yi} \right|$, from which we get

$$\bar{\bar{\sigma}} = \begin{vmatrix} \sigma_{xx} & 0 \\ 0 & \sigma_{yy} \end{vmatrix}$$

Because there is some resistive coupling with the mantle, these averages are slightly different from a series and parallel average. After these are determined we have all the information to compute fields in the entire region shown in step 2. Solving equations (2.2.7) (with $J_x = \sigma_{xx} E_x$ and $J_y = \sigma_{yy} E_y$), the fields in all the zones at the second level can be computed.

Having determined the fields in level 2, we replace the three equivalent zones in the middle by the inner region representing the true properties of the medium (with spacing d_1). At the spacing each of the outer zones can be divided into three zones ($d_2 = 3d_1$). Now the fields in the inner zone are recalculated, assuming the entire region of interest to be subdivided with spacing d_1, with the zones outside the inner region having average E values determined in step 2 (step 4). While computing the solution in the inner region, part of the convolution (Y * E) involving E in the outer region is known and so moved to the right-hand side of the simultaneous equations. The final result therefore appears as in step 5: fields being determined at close spacings around the point of measurement, fields farther away being determined at larger spacings.

The thin sheet model used in testing is shown in Fig. 4.1-2 for both methods of computation. The two solutions are compared for four different models of the layered medium below the thin sheet. These results are summarized in Figs. 4.1-3 to 4.1-10 and Tables 4.1-1 and 4.1-2. As can be seen from these figures and tables, the agreement between the two results is almost perfect.

Such elaborate testing is not possible for two-dimensional variation in the conductivity of the thin sheet as it is very difficult or almost impossible to calculate true model solutions using a uniform spacing equal to that of the lowest level in the imbedding method. When the source field varies in both the x and y directions, even for one-dimensional conductivity variation in the thin sheet, we would get coupled equations (i.e. H_x incidence field excites both E_x and E_y and, similarly, H_y incidence excites both E_x and E_y) just as in two-dimensional conductivity variation in the thin sheet. Therefore it would be instructive to compare the solutions obtained with the two methods for a source field varying in both the x and y directions.

Imbedding for this case would be only slightly different from that for the previous case. First of all, source field variation in the y direction enters calculations only indirectly through the operators $[Y^+]$ and $[Y^-]$ so that one need not calculate the solutions for different y positions directly, as the medium is uniform along the y direction and y dependence of the solution can be expressed as $e^{ik_y y}$. However, while finding the average properties of the

medium, uniform source fields are employed, i.e. σ_{xx} and σ_{yy} are determined using decoupled equations. Source field is specified at spacings equal to the spacing at the lowest level (d_1). Source fields at higher levels are computed from these by averaging over appropriate distances. In our example the source field at the first point (represented by the strip of conductivity σ_1') would be the average of the first nine points, at the second point, the average of the next nine points, and so on. The source field for the second level would be the middle nine points (at spacings d_1). Solutions were also obtained using uniform spacing throughout. These results are summarized in Figs. 4.1-11 to 4.1-22 and Tables 4.1-3 to 4.1-6. As can be seen, the two results are in reasonably good agreement, especially at the point of measurement. The only appreciable errors occur at the transition between zones of different scale lengths, which is in the buffer region and not expected to be accurate.

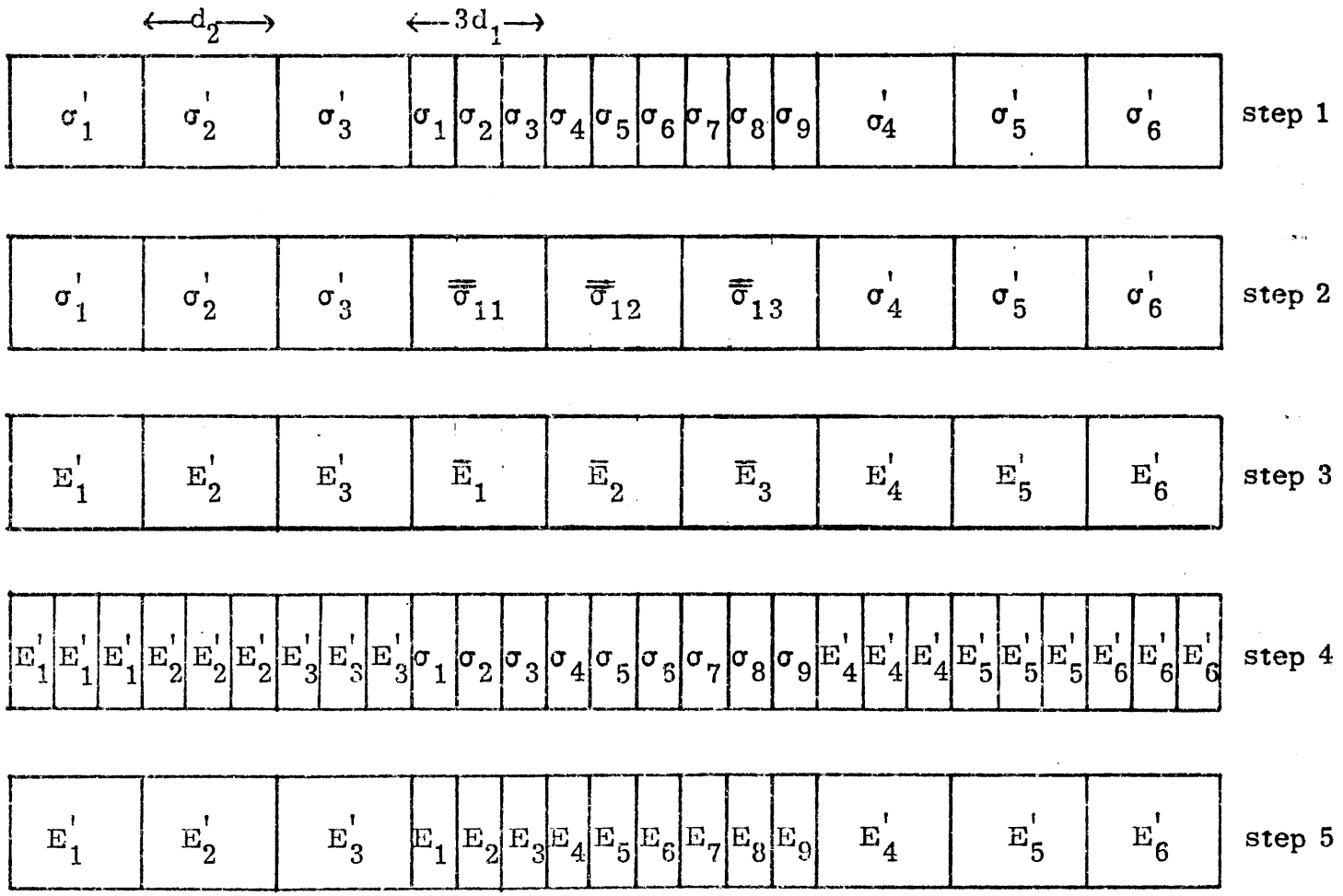
$\leftarrow d_2 \rightarrow$
$\leftarrow 3d_1 \rightarrow$
σ'_1 σ'_2 σ'_3 σ_1 σ_2 σ_3 σ_4 σ_5 σ_6 σ_7 σ_8 σ_9 σ'_4 σ'_5 σ'_6
step 1
σ'_1 σ'_2 σ'_3 $\overline{\overline{\sigma}}_{11}$ $\overline{\overline{\sigma}}_{12}$ $\overline{\overline{\sigma}}_{13}$ σ'_4 σ'_5 σ'_6
step 2
E'_1 E'_2 E'_3 $\overline{\overline{E}}_1$ $\overline{\overline{E}}_2$ $\overline{\overline{E}}_3$ E'_4 E'_5 E'_6
step 3
E'_1 E'_1 E'_1 E'_2 E'_2 E'_2 E'_3 E'_3 E'_3 σ_1 σ_2 σ_3 σ_4 σ_5 σ_6 σ_7 σ_8 σ_9 E'_4 E'_4 E'_4 E'_5 E'_5 E'_5 E'_6 E'_6 E'_6
step 4
E'_1 E'_2 E'_3 E_1 E_2 E_3 E_4 E_5 E_6 E_7 E_8 E_9 E'_4 E'_5 E'_6
step 5

Fig. 4.1-1

Imbedding Model

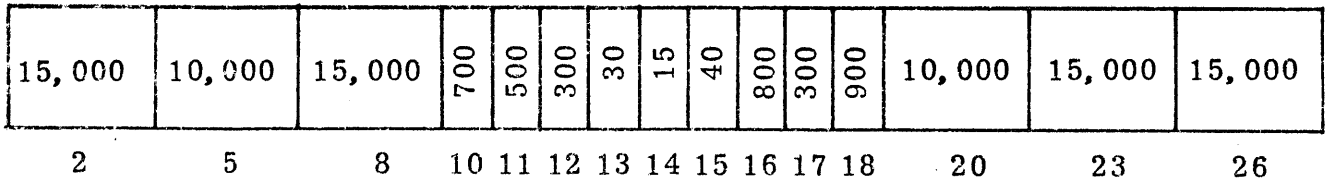

Uniform Spacing Model

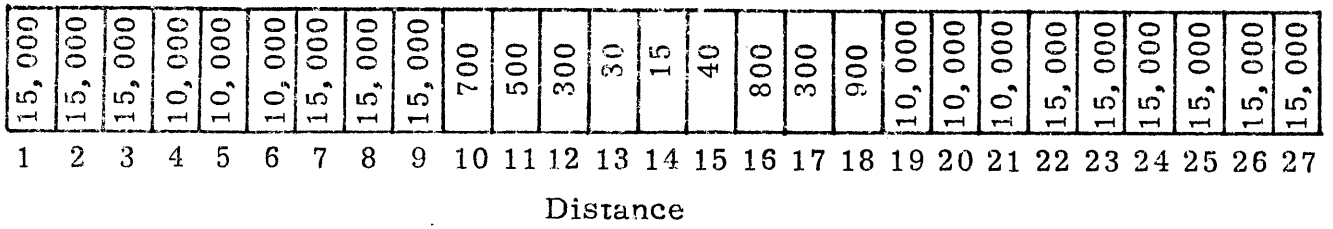

Fig. 4.1-2 Conductance of the Thin Sheet (in mhos)

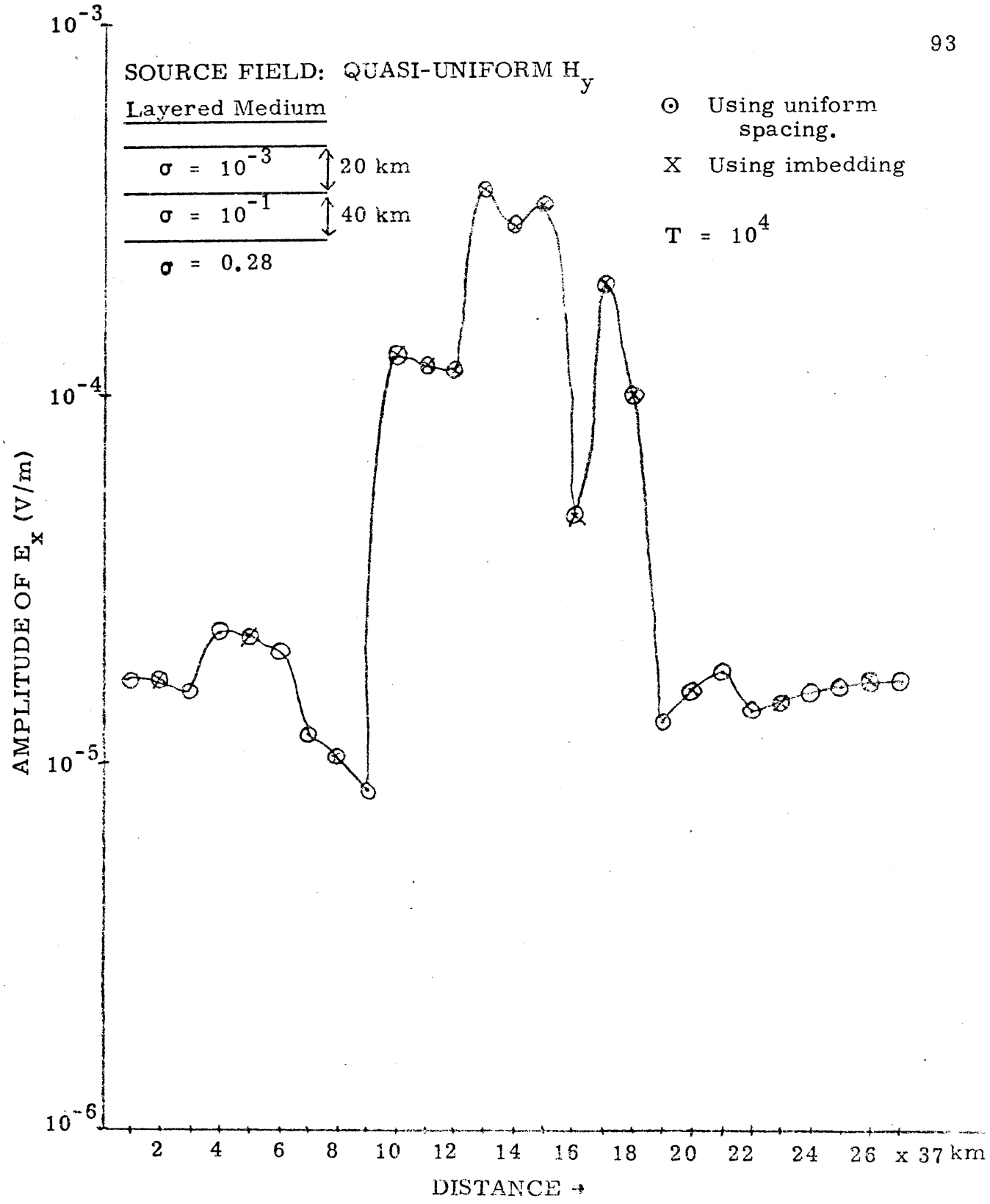

A comparison of the two solutions for the thin sheet conductance given in Fig. 4.1-2. Phases of the two solutions are given in Fig. 4.1-4.

Fig. 4.1-3

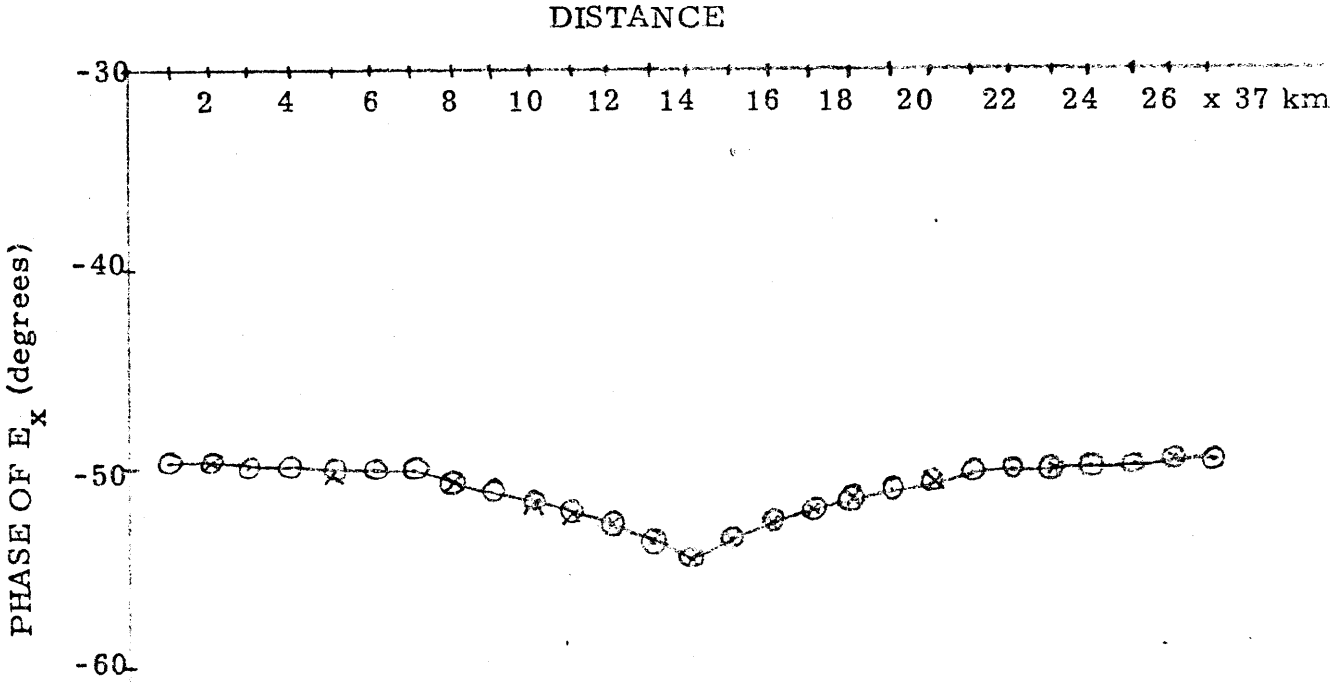

Refer to Fig. 4.1-3 for details

Fig. 4.1-4

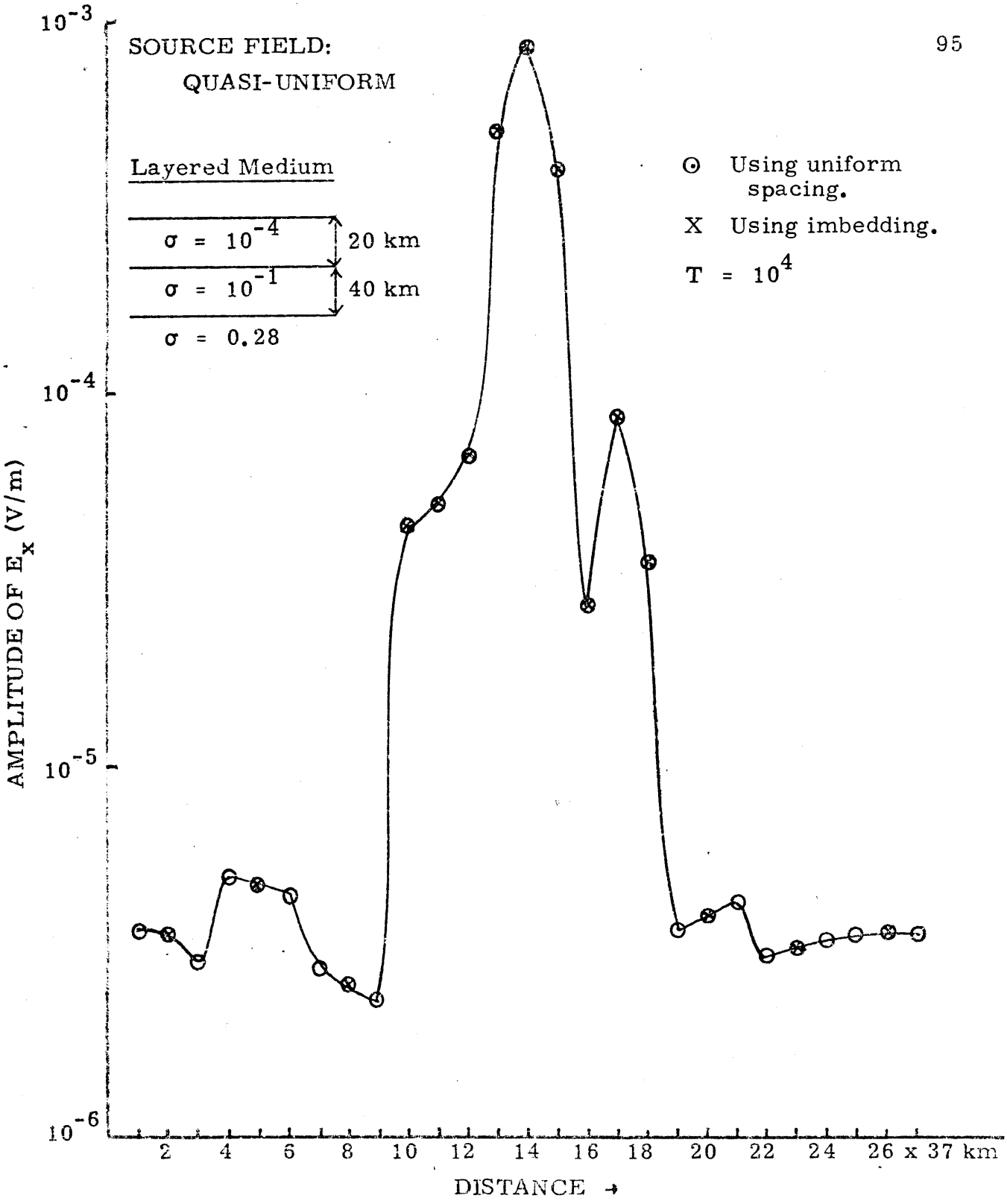

Refer to Fig. 4.1-2 for thin sheet conductance used in this calculation.
Phases of the two solutions are given in Fig. 4.1-6

Fig. 4.1-5

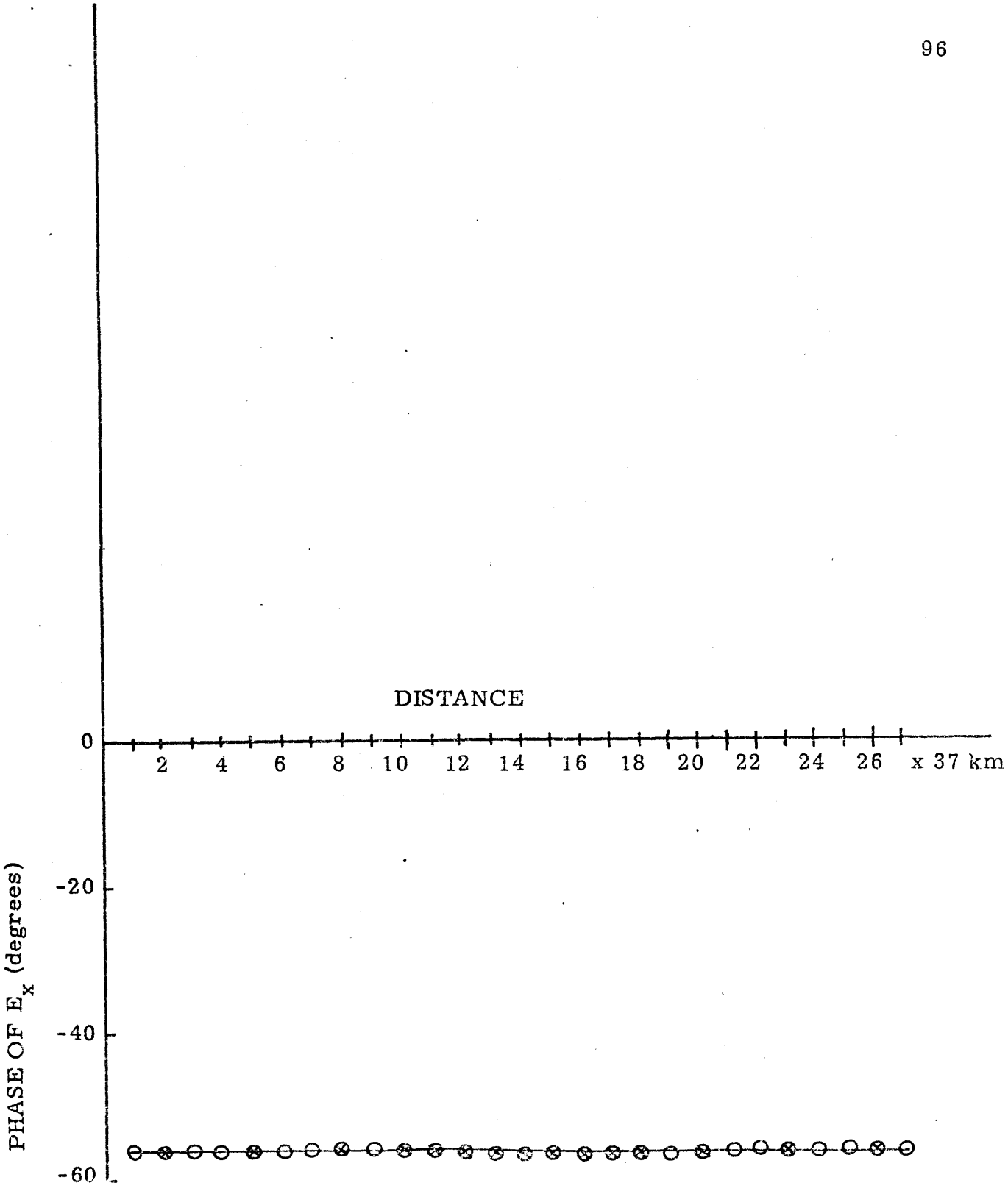

Refer to Fig. 4.1-5 for details.

Fig. 4.1-6

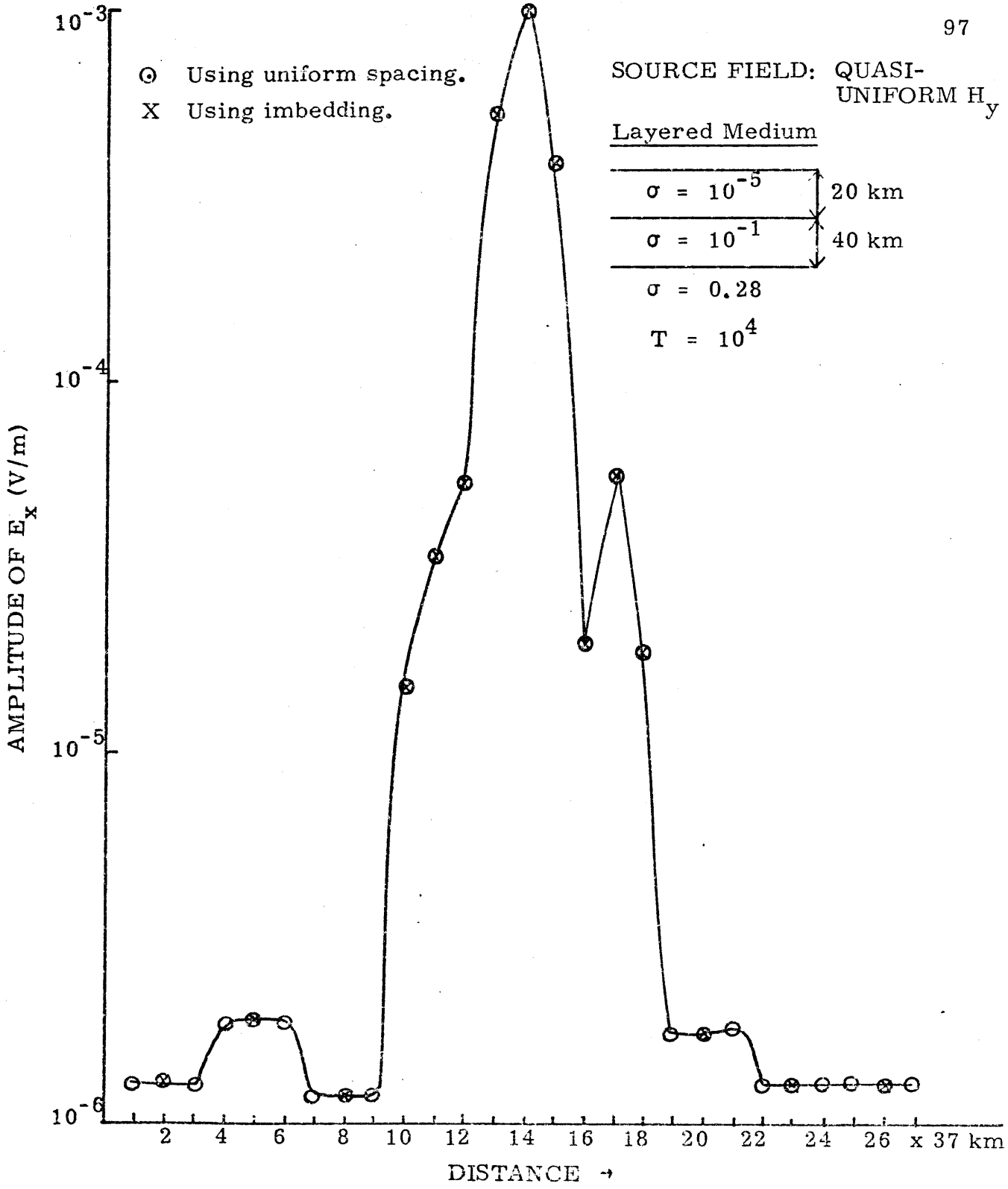

Refer to Fig. 4.1-2 for thin sheet conductance used in this calculation. The two solutions give a constant phase of -59.3°.

Fig. 4.1-7

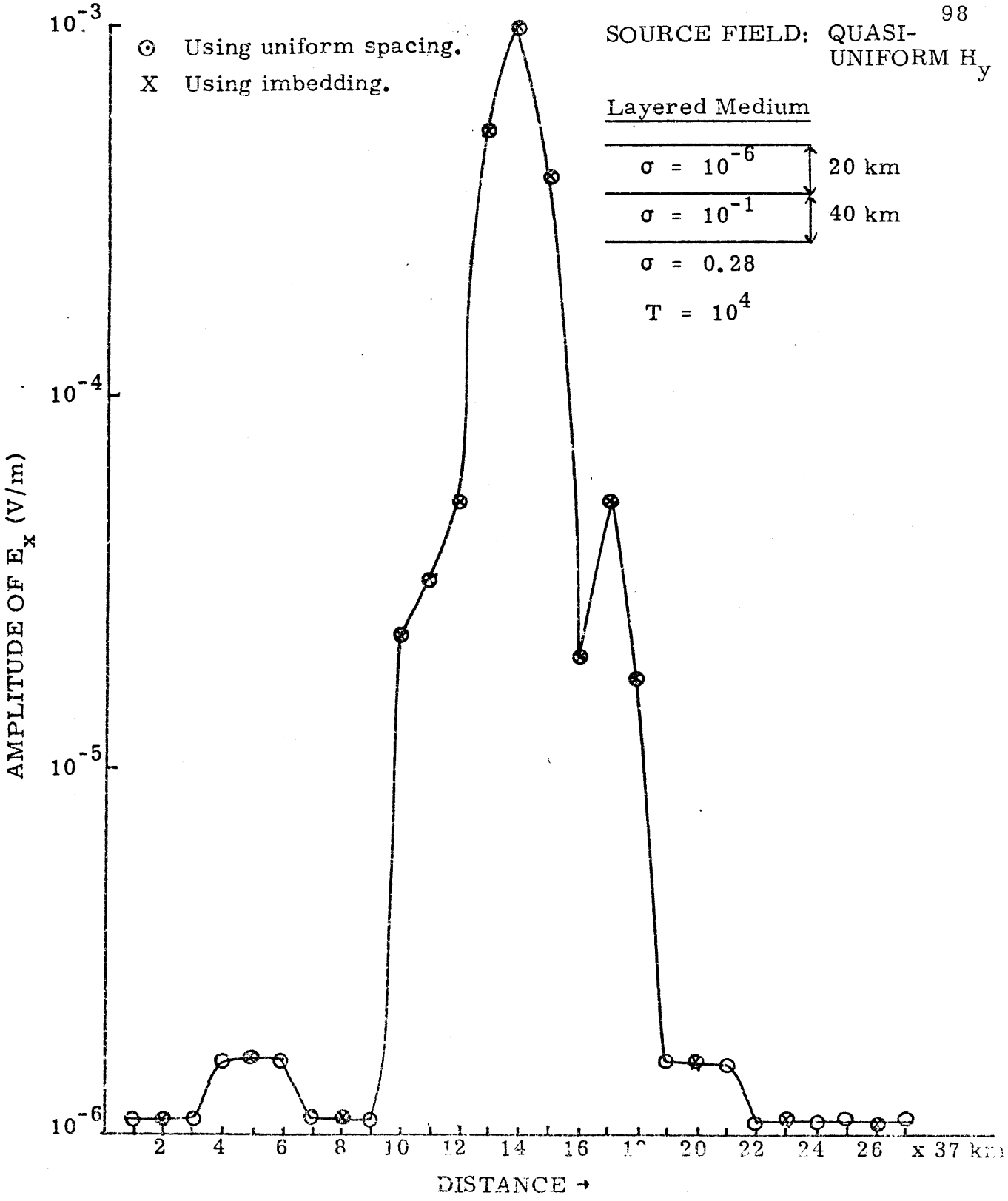

Refer to Fig. 4.1-2 for thin sheet conductance used. The two solutions give a constant phase of -59.4°.

Fig. 4.1-8

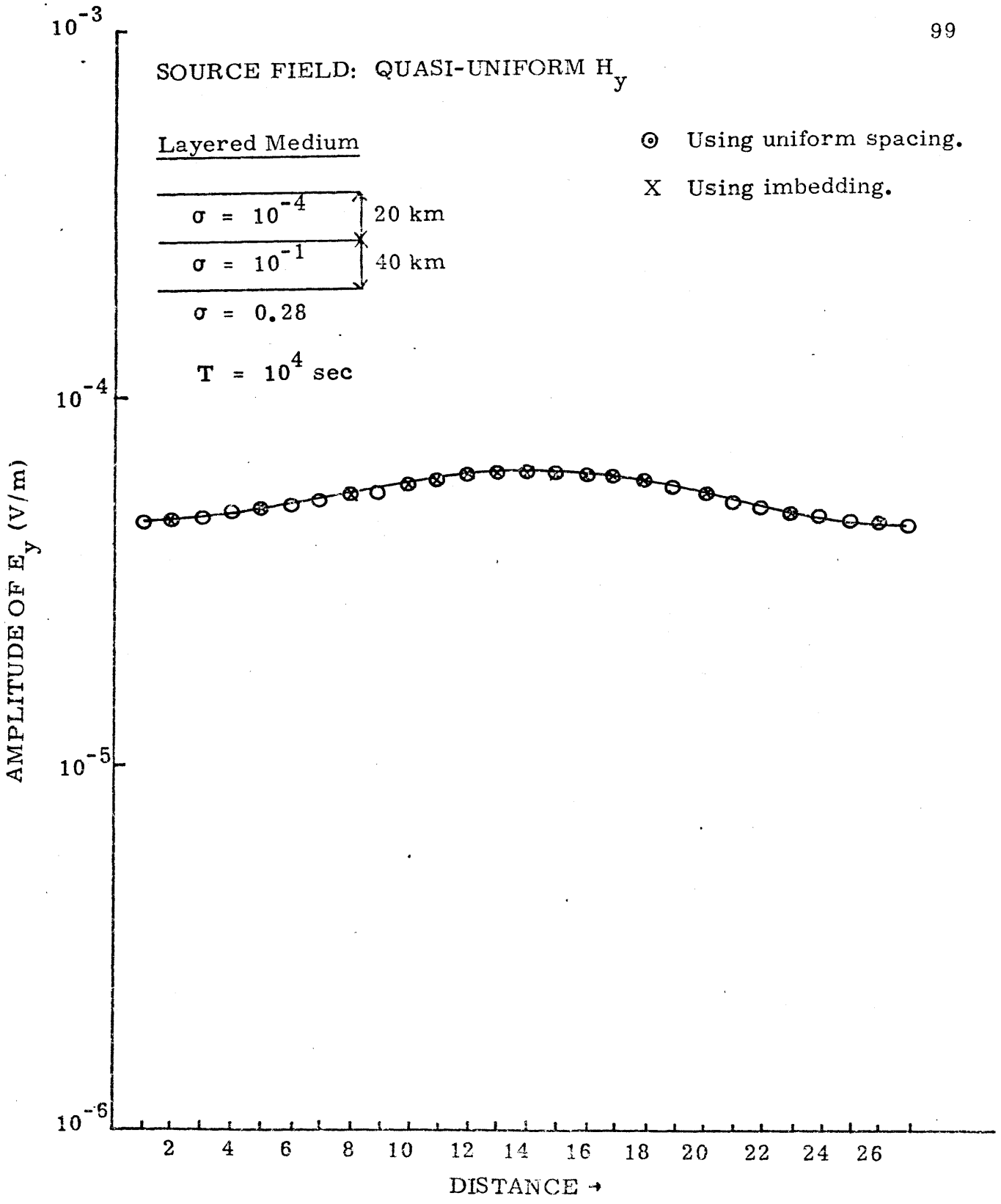

Refer to Fig. 4.1-2 for thin sheet conductance used in this study. Phases of the two solutions are given in Fig. 4.1-10.

Fig. 4.1-9

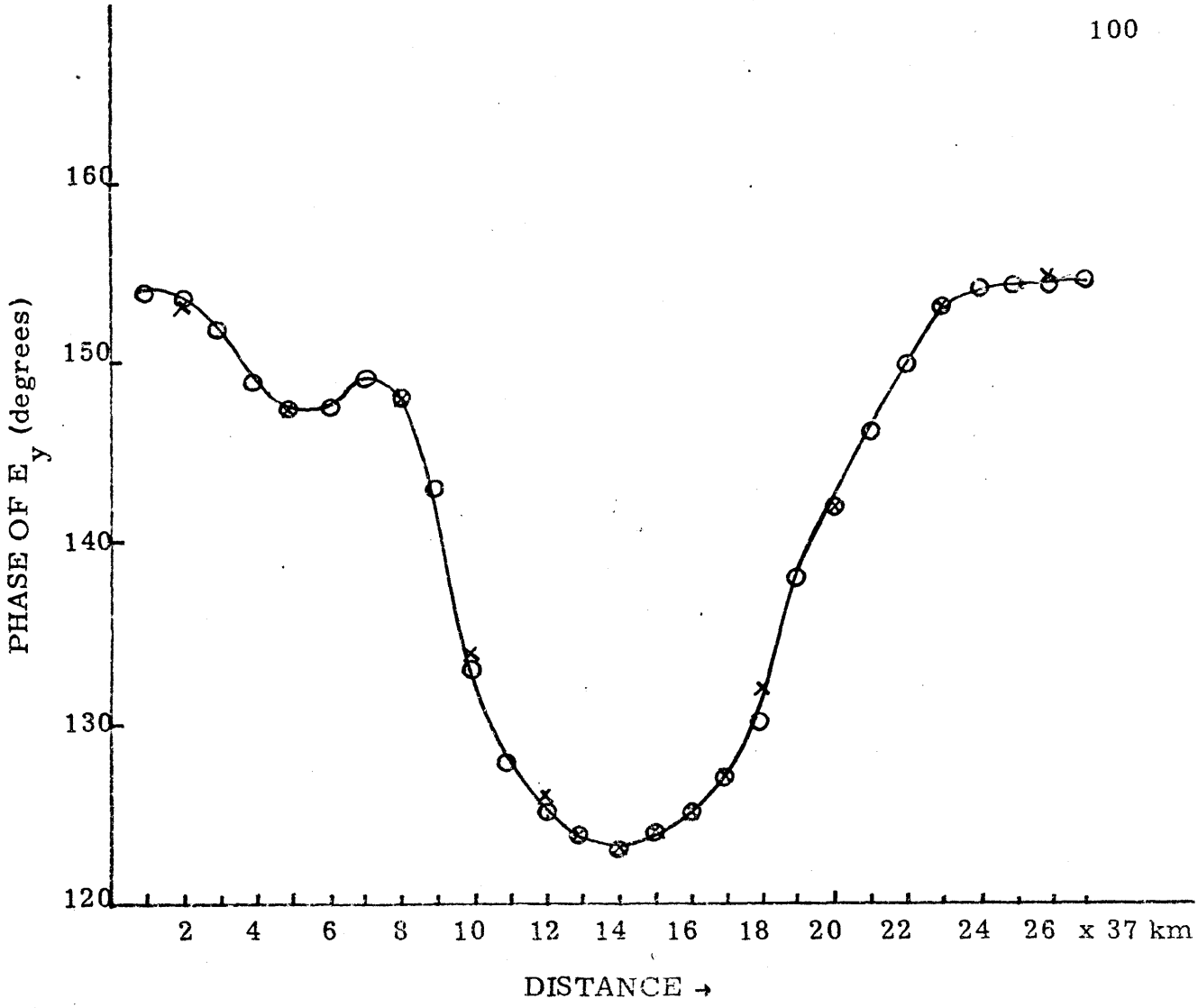

Refer to Fig. 4.1-9 for details.

Fig. 4.1-10

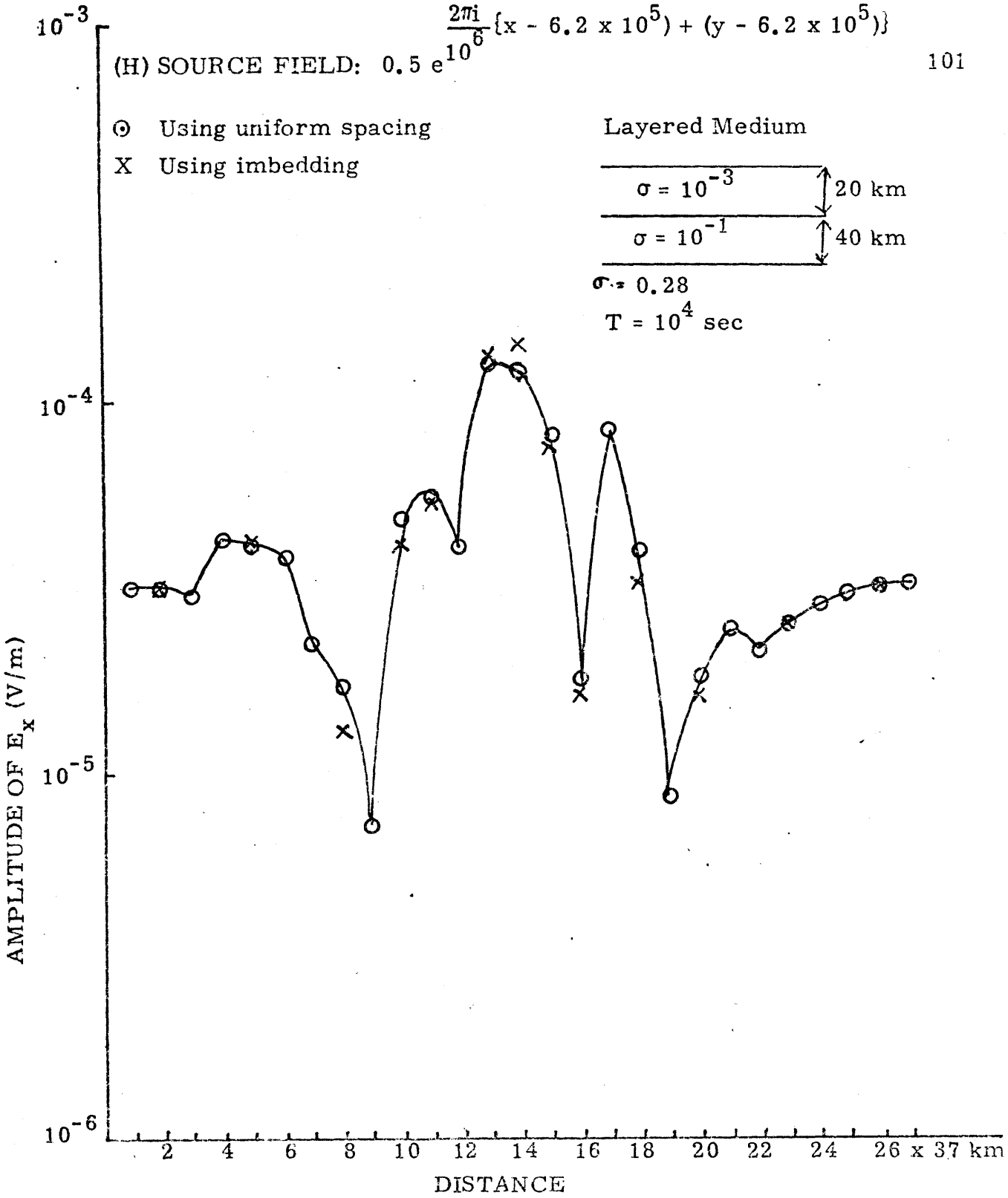

Refer to Fig. 4.1-2 for thin sheet model Phases for the two cases are plotted in Fig. 4.1-12.

Fig. 4.1-11

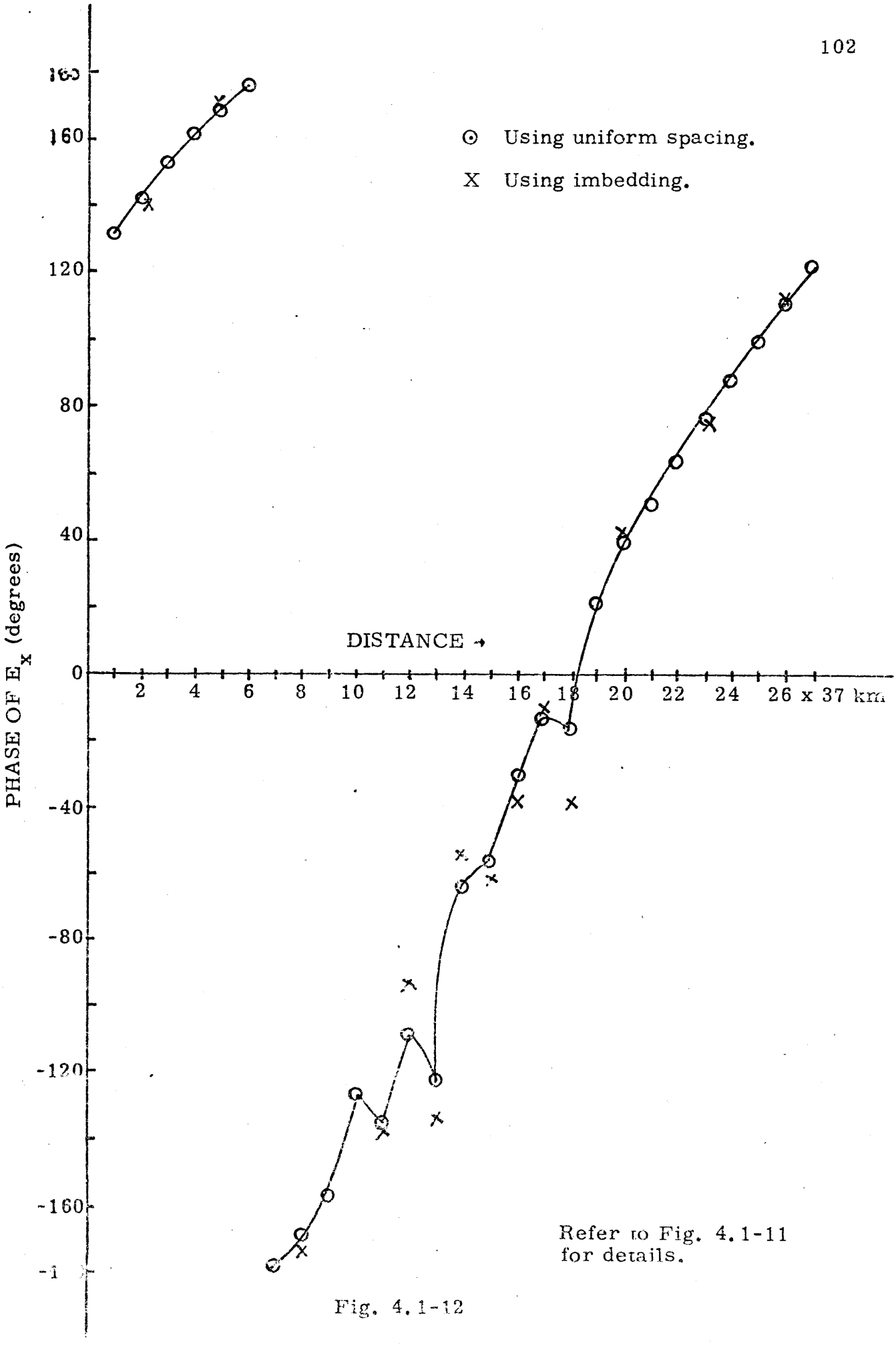

Refer to Fig. 4.1-11 for details.

Fig. 4.1-12

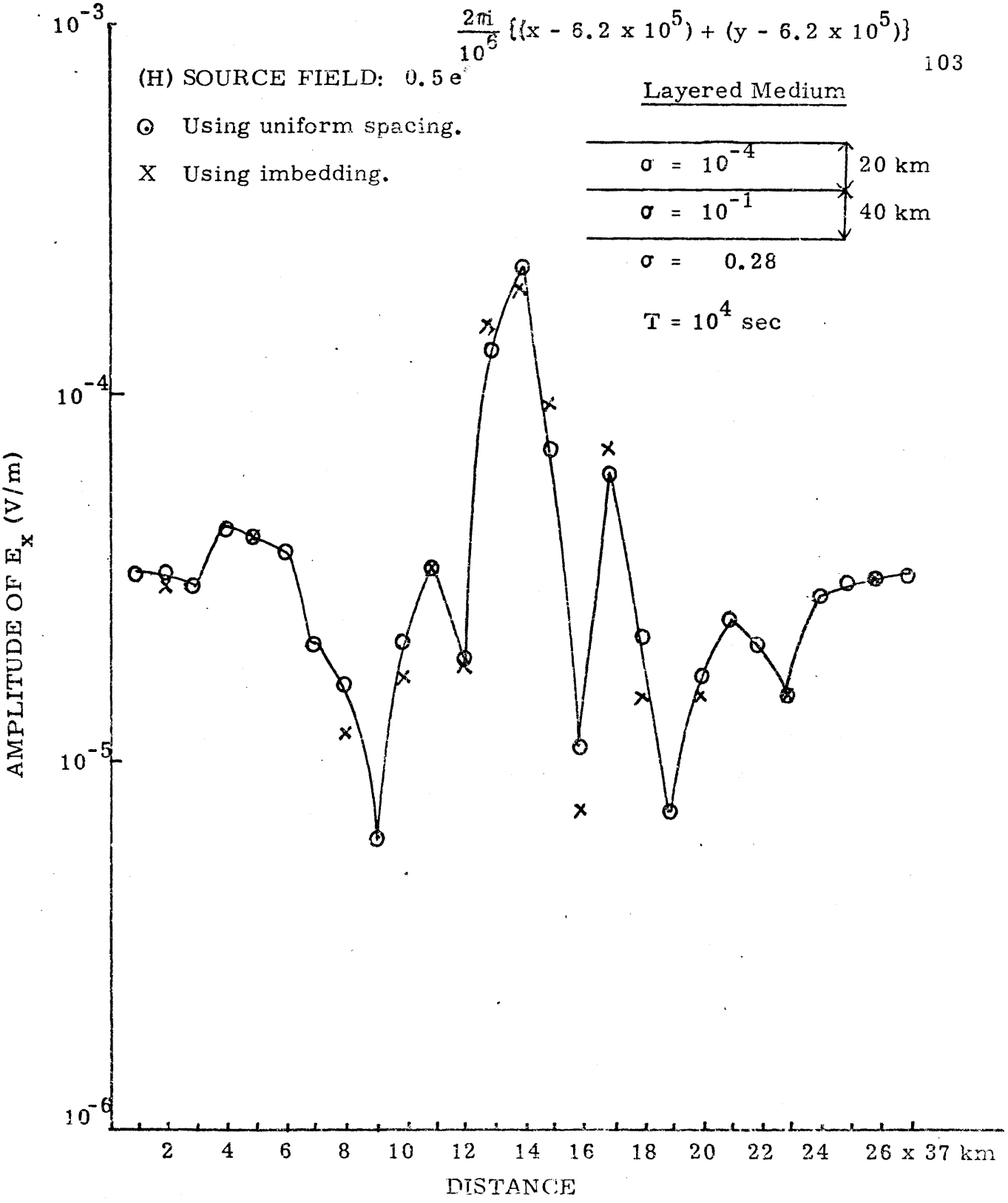

Refer to Fig. 4.1-2 for thin sheet model. Phases for the two cases are plotted in Fig. 4.1-14.

Fig. 4.1-13

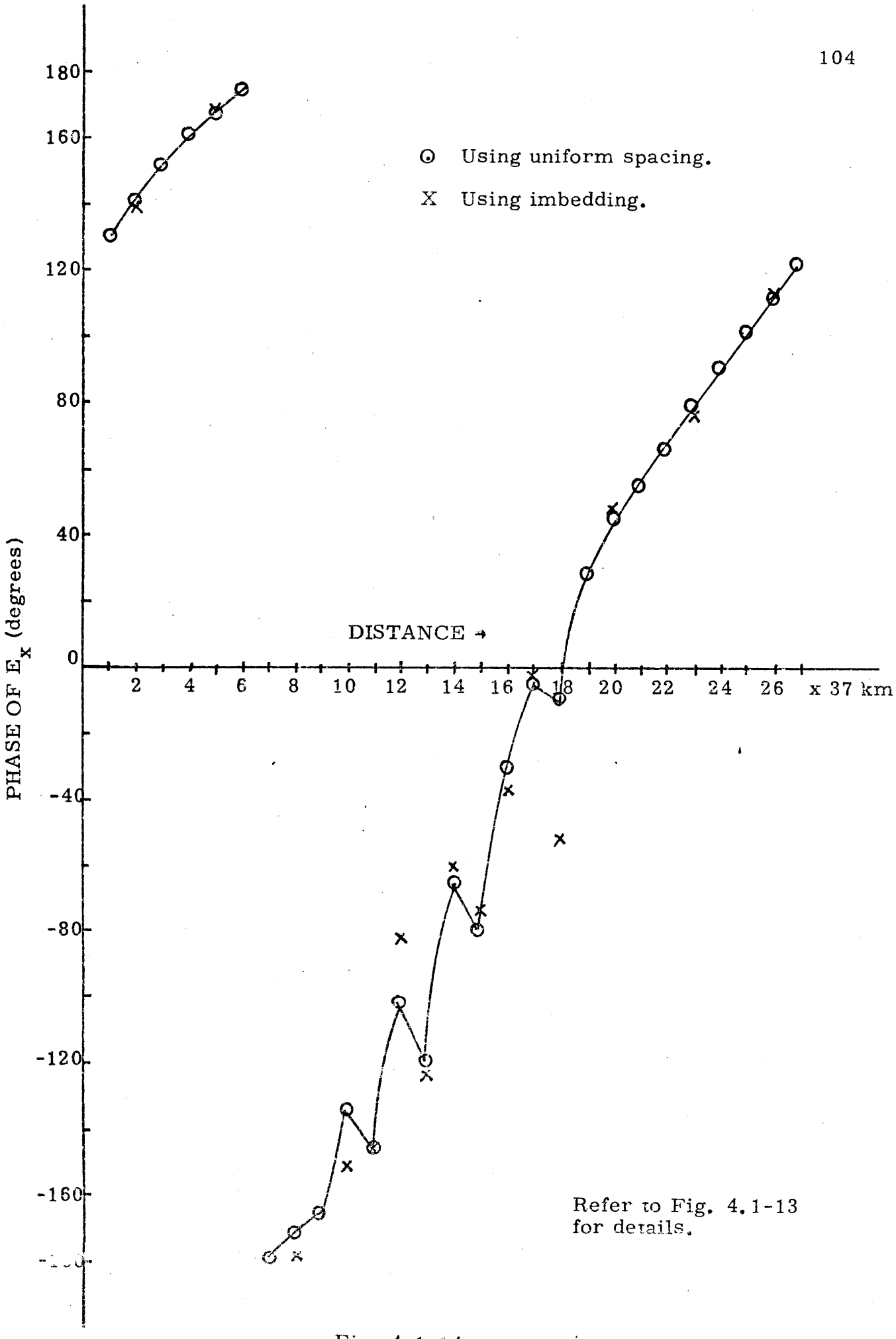
⊙ Using uniform spacing.
X Using imbedding.
PHASE OF E_x (degrees)
DISTANCE →
180
160
120
80
40
0
-40
-80
-120
-160
2
4
6
8
10
12
14
16
18
20
22
24
26
x 37 km
Refer to Fig. 4.1-13 for details.

Fig. 4.1-14

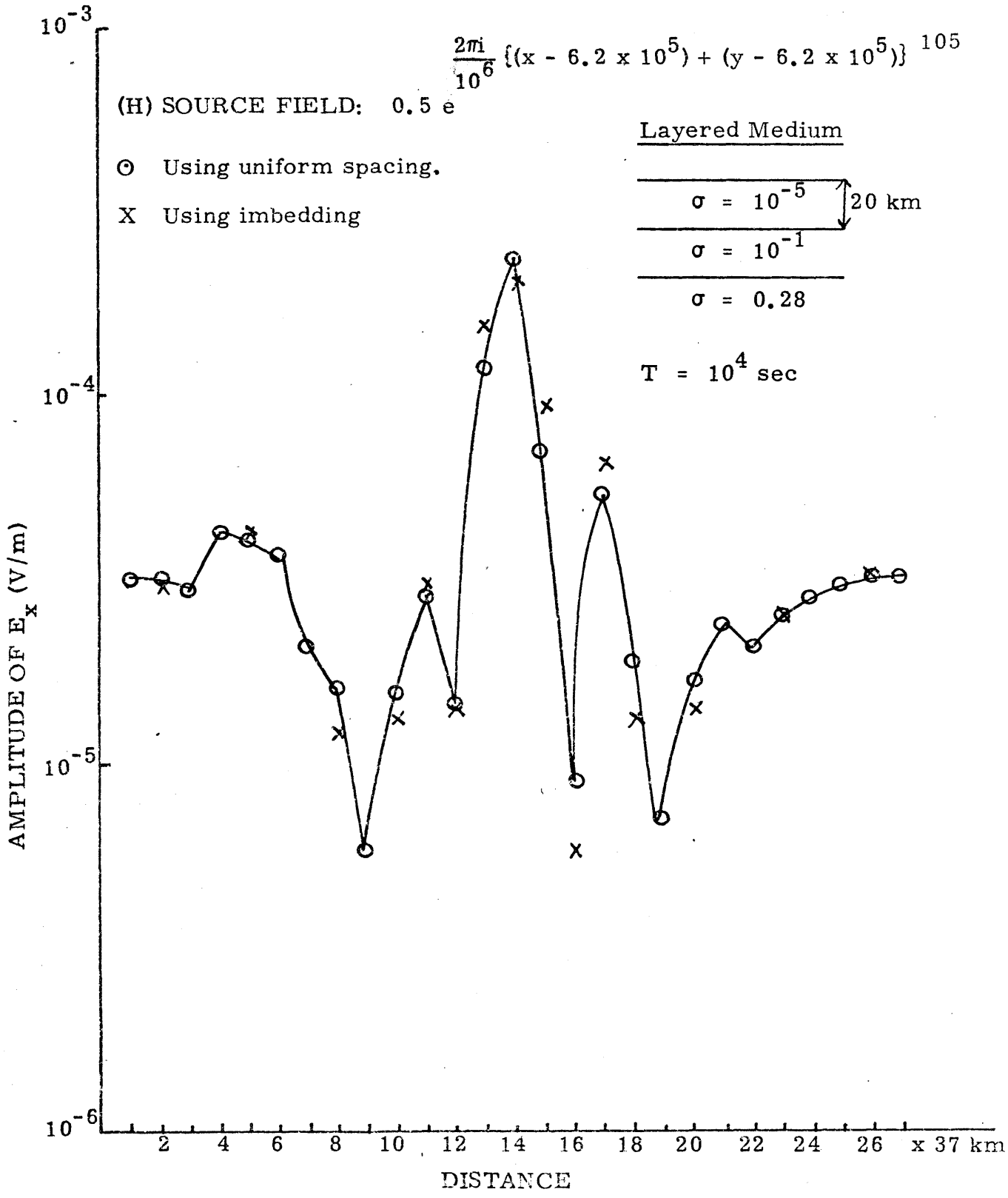

Refer to Fig. 4.1-2 for thin sheet model. Phases for the two cases are plotted in Fig. 4.1-16.

Fig. 4.1-15

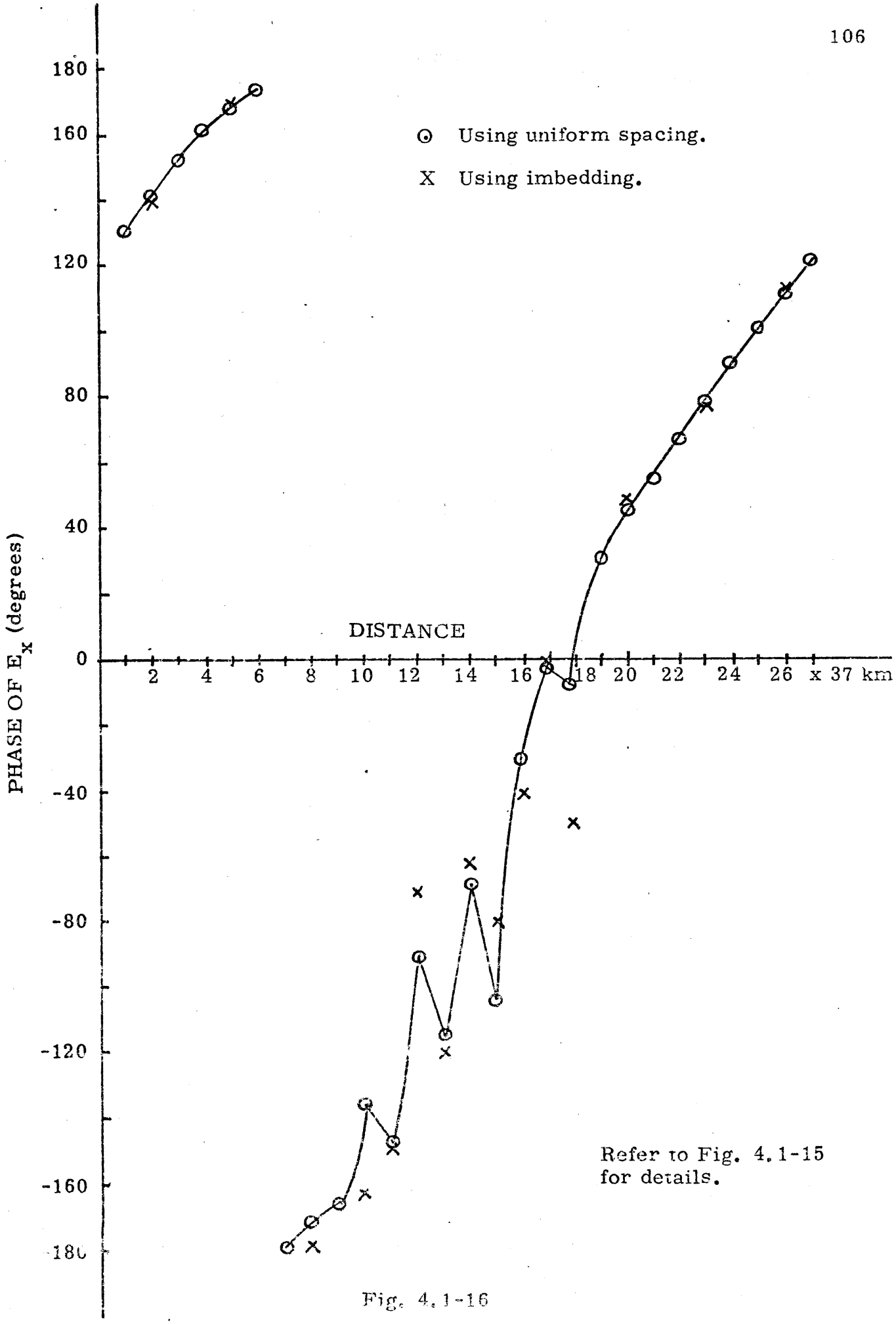

Refer to Fig. 4.1-15 for details.

Fig. 4.1-16

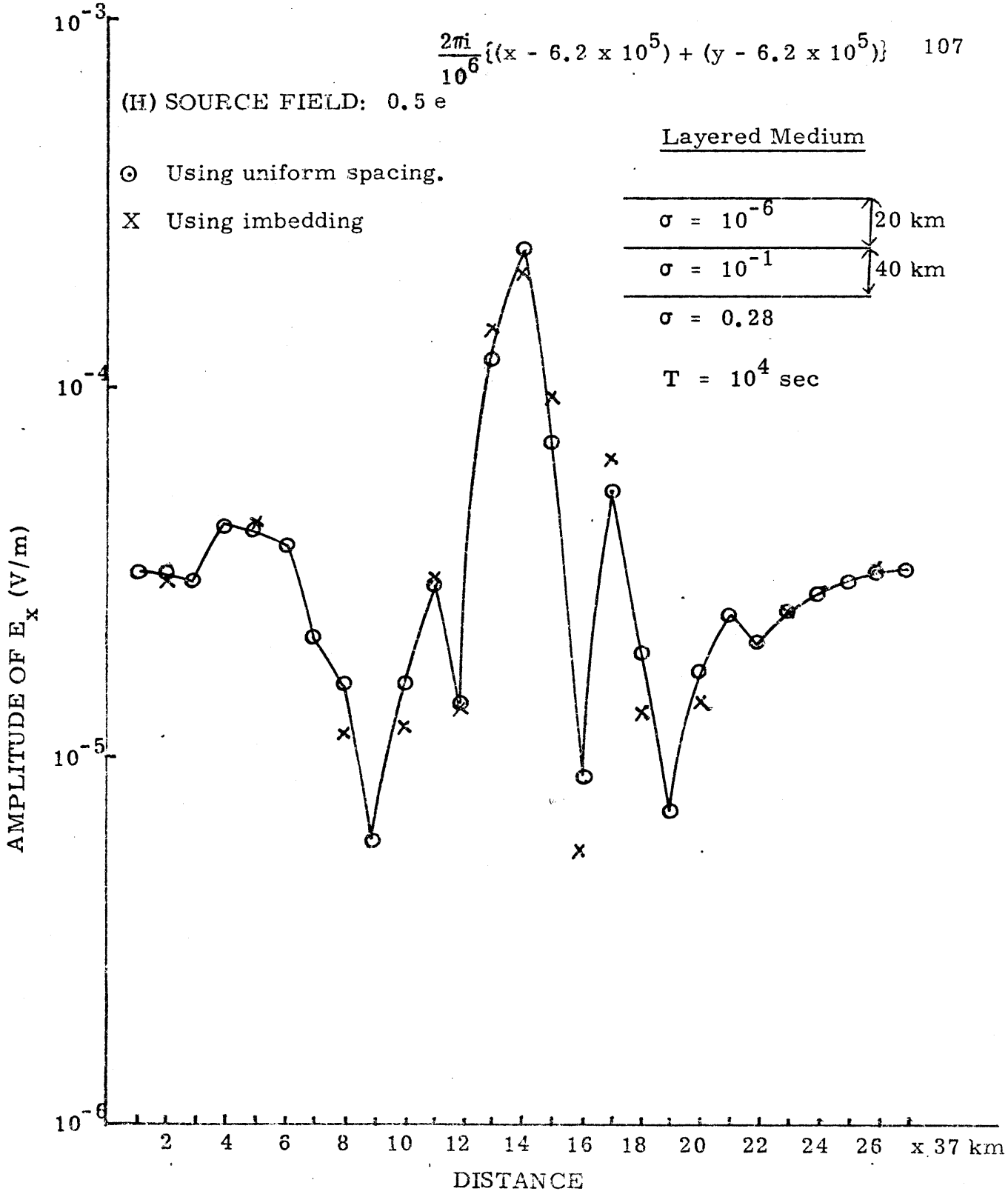

Refer to Fig. 4.1-2 for thin sheet model. Phases for the two cases are plotted in Fig. 4.1-18.

Fig. 4.1-17

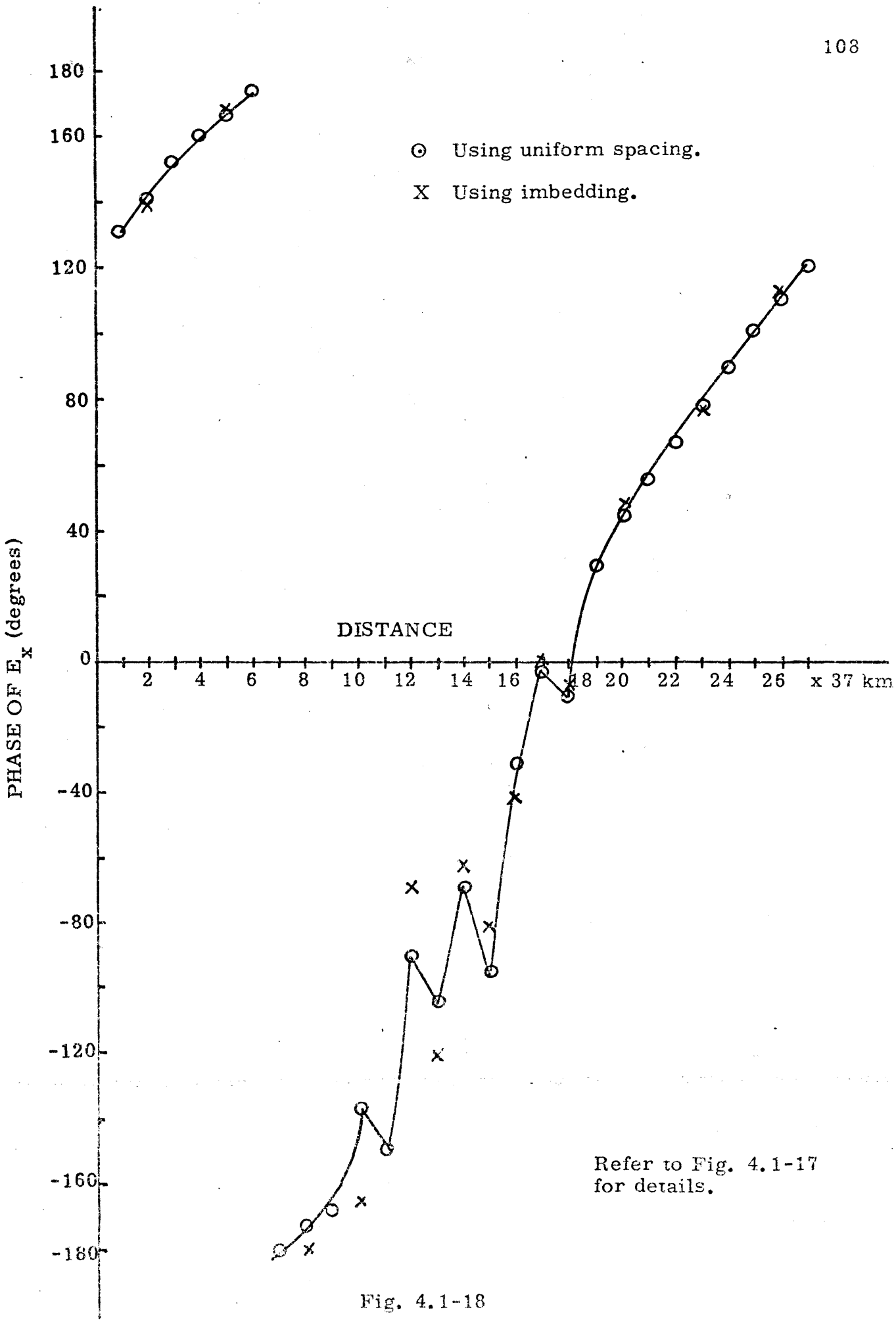

Refer to Fig. 4.1-17 for details.

Fig. 4.1-18

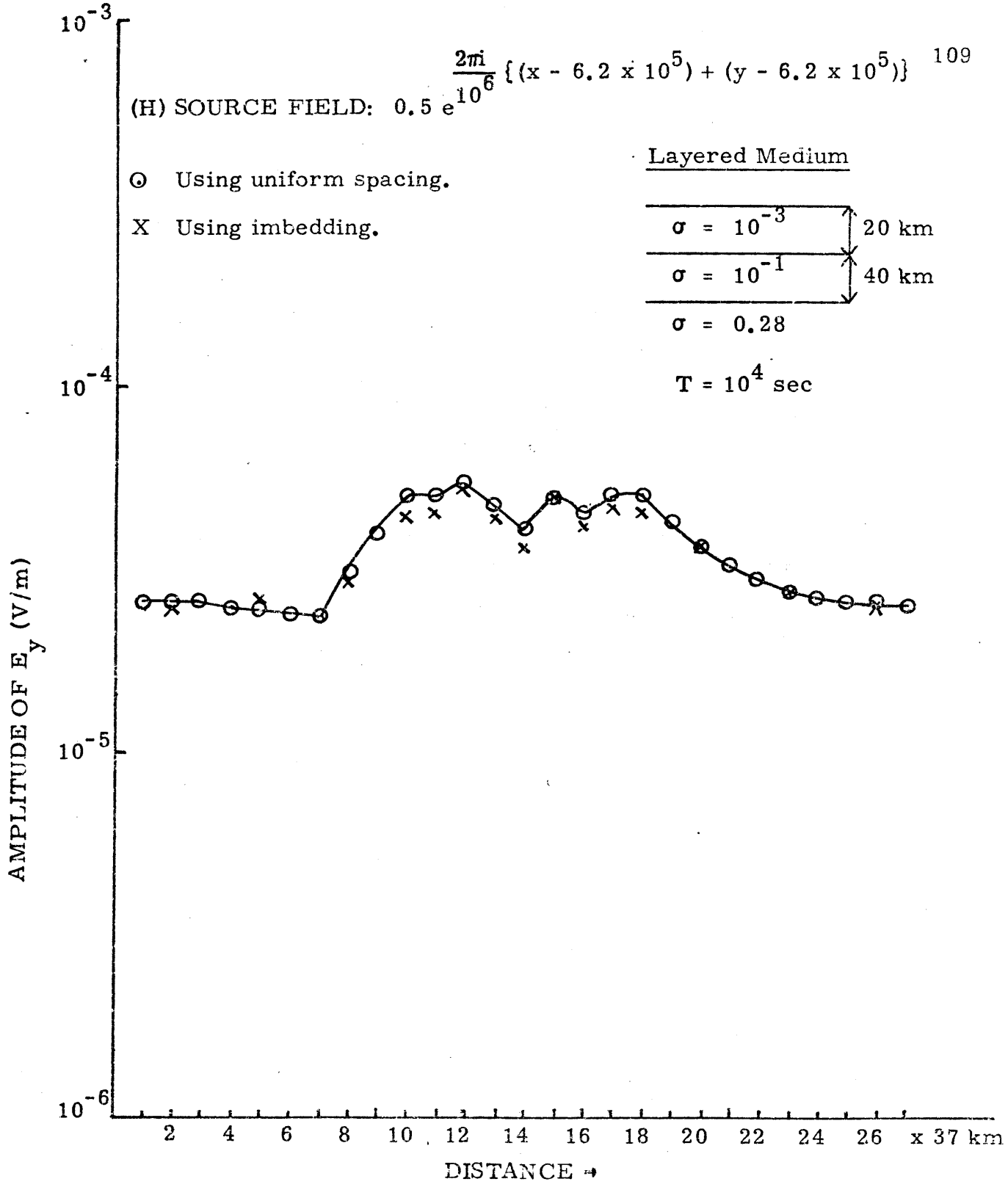

Refer to Fig. 4.1-2 for thin sheet conductance used in these calculations. Phases of the two solutions are given in Fig. 4.1-20.

Fig. 4.1-19

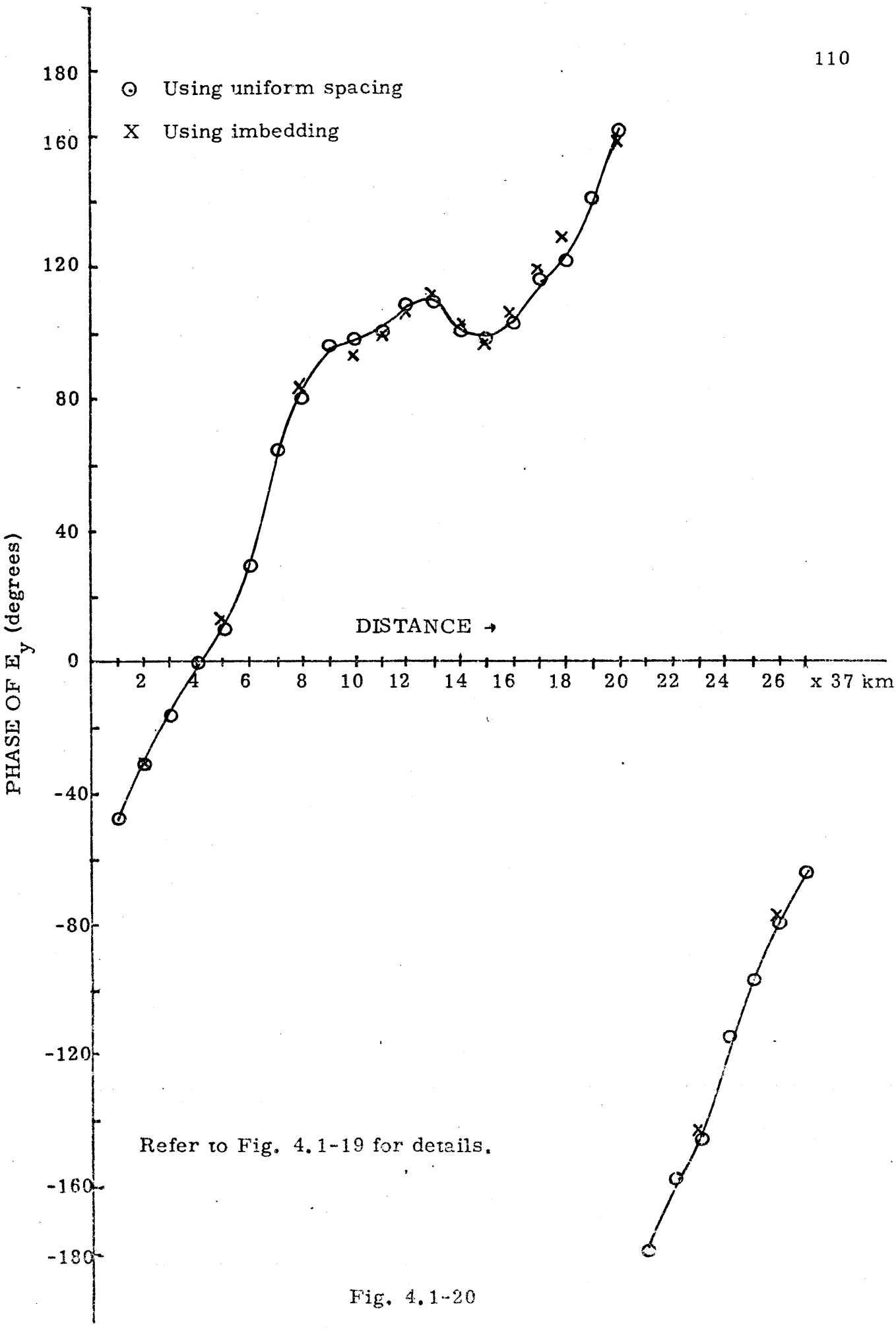
⊙ Using uniform spacing
X Using imbedding
PHASE OF E_y (degrees)
180
160
120
80
40
0
-40
-80
-120
-160
-180
DISTANCE →
2
4
6
8
10
12
14
16
18
20
22
24
26
x 37 km
Refer to Fig. 4.1-19 for details.

Fig. 4.1-20

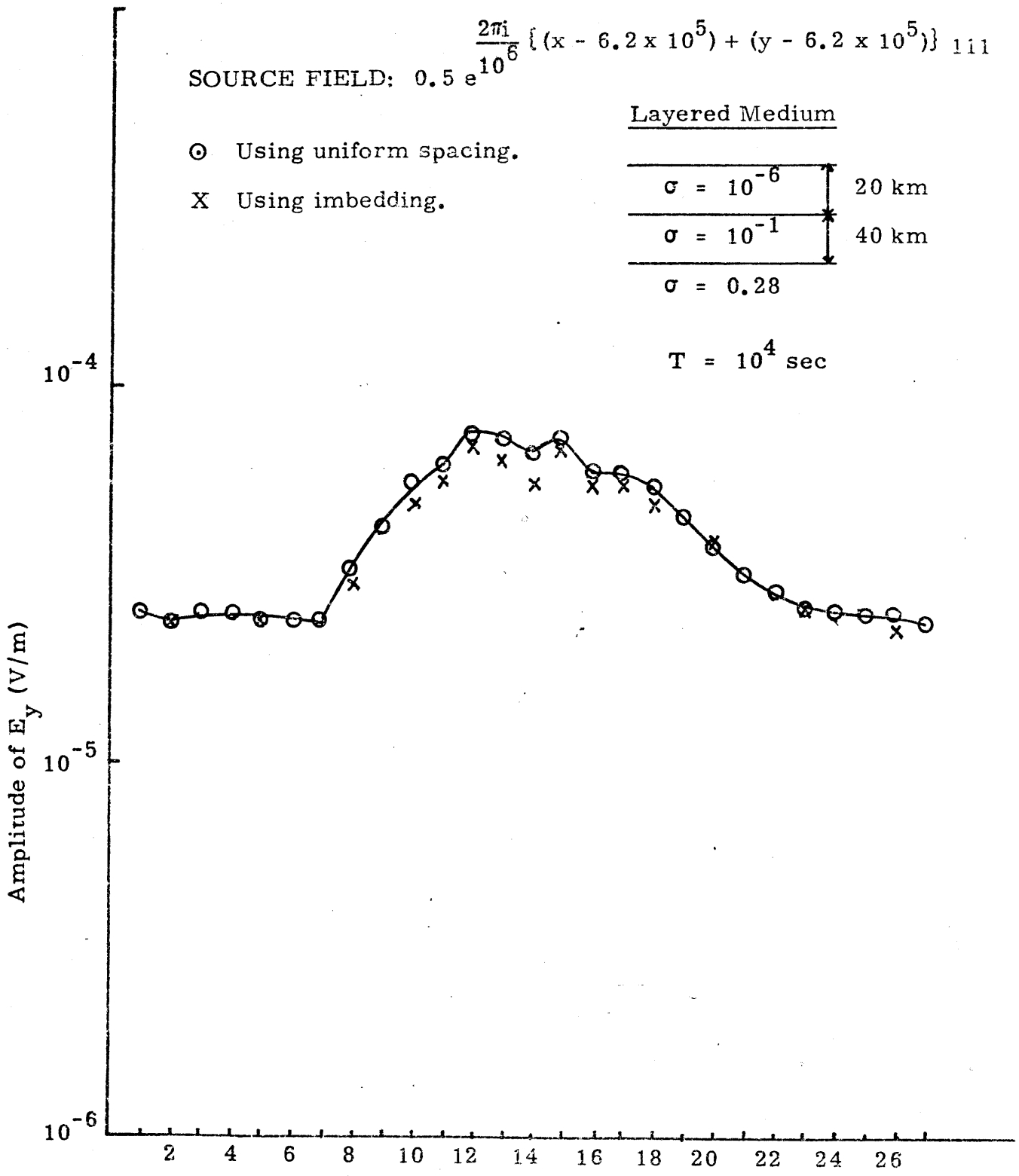

Refer to Fig. 4.1-2 for thin sheet conductance used here. Phases of the two solutions are given in Fig. 4.1-22.

Fig. 4.1-21

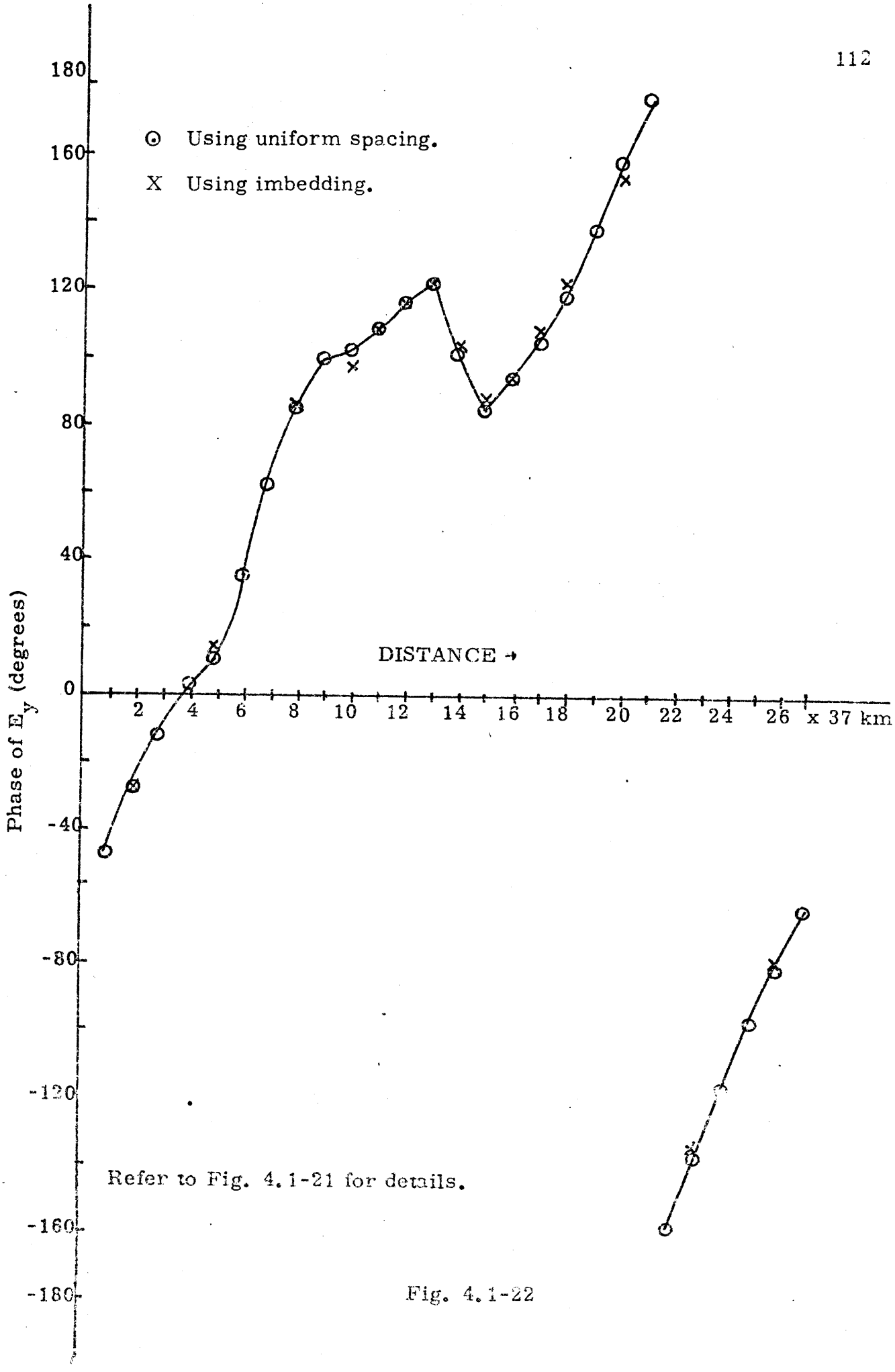

Refer to Fig. 4.1-21 for details.

Fig. 4.1-22

TABLE 4.1-1

Distance x 37 km	Amplitude of E_y (V/m) Using		Phase of E_y (deg) Using		Amplitude of H_x (At/m) Using		Phase of H_x (deg) Using	
	Imbedding	Uniform Spacing	Imbedding	Uniform Spacing	Imbedding	Uniform Spacing	Imbedding	Uniform Spacing
	$\times 10^{-4}$	$\times 10^{-4}$						
2	.4708	.4709	153.2	153.5	1.092	1.094	-0.2	-0.2
[illegible]	.5027	.5030	147.8	147.5	1.007	1.005	0.3	0.4
8	.5337	.5355	147.7	148.1	1.151	1.155	-4.7	-6.7
10	.5645	.5817	134.4	132.6	.8485	.8486	5.0	4.7
11	.5949	.6074	128.3	127.6	.8348	.8400	4.8	4.4
12	.6147	.6254	125.6	125.1	.8334	.8386	4.3	4.0
13	.6276	.6370	124.0	123.7	.8295	.8353	4.3	4.0
14	.6328	.6419	123.5	123.3	.8303	.8359	4.1	3.8
15	.6313	.6406	123.9	123.6	.8307	.8363	4.1	3.8
16	.6226	.6329	125.3	124.9	.8427	.8473	3.1	2.9
17	.6070	.6192	127.2	126.5	.8336	.8383	4.6	4.3
18	.5822	.5988	131.9	130.3	.8495	.8499	4.2	3.9
20	.5514	.5522	142.0	142.3	1.032	1.033	-3.2	-3.2
23	.4888	.4896	152.7	152.7	1.117	1.117	-1.2	-1.2
26	.4634	.4644	154.6	154.4	1.091	1.091	-0.4	0.4

Layered Medium $\quad T = 10^4$ sec

$\sigma = 10^{-3}$ — 20 km

$\sigma = 10^{-1}$ — 40 km

$\sigma = 0.28$

Source Field: Quasi-Uniform H_x

Thin sheet model in Fig. 4.1-2

TABLE 4.1-2

Distance x 37 km	Amplitude of E_y (V/m) Using		Phase of E_y (Deg) Using		Amplitude of H_x (At/m) Using		Phase of H_x (Deg) Using	
	Imbedding	Uniform Spacing	Imbedding	Uniform Spacing	Imbedding	Uniform Spacing	Imbedding	Uniform Spacing
	$\times 10^{-4}$	$\times 10^{-4}$						
2	.4712	.4713	153.2	153.5	1.092	1.094	-0.2	-0.2
5	.5031	.5034	147.7	147.5	1.007	1.005	0.3	0.4
8	.5341	.5359	147.6	148.1	1.151	1.155	-4.7	-4.6
10	.5649	.5821	134.3	132.5	.8484	.8485	5.0	4.7
11	.5953	.6078	128.2	127.5	.8347	.8400	4.8	4.4
12	.6150	.6258	125.5	125.1	.8334	.8385	4.3	4.0
13	.6280	.6374	123.9	123.7	.8294	.8352	4.3	4.0
14	.6332	.6423	123.5	123.3	.8303	.8358	4.1	3.9
15	.6317	.6410	123.8	123.6	.8306	.8362	4.1	3.9
16	.6230	.6333	125.2	124.8	.8420	.8472	3.2	2.9
17	.6074	.6196	127.2	126.5	.8335	.8382	4.6	4.3
18	.5826	.5992	131.9	130.3	.8494	.8498	4.2	4.0
20	.5518	.5526	142.0	142.2	1.032	1.033	-3.2	-3.2
23	.4892	.4899	152.7	152.7	1.117	1.118	-1.2	-1.2
26	.4638	.4648	154.6	154.4	1.091	1.091	0.4	0.4

Layered Medium $T = 10^4$ sec

$\sigma = 10^{-6}$ — 20 km

$\sigma = 10^{-1}$ — 40 km

$\sigma = 0.28$

Source Field: Quasi-Uniform H_x

Thin sheet model in Fig. 4.1-2

TABLE 4.1-3

Distance x 37 km	Amplitude of H_x (At/m) Using		Phase of H_x (deg) Using		Amplitude of H_y (At/m) Using		Phase of H_y (deg) Using	
	Imbedding	Uniform Spacing	Imbedding	Uniform Spacing	Imbedding	Uniform Spacing	Imbedding	Uniform Spacing
2	.7075	.7231	-174.7	-174.8	0.7184	0.7432	-177.2	-177.2
5	.6673	.6713	-131.4	-131.4	0.7003	0.7012	-139.0	-138.6
8	.7790	.8029	-87.6	-88.1	0.6033	0.6296	-94.4	-96.3
10	.5976	.6099	-58.3	-58.9	0.6000	0.6047	-60.8	-61.4
11	.5904	.5996	-46.1	-46.1	0.5926	0.5959	-48.0	-48.4
12	.5866	.5945	-33.2	-33.2	0.5927	0.5932	-34.5	-34.9
13	.5789	.5856	-19.8	-19.9	0.5856	0.5875	-21.5	-21.6
14	.5756	.5814	-6.6	-6.9	0.5842	0.5850	-8.3	-8.4
15	.5730	.5774	6.7	6.2	0.5788	0.5808	4.9	4.9
16	.5709	.5731	18.6	18.0	0.5758	0.5797	18.1	18.1
17	.5725	.5721	33.2	32.6	0.5762	0.5795	31.3	31.3
18	.5778	.5686	44.2	44.4	0.5640	0.5746	44.7	44.6
20	.5754	.5964	56.0	56.8	0.6148	0.6357	70.2	69.5
23	.6717	.6775	98.9	99.1	0.6980	0.7126	106.0	106.8
26	.6953	.7089	143.5	143.1	0.7415	0.7467	144.8	144.5

Layered Medium $T = 10^4$ sec

$\sigma = 10^{-3}$ — 20 km

$\sigma = 10^{-1}$ — 40 km

$\sigma = 0.28$

(H) Source Field: $0.5\, e^{\frac{2\pi i}{10^6}\{(x - 6.21 \times 10^5) + (y - 6.21 \times 10^5\}}$

Thin sheet model: Figure 4.1-2

TABLE 4.1-4

Distance x 37 km	Amplitude of H_x (At/m) Using		Phase of H_x (deg) Using		Amplitude of H_y (At/m) Using		Phase of H_y (deg) Using	
	Imbedding	Uniform Spacing	Imbedding	Uniform Spacing	Imbedding	Uniform Spacing	Imbedding	Uniform Spacing
2	.7093	.7224	-174.7	-174.6	.7180	.7432	-177.3	-177.3
5	.6655	.6689	-130.7	-131.4	.6973	.6994	-139.2	-138.7
8	.7823	.8112	-87.6	-87.6	.5949	.6238	-94.0	-96.2
10	.5905	.6025	-58.4	-59.1	.5930	.5992	-60.2	-60.8
11	.5836	.5930	-46.1	-46.0	.5890	.5923	-47.5	-47.9
12	.5805	.5884	-33.0	-33.0	.5887	.5904	-34.0	-34.4
13	.5725	.5792	-19.4	-19.5	.5834	.5853	-21.1	-21.2
14	.5715	.5772	-6.1	-6.3	.5808	.5824	-7.9	-8.0
15	.5715	.5757	7.3	6.9	.5757	.5776	5.2	5.3
16	.5685	.5705	19.0	18.4	.5717	.5760	18.5	18.5
17	.5752	.5743	33.8	33.2	.5726	.5757	31.7	31.8
18	.5815	.5723	44.6	44.9	.5600	.5705	45.4	45.1
20	.5725	.5929	55.8	56.7	.6130	.6337	70.8	70.0
23	.6680	.6717	99.2	99.2	.6975	.7127	106.3	107.0
26	.6876	.7066	143.4	143.0	.7423	.7474	144.9	144.5

Layered Medium $T = 10^4$ sec

$\sigma = 10^{-4}$ — 20 km

$\sigma = 10^{-1}$ — 40 km

$\sigma = 0.28$

(H) Source Field: $0.5\, e^{\frac{2\pi i}{10^6}\{(x - 6.2 \times 10^5) + (y - 6.2 \times 10^5)\}}$

Thin sheet model: Figure 4.1-2

TABLE 4.1-5

Distance x 37 km	Amplitude of H_x (At/m) Using		Phase of H_x (deg) Using		Amplitude of H_y (At/m) Using		Phase of H_y (deg) Using	
	Imbedding	Uniform Spacing	Imbedding	Uniform Spacing	Imbedding	Uniform Spacing	Imbedding	Uniform Spacing
2	.7096	.7225	-174.7	-174.6	.7179	.7432	-177.4	-177.3
5	.6654	.6685	-130.6	-131.3	.6966	.6992	-139.2	-138.8
8	.7826	.8125	-87.6	-87.6	.5936	.6230	-93.9	-96.2
10	.5895	.6014	-58.4	-59.1	.5920	.5984	-60.1	-60.7
11	.5826	.5921	-46.1	-46.0	.5385	.5918	-47.4	-47.8
12	.5796	.5874	-33.0	-33.0	.5882	.5900	-33.9	-34.3
13	.5714	.5782	-19.3	-19.4	.5831	.5850	-21.0	-21.1
14	.5709	.5766	-6.0	-6.2	.5804	.5820	-7.8	-7.9
15	.5713	.5755	7.4	7.0	.5752	.5771	5.3	5.3
16	.5680	.5701	19.1	18.4	.5711	.5754	18.6	18.6
17	.5756	.5747	33.9	33.3	.5721	.5752	31.8	31.8
18	.5821	.5729	44.7	45.0	.5594	.5699	45.5	45.2
20	.5721	.5925	55.7	56.7	.6127	.6334	70.9	70.1
23	.6674	.6709	99.2	99.3	.6974	.7128	106.4	107.1
26	.6863	.7062	143.4	143.0	.7424	.7475	144.9	144.5

Layered Medium $T = 10^4$ sec

$\sigma = 10^{-5}$ — 20 km

$\sigma = 10^{-1}$ — 40 km

$\sigma = 0.28$

(H) Source Field: $0.5\, e^{\frac{2\pi i}{10^6}\{(x - 6.2 \times 10^5) + (y - 6.2 \times 10^5)\}}$

Thin sheet model in Figure 4.1-2

TABLE 4.1-6

Distance x 37 km	Amplitude of H_x (At/m) Using		Phase of H_x (deg) Using		Amplitude of H_y (At/m) Using		Phase of H_y (deg) Using	
	Imbedding	Uniform Spacing	Imbedding	Uniform Spacing	Imbedding	Uniform Spacing	Imbedding	Uniform Spacing
2	.7097	.7225	-174.7	-174.6	.7179	.7432	-177.4	-177.3
5	.6654	.6685	-130.6	-131.3	.6966	.6911	-139.2	-138.8
8	.7826	.8126	-87.6	-87.6	.5935	.6229	-93.9	-96.2
10	.5894	.6013	-58.4	-59.1	.5919	.5983	-60.1	-60.6
11	.5825	.5920	-46.1	-46.0	.5885	.5918	-47.4	-47.8
12	.5795	.5873	-33.0	-33.0	.5882	.5900	-33.9	-34.3
13	.5713	.5781	-19.3	-19.4	.5831	.5850	-21.0	-21.1
14	.5708	.5765	-6.0	-6.2	.5803	.5820	-7.8	-7.9
15	.5713	.5755	7.4	7.0	.5751	.5770	5.3	5.3
16	.5680	.5701	19.1	18.5	.5711	.5754	18.6	18.6
17	.5756	.5747	33.9	33.3	.5720	.5751	31.8	31.8
18	.5822	.5730	44.7	45.0	.5593	.5699	45.6	45.2
20	.5720	.5925	55.7	56.7	.6127	.6334	70.9	70.1
23	.6674	.6708	99.3	99.3	.6974	.7128	106.4	107.1
26	.6862	.7061	143.4	143.0	.7425	.7476	144.9	144.5

Layered Medium $T = 10^4$ sec

$\sigma = 10^{-6}$ — 20 km

$\sigma = 10^{-1}$ — 40 km

$\sigma = 0.28$

(H) Source Field: $0.5\, e^{\frac{2\pi i}{10^6}\{(x - 6.2 \times 10^5) + (y - 6.2 \times 10^5)\}}$

Thin sheet model in Figure 4.1-2

4.2 Application to One-Dimensional Generalized Thin Sheet

The imbedding scheme is shown in Fig. 4.2-00. The only difference in this case is that there is one additional variable ρ_s (the resistivity thickness product of the resistive sheet) for which an average property has to be determined as for σ_s. This is determined by computing $\rho_{zz} = |\sum_i E_{zi} / \sum_i J_{zi}|$. The rest of the steps involved in calculating the solution using imbedding are exactly the same as for the thin sheet model. As in thin sheet models, two types of source fields were employed: (1) a quasi-uniform source filed; (2) a source field with variation in both the x and y directions.

The solutions were computed using equations (2.3.5) and (2.3.6), which resulted in four unknowns at each grid point, viz. E_x^-, E_y^-, E_x^+, E_y^+, instead of just E_x^-, E_y^- (with (2.3.7)). The advantage is that with four unknowns we get rather simple equations for the case of the source field, varying in the x and y directions, whereas with (2.3.7) (although it results in half the number of equations which is not an enormous advantage in the case of one-dimensional variation in generalized thin sheet) we lose this simple nature of equations.

The results are summarized in Figs. 4.2-1 to 4.2-11 and Tables 4.2-1 to 4.2-3. A comparison of the Figs. 4.2-1, 3, 4, 5, for which the generalized thin sheet models (ρ_s being constant) are similar to the thin sheet models, with Figs. 4.1-3, 5, 7 shows that scatter is greater in the generalized thin sheet models. This may be due to the method of computation which resulted in using four averages (E_x^-, E_y^-, E_x^+, E_y^+) outside the inner region instead of just

two ($\bar{E}_x$, $\bar{E}_y$). However, the agreement between the 'true model' solution and the 'imbedding solution' is still satisfactory.

Thus in the 'imbedding' method the entire problem is solved by solving a much smaller sized problem several times. For instance, in the above example (for the case of a quasi-uniform source field) we essentially solve a system of 9 simultaneous equations twice. Using a uniform spacing throughout we have to solve a system of 27 simultaneous equations once. For a non-uniform source field with variation in the x and y directions or only the y direction, we would have to solve a system of 18 equations twice for the imbedding method, or a system of 54 equations once for the uniform spacing method. For a three-level imbedding with non-uniform source field, the difference is solving a system of 18 equations thrice (imbedding) or solving 162 equations once (uniform spacing).

σ'_1	σ'_2	σ'_3	σ_1	σ_2	σ_3	σ_4	σ_5	σ_6	σ_7	σ_8	σ_9	σ'_4	σ'_5	σ'_6
ρ'_1	ρ'_2	ρ'_3	ρ_1	ρ_2	ρ_3	ρ_4	ρ_5	ρ_6	ρ_7	ρ_8	ρ_9	ρ'_4	ρ'_5	ρ'_6

σ'_1	σ'_2	σ'_3	$\bar{\bar{\sigma}}_{11}$	$\bar{\bar{\sigma}}_{12}$	$\bar{\bar{\sigma}}_{13}$	σ'_4	σ'_5	σ'_6
ρ'_1	ρ'_2	ρ'_3	$\bar{\bar{\rho}}_{11}$	$\bar{\bar{\rho}}_{12}$	$\bar{\bar{\rho}}_{13}$	ρ'_4	ρ'_5	ρ'_6

E'^-_1	E'^-_2	E'^-_3	$\bar{E}^-_1$	$\bar{E}^-_2$	$\bar{E}^-_3$	E'^-_4	E'^-_5	E'^-_6
E'^+_1	E'^+_2	E'^+_3	$\bar{E}^+_1$	$\bar{E}^+_2$	$\bar{E}^+_3$	E'^+_4	E'^+_5	E'^+_6

E'^-_1	E'^-_1	E'^-_1	E'^-_2	E'^-_2	E'^-_2	E'^-_3	E'^-_3	E'^-_3	σ_1	σ_2	σ_3	σ_4	σ_5	σ_6	σ_7	σ_8	σ_9	E'^-_4	E'^-_4	E'^-_4	E'^-_5	E'^-_5	E'^-_5	E'^-_6	E'^-_6	E'^-_6
E'^+_1	E'^+_1	E'^+_1	E'^+_2	E'^+_2	E'^+_2	E'^+_3	E'^+_3	E'^+_3	ρ_1	ρ_2	ρ_3	ρ_4	ρ_5	ρ_6	7	ρ_8	ρ_9	E'^+_4	E'^+_4	E'^+_4	E'^+_5	E'^+_5	E'^+_5	E'^+_6	E'^+_6	E'^+_6

E'^-_1	E'^-_2	E'^-_3	E^-_1	E^-_2	E^-_3	E^-_4	E^-_5	E^-_6	E^-_7	E^-_8	E^-_9	E'^-_4	E'^-_5	E'^-_6
E'^+_1	E'^+_2	E'^+_3	E^+_1	E^+_2	E^+_3	E^+_4	E^+_5	E^+_6	E^+_7	E^+_8	E^+_9	E'^+_4	E'^+_5	E'^+_6

Fig. 4.2-00

Imbedding Model

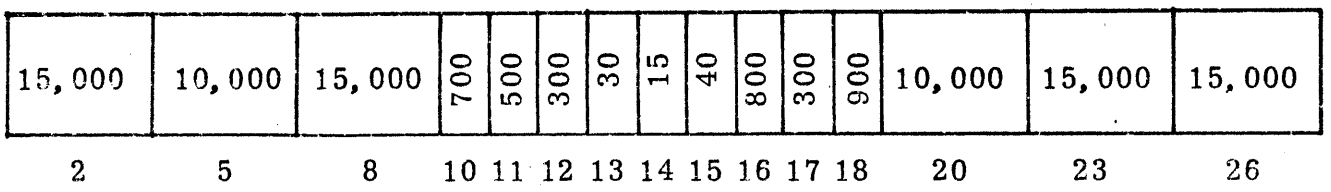

Uniform Spacing Model

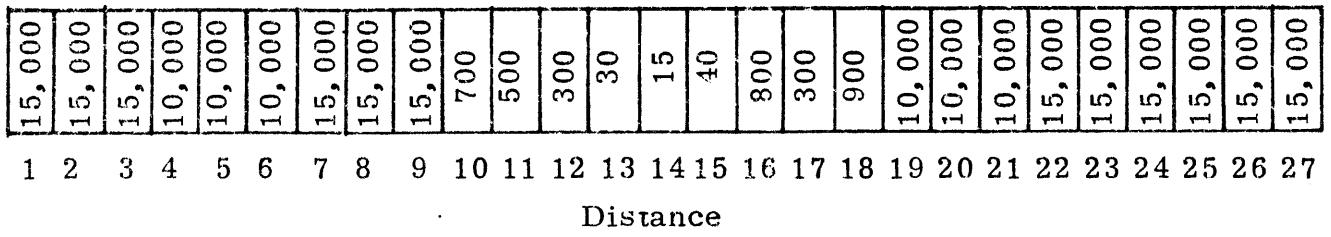

Fig. 4.2-0 Conductance of the Thin Sheet (in mhos)

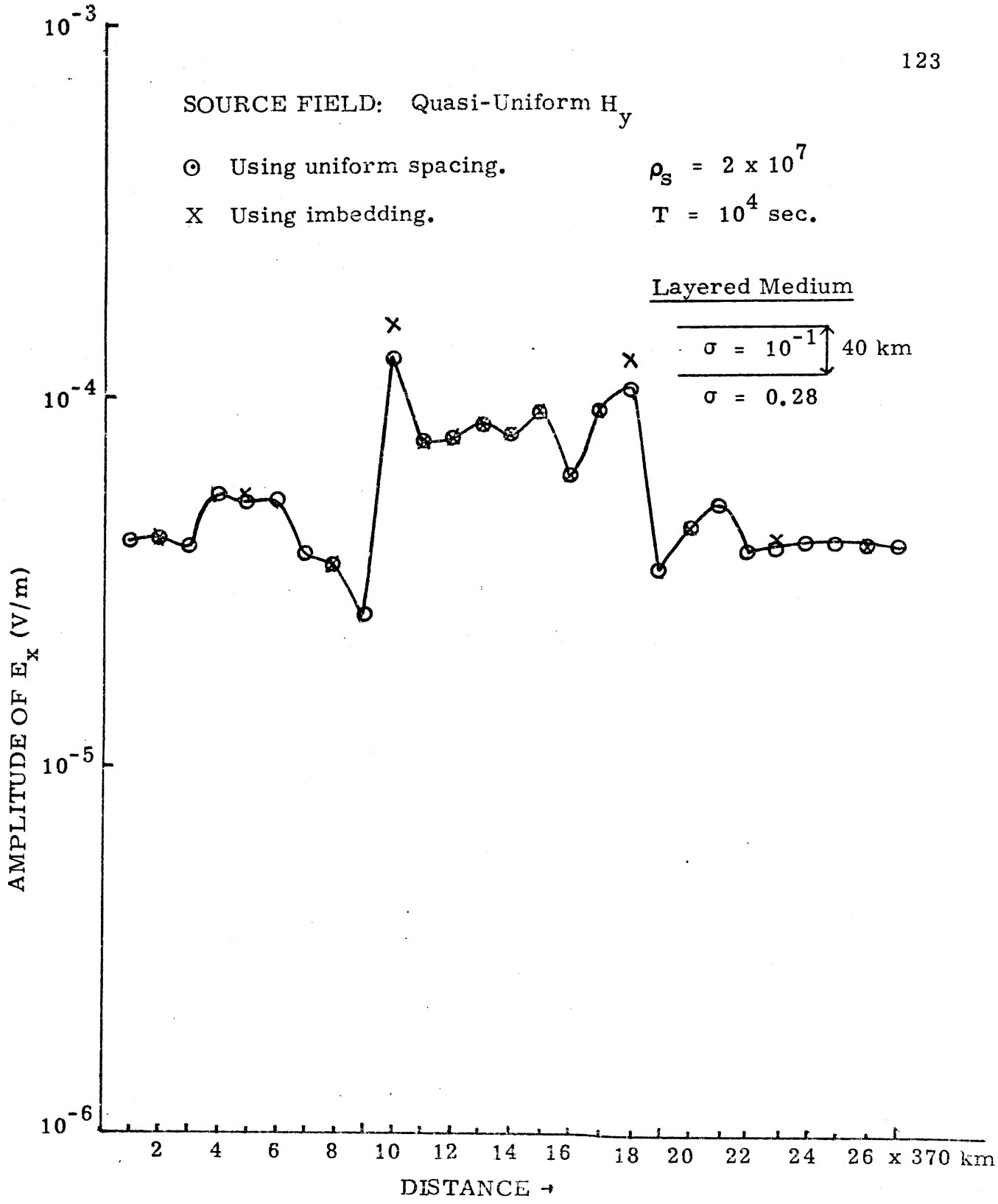

Refer to Fig. 4.2-0 for thin sheet model used in the study. Phases for the two cases are plotted in Fig. 4.2-2.

Fig. 4.2-1

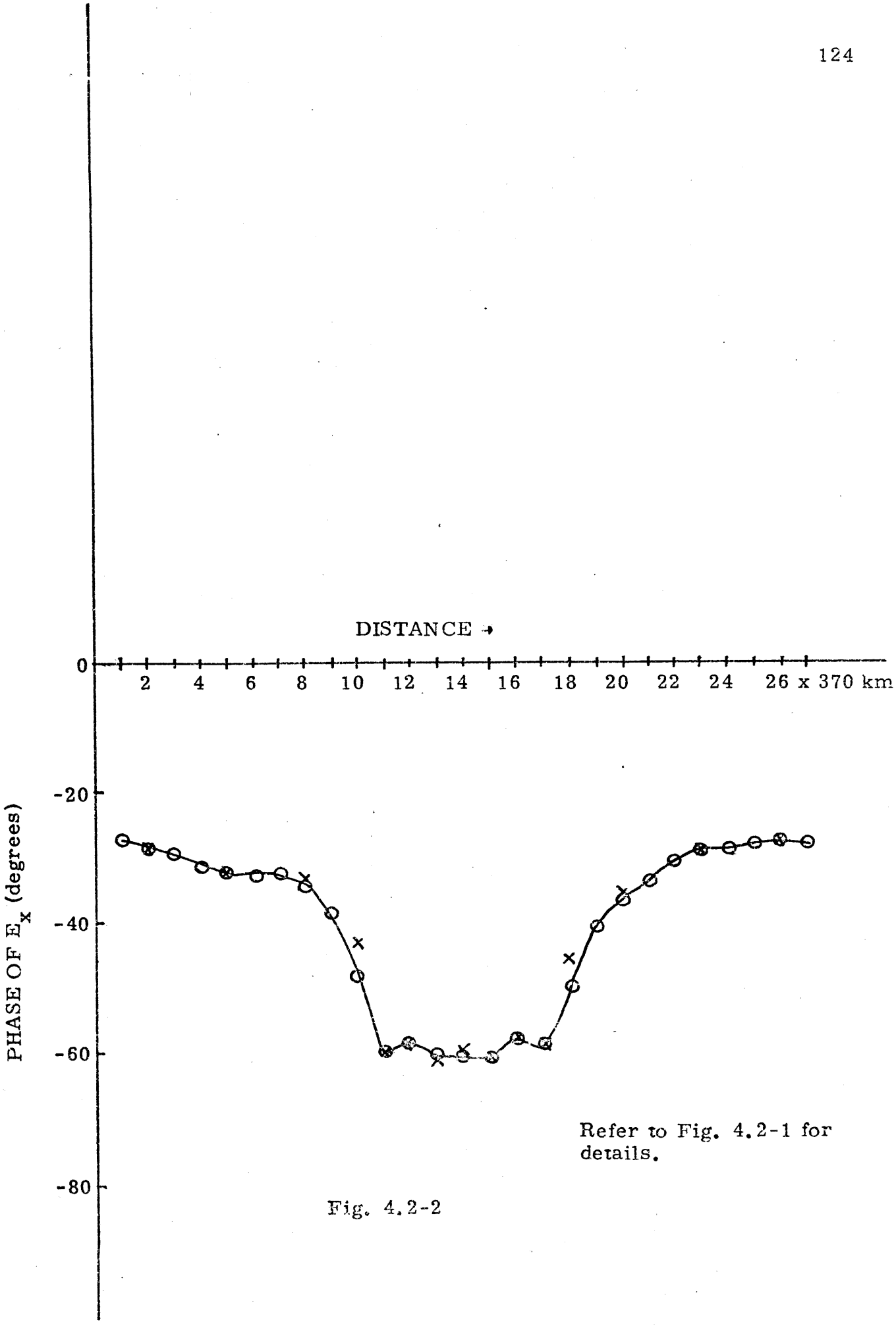

Refer to Fig. 4.2-1 for details.

Fig. 4.2-2

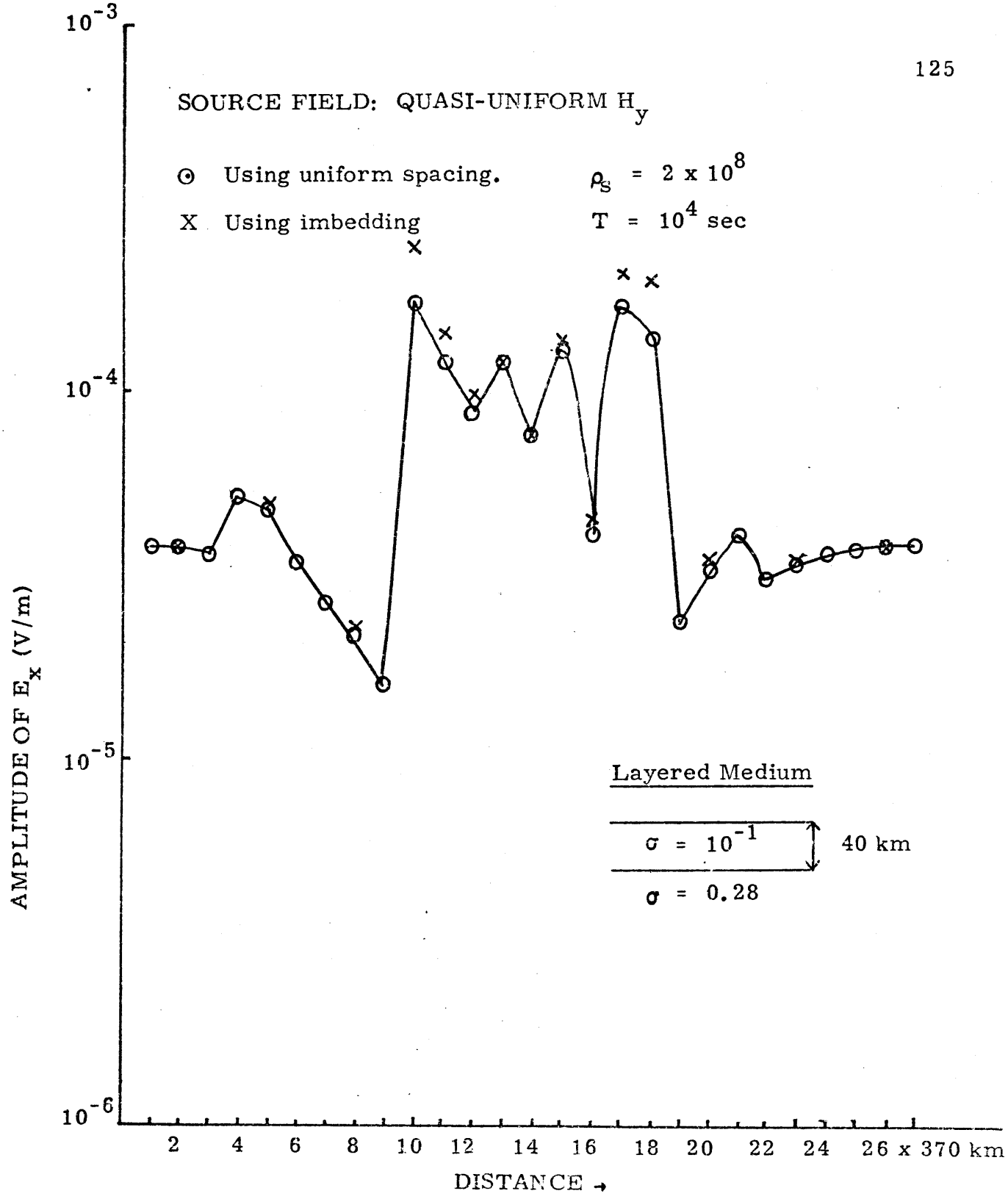

Refer to Fig. 4.2-0 for thin sheet model used in the study. Phases for the two cases are tabulated in Table 4.2-1a.

Fig. 4.2-3

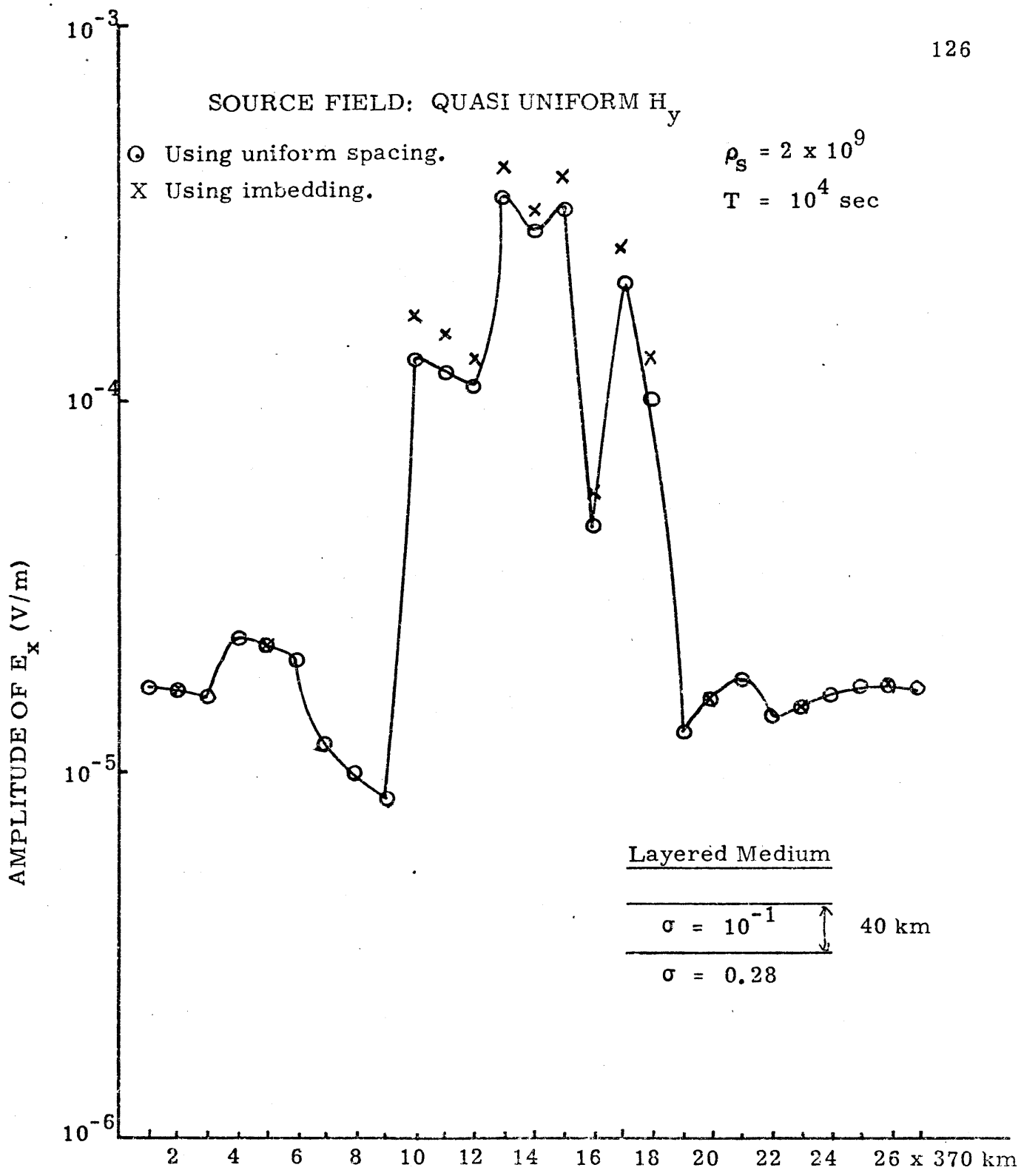

Refer to Fig. 4.2-0 for thin sheet model used in this comparison. Phases for the two cases are tabulated in Table 4.2-1b.

Fig. 4.2-4

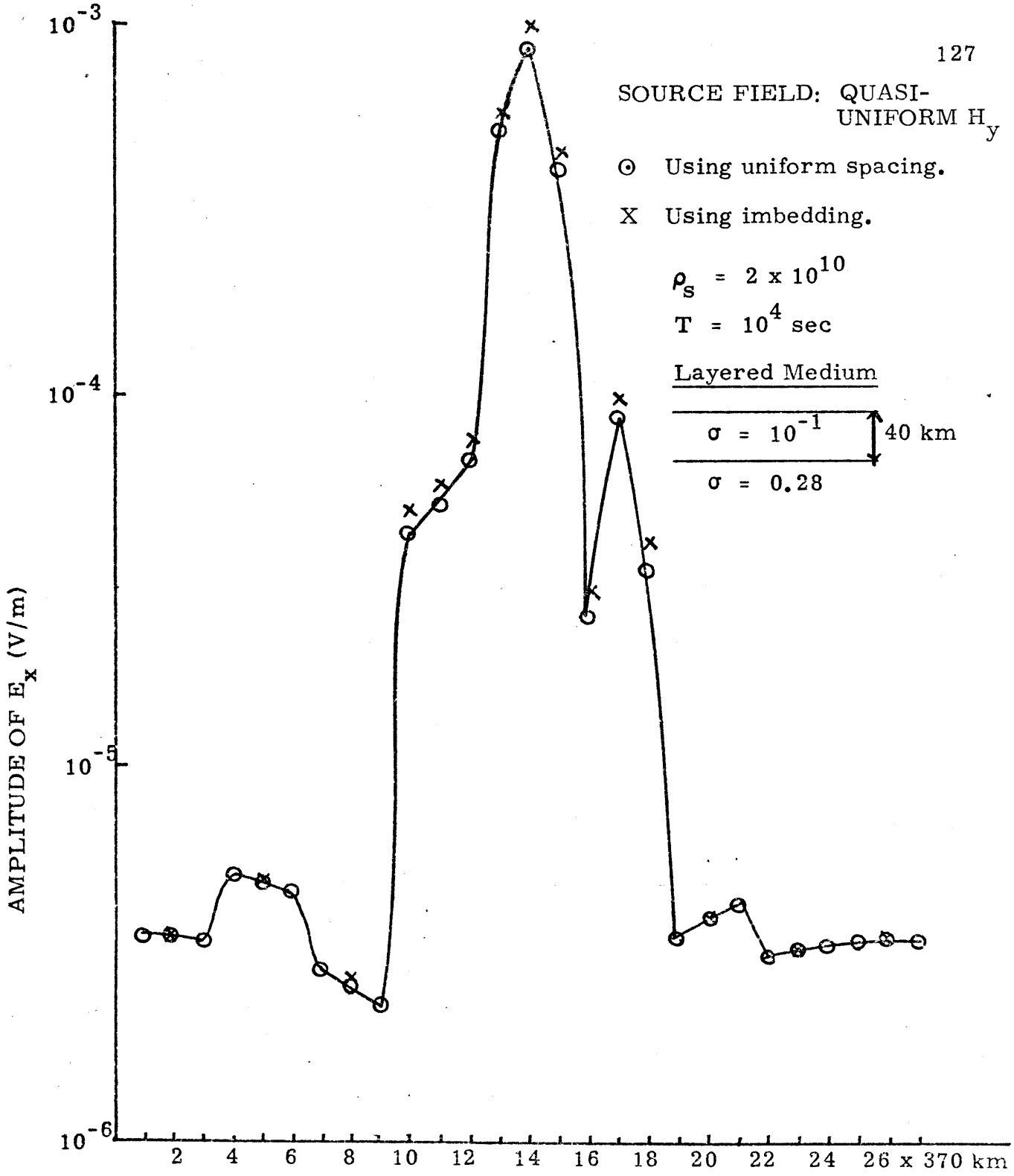

Refer to Fig. 4.2-0 for sheet model used in this comparison. Phases for the two cases are tabulated in Table 4.2-1c.

Fig. 4.2-5

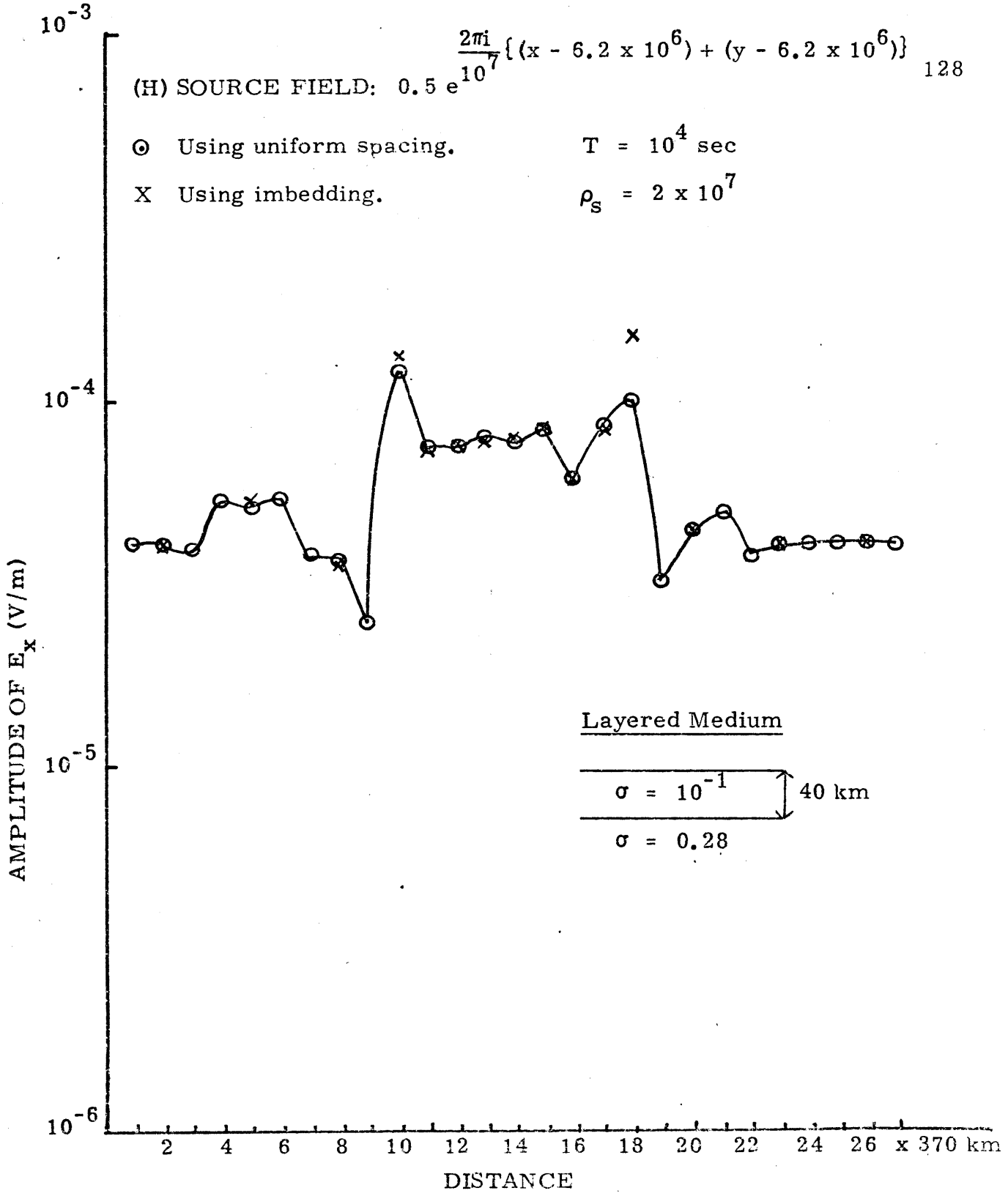

Refer to Fig. 4.2-0 for thin sheet model used in this comparison. Phases for the two cases are plotted in Fig. 4.2-7.

Fig. 4.2-6

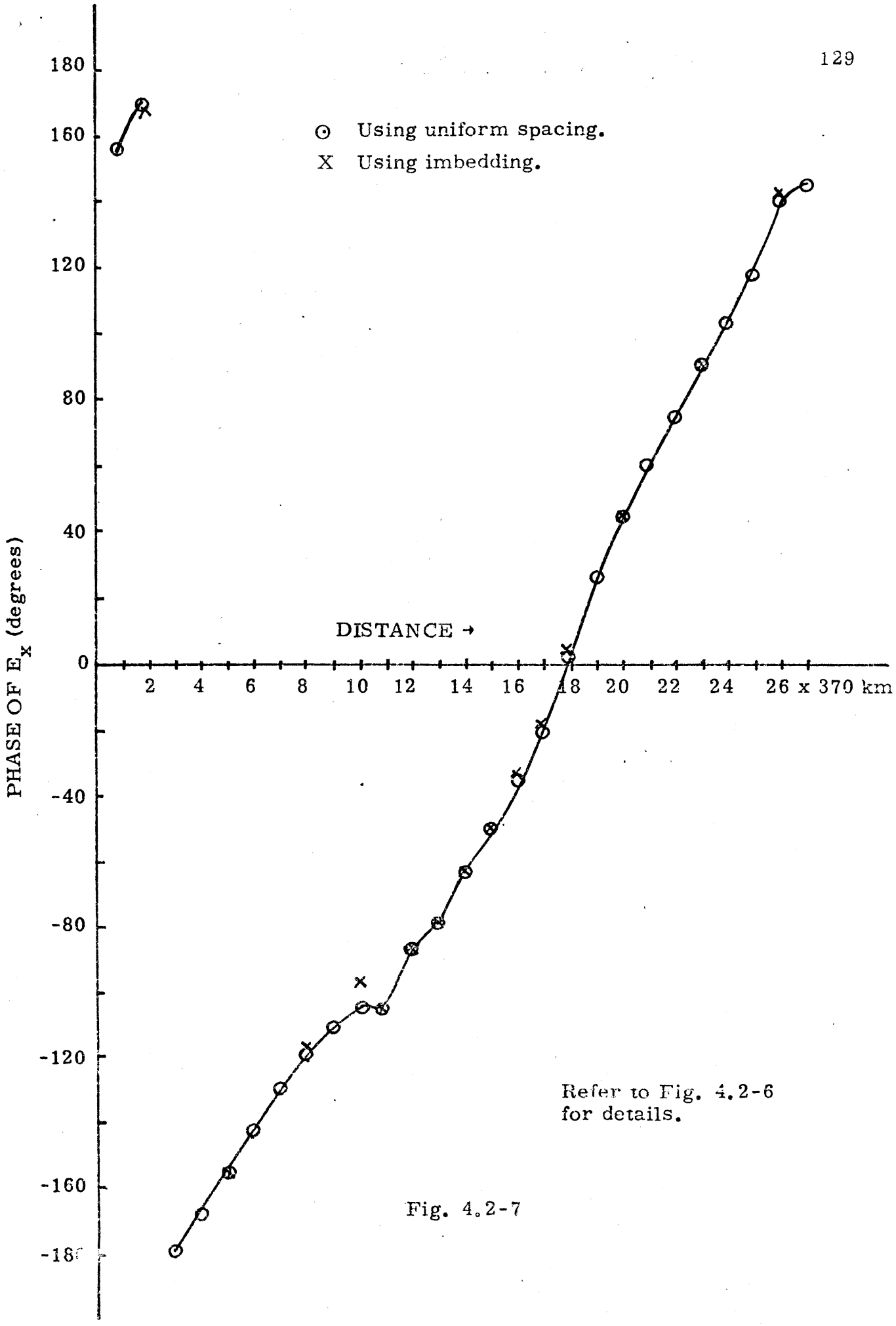

Refer to Fig. 4.2-6 for details.

Fig. 4.2-7

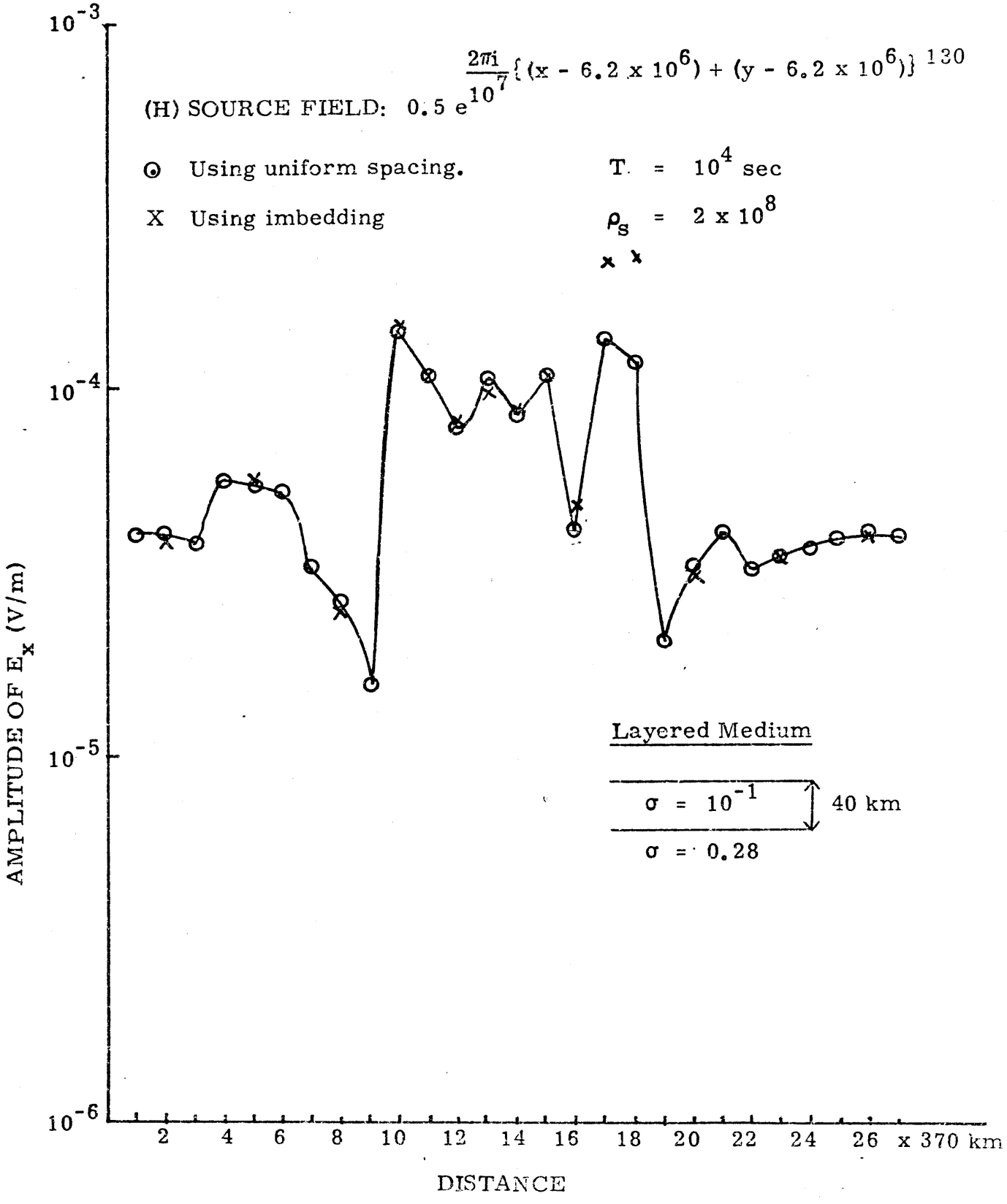

Refer to Fig. 4.2-0 for thin sheet model used in the comparison. Phases for the two cases are plotted in Fig. 4.2-9.

Fig. 4.2-8

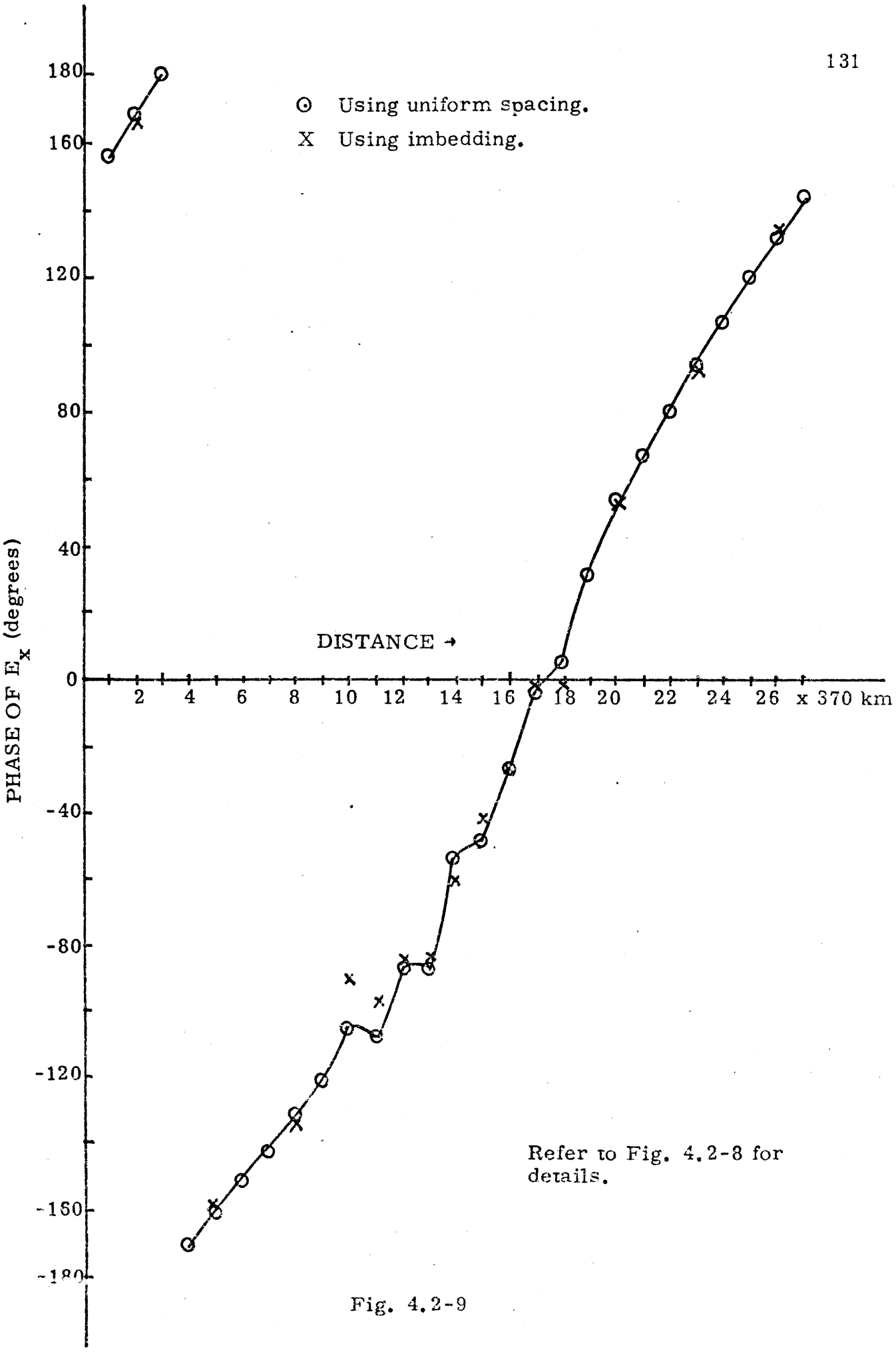

Refer to Fig. 4.2-8 for details.

Fig. 4.2-9

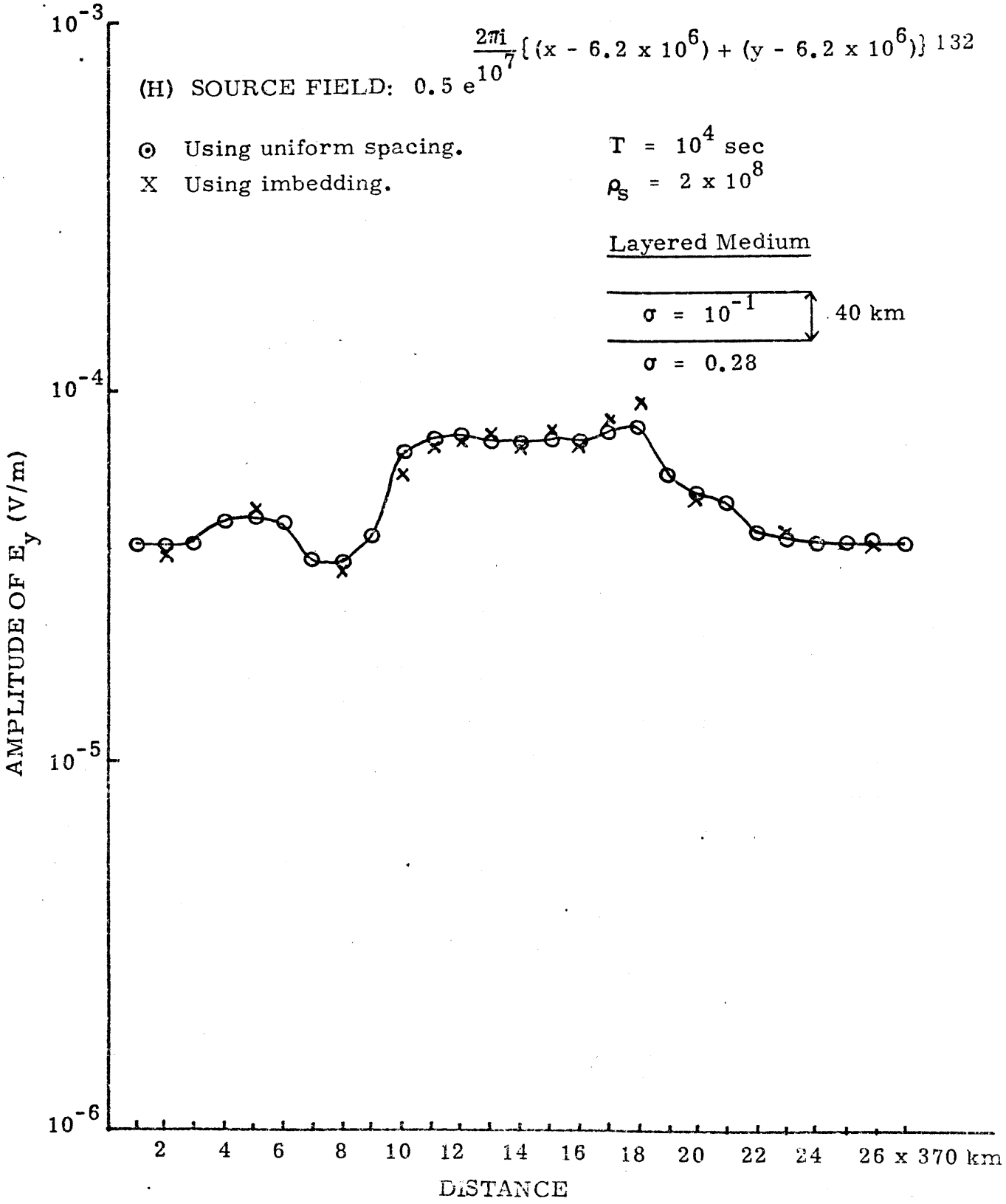

Refer to Fig. 4.2-0 for thin sheet model used in this comparison. Phases for the two cases are plotted in Fig. 4.2-11.

Fig. 4.2-10

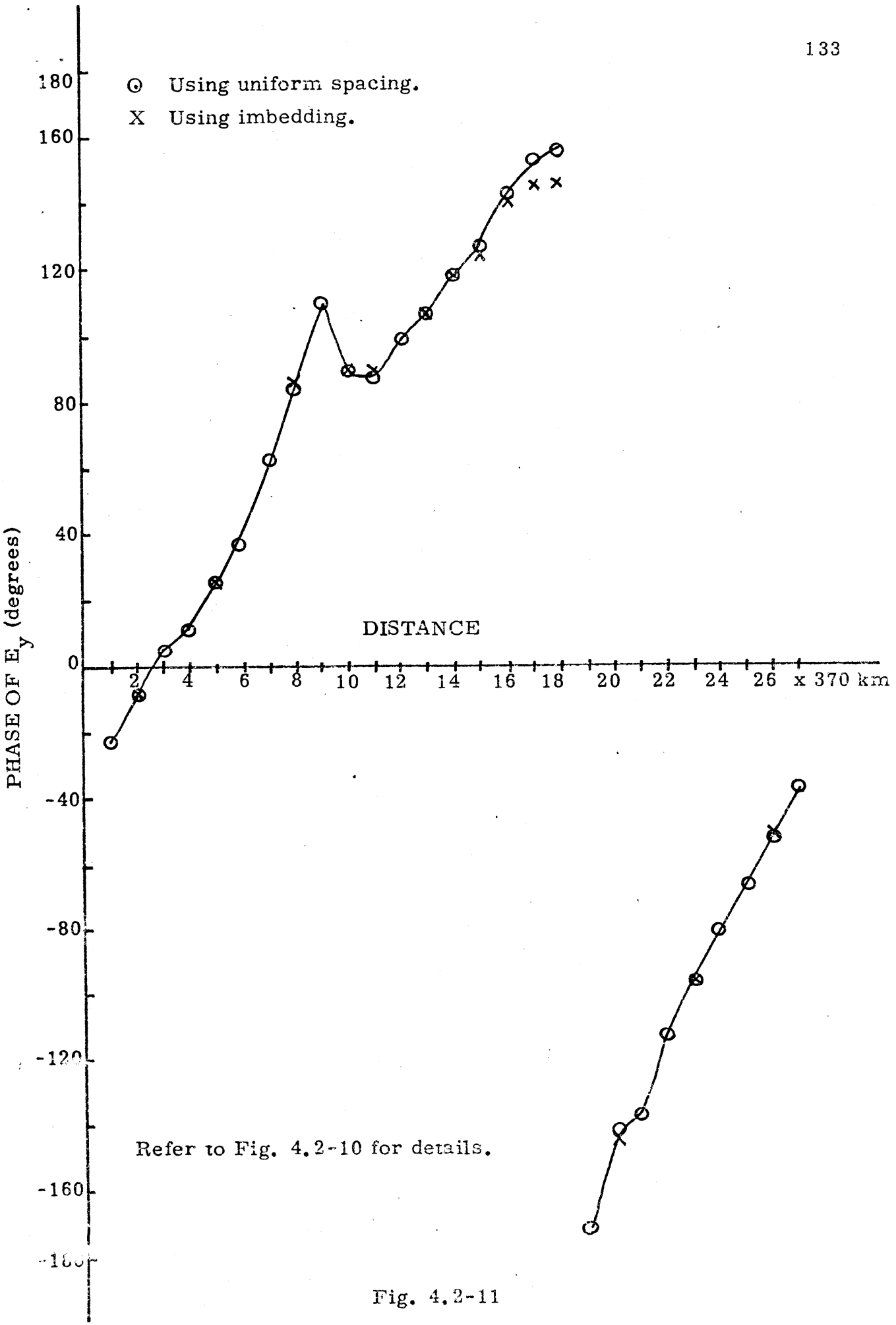

Refer to Fig. 4.2-10 for details.

Fig. 4.2-11

TABLE 4.2-1

Distance x 370 km	Phase of E_x (deg) Using	
	Imbedding	Uniform Spacing
2	-33.2	-33.5
5	-35.5	-35.9
8	-39.5	-40.2
10	-42.8	-45.1
11	-47.1	-49.8
12	-52.0	-54.2
13	-57.5	-58.3
14	-60.7	-60.6
15	-56.8	-57.8
16	-52.6	-54.7
17	-46.9	-49.7
18	-42.1	-44.6
20	-38.9	-39.6
23	-34.8	-33.9
26	-32.9	-38.1

$\rho_s = 2 \times 10^8$

a

Phase of E_x (deg) Using	
Imbedding	Uniform Spacing
-49.2	-49.4
-49.6	-49.8
-50.4	-50.6
-51.3	-51.4
-51.8	-52.0
-52.3	-52.6
-53.3	-53.7
-54.4	-55.1
-53.1	-53.6
-52.2	-52.7
-51.7	-52.0
-51.2	-51.4
-50.3	-50.5
-49.5	-49.7
-49.2	-49.4

$\rho_s = 2 \times 10^9$

b

Phase of E_x (deg) Using	
Imbedding	Uniform Spacing
-57.9	-57.9
-57.9	-58.0
-58.0	-58.1
-58.3	-58.1
-58.3	-58.2
-58.4	-58.2
-58.4	-58.3
-58.4	-58.3
-58.4	-58.3
-58.3	-58.2
-58.3	-58.2
-58.3	-58.1
-58.0	-58.1
-57.9	-58.0
-57.9	-57.9

$\rho_s = 2 \times 10^{10}$

c

Layered Medium

$T = 10^4$ sec

$\sigma = 10^{-1}$ ↕ 40 km

$\sigma = 0.28$

Source Field: Quasi-Uniform H_y

Thin sheet model: Figure 4.2-0

TABLE 4.2-2

Distance x 370 km	Amplitude of H_x (At/m) Using		Phase of H_x (deg) Using		Amplitude of H_y (At/m) Using		Phase of H_y (deg) Using	
	Imbedding	Uniform Spacing	Imbedding	Uniform Spacing	Imbedding	Uniform Spacing	Imbedding	Uniform Spacing
2	.9541	.9746	-162.0	-162.1	.9547	.9773	-162.6	-162.5
5	.9438	.9589	-122.6	-122.5	.9582	.9690	-122.7	-122.7
8	.9711	.9828	-80.6	-81.0	.9388	.9633	-82.5	-82.7
10	.8978	.8786	-54.5	-52.8	.9420	.9448	-55.2	-54.8
11	.9268	.9219	-41.3	-41.4	.9366	.9372	-42.4	-42.3
12	.9295	.9302	-28.8	-28.3	.9362	.9368	-29.1	-29.0
13	.9322	.9294	-15.3	-15.3	.9322	.9321	-15.8	-15.8
14	.9250	.9298	-2.4	-2.4	.9333	.9333	-2.6	-2.5
15	.9263	.9255	10.6	10.7	.9317	.9311	10.6	10.8
16	.9256	.9358	23.0	23.0	.9346	.9348	23.8	24.1
17	.9109	.9164	36.4	36.7	.9381	.9377	37.2	37.4
18	.8369	.8835	51.2	49.5	.9347	.9395	49.2	50.0
20	.9542	.9766	75.0	75.9	.9380	.9601	77.2	77.4
23	.9650	.9772	117.0	117.2	.9578	.9729	117.5	117.7
26	.9570	.9739	157.7	157.5	.9609	.9768	157.9	157.6

$\rho_s = 2 \times 10^7$ Layered Medium $T = 10^4$ sec

$\sigma = 10^{-1}$ ↕ 40 km

$\sigma = 0.28$

(H) Source Field: $0.5\, e^{\frac{2\pi i}{10^7}\{(x - 6.2 \times 10^6) + (y - 6.2 \times 10^6)\}}$

Thin sheet model: Figure 4.2-0

TABLE 4.2-3

Distance x 370 km	Amplitude of H_x (At/m) Using		Phase of H_x (deg) Using		Amplitude of H_y (At/m) Using		Phase of H_y (deg) Using	
	Imbedding	Uniform Spacing	Imbedding	Uniform Spacing	Imbedding	Uniform Spacing	Imbedding	Uniform Spacing
2	.9528	.9734	-162.1	-162.2	.9549	.9776	-162.7	-162.5
5	.9449	.9587	-122.5	-122.5	.9587	.9685	-122.7	-122.8
8	.9625	.9757	-80.0	-80.7	.9331	.9612	-82.6	-82.8
10	.9116	.8770	-54.8	-54.4	.9386	.9363	-55.8	-54.9
11	.9330	.9218	-42.5	-41.9	.9366	.9335	-42.7	-42.4
12	.9322	.9277	-28.3	-28.6	.9347	.9337	-29.4	-29.0
13	.9183	.9270	-16.3	-15.5	.9317	.9304	-16.1	-15.8
14	.9311	.9266	-2.1	-2.4	.9311	.9316	-3.0	-2.5
15	.8965	.9229	10.4	10.8	.9287	.9297	10.3	10.8
16	.9270	.9310	23.7	23.2	.9265	.9326	23.1	24.0
17	.8648	.9119	38.2	37.0	.9269	.9348	36.5	37.3
18	.8087	.8792	57.9	50.6	.9007	.9331	47.8	49.9
20	.9516	.9744	74.5	75.6	.9329	.9574	77.2	77.4
23	.9665	.9775	116.9	117.0	.9581	.9718	117.5	117.8
26	.9548	.9728	157.7	157.5	.9604	.9770	157.9	157.6

$\rho_s = 2 \times 10^8$ Layered Medium $\sigma = 10^{-1}$ ↕ 40 km $\sigma = 0.28$ $T = 10^4$ sec

(H) Source Field: $0.5\, e^{\frac{2\pi i}{10^7}\{(x - 6.2 \times 10^6) + (y - 6.2 \times 10^6)\}}$

Thin sheet model: Figure 4.2-0

CHAPTER V

TWO-DIMENSIONAL SURFACE VARIATIONS

In this chapter we treat cases in which crustal electrical properties vary in both the x and y directions. Several times in the interpretation of magnetotelluric data we encounter situations in which conductivity variations do not have any well defined strike direction (e.g. see Kasamayer, 1974). In these cases two-dimensional models cannot be employed, as the conductivity variations are three-dimensional in nature. Even situations that appear quite two-dimensional may be far different from them as the criteria for two-dimensionality is that the consistency along strike must extend well beyond the adjustment distance. If the frequencies of fields being studied are low, the surface layer in which the conductivity and the resistivity vary in both directions can be treated as an anisotropic thin sheet and we obtain a quasi-three-dimensional conductivity model. We showed in Chapters II and III that the anisotropic thin sheet can physically be thick and yet be treated as thin.

In this chapter we restrict our discussion to cases in which only the conductivity varies and therefore the resistive thin sheet is made the top layer of the layered medium. We first check the accuracy of the two-dimensional calculations. Then the imbedding technique for two-dimensional conductivity variation is described and the accuracy of the two-dimensional imbedding solution is checked. Finally the method is applied to find the island effect on Oahu,

Hawaii. These results are used to investigate the accuracy of the assumptions made by Larsen (1975) in the interpretations of his very long period magnetotelluric measurements on Oahu. These measurements are of special interest because they are the most extensive long period magnetotelluric measurements that exist to date and the most reliable measurements that sample the suboceanic mantle.

5.1 Checking Two-Dimensional Calculations

The two-dimensional calculations were checked by comparing the solution obtained with two-dimensional calculations for a one-dimensional problem with that obtained using one-dimensional calculations. The results of this comparison are shown in Figs. 5.1-2 to 5.1-7. The σ_s model is shown in Fig. 5.1-1. From these figures we see that the agreement between the two solutions is perfect.

y↓ \ x→	111	222	333	444	555	666	777	888	999
111	15,000	10,200	8,000	40	30	50	10,000	8,000	15,000
222	15,000	10,200	8,000	40	30	50	10,000	8,000	15,000
333	15,000	10,200	8,000	40	30	50	10,000	8,000	15,000
444	15,000	10,000	8,000	40	30	50	10,000	8,000	15,000
555	15,000	10,200	8,000	40	30	50	10,000	8,000	15,000
666	15,000	10,200	8,000	40	30	50	10,000	8,000	15,000
777	15,000	10,200	8,000	40	30	50	10,000	8,000	15,000
888	15,000	10,200	8,000	40	30	50	10,000	8,000	15,000
999	15,000	10,200	8,000	40	30	50	10,000	8,000	15,000

(km)

(km)

Fig. 5.1-1 Conductance of the thin sheet model.

Map of the Amplitude of E_y ($\times 10^{-4}$) (V/m)

Layered Medium

20 km | $\sigma = 10^{-3}$ mho/m

40 km | $\sigma = 0.1$ mho/m

$\sigma = 0.28$ mho/m

$T = 10^4$ secs

Source Field: Quasi-Uniform H_x

y ↓ \ x →	111	222	333	444	555	666	777	888	999	(km)
111	.4957	.5404	.5975	.6528	.6743	.6479	.5921	.5466	.4987	
222	.4957	.5404	.5975	.6528	.6743	.6479	.5921	.5466	.4987	
333	.4957	.5404	.5975	.6528	.6743	.6479	.5921	.5466	.4987	
444	.4957	.5404	.5975	.6528	.6743	.6479	.5921	.5466	.4987	
555	.4957	.5404	.5975	.6528	.6743	.6479	.5921	.5466	.4987	
666	.4957	.5404	.5975	.6528	.6743	.6479	.5921	.5466	.4987	
777	.4957	.5404	.5975	.6528	.6743	.6479	.5921	.5466	.4987	
888	.4957	.5404	.5975	.6528	.6743	.6479	.5921	.5466	.4987	
999	.4957	.5404	.5975	.6528	.6743	.6479	.5921	.5466	.4987	
(km)	(.4957)	(.5404)	(.5975)	(.6528)	(.6743)	(.6479)	(.5921)	(.5466)	(.4987)	

Fig. 5.1-2 The conductivity thickness product of the thin sheet model is shown in Fig. 5.1-1. The amplitudes of E_x and H_y were zeros. Values in the brackets indicate the amplitude of E_y, obtained using one-dimensional model of the thin sheet. Phases for the two cases are shown in Fig. 5.1-3.

Map of the Phase of E_y (Degrees)

y ↓ \ x →	111	222	333	444	555	666	777	888	999	(km)
111	153.8	146.2	138.2	125.2	122.5	125.8	140.6	143.9	153.2	
222	153.8	146.2	138.2	125.2	122.5	125.8	140.6	143.9	153.2	
333	153.8	146.2	138.2	125.2	122.5	125.8	140.6	143.9	153.2	
444	153.8	146.2	138.2	125.2	122.5	125.8	140.6	143.9	153.2	
555	153.8	146.2	138.2	125.2	122.5	125.8	140.6	143.9	153.2	
666	153.8	146.2	138.2	125.2	122.5	125.8	140.6	143.9	153.2	
777	153.8	146.2	138.2	125.2	122.5	125.8	140.6	143.9	153.2	
888	153.8	146.2	138.2	125.2	122.5	125.8	140.6	143.9	153.2	
999	153.8	146.2	138.2	125.2	122.5	125.8	140.6	143.9	153.2	
(km)	(153.8)	(146.2)	(138.2)	(125.2)	(122.5)	(125.8)	(140.6)	(143.9)	(153.2)	

Fig. 5.1-3 The conductance of the thin sheet model is shown in Fig. 5.1-1. Values in the brackets indicate the phase of E_y, obtained using a one-dimensional model of the thin sheet. For details refer to Fig. 5.1-2.

Map of the Amplitude of H_x (At/m)

y ↓ \ x →	111	222	333	444	555	666	777	888	999	(km)
111	1.139	1.052	1.022	0.862	0.863	0.862	1.072	1.002	1.138	
222	1.139	1.052	1.022	0.862	0.863	0.862	1.072	1.002	1.138	
333	1.139	1.052	1.022	0.862	0.863	0.862	1.072	1.002	1.138	
444	1.139	1.052	1.022	0.862	0.863	0.862	1.072	1.002	1.138	
555	1.139	1.052	1.022	0.862	0.863	0.862	1.072	1.002	1.138	
666	1.139	1.052	1.022	0.862	0.863	0.862	1.072	1.002	1.138	
777	1.139	1.052	1.022	0.862	0.863	0.862	1.072	1.002	1.138	
888	1.139	1.052	1.022	0.862	0.863	0.862	1.072	1.002	1.138	
999	1.139	1.052	1.022	0.862	0.863	0.862	1.072	1.002	1.138	
(km)	(1.139)	(1.052)	(1.022)	(0.862)	(0.863)	(0.862)	(1.072)	(1.002)	(1.138)	

Fig. 5.1-4 The conductivity thickness product of the thin sheet model is shown in Fig. 5.1-1. Values in the brackets indicate amplitude of H_x, obtained using a one-dimensional model of the thin sheet. For details refer to Fig. 5.1-2.

Map of the Phase of H_x (Degrees)

y ↓ \ x →	111	222	333	444	555	666	777	888	999	(km)
111	-0.38	-0.98	-3.16	4.03	3.23	4.20	-4.32	0.21	-0.68	
222	-0.38	-0.98	-3.16	4.03	3.23	4.20	-4.32	0.21	-0.68	
333	-0.38	-0.98	-3.16	4.03	3.23	4.20	-4.32	0.21	-0.68	
444	-0.38	-0.98	-3.16	4.03	3.23	4.20	-4.32	0.21	-0.68	
555	-0.38	-0.98	-3.16	4.03	3.23	4.20	-4.32	0.21	-0.68	
666	-0.38	-0.98	-3.16	4.03	3.23	4.20	-4.32	0.21	-0.68	
777	-0.38	-0.98	-3.16	4.03	3.23	4.20	-4.32	0.21	-0.68	
888	-0.38	-0.98	-3.16	4.03	3.23	4.20	-4.32	0.21	-0.68	
999	-0.38	-0.98	-3.16	4.03	3.23	4.20	-4.32	0.21	-0.68	
(km)	(-0.38)	(-0.98)	(-3.16)	(4.03)	(3.23)	(4.20)	(-4.32)	(0.21)	(-0.68)	

Fig. 5.1-5 The conductance of the thin sheet model is shown in Fig. 5.1-1. Values in the brackets indicate the phase of H_x, obtained using one-dimensional model of the thin sheet. For details refer to Fig. 5.1-2.

Map of the Amplitude of E_x ($\times 10^{-4}$) (V/m)

Layered Medium

20 km | $\sigma = 10^{-3}$ mho/m

40 km | $\sigma = 0.1$ mho/m

$\sigma = 0.28$ mho/m

$T = 10^4$ secs

Source Field: Quasi-Uniform H_y

y ↓ \ x →	111	222	333	444	555	666	777	888	999	(km)
111	.1390	.1710	.1282	2.673	.6616	2.612	.1041	.2175	.1388	
222	.1390	.1710	.1282	2.673	.6616	2.612	.1041	.2175	.1388	
333	.1390	.1710	.1282	2.673	.6616	2.612	.1041	.2175	.1388	
444	.1390	.1710	.1282	2.673	.6616	2.612	.1041	.2175	.1388	
555	.1390	.1710	.1282	2.673	.6616	2.612	.1041	.2175	.1388	
666	.1390	.1710	.1282	2.673	.6616	2.612	.1041	.2175	.1388	
777	.1390	.1710	.1282	2.673	.6616	2.612	.1041	.2175	.1388	
888	.1390	.1710	.1282	2.673	.6616	2.612	.1041	.2175	.1388	
999	.1390	.1710	.1282	2.673	.6616	2.612	.1041	.2175	.1388	
(km)	(.1390)	(.1710)	(.1282)	(2.673)	(.6616)	(2.612)	(.1041)	(.2175)	(.1388)	

Fig. 5.1-6 The conductivity thickness product of the thin sheet model is shown in Fig. 5.1-1. The amplitudes of E_y and H_x were zeroes. Values in the brackets indicate the amplitude of E_x obtained using one-dimensional model of the thin sheet. Phases for the two cases are shown in Fig. 5.1-7. Amplitude of H_y for both cases is constant and equal to 1.0 (At/m) and phase for both cases is 0.0 degrees.

Map of the Phase of E_x (Degrees)

y↓ \ x→	111	222	333	444	555	666	777	888	999	(km)
111	-51.49	-51.87	-52.56	-54.41	-61.57	-54.38	-52.58	-51.88	-51.49	
222	-51.49	-51.87	-52.56	-54.41	-61.57	-54.38	-52.58	-51.88	-51.49	
333	-51.49	-51.87	-52.56	-54.41	-61.57	-54.38	-52.58	-51.88	-51.49	
444	-51.49	-51.87	-52.56	-54.41	-61.57	-54.38	-52.58	-51.88	-51.49	
555	-51.49	-51.87	-52.56	-54.41	-61.57	-54.38	-52.58	-51.88	-51.49	
666	-51.49	-51.87	-52.56	-54.41	-61.57	-54.38	-52.58	-51.88	-51.49	
777	-51.49	-51.87	-52.56	-54.41	-61.57	-54.38	-52.58	-51.88	-51.49	
888	-51.49	-51.87	-52.56	-54.41	-61.57	-54.38	-52.58	-51.88	-51.49	
999	-51.49	-51.87	-52.56	-54.41	-61.57	-54.38	-52.58	-51.88	-51.49	
(km)	(-51.49)	(-51.87)	(-52.56)	(-54.41)	(-61.57)	(-54.38)	(-52.58)	(-51.88)	(-51.49)	

Fig. 5.1-7 The conductance of the thin sheet model is shown in Fig. 5.1-1. Values in the brackets indicate phase of E_x obtained using a one-dimensional model of the thin sheet. For details refer to Fig. 5.1-6.

5.2 Method of Imbedding for Two-Dimensional Conductivity Variation

The imbedding method for two-dimensional calculations is essentially the same as that for one-dimensional problems (Chapter IV). One-dimensional strips in a one-dimensional problem are now replaced by two-dimensional zones. The conductivity tensor in one-dimensional calculations has zero off-diagonal terms, while in the two-dimensional variation the off-diagonal terms are not necessarily zero.

The imbedding scheme for two-dimensional conductivity variation is shown in Fig. 5.2-1. Starting at the smallest scale, average properties of the medium surrounding the point of measurement are found. To find the average conductivity tensor, the electric fields E_x, E_y and current densities J_x, J_y at each grid point are first determined for the H_x incidence field and the H_y incidence field. Let us define: $\bar{E}_{x1} = \sum_i \sum_j (E_x)_{ij}$, $\bar{E}_{y1} = \sum_i \sum_j (E_y)_{ij}$, $\bar{J}_{x1} = \sum_i \sum_j (J_x)_{ij}$, $\bar{J}_{y1} = \sum_i \sum_j (J_y)_{ij}$ for the H_x incidence field and $\bar{E}_{x2} = \sum_i \sum_j (E_x)_{ij}$, $\bar{E}_{y2} = \sum_i \sum_j (E_y)_{ij}$, $\bar{J}_{x2} = \sum_i \sum_j (J_x)_{ij}$, $\bar{J}_{y2} = \sum_i \sum_j (J_y)_{ij}$ for the H_y incidence field. From these, average conductivity tensor is obtained as

$$\begin{bmatrix} \sigma_{xx} & \sigma_{xy} \\ \sigma_{yx} & \sigma_{yy} \end{bmatrix} = \begin{bmatrix} \bar{J}_{x1} & \bar{J}_{x2} \\ \bar{J}_{y1} & \bar{J}_{y2} \end{bmatrix} \begin{bmatrix} \bar{E}_{x1} & \bar{E}_{x2} \\ \bar{E}_{y1} & \bar{E}_{y2} \end{bmatrix}^{-1}$$

Similarly, average conductivity tensors at larger scales are determined. Having determined the conductivity tensors at all scales,

fields are computed from the largest to the smallest scale. First fields at the largest scale are calculated. Then the inner zone is replaced by a set of smaller zones. The field in the middle zone is recalculated using the outer zone fields as knowns. The process is continued until the smallest scale is reached at which conductivity variations represent the true variations in the conductivity values of the medium.

As mentioned earlier (Chapter IV), checking the imbedding solution for two-dimensional conductivity variation is not easy, as a 'true model solution' at a spacing equal to the spacing at the smallest scale of imbedding is very difficult or almost impossible. However, when $\sigma_s \rho_s$ is small, the distance over which a discontinuity in surface value affects the surface current and electric field variation is small. Therefore to check the imbedding solution a very conductive layered medium was used and the model solutions were obtained in the region made up of the inner zone and its surrounding region using a uniform grid size throughout (equal to the size of the grid at which the imbedded solution was obtained). The conductivity variation employed, the imbedding scheme used, and the region in which uniform spacing solutions were obtained are shown in Fig. 5.2-2. The results of this study are summarized in Figs. 5.2-3 to 5.2-12. From these we find that the agreement between the two solutions is quite good.

In the above example, conductivity in the middle region and outside were uniform. In the other example shown in Figs. 5.2-13 to 5.2-23 the conductivity variation is more complex. Even in this

case the imbedding solutions agree well with those obtained using uniform spacing throughout. There is no reason to expect the accuracy of the imbedding technique to be any worse in two dimensions than in one dimension, so the results shown in Chapter IV can probably serve as a good indication of the level of accuracy to be expected.

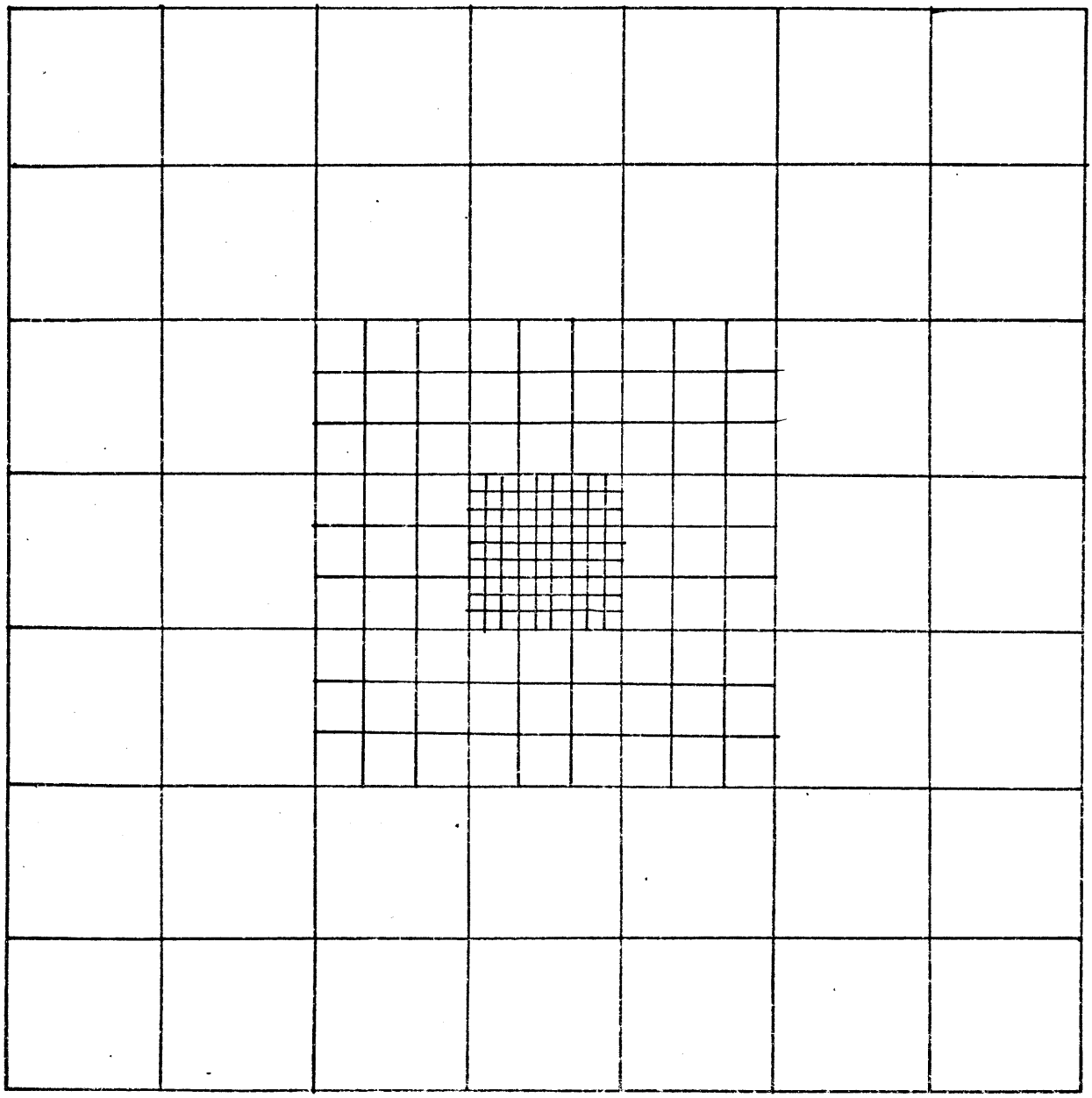

Fig. 5.2-1 Imbedding scheme for two-dimensional conductivity variation.

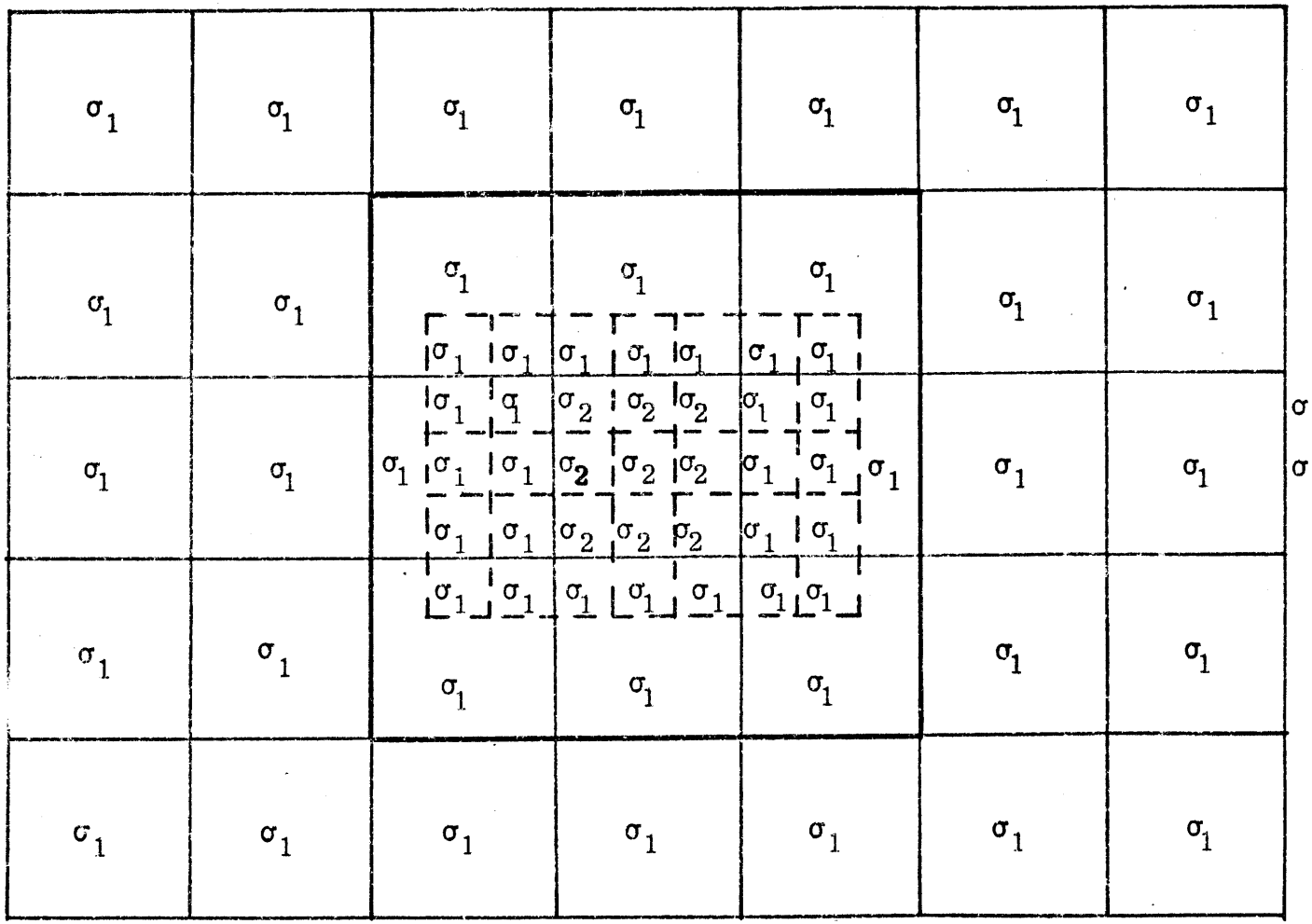

Fig. 5.2-2 Imbedding scheme used. σ_1 and σ_2 represent conductance of the grid in mhos. The region drawn in dashed lines represents the region in which the final (of 2 scale) imbedding solution is obtained. The region enclosed within the dark lines is the region in which uniform spacing solution was obtained.

Map of the Amplitude of the Electric Field (V/m)

$E_x \times 10^{-4}$

y \ x	-1800	-1200	-600	0	600	1200	1800	(km)
-1200	.0027	.0036	.0068	.0000	.0068	.0036	.0027	
-600	.0052	.0060	.0152	.0000	.0152	.0060	.0052	
0	.0000	.0000	.0000	.0000	.0000	.0000	.0000	
600	.0052	.0060	.0152	.0000	.0152	.0060	.0052	
1200	.0027	.0036	.0068	.0000	.0068	.0036	.0027	
(km)								

$E_y \times 10^{-4}$

y \ x	-1800	-1200	-600	0	600	1200	1800	(km)
-1200	.404	.404	.404	.404	.404	.404	.404	
-600	.404	.405	.405	.396	.405	.405	.404	
0	.405	.403	.422	.649	.422	.403	.405	
600	.404	.405	.405	.396	.405	.405	.404	
1200	.404	.404	.404	.404	.404	.404	.404	
(km)								

Source Field: Quasi-Uniform H_x. $T = 10^4$ secs.

Layered Medium

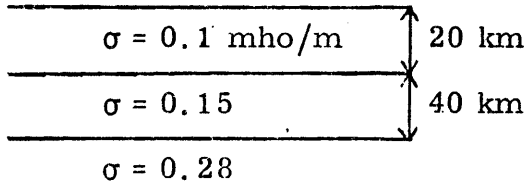

Fig. 5.2-3 Large scale 'imbedding' solution. Conductance of the thin sheet is given in Fig. 5.2-2. The region enclosed within the double lines represents the area in which 'uniform spacing' solution was obtained.

Map of the amplitude of the electric field (V/m)

E_x

y \ x	-600	-400	-200	0	200	400	600	(km)
-400	.008	.048	.042	0.0	.042	.048	.008	
	(.010)	(.046)	(.040)	(0.0)	(.040)	(.046)	(.010)	
-200	.003	.024	.038	0.0	.038	.024	.003	
	(.004)	(.024)	(.037)	(0.0)	(.037)	(.024)	(.004)	
0	0.0	0.0	0.0	0.0	0.0	0.0	0.0	
	(0.0)	(0.0)	(0.0)	(0.0)	(0.0)	(0.0)	(0.0)	
200	.003	.024	.038	0.0	.038	.024	.003	
	(.004)	(.024)	(.037)	(0.0)	(.037)	(.024)	(.004)	
400	(.008)	.048)	(.042)	0.0	.042	.048	.008	
(km)	(.010)	(.046	(.040)	0.0	(.040)	(.046)	(.010)	

E_y

y \ x	-600	-400	-200	0	200	400	600	(km)
-400	.410	.401	.372	.357	.372	.407	.410	
	(.4097)	(.4128)	(.3685)	(.3599)	(.3635)	(.4128)	(.4097)	
-200	.412	.461	.649	.707	.649	.461	.412	
	(.4129)	(.4596)	(.6539)	(.7064)	(.6539)	(.4596)	(.4129)	
0	.416	.455	.579	.638	.579	.455	.416	
	(.4167)	(.4568)	(.5779)	(.6409)	(.5779)	(.4568)	(.4167)	
200	.412	.461	.649	.707	.649	.461	.412	
	(.4129)	(.4596)	(.6539)	(.7064)	(.6539)	(.4596)	(.4129)	
400	.410	.407	.372	.357	.372	.407	.410	
(km)	(.4097)	(.4128)	(.3685)	(.3599)	(.3685)	(.4128)	(.4097)	

Source Field: Quasi-Uniform H_x

Fig. 5.2-4 Small scale 'imbedding' solution. The conductivity thickness product of the thin sheet is shown in Fig. 5.2-2. Values in the brackets indicate solution obtained using uniform spacing over the region shown in Fig. 5.2-2.

Map of the Phase of the Electric Field (degrees)

E_x

y \ x	-600	-400	-200	0	200	400	600
-400	144	-14	-18	-	162	166	-36
	(147)	(-17)	(-18)		(162)	(163)	(-33)
-200	126	-20	-37	-	143	160	-54
	(126)	(-22)	(-38)		(142)	(158)	(-54)
0	-	-	-	-	-	-	-
200	-54	160	143		-37	-20	126
	(-54)	(158)	(142)	-	(-38)	(-22)	(126)
400	-36	166	162		-18	-14	144
	(-33)	(163)	(162)	-	(-18)	(-17)	(147)

(km)

E_y

y \ x	-600	-400	-200	0	200	400	600
-400	153	152	151	149	151	152	153
	(153)	(153)	(150)	(149)	(150)	(152)	(153)
-200	154	152	131	129	131	152	154
	(153)	(152)	(132)	(130)	(132)	(152)	(153)
0	153	151	128	126	128	151	153
	(154)	(151)	(127)	(126)	(127)	(151)	(154)
200	154	152	131	129	131	152	154
	(153)	(152)	(132)	(130)	(132)	(152)	(153)
400	153	152	151	149	151	152	153
	(153)	(153)	(150)	(149)	(150)	(153)	(153)

(km)

Source field: Quasi-uniform H_x

Fig. 5.2-5 Small scale 'imbedding' solution. Values in the brackets indicate solution obtained using uniform spacing over the region shown in Fig. 5.2-2.

Map of the Amplitude of the Magnetic Field (At/m)

H_x

y \ x	-600	-400	-200	0	200	400	600	(Km)
-400	1.01	1.01	0.980	0.963	0.980	1.01	1.01	
	(1.014)	(1.020)	(0.974)	(0.964)	(0.974)	(1.020)	(1.014)	
-200	1.03	1.09	0.897	0.929	0.897	1.09	1.03	
	(1.027)	(1.092)	(0.901)	(0.932)	(0.901)	(1.092)	(1.027)	
0	1.03	1.09	0.891	0.929	0.891	1.09	1.03	
	(1.034)	(1.095)	(0.891)	(0.929)	(0.891)	(1.095)	(1.034)	
200	1.03	1.09	0.897	0.929	0.897	1.09	1.03	
	(1.027)	(1.092)	(0.901)	(0.932)	(0.901)	(1.092)	(1.027)	
400	1.01	1.01	0.980	0.963	0.980	1.01	1.01	
(Km)	(1.014)	(1.020)	(0.974)	(0.964)	(1.974)	(1.020)	(1.014)	

H_y

y \ x	-600	-400	-200	0	200	400	600	(Km)
	.010	.067	.062	0.0	.062	.067	.010	
	(.008)	(.064)	(.058)	(0.0)	058)	(.064)	(.008)	
	.006	.041	.030	0·0	.030	.041	.006	
	(.006)	(.040)	(.030)	(0.0)	(.030)	(.040)	(.006)	
	0.0	0.0	0.0	0.0	0.0	0.0	0.0	
	(0.0)	(0.0)	(0.0)	(0.0)	(0.0)	(0.0)	(0.0)	
	.006	.041	.030	0.0	.030	.041	.006	
	(.006)	(.040)	(.030)	(0.0)	(.030)	(.040)	(.006)	
	.010	.067	.062	0.0	.062	.067	.010	
(Km)	(.008)	(.064)	(.058)	(0.0)	(.058)	(.064)	(.008)	

Source Field: Quasi-Uniform H_x

Fig. 5.2-6 Small scale 'imbedding' solution. Values in the brackets refer to 'uniform spacing' solution. Refer to Fig. 5.2-2 for details.

Map of the Phase of Magnetic Field (Degrees)

H_x

y \ x	-600	-400	-200	0	200	400	600	(Km)
-400	0	0	0	0	0	0	0	
	(0)	(0)	(0)	(0)	(0)	(0)	(0)	
-200	1	-1	1	0	1	-1	1	
	(0)	(-2)	(1)	(0)	(1)	(-2)	(0)	
0	0	-2	2	0	2	-2	0	
	(0)	(-2)	(2)	(0)	(2)	(-2)	(0)	
200	1	-1	1	0	1	-1	1	
	(0)	(-2)	(1)	(0)	(1)	(-2)	(0)	
400	0	0	0	0	0	0	0	
(Km)	(0)	(0)	(0)	(0)	(0)	(0)	(0)	

H_y

y \ x	-600	-400	-200	0	200	400	600	(Km)
	86	-5	-9	-	171	175	-94	
	(103)	(-9)	(-10)	(-)	(170)	(171)	(-77)	
	58	-7	-9	-	171	173	-122	
	(64)	(-10)	(-11)	(-)	(169)	(170)	(-116)	
	-	-	-	-	-	-	-	
	(-)	(-)	(-)	(-)	(-)	(-)	(-)	
	-122	173	171	-	-9	-7	58	
	-116	(170)	(169)	(-)	(-11)	(-10)	(64)	
	-94	175	171	-	-9	-5	86	
(Km)	(-77)	(171)	(170)	(-)	(-10)	(-9)	(103)	

Source Field: Quasi-Uniform H_x

Fig. 5.2-7 Small scale 'imbedding' solution. Values in the brackets refer to solution obtained using uniform spacing throughout. Refer to Fig. 5.2-9 for details.

Map of the Amplitude of the Electric Field (V/m)

$E_x \times 10^{-4}$

y \ x	-1800	-1200	-600	0	600	1200	1800	(km)
-1200	.404	.404	.405	.404	.405	.404	.404	
-600	.404	.404	.405	.422	.405	.404	.404	
0	404	.405	.396	.650	.398	.405	.404	
600	.404	.404	.405	.422	.405	.404	.400	
1200	.404	.404	.405	.404	.405	.404	.404	
(km)								

$E_y \times 10^{-4}$

y \ x	-1800	-1200	-600	0	600	1200	1800	(km)
-1200	.0027	.0036	.0068	.0000	.0068	.0036	.0027	
-600	.0052	.0060	.0153	.0000	.0153	.0060	.0052	
0	.0000	.0000	.0000	.0000	.0000	.0000	.0000	
600	.0052	.0060	.0153	.0000	.0153	.0060	.0052	
1200	.0027	.0036	.0068	.0000	.0068	.0036	.0027	
(km)								

Source Field: Quasi-Uniform H_y. $T = 10^4$ secs

Layered Medium

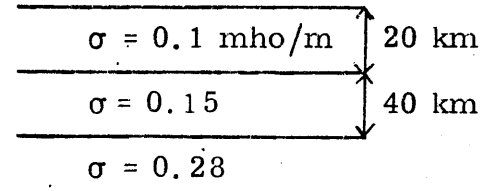

Fig. 5.2-8 Large scale 'imbedding' solution. Conductance of the thin sheet is given in Fig. 5.2-2. The region enclosed in double lines represents area in which 'uniform spacing' solution was obtained.

Map of the Amplitude of the Electric Field (V/m)

$E_x \times 10^{-4}$

y \ x	-600	-400	-200	0	200	400	600	(Km)
-400	.405	.408	.466	.456	.466	.408	.405	
	(.404)	(.413)	(.460)	(.457)	(.460)	(.413)	(.404)	
-200	.405	.371	.649	.579	.649	.371	.405	
	(.405)	(.369)	(.654)	(.578)	(.654)	(.369)	(.405)	
0	.403	.357	.709	.638	.709	.357	.403	
	(.405)	(.360)	(.706)	(.641)	(.706)	(.360)	(.405)	
200	.405	.371	.649	.579	.649	.371	.405	
	(.405)	(.369)	(.654)	(.578)	(.654)	(.369)	(.405)	
400	.405	.408	.466	.456	.466	.408	.405	
(Km)	(.404)	(.413)	(.460)	(.457)	(.460)	(.412)	(.404)	

$E_y \times 10^{-4}$

y \ x	-600	-400	-200	0	200	400	600	(Km)
	.008	.0402	.0243	0.0	.0243	.0402	.008	
	(.0106)	(.0457)	(.0243)	(0.0)	(.0243)	(.0457)	(.0106)	
	.0085	.0406	.0377	0.0	.0377	.0406	.0085	
	(.0077)	(.0398)	(.0374)	(0.0)	(.0374)	(.0398)	(.0077)	
	0.0	0.0	0.0	0.0	0.0	0.0	0.0	
	(0.0)	(0.0)	(0.0)	(0.0)	(0.0)	(0.0)	(0.0)	
	.0085	.0406	.0377	0.0	.0377	.0406	.0085	
	(.0077)	(.0398)	(.0374)	(0.0)	(.0374)	(.0398)	(.0077)	
	.008	.0402	.0243	0.0	.0243	.0402	.008	
(Km)	(.0106)	(.0457)	(.0243)	(0.0)	(.0243)	(.0457)	(.0106)	

Source Field: Quasi-Uniform H_y

Fig. 5.2-9 Small scale 'imbedding' solution. Values in the brackets refer to 'uniform spacing' solution. For details refer to Fig. 5.2-2.

Map of the Phase of the Electric Field (degrees)

E_x

y \ x	-600	-400	-200	0	200	400	600	(km)
-400	-27	-28	-27	-30	-27	-28	-27	
	(-27)	(-27)	(-28)	(-29)	(-28)	(-27)	(-27)	
-200	-27	-30	-49	-52	-49	-30	-27	
	(-28)	(-30)	(-48)	(-53)	(-48)	(-30)	(-28)	
0	-28	-31	-50	-54	-50	-31	-28	
	(-28)	(-31)	(-50)	(-54)	(-50)	(-31)	(-28)	
200	-27	-30	-49	-52	-49	-30	-27	
	(-28)	(-30)	(-48)	(-53)	(-48)	(-30)	(-28)	
400	-27	-28	-27	-30	-27	-28	-27	
	(-27)	(-27)	(-28)	(-29)	(-28)	(-27)	(-27)	

E_y

y \ x	-600	-400	-200	0	200	400	600	(km)
	-64	156	158	-	-22	-24	116	
	(-32)	(163)	(158)		(-22)	(-174)	(148)	
	-34	162	142	-	-38	-18	146	
	(-37)	(162)	(142)		(-38)	(-18)	(143)	
	-	-	-	-	-	-	-	
	146	-18	-38	-	142	162	-34	
	(143)	(-18)	(-38)		(142)	(162)	(-37)	
	116	-24	-22	-	158	156	-64	
	(148)	(-17)	(-22)		(158)	(163)	(-32)	

Source Field: Quasi-Uniform H_y

Fig. 5.2-10 Small scale 'imbedding' solution. Values in the brackets refer to 'uniform spacing' solution. For details refer to Fig. 5.2-2.

Map of the Amplitude of Magnetic Field (At/m)

H_x

y \ x	-600	-400	-200	0	200	400	600	(km)
-400	.013	.058	.040	0.0	.040	.058	.013	
	(.009)	(.064)	(.040)	(0.0)	(.040)	(.064)	(.009)	
-200	.008	.059	.030	0.0	.030	.059	.008	
	(.007)	(.058)	(.030)	(0.0)	(.030)	(.058)	(.007)	
0	0.0	0.0	0.0	0.0	0.0	0.0	0.0	
	(0.0)	(0.0)	(0.0)	(0.0)	(0.0)	(0.0)	(0.0)	
200	.008	.059	.030	0.0	.030	.059	.008	
	(.007)	(.058)	(.030)	(0.0)	(.030)	(.058)	(.007)	
400	.013	.058	.040	0.0	.040	.058	.013	
	(.009)	(.064)	(.040)	(0.0)	(.040)	(.064)	(.009)	

H_y

y \ x	-600	-400	-200	0	200	400	600	(km)
	1.00	1.00	1.10	1.09	1.10	1.01	1.00	
	(1.00)	(1.02)	(1.09)	(1.10)	(1.09)	(1.02)	(1.00)	
	0.993	0.977	0.898	0.892	0.898	0.977	0.993	
	(0.994)	(0.974)	(0.901)	(0.891)	(0.901)	(0.974)	(0.994)	
	0.984	0.961	0.931	0.929	0.931	0.961	0.984	
	(0.990)	(0.964)	(0.932)	(0.929)	(0.932)	(0.964)	(0.990)	
	0.993	0.977	0.898	0.892	0.898	0.977	0.993	
	(0.994)	(0.974)	(0.901)	(0.891)	(0.801)	(0.974)	(0.994)	
	1.00	1.01	1.10	1.09	1.10	1.01	1.00	
	(1.00)	(1.02)	(1.09)	(1.10)	(1.09)	(1.02)	(1.00)	

Source Field: Quasi-Uniform H_y

Fig. 5.2-11 Small scale 'imbedding' solution. Values in the brackets refer to 'uniform spacing' solution. For details refer to Fig. 5.2-2.

Map of the Phase of the Magnetic Field (degrees)

H_x

y \ x	-600	-400	-200	0	200	400	600	(Km)
-400	71	-12	-10	-	170	168	-109	
	(104)	(9)	(-10)		(170)	(171)	(-75)	
-200	104	-11	-11	-	169	169	-76	
	(94)	(-10)	(-11)		(169)	(170)	(-86)	
0	-	-	-	-	-	-	-	
200	-76	169	169	-	-11	-10	104	
	(-86)	(170)	(169)		(-11)	(-10)	(94)	
400	-109	168	170	-	-10	-12	71	
(Km)	(-75)	(171)	(170)		(-10)	(-9)	(105)	

H_y

y \ x	-600	-400	-200	0	200	400	600	(Km)
	0	0	-1	-2	-1	0	0	
	(0)	(0)	(-2)	(-2)	(-2)	(0)	(0)	
	0	0	1	2	1	0	0	
	(0)	(0)	(1)	(2)	(1)	(0)	(0)	
	0	0	0	0	0	0	0	
	(0)	(0)	(0)	(0)	(0)	(0)	(0)	
	0	0	1	2	1	0	0	
	(0)	(0)	(1)	(2)	(1)	(0)	(0)	
	0	0	-1	-2	-1	0	0	
(Km)	(0)	(0)	(-2)	(-2)	(-2)	(0)	(0)	

Source Field: Quasi-Uniform H_y

Fig. 5.2-12 Small scale 'imbedding' solution. Values in the brackets refer to 'uniform spacing' solution. For details refer to Fig. 5.2-2.

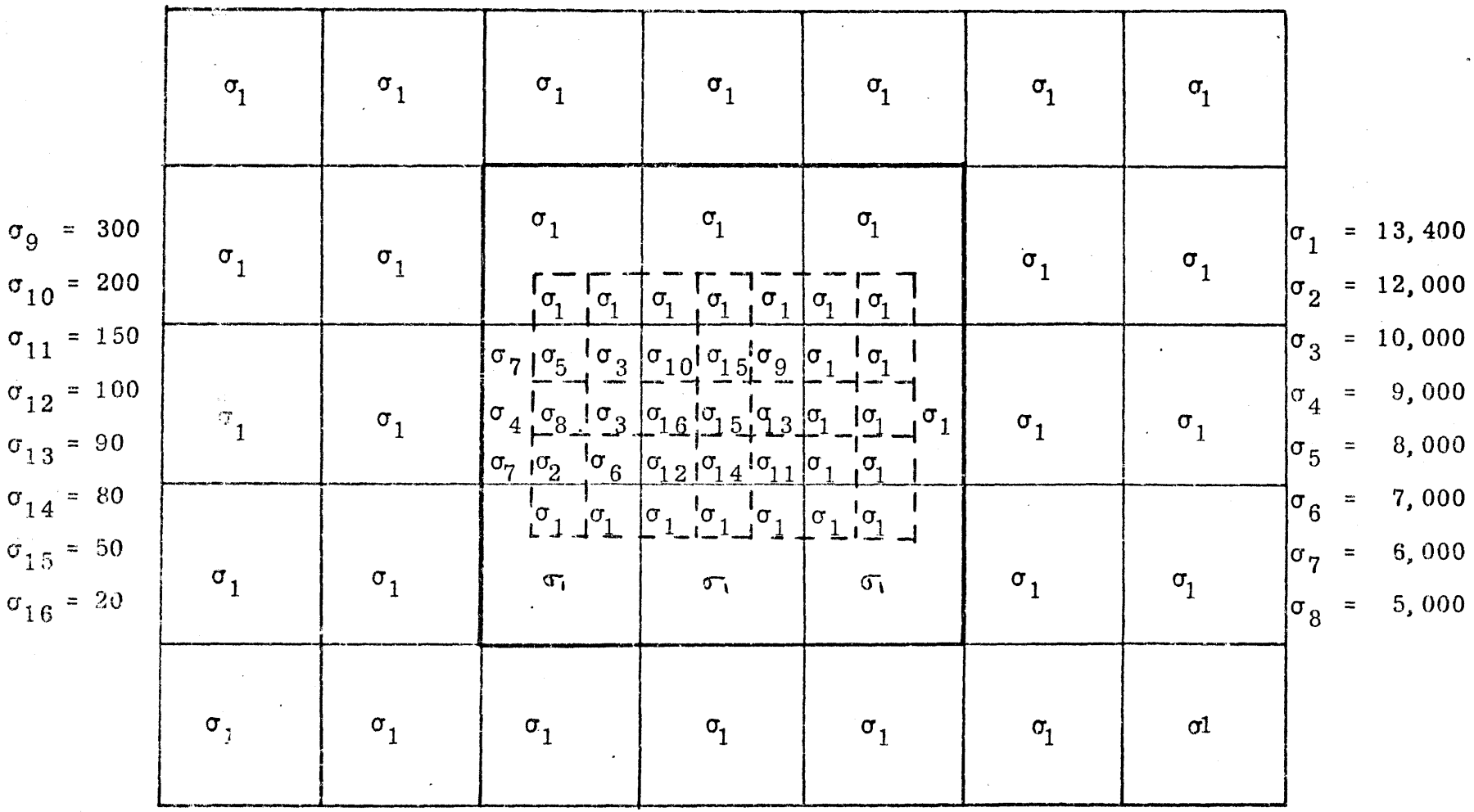

Fig. 5.2-13 Imbedding scheme used. σ_1, σ_2, etc. represent conductance of the grid in mhos. The region drawn in dashed lines represents the region in which the final (of 2 scale) imbedding solution is obtained. The region enclosed within the dark lines represents the area in which a 'uniform spacing' solution was obtained.

Map of the Amplitude of the Electric Field (V/m)

$E_x \times 10^{-4}$

y \ x	-1800	-1200	-600	0	600	1200	1800	(km)
-1200	.0017	.0017	.0068	.0022	.0057	.0028	.0019	
-600	.0034	.0020	.0154	.0048	.0135	.0044	.0037	
0	.0000	.0000	.0014	.0000	.0000	.0000	.0000	
600	.0035	.0020	.0152	.0049	.0135	.0040	.0037	
1200	.0017	.0017	.0068	.0022	.0057	.0028	.0019	

$E_y \times 10^{-4}$

y \ x	-1800	-1200	-600	0	600	1200	1800	(km)
-1200	.404	.404	.404	.404	.404	.404	.404	
-600	.405	.405	.403	.396	.406	.405	.405	
0	.405	.409	.508	.656	.422	.403	.405	
600	.405	.405	.403	.396	.405	.405	.405	
1200	.404	.404	.404	.404	.404	.404	.404	

Source Field: Quasi-Uniform H_x. $T = 10^4$ secs.

Layered Medium

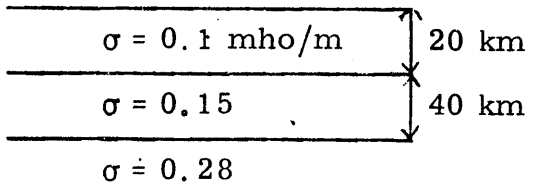

Fig. 5.2-14 Large scale 'imbedding' solution. Conductance of the thin sheet is given in 5.2-13. The region enclosed within the double line represents area in which 'uniform spacing' solution was obtained.

Map of the Amplitude of the Electric Field (V/m)

$E_x \times 10^{-4}$

y \ x	-600	-400	-200	0	200	400	600	(Km)
-400	.0140	.0455	.0279	.0026	.0458	.0440	.0055	
	(.0209)	(.0458)	(.0237)	(.0045)	(.0464)	(.0366)	(.0018)	
-200	.0088	.0036	.0403	.0084	.0349	.0266	.0050	
	(.0060)	(.0049)	(.0424)	(.0113)	(.0300)	(.0300)	(.0095)	
0	.0085	.0161	.0228	.0109	.0067	.0024	.0025	
	(.0125)	(.0150)	(.0226)	(.0118)	(.0082)	(.0040)	(.0046)	
200	.0064	.0084	.0378	.0066	.0354	.0258	.0039	
	(.0030)	(.0086)	(.0386)	(.0087)	(.0317)	(.0279)	(.0078)	
400	.0082	.05?1	.0161	.0069	.0494	.0421	.0035	
(Km)	(.0136)	(.0552)	(.0137)	(.0088)	(.0498)	(.0344)	(.0026)	

$E_y \times 10^{-4}$

y \ x	-600	-400	-200	0	200	400	600	(Km)
	.398	.404	.372	.358	.375	.406	.412	
	(.404)	(.410)	(.369)	(.362)	(.372)	(.413)	(.412)	
	.497	.517	.664	.707	.645	.460	.413	
	(.499)	(.519)	(.668)	(.709)	(.649)	(.462)	(.414)	
	.552	.513	.596	.647	.578	.458	.413	
	(.560)	(.511)	(.601)	(.647)	(.582)	(.460)	(.421)	
	.454	.559	.682	.705	.654	.458	.416	
	(.449)	(.564)	(.682)	(.708)	(.656)	(.460)	(.415)	
	.408	.395	.370	.360	.373	.408	.410	
(Km)	(.412)	(.318)	(.369)	(.363)	(.370)	(.414)	(.411)	

Source Field: Quasi-Uniform H_x

Fig. 5.2-15 Small scale 'imbedding' solution. Values in the brackets refer to 'uniform spacing' solution. For details refer to Fig. 5.2-13.

Map of the Phase of the Electric Field (degrees)

E_x

y \ x	-600	-400	-200	0	200	400	600	(km)
-400	157	-18	-23	-79	163	168	-30	
	(159)	(-21)	(-24)	(-24)	(162)	(164)	(-71)	
-200	122	-57	-45	119	149	156	-75	
	(145)	(-94)	(-42)	(143)	(143)	(158)	(-31)	
0	-52	-12	148	-33	141	-30	125	
	(-19)	(-13)	(15)	(-27)	(152)	(-7)	(167)	
200	-51	129	137	-49	-33	-22	111	
	(-34)	(112)	(137)	(-36)	(-38)	(-22)	(146)	
400	-14	165	145	150	-17	-12	159	
	(-28)	(161)	(148)	(160)	(-17)	(-17)	(25)	

E_y

y \ x	-600	-400	-200	0	200	400	600	(km)
	152	151	151	149	151	152	153	
	(151)	(152)	(149)	(149)	(150)	(153)	(153)	
	147	148	132	130	132	152	154	
	(146)	(148)	(132)	(130)	(132)	(152)	(154)	
	141	146	128	127	128	151	153	
	(143)	(146)	(128)	(126)	(128)	(151)	(154)	
	152	144	132	130	132	152	154	
	(150)	(145)	(132)	(130)	(132)	(152)	(154)	
	152	151	150	149	150	152	153	
	(152)	(151)	(149)	(149)	(150)	(153)	(153)	

Source Field: Quasi-Uniform H_x

Fig. 5.2-16 Small scale 'imbedding' solution. Values in the brackets refer to 'uniform spacing' solution. For details refer to Fig. 5.2-13.

Map of the Amplitude of the Magnetic Field (At/m)

H_x

y \ x	-600	-400	-200	0	200	400	600	(Km)
-400	1.00	1.01	0.982	0.964	0.984	1.01	1.01	
	(1.01)	(1.02)	(0.977)	(0.967)	(0.979)	(1.02)	(1.02)	
-200	1.00	1.03	0.918	0.934	0.904	1.09	1.03	
	(1.01)	(1.08)	(0.922)	(0.939)	(0.909)	(1.10)	(1.03)	
0	0.970	1.09	0.911	0.938	0.894	1.09	1.03	
	(0.981)	(1.09)	(0.915)	(0.938)	(0.897)	(1.10)	(1.05)	
200	1.06	1.03	0.926	0.935	0.905	1.09	1.03	
	(1.05)	(1.04)	(0.928)	(0.941)	(0.909)	(1.10)	(1.04)	
400	1.01	1.00	0.980	0.967	0.981	1.01	1.01	
(Km)	(1.02)	(1.01)	(0.977)	(0.969)	(0.977)	(1.02)	(1.02)	

H_y

y \ x	-600	-400	-200	0	200	400	600	(Km)
	.012	.060	.043	.005	.066	.064	.008	
	(.018)	(.058)	(.039)	(.003)	(.065)	(.054)	(.005)	
	.008	.013	.026	.004	.031	.042	.009	
	(.005)	(.012)	(.027)	(.005)	(.029)	(.045)	(.007)	
	.007	.015	.010	.004	.002	.002	.003	
	(.010)	(.015)	(.010)	(.004)	(.003)	(.003)	(.005)	
	.007	.015	.027	.004	.031	.041	.007	
	(.004)	(.014)	(.027)	(.005)	(.028)	(.043)	(.006)	
	.006	.074	.029	.006	.069	.062	.007	
(Km)	(.011)	(.070)	(.027)	(.007)	(.068)	(.052)	(.007)	

Source Field: Quasi-Uniform H_x

Fig. 5.2-17 Small scale 'imbedding' solution. Values in the brackets refer to 'uniform spacing' solution. For details refer to Fig. 5.2-13.

Map of the Phase of Magnetic Field (Degrees)

y \ x	-600	-400	-200	0	200	400	600	(Km)
-400	0	0	0	0	0	0	0	
	(0)	(0)	(0)	(0)	(0)	(0)	(0)	
-200	0	-2	1	0	1	1	1	
	(0)	(-2)	(1)	(0)	(1)	(-1)	(1)	
0	0	-2	2	0	2	2	0	
	(1)	(-2)	(2)	(0)	(2)	(-2)	(1)	
200	0	-1	1	0	1	-1	1	
	(-1)	(-1)	(1)	(0)	(1)	(-1)	(1)	
400	0	0	0	0	0	0	0	
(Km)	(0)	(0)	(0)	(0)	(0)	(0)	(0)	

y \ x	-600	-400	-200	0	200	400	600	(Km)
	125	-10	-14	-114	173	177	-108	
	(146)	(-16)	(-15)	(-65)	(170)	(173)	(-137)	
	90	-4	-22	165	175	170	-115	
	78	(-19)	(-22)	(172)	(172)	(169)	(-55)	
	-32	-9	161	-30	150	-35	126	
	(-9)	(-9)	(162)	(-23)	(162)	(-9)	(168)	
	-80	168	161	-5	-6	-9	62	
	(-106)	(157)	(160)	(-5)	(-9)	(-12)	(118)	
	-91	171	162	119	-8	-2	55	
(Km)	(-59)	(166)	(164)	(141)	(-10)	(-7)	(21)	

Source Field: Quasi-Uniform H_x

Fig. 5.2-18 Small scale 'imbedding' solution. Values in the brackets reflect 'uniform spacing' solution. For details refer to Fig. 5.2-13.

Map of the Amplitude of the Electric Field (V/m)

$E_x \times 10^{-4}$

y \ x	-1800	-1200	-600	0	600	1200	1800	(km)
-1200	.404	.405	.404	.404	.405	.404	.404	
-600	.404	.404	.411	.422	.405	.404	.404	
0	.404	.403	.477	.645	.396	.405	.404	
600	.404	.404	.411	.422	.405	.404	.404	
1200	.404	.405	.405	.404	.405	.404	.404	
(km)								

$E_y \times 10^{-4}$

y \ x	-1800	-1200	-600	0	600	1200	1800	(km)
-1200	.0017	.0018	.0067	.0020	.0057	.0028	.0019	
-600	.0035	.0021	.0150	.0046	.0133	.0044	.0037	
0	.0000	.0000	.0013	.0001	.0000	.0000	.0000	
600	.0035	.0021	.015	.0046	.0133	.0044	.0037	
1200	.0017	.0018	.0067	.0020	.0057	.0028	.0019	
(km)								

Source Field: Quasi-Uniform H_y. $T = 10^4$ secs.

Layered Medium

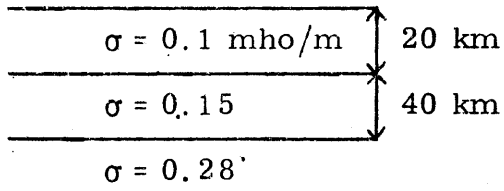

Fig. 5.2-19 Large scale 'imbedding' solution. Conductance of the thin sheet is given in Fig. 5.2-13. The region enclosed in double lines represents area in which 'uniform spacing' solution was obtained.

Map of the Amplitude of the Electric Field (V/m)

$E_x \times 10^{-4}$

y \ x	-600	-400	-200	0	200	400	600	(Km)
-400	.421	.422	.463	.455	.465	.406	.406	
	(.420)	(.426)	(.458)	(.457)	(.459)	(.412)	(.404)	
-200	.492	.405	.640	.582	.641	.372	.405	
	(.484)	(.407)	(.643)	(.583)	(.644)	(.370)	(.406)	
0	.519	.405	.700	.639	.701	.360	.400	
	(.538)	(.401)	(.703)	(.637)	(.701)	(.360)	(.405)	
200	.428	.460	.630	.578	.648	.369	.408	
	(.417)	(.464)	(.630)	(.580)	(.650)	(.367)	(.407)	
400	.410	.428	.463	.457	.464	.409	.404	
(Km)	(.413)	(.430)	(.459)	(.458)	(.458)	(.413)	(.404)	

$E_y \times 10^{-4}$

y \ x	-600	-400	-200	0	200	400	600	(Km)
	.0096	.0347	.0146	.0028	.0276	.0371	.0053	
	(.0214)	(.0430)	(.0106)	(.0072)	(.0324)	(.0363)	(.0025)	
	.0219	.0226	.0420	.0067	.0355	.0411	.0103	
	(.0010)	(.0192)	(.0450)	(.0098)	(.0300)	(.0431)	(.0133)	
	.0166	.0110	.0178	.0073	.0045	.0015	.0026	
	(.0106)	(.0115)	(.0195)	(.0093)	(.0070)	(.0032)	(.0048)	
	.0135	.0286	.0335	.0028	.0375	.0408	.0093	
	(.0051)	(.0254)	(.0353)	(.0044)	(.0380)	(.0417)	(.0116)	
	.0062	.0414	.0063	.0070	.0300	.0358	.0041	
(Km)	(.0159)	(.0502)	(.0040)	(.0118)	(.0353)	(.0338)	(.0022)	

Source Field: Quasi-Uniform H_y

Fig. 5.2-20 Large scale 'imbedding' solution. Values in the brackets refer to 'uniform spacing' solution. For details refer to Fig. 5.2-13.

Map of the Phase of the Electric Field (degrees)

y \ x	-600	-400	-200	0	200	400	600	(km)
-400	-26	-28	-27	-30	-27	-29	-27	
	(-27)	(-27)	(-28)	(-29)	(-28)	(-27)	(-27)	
-200	-35	-35	-49	-52	-48	-30	-27	
	(-35)	(-35)	(-49)	(-52)	(-48)	(-30)	(-28)	
0	-41	-36	-52	-54	-50	-31	-28	
	(-39)	(-37)	(-51)	(-54)	(-50)	(-32)	(-28)	
200	-30	-38	-50	-52	-48	-30	-27	
	(-32)	(-37)	(-50)	(-52)	(-48)	(-31)	(-28)	
400	-27	-28	-28	-29	-27	-28	-27	
	(-27)	(-27)	(-28)	(-29)	(-28)	(-27)	(-27)	

y \ x	-600	-400	-200	0	200	400	600	(km)
	-31	147	161	126	-26	-21	110	
	(-20)	(158)	(144)	(164)	(-21)	(-16)	(129)	
	-18	151	136	-60	-33	-20	136	
	(-32)	(149)	(139)	(-38)	(-38)	(-19)	(151)	
	171	166	-37	138	-54	132	-46	
	(158)	(165)	(-32)	(151)	(-27)	(173)	(-12)	
	163	-33	-45	110	144	161	-39	
	(141)	(-34)	(-45)	(129)	(144)	(161)	(-31)	
	93	-29	-30	-30	154	159	-85	
	(157)	(-21)	(-81)	(-15)	(160)	(163)	(-144)	

Source Field: Quasi-Uniform H_y

Fig. 5.2-21 Small scale 'imbedding' solution. Values in the brackets refer to 'uniform spacing' solution. For details refer to Fig. 5.2-13.

Map of the Amplitude of the Magnetic Field (At/m)

H_x

y \ x	-600	-400	-200	0	200	400	600	(Km)
-400	.008	.047	.028	.003	.043	.055	.011	
	(.019)	(.055)	(.023)	(.006)	(.048)	(.054)	(.004)	
-200	.014	.032	.028	.003	.031	.059	.010	
	(.006)	(.029)	(.029)	(.004)	(.028)	(.061)	(.011)	
0	.013	.011	.008	.002	.002	.001	.003	
	(.008)	(.011)	(.009)	(.003)	(.003)	(.003)	(.005)	
200	.010	.032	.025	.002	.031	.059	.009	
	(.005)	(.030)	(.026)	(.002)	(.029)	(.059)	(.009)	
400	.013	.055	.018	.006	.046	.054	.011	
(Km)	(.012)	(.064)	(.013)	(.010)	(.051)	(.051)	(.007)	

H_y

y \ x	-600	-400	-200	0	200	400	600	(Km)
	1.03	1.04	1.10	1.09	1.10	1.01	1.00	
	(1.03)	(1.04)	(1.09)	(1.10)	(1.09)	(1.02)	(1.00)	
	0.972	0.953	0.898	0.893	0.900	0.978	0.993)	
	(0.969)	(0.954)	(0.901)	(0.892)	(0.903)	(0.975)	(0.991)	
	.912	.957	.925	.927	.928	.963	.982	
	(.933)	(.952)	(.929)	(.926)	(.930)	(.963)	(.987)	
	1.01	.935	.895	.889	.901	.973	.997	
	(.997)	(.939)	(.895)	(.890)	(.902)	(.972)	(.993)	
	1.02	1.04	1.10	1.09	1.10	1.01	1.00	
(Km)	(1.02)	(1.05)	(1.09)	(1.10)	(1.09)	(1.02)	(1.00)	

Source Field: Quasi-Uniform H_y

Fig. 5.2-22 Small scale 'imbedding' solution. Values in the brackets refer to 'uniform spacing' solution. For details refer to Fig. 5.2-13.

Map of the Phase of Magnetic Field (degrees)

y \ x	-600	-400	-200	0	200	400	600	(Km)
-400	111	-22	-10	-91	168	170	-120	
	(149)	(-16)	(-16)	(-26)	(169)	(172)	(-125)	
-200	158	-17	-21	157	171	169	-78	
	(98)	(-15)		(-20)	(171)	(169)	(-47)	
0	2	-6	155	-44	134	-60	138	
	(-15)	(-11)	(159)	(-28)	(163)	(-8)	(170)	
200	-20	160	161	-8	-10	-11	103	
	(-11)	(162)	(161)	(-12)	(-9)	(-11)	(129)	
400	-127	10	170	133	-13	-9	50	
(Km)	(-45)	(165)	(163)	(158)	(-11)	(-8)	(26)	

y \ x	-600	-400	-200	0	200	400	600	(Km)
	0	0	-1	-2	-1	0	0	
	(0)	(0)	(-1)	(-2)	(-1)	(0)	(0)	
	-1	0	1	2	1	0	0	
	(-1)	(0)	(1)	(1)	(1)	(0)	(0)	
	0	-1	0	0	0	0	0	
	(0)	(-1)	(0)	(0)	(0)	(0)	(0)	
	0	0	1	2	1	0	0	
	(-1)	(0)	(1)	(1)	(1)	(0)	(0)	
	0	0	-1	-2	-1	(0)	(0)	
(Km)	(0)	(0)	(-2)	(-2)	(-2)	(0)	(0)	

Source Field: Quasi-Uniform H_y

Fig. 5.2-23 Small scale 'imbedding' solution. Values in the brackets refer to 'uniform spacing' solution. For details refer to Fig. 5.2-13.

5.3 Application to the Magnetotelluric Measurements on Oahu, Hawaii

Larsen (1975) computed the E over B response of low frequency (0.1 - 6 cpd) magnetotelluric measurements on the island of Oahu. He corrected for the island effect by treating the disturbance field to be essentially static and by pinning the low frequency impedance to the value obtained from magnetic variation studies. The conductivity model of the earth that he obtained by applying Schmucker's inversion scheme to his data is shown in Table 5.3-1. In our study we used the same conductivity model for the layered medium but the top 20 km was assumed to have a conductivity of 10^{-10} mho/m so that the electric currents in the surface sheet remain essentially in the surface sheet as in Price's model. We assumed the ocean depth to be 5,500 meters and the thickness of the ocean sediments to be 200 m. The ocean and its sediments therefore had a conductivity thickness product of 17,810 mhos (conductivity of the ocean water was taken as 3.32 mho/m and the conductivity of the ocean sediments was set at 1 mho/m). Island conductivity was taken as 0.036 mho/m (see Larsen, 1975), which gave the conductance of the island as 191 mhos.

In Fig. 5.3-1 is shown the bathymetry map of the Hawaiian islands. The region over which the large scale solution was obtained was much larger than the region shown in the figure. The region enclosed within the dark line represents the area in which the final small scale solution was obtained. Because of the still rather large grid size (55.5 km), average conductivity tensors (obtained

from much smaller grid spacing of 18.5 km) were used even at the final scale. (A two scale imbedding scheme was used.) The impedance obtained therefore gives the average value for the island and its surrounding shallow ocean. The conductivity model is shown in Fig. 5.3-2.

To check the reasonableness of the calculations, E-fields were computed for different values of resistivity of the resistive sheet. The average amplitude of E fields within the middle 3 x 5 grids was compared with the corresponding solution for the one-dimensional model of the rise discussed in Chapter III. For example, average E_x was compared with E_{11} (i.e. E_y) of the one-dimensional model (Chapter III). Average amplitude of E_y was compared with $|E_\perp|$ (i.e. $|E_x|$) of the one-dimensional model. When the resistivity thickness product of the resistive sheet was 2×10^9 ohm-m-m, the average amplitudes of E_x and E_y (within the middle 3 x 5 grids) were 0.33×10^{-4} and 0.69×10^{-4}, which compare well with 0.3×10^{-4} and 0.78×10^{-4} that were the amplitudes of $E_\parallel$ and $E_\perp$ for the one-dimensional model (for the same ρ_s and frequency, Chapter III).

Varying the resistivity value of the resistive sheet from 10^{-3} to 10^{-5} did not have any profound effect on the surface electric field variation (just as in the one-dimensional model). The surface electric field variation for a resistivity of 10^{10} ohm-m (of the resistive sheet) was about the same as that at a resistivity of 10^5 ohm-m. This is probably due to the dimensions of the resistive zones being much smaller than the adjustment distance, so that much

of the current would flow around the resistive zones rather than go down into the mantle. Some changes did occur in the one-dimensional models when the $\rho\sigma$ values were much smaller, but since these effects are relatively frequency-independent and since we cannot compare the absolute values of our results with Larsen's, we did not incorporate small $\rho\sigma$ values in the two-dimensional models.

E over B response was calculated for six frequencies. The Hawaiian rise has a fairly well defined strike direction. The calculated impedance was therefore rotated into the direction which maximized Cagniard elements of the impedance tensor (Swift, 1967) so that we could obtain two principal impedance values, one parallel to the strike and the other perpendicular to the strike. These values are tabulated in Table 5.3-2 along with the impedance on the surface of the (uniform) ocean.

To compare our predictions with Larsen's data the computed impedances were rotated into the geographic coordinate system so that y represented the true north and x represented the true east. From these tensors (defined for geographic coordinates) the following four quantities were determined:

$$Z_1 = \frac{Z_{xx} + Z_{yy}}{2} \qquad Z_2 = \frac{Z_{xy} + Z_{yx}}{2}$$

$$Z_3 = \frac{Z_{xy} - Z_{yx}}{2} \qquad Z_4 = \frac{Z_{xx} - Z_{yy}}{2}$$

In Table 5.3-3 are listed the calculated amplitudes and phases of Z_1,

Z_2, Z_3, Z_4 along with those observed on Oahu (Larsen, 1975).

From Table 5.3-3 we see that the amplitude of the impedance calculated on the basis of the layered model given by Larsen is much smaller than the observed values. In Larsen's calculations the ocean was assumed to have a uniform conductance of 15,800 mhos, whereas in our model the ocean was assumed to have a uniform conductance of 17,810 mhos. Reducing the conductance of the ocean to 15,800 mhos reduced the impedance calculated on the island. Changing the island conductivity from 0.036 mho/m to 0.0036 mho/m changed the surface E-field amplitude by less than a percent. Therefore the differences in the measured and calculated impedances do not appear to be due to differences in the thin sheet model.

These differences could be due to various reasons. First of all the calculated impedance is the average impedance for the entire island and a small portion of the shallow ocean (as shown in Fig. 5.2-1). Therefore the calculated impedance is expected to be lower than the island value. However, the difference is not expected to be too great. Secondly, electric fields are greatly affected by local conductivity and resistivity variations. Hence the measured impedance could be reflecting the local conductivity and resistivity variations. Thirdly, in Larsen's calculations, mutual-induction and self-induction terms were neglected, whereas in our calculations no term was dropped. It is known that including mutual- and self-induction terms reduces the currents and therefore the E-fields in the surface sheet (Bullard and Parker, 1970; Honkura,

1972). Finally, part of the difference could be due to the method in which island effect was corrected by Larsen. He assumed that the magnetic field on the island was the same as that at half the depth of the ocean. In our calculations the magnetic field on the island is slightly lower than at the ocean. Further study is necessary to determine the contribution of each one of the above possible causes. Of all these effects none other than that of local resistivity variations can account for the large discrepancy. Larsen realized this problem and bypassed it by pinning his results to the extra low frequency impedance determined by magnetic variation studies. The phase and frequency variations of the impedance are not dependent on local effects, however, and therefore critical comparisons can be made between our results and Larsen's.

Figures 5.3-3 to 5.3-8 show the comparison between the calculated and the observed amplitudes and phases. From Figs. 5.3-3 to 5.3-5 we see that the agreement between observed impedance and the impedance at half the ocean depth is good. The comparison between the slopes of calculated and observed impedances shows that towards the high frequency the calculated slope is higher than the observed slope. The comparison between the observed and calculated phases (Figs. 5.3-7 and 5.3-8) also shows that the difference is higher towards the high frequency end. This phase difference is maximum in the case of Z_2. These differences could be due to induction effects which were neglected by Larsen while correcting for the island effect. From amplitudes (ratios) and phases listed in Table 5.3-2 we see that the induction effect cannot be

neglected. Larsen's model therefore needs a slight modification. The conductivity of the top layers should be slightly increased.

Thus we see that the induction effects which were neglected by Larsen cannot be neglected towards the high frequency end of the frequency range he studied.

The actual values of the impedance calculated are much smaller than those observed. The discrepancy between the measured and calculated impedance values can be explained in several ways. The most important of these are: (1) The calculated impedance is low because it is the average value and does not take into consideration the actual variations in the conductivity at the point of measurement. (2) The measured impedance is high because of the conductivity and resistivity variations at the point of measurement. (3) Error caused by pinning. In order to obtain island correction Larsen pinned his result to low frequency impedance determined by magnetic variation studies. The accuracy of the pinning impedance is not known.

The first possibility can be eliminated by computing the impedance at much closer spacings (by using one more 'smaller' scale imbedding). To eliminate the second possibility, E-fields should be measured at a number of locations on the island to determine if high E-fields are peculiar to the measurement point. If these two possibilities are eliminated, the discrepancy between the calculated and measured values can be attributed to the third possibility. In such a case a new conductivity model would have to be determined. Such a model would have to have lower conductivities than Larsen's model.

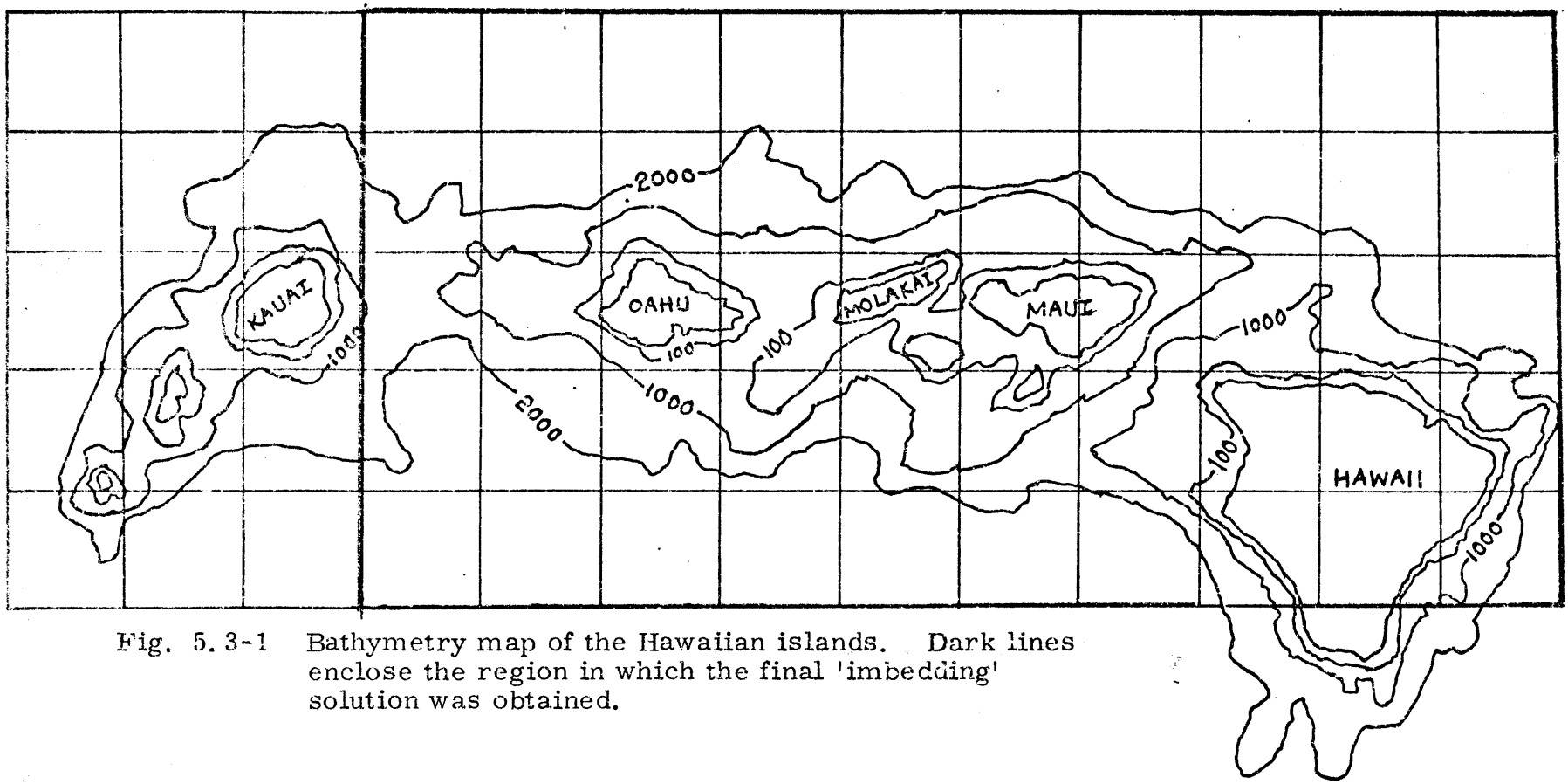

Fig. 5.3-1 Bathymetry map of the Hawaiian islands. Dark lines enclose the region in which the final 'imbedding' solution was obtained.

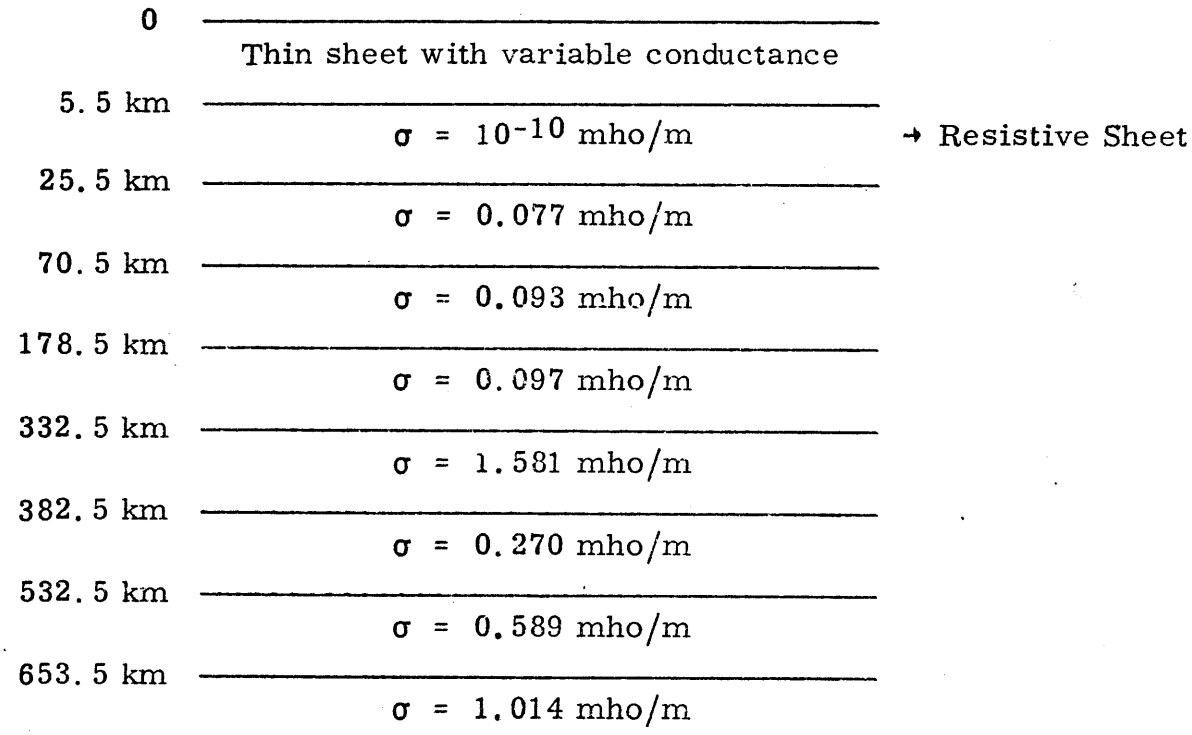

Fig. 5.3-2 Conductivity Model

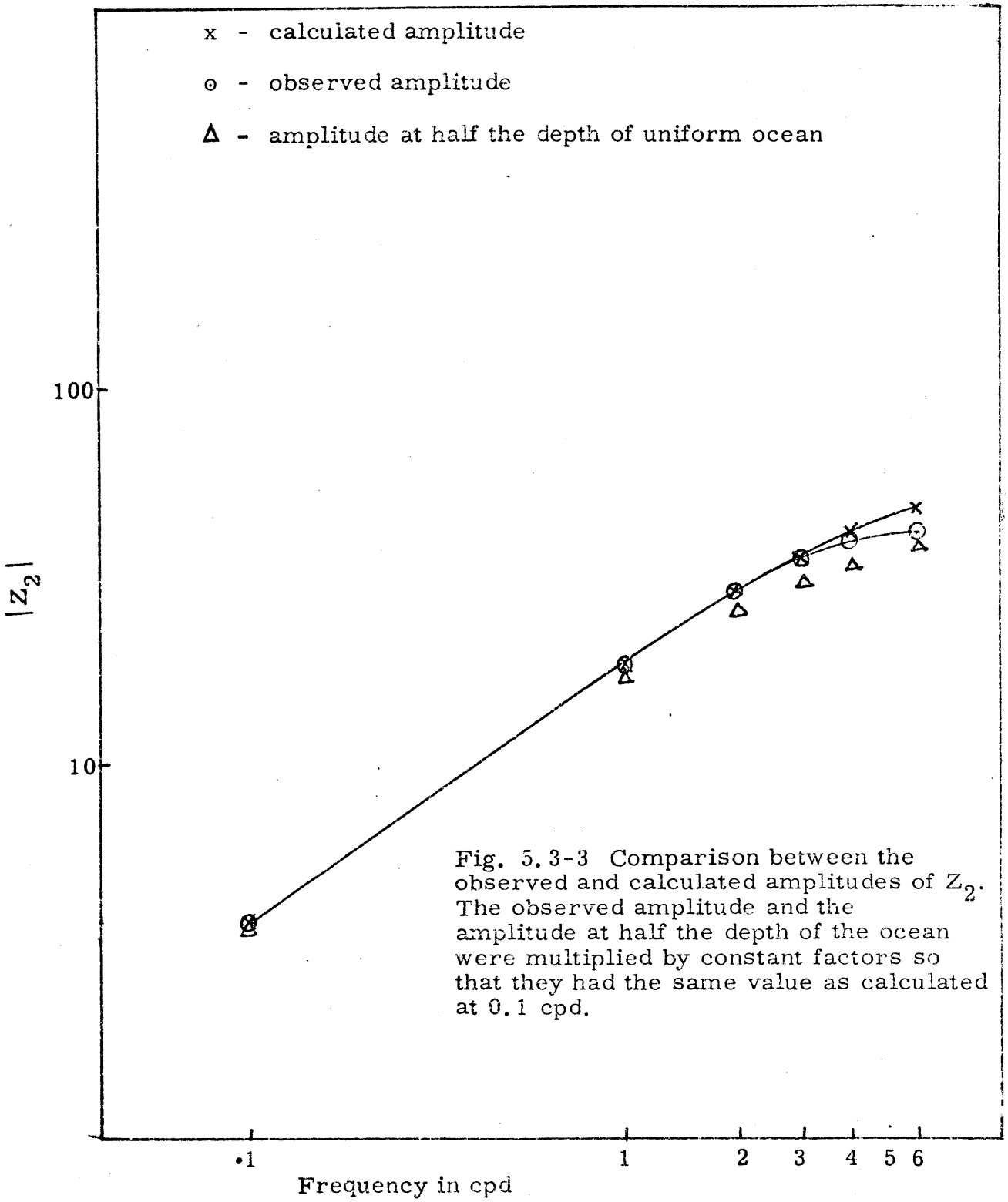

Fig. 5.3-3 Comparison between the observed and calculated amplitudes of Z_2. The observed amplitude and the amplitude at half the depth of the ocean were multiplied by constant factors so that they had the same value as calculated at 0.1 cpd.

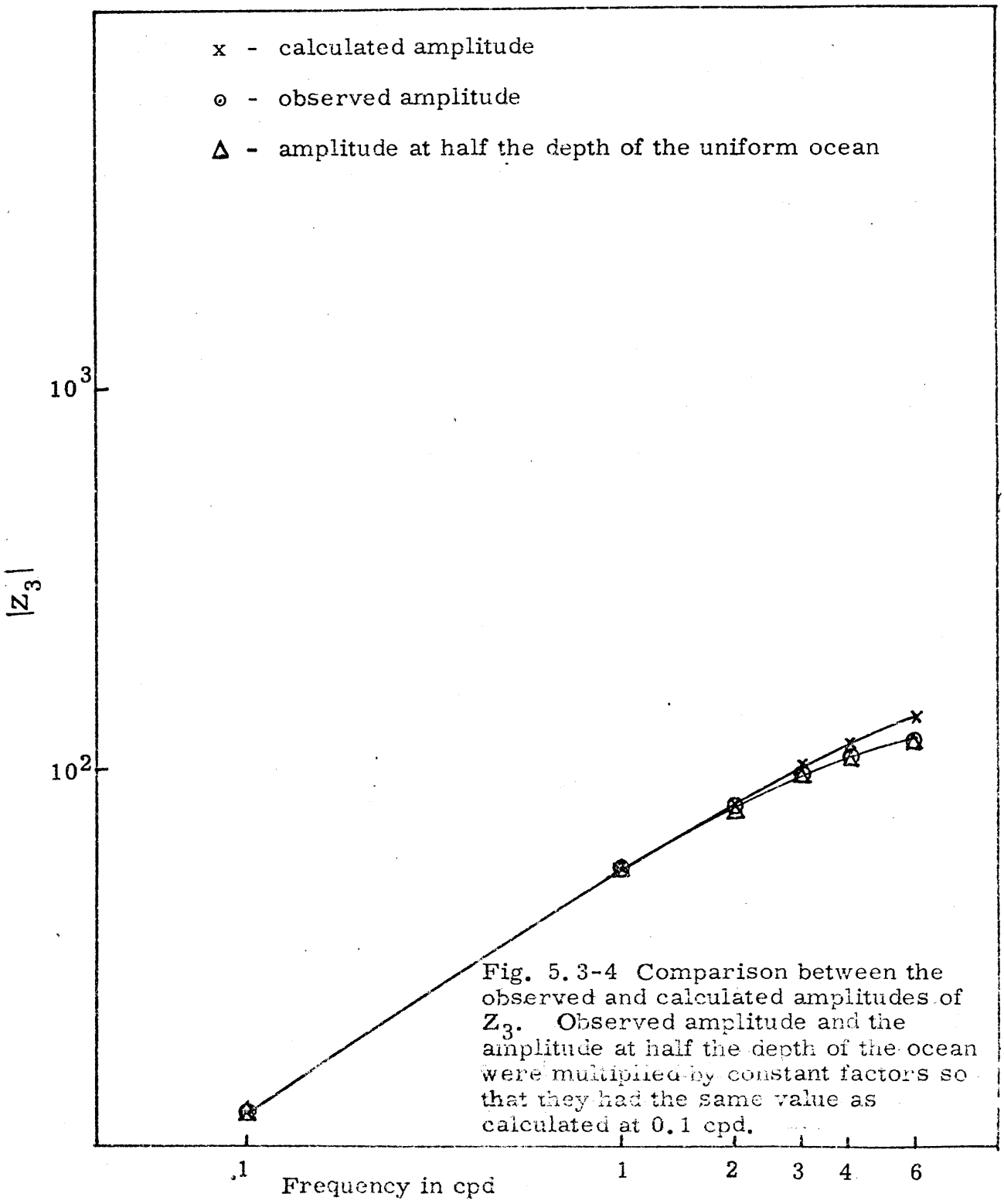

Fig. 5.3-4 Comparison between the observed and calculated amplitudes of Z_3. Observed amplitude and the amplitude at half the depth of the ocean were multiplied by constant factors so that they had the same value as calculated at 0.1 cpd.

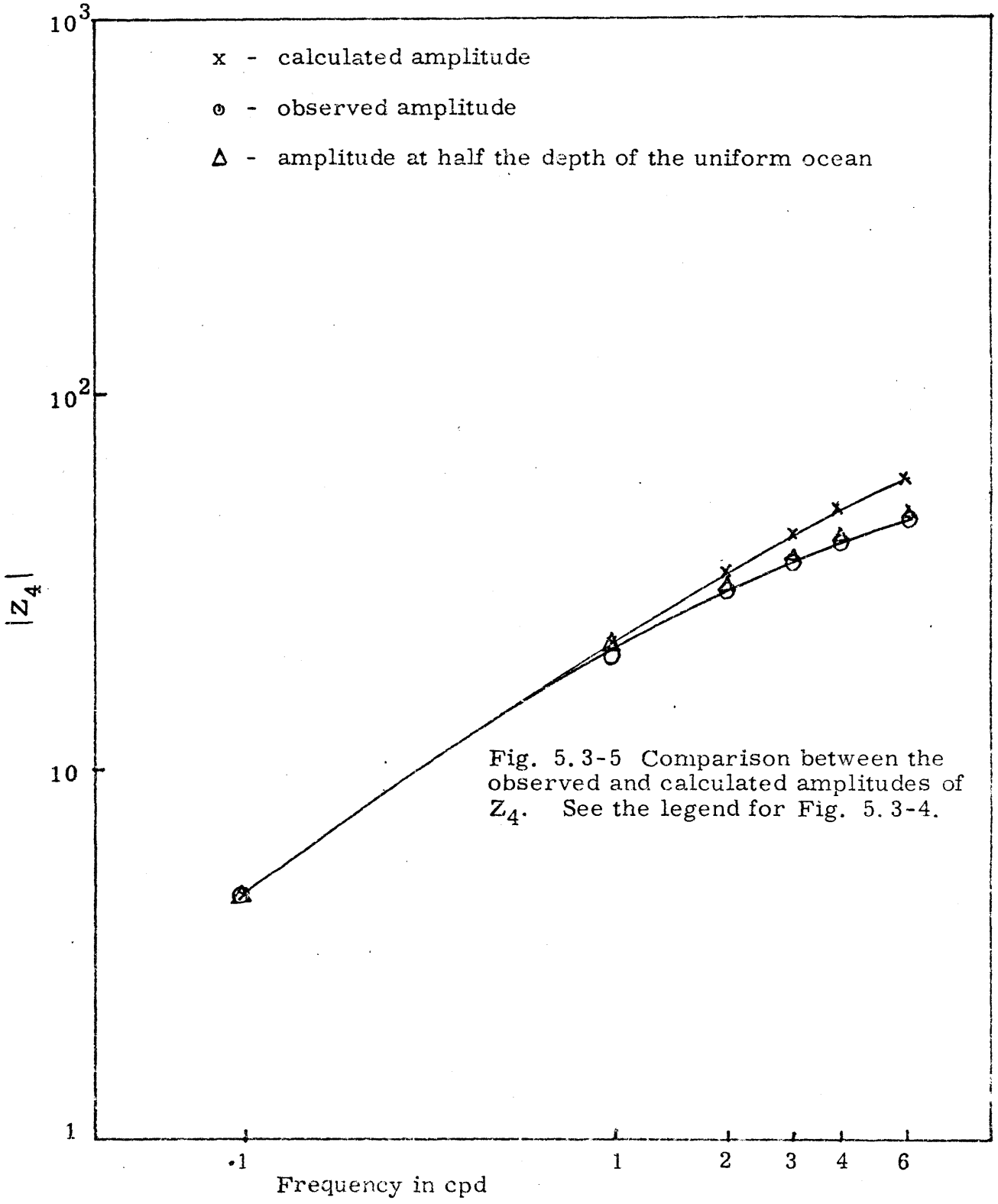

Fig. 5.3-5 Comparison between the observed and calculated amplitudes of Z_4. See the legend for Fig. 5.3-4.

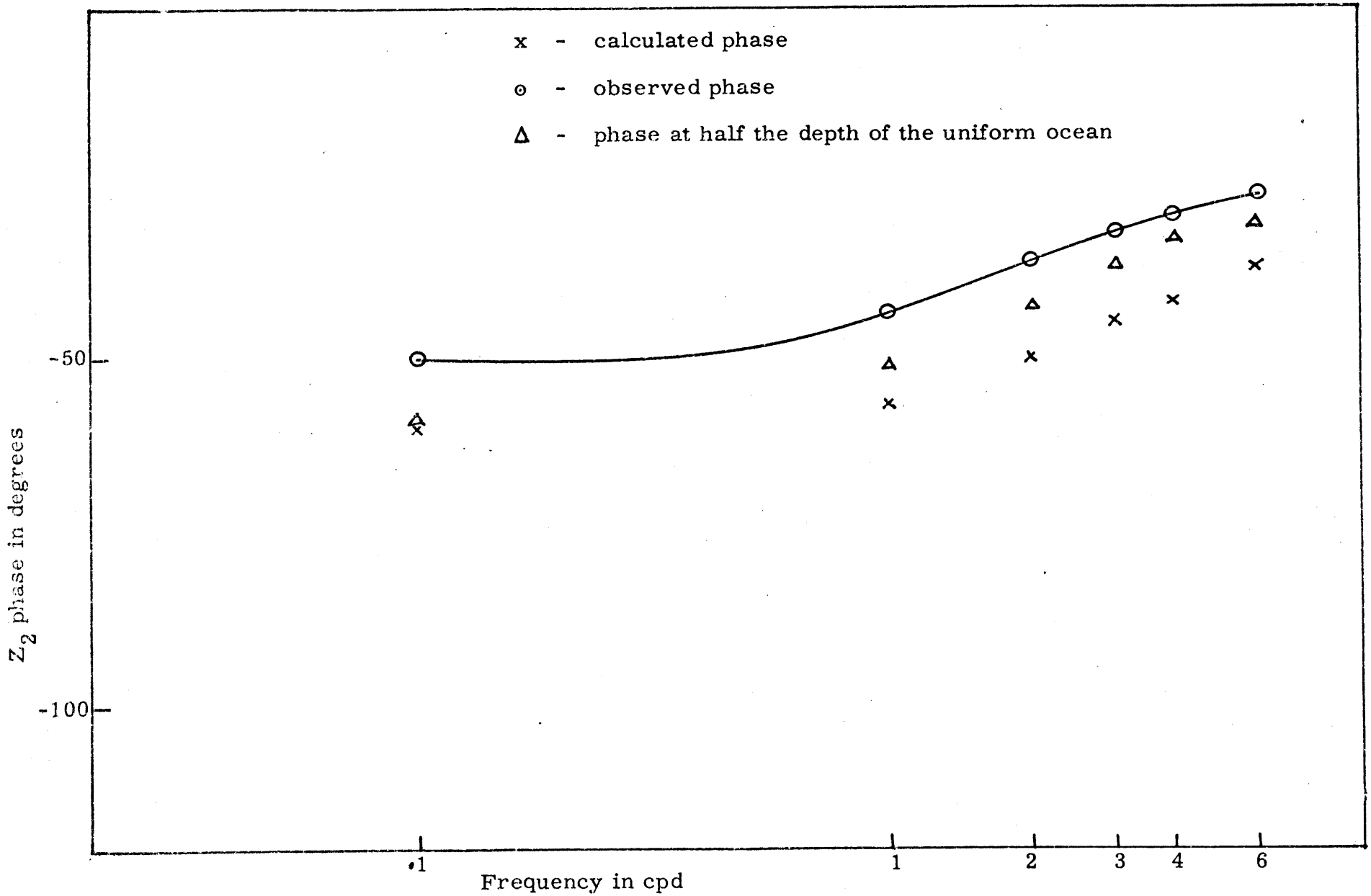

Fig. 5.3-6 Comparison between observed and calculated phases of Z_2.

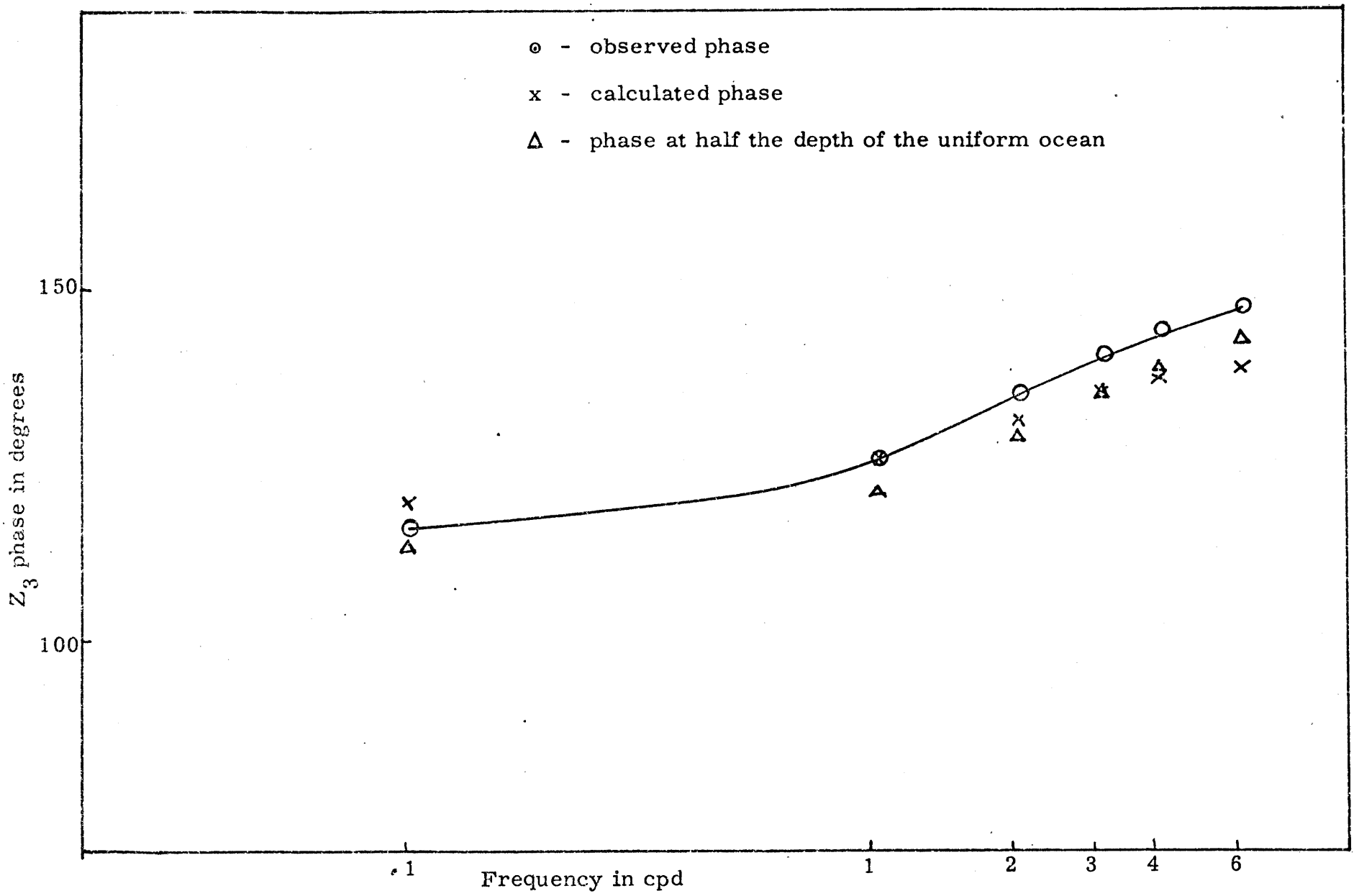

Fig. 5.3-7 Comparison between observed and calculated phases of Z_3.

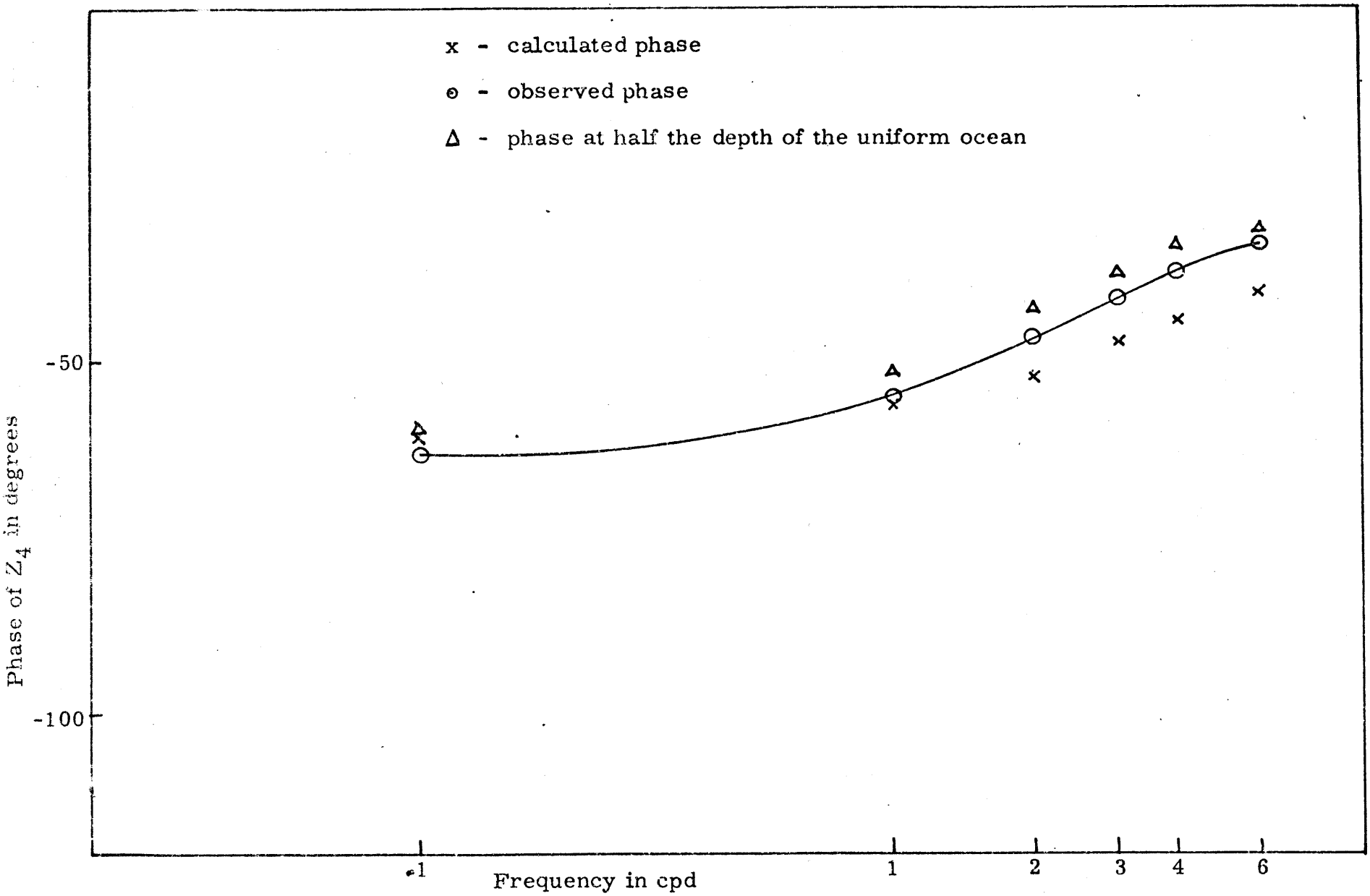

Fig. 5.3-8 Comparison between observed and calculated phases of Z_4.

TABLE 5.3-1

LARSEN'S LAYERED MEDIUM MODEL

Layer	Layer Thickness (km)	Conductivity (mho/m)
1	65	0.077
2	108	0.093
3	154	0.097
4	50	1.581
5	150	0.270
6	121	0.589
7	107	1.014
8	half space	1.014

Table 5.3-2

Impedance Tensor referred to Principal Axes

amp - amplitude in m/sec
pha - phase in radians

Frequency cpd	Z_{11}		Z_{12}		Z_{21}		Z_{22}		Impedance on the surface of uniform ocean		Impedance at half the depth of uniform ocean	
	amp	pha	amp	pha	amp	pha	amp	pha	amp	pha	amp	pha
.1	0.22	-0.40	5.94	-1.05	17.79	2.11	0.35	1.97	4.39	-0.99	4.49	-1.03
1	0.32	0.44	25.94	-0.91	81.36	2.18	1.52	1.93	17.76	-0.74	20.48	-0.89
2	0.74	1.19	38.40	-0.82	125.86	2.28	3.04	1.78	24.06	-0.57	30.53	-0.74
3	1.03	2.03	46.26	-0.76	156.00	2.35	4.72	1.84	27.03	-0.47	36.35	-0.64
4	1.57	2.36	51.85	-0.74	178.40	2.39	6.22	1.93	28.73	-0.41	40.04	-0.57
6	2.55	2.59	60.61	-0.74	212.60	2.44	8.64	2.08	30.86	-0.36	44.84	-0.50

Table 5.3-3

Impedance referred to geographic coordinates

Amplitude in m/s

Phase in radians

Frequency	Z_2				Z_3				Z_4			
	Amplitude		Phase		Amplitude		Phase		Amplitude		Phase	
cpd	Calc.	Obs.	Calc.	Obs.	Calc.	Obs.	Calc.	Obs.	Calc.	Obs.	Calc.	Obs.
.1	3.68	7.35	-1.04	-0.88	11.87	43.14	2.10	2.02	4.64	33.03	-1.03	-1.10
1	17.84	36.02	-1.00	-0.75	53.63	193.22	2.19	2.18	21.24	144.22	-0.98	-0.96
2	28.24	57.05	-0.88	-0.63	82.11	287.90	2.29	2.35	33.43	212.61	-0.90	-0.81
3	35.15	70.23	-0.79	-0.56	101.12	344.98	2.35	2.45	42.17	254.40	-0.82	-0.71
4	40.19	77.50	-0.73	-0.53	115.13	381.09	2.39	2.51	48.89	281.05	-0.77	-0.64
6	47.70	79.32	-0.65	-0.47	136.58	421.13	2.43	2.57	59.24	307.09	-0.70	-0.57

$$\begin{bmatrix} E_x \\ E_y \end{bmatrix} = \begin{bmatrix} Z_{xx} & Z_{xy} \\ Z_{yx} & Z_{yy} \end{bmatrix} \begin{matrix} H_x \\ H_y \end{matrix}$$

Calc. = calculated

Obs. = observed

where x is true east and y is true north.

$$Z_1 = (Z_{xx} + Z_{yy})/2 \qquad Z_2 = (Z_{xy} + Z_{yx})2 \qquad Z_3 = (Z_{xy} - Z_{yx})/2 \qquad Z_4 = (Z_{xx} - Z_{yy})/2$$

Z_1 values are not tabulated as they were not used in the analysis because of their error (Larsen, 1975).

SUMMARY

Conductivity and resistivity variations in the crust cause great complications in the surface distribution of electric currents and fields. At low frequencies this surface layer effect can be corrected by treating the surface layer as a thin sheet. Up to the present all studies involving the thin sheet approximation assumed the layer below the thin sheet to be a perfect insulator. In the models used in the thesis, this restriction is removed by generalizing the boundary condition at the thin sheet, and by generalizing the thin sheet conductivity and resistivity variations. This latter modification is done by treating the thin sheet as anisotropic with different parallel and perpendicular conductivities. In the model developed the thin sheet is actually made up of two thin sheets, a conductive thin sheet lying on top of a resistive thin sheet. Now both conductivity and resistivity variations in the crust can be modelled.

It is found that the resistivity thickness product of the thin sheet has a profound effect on the surface distribution of electric currents and fields. A new parameter, called the adjustment distance, appears which is equal to the square root of the thin layer conductivity thickness product times the resistivity thickness product. Adjustment distance represents the distance over which surface electric currents reequilibrate themselves with respect to the mantle electric currents. Typical values of conductivity thickness and resistivity thickness products suggest this distance to be of the order of hundreds of kilometers. Thus electric fields measured at a point

are influenced by conductivity and resistivity values of the medium considerable distance away.

Since the variations in the electrical properties of the medium hundreds of kilometers away have to be taken into consideration while interpreting magnetotelluric measurements made at a point one needs to develop efficient computational methods to model the magnetotelluric fields. A new method called 'the method of imbedding' is developed. In this method fields close to the point of measurement are computed at close spacings while fields far away are determined at large spacings. This method worked very well with the models studied, but it needs further development to be more generally applicable.

The method was applied to modelling the Hawaiin island chain in order to reevaluate the results of Larsen's low frequency magnetotelluric studies on Oahu. Using Larsen's final model we found his measured data gave significantly higher electric fields than our predicted values. Unfortunately these results are not conclusive since they could be accounted for by local resistivity variations at the measurement site. Some small discrepancies also appear at the shorter period end of the spectrum due to the neglect of inductive coupling in Larsen's analysis.

SUGGESTIONS FOR FUTURE WORK

The models developed in the thesis enable us to treat cases in which surface variations are three-dimensional in nature. We also found that in order to apply two-dimensional models, uniformity along strike direction should extend further than the adjustment distance. Hence even situations which appear two-dimensional may actually represent three-dimensional variation. Therefore the most important suggestion would be the application to several cases so that we can quantitatively understand the effects of three-dimensional features on low frequency magnetotelluric fields.

More work can be done to improve the efficiency of the 'imbedding' technique.

The theory of electromagnetic induction in nonuniform thin shells surrounding a stratified spherical conductor (with nonzero conductivity in every shell) should be developed. Then the theory could be applied to find the effect of the oceans on low frequency magnetic variations at the land based observatories.

APPENDIX I

LAYERED MEDIUM SOLUTION

In the medium below the thin sheet, assuming a dependence of $e^{ik_x x + ik_y y - i\omega t}$ (Madden, 1972), we have

$$\nabla \times \vec{E} = i\mu\omega\vec{H} \qquad \text{(A.1.1)}$$

$$\nabla \times \vec{H} = \sigma\vec{E} \qquad \text{(A.1.2)}$$

From (A.1.1) we get

$$\frac{\partial E_y}{\partial z} = ik_y E_z - i\mu\omega H_x \qquad \text{(A.1.1a)}$$

$$\frac{\partial E_x}{\partial z} = ik_x E_z + i\mu\omega H_y \qquad \text{(A.1.1b)}$$

$$k_x E_y - k_y E_x = \mu\omega H_z \qquad \text{(A.1.1c)}$$

From (A.1.2) we get

$$\frac{\partial H_y}{\partial z} = ik_y H_z - \sigma E_x \qquad \text{(A.1.2a)}$$

$$\frac{\partial H_x}{\partial z} = ik_x H_z + \sigma E_y \qquad \text{(A.1.2b)}$$

$$ik_x H_y - ik_y H_x = \sigma E_z \qquad \text{(A.1.2c)}$$

Substituting for E_z and H_z from (A.1.1c) and (A.1.2c) we get:

$$\frac{\partial}{\partial z}\begin{vmatrix} E_x \\ E_y \\ H_x \\ H_y \end{vmatrix} = \begin{vmatrix} 0 & 0 & \frac{k_x k_y}{\sigma} & \left(\frac{-k_x^2}{\sigma} + i\mu\omega\right) \\ 0 & 0 & \left(\frac{k_y^2}{\sigma} - i\mu\omega\right) & \frac{-k_x k_y}{\sigma} \\ \frac{-ik_x k_y}{\mu\omega} & \left(\frac{ik_x^2}{\mu\omega} + \sigma\right) & 0 & 0 \\ -\left(\frac{ik_y^2}{\mu\omega} + \sigma\right) & \frac{ik_x k_y}{\mu\omega} & 0 & 0 \end{vmatrix} \begin{vmatrix} E_x \\ E_y \\ H_x \\ H_y \end{vmatrix} \qquad \text{(A.1.3)}$$

Let

$$V = \begin{vmatrix} E_x \\ E_y \end{vmatrix} \qquad I = \begin{vmatrix} H_x \\ H_y \end{vmatrix}$$

Then from (A.1.3) we have

$$\frac{\partial V}{\partial z} = ZI \qquad \text{(A.1.4a)}$$

$$\frac{\partial I}{\partial z} = YV \qquad \text{(A.1.4b)}$$

where

$$Z = \begin{vmatrix} \frac{k_x k_y}{\sigma} & \left(\frac{-k_x^2}{\sigma} + i\mu\omega\right) \\ \left(\frac{k_y^2}{\sigma} - i\mu\omega\right) & \frac{-k_x k_y}{\sigma} \end{vmatrix} \qquad \text{(A.1.4c)}$$

$$Y = \begin{vmatrix} \frac{-ik_x k_y}{\mu\omega} & \frac{ik_x^2}{\mu\omega} + \sigma \\ \frac{-ik_y^2}{\mu\omega} - \sigma & \frac{ik_x k_y}{\mu\omega} \end{vmatrix} \qquad \text{(A.1.4d)}$$

From (A.1.4) we get

$$\frac{d^2V}{dz^2} = \left[Z\right]\left[Y\right]V$$

$$V = e^{+\sqrt{ZY}\,z} A_1 + e^{-\sqrt{ZY}\,z} A_2$$

where $\sqrt{ZY}$, the propagation matrix, is

$$\left[ZY\right]^{\frac{1}{2}} = \begin{vmatrix} \sqrt{k_x^2 + k_y^2 - i\sigma\mu\omega} & 0 \\ 0 & \sqrt{k_x^2 + k_y^2 - i\sigma\mu\omega} \end{vmatrix}$$

and

$$A_1 = \begin{vmatrix} a_1 \\ a_1' \end{vmatrix} \qquad A_2 = \begin{vmatrix} a_2 \\ a_2' \end{vmatrix}$$

Therefore

$$V = \begin{vmatrix} e^{\gamma_z z} & 0 \\ 0 & e^{\gamma_z z} \end{vmatrix} \begin{vmatrix} a_1 \\ a_1' \end{vmatrix} + \begin{vmatrix} e^{-\gamma_z z} & 0 \\ 0 & e^{-\gamma_z z} \end{vmatrix} \begin{vmatrix} a_2 \\ a_2' \end{vmatrix} \qquad \text{(A.1.5)}$$

where $\gamma_z = \sqrt{k_x^2 + k_y^2 - i\sigma\mu\omega}$.

From (A.1.4a) we get:

$$\left[Z\right] I = \gamma_z \begin{vmatrix} e^{\gamma_z z} & 0 \\ 0 & e^{\gamma_z z} \end{vmatrix} \begin{vmatrix} a_1 \\ a_1' \end{vmatrix} - \gamma_z \begin{vmatrix} e^{-\gamma_z z} & 0 \\ 0 & e^{-\gamma_z z} \end{vmatrix} \begin{vmatrix} a_2 \\ a_2' \end{vmatrix}$$

where

$$\left[K\right] = \gamma_z^{-1} \left[Z\right]$$

is called the characteristic impedance matrix of the medium

$$I = \left[K\right]^{-1} \left[e^{\gamma_z z}\right] A_1 - \left[K\right]^{-1} \left[e^{-\gamma_z z}\right] A_2 \qquad \text{(A.1.6)}$$

using abbreviations

$$\left[e^{\gamma_z z}\right] = \begin{vmatrix} e^{\gamma_z z} & 0 \\ 0 & e^{\gamma_z z} \end{vmatrix}; \quad \left[e^{-\gamma_z z}\right] = \begin{vmatrix} e^{-\gamma_z z} & 0 \\ 0 & e^{-\gamma_z z} \end{vmatrix}$$

From (A.1.5) and (A.1.6), the impedance Z^z at a depth 'd' is determined from

$$\left[V\right]_{z=d} = \left[Z^z\right]\left[I\right]_{z=d}$$

Example

Consider a two-layered medium with the conductivities of top and bottom layers being σ_1 and σ_2, respectively (as shown in the figure). The first layer extends to depth d and the second layer extends to infinity.

$$\frac{\qquad\qquad}{\sigma_1} \quad z = 0$$

$$\frac{\qquad\qquad}{\sigma_2} \quad z = d$$

In the second layer only downgoing waves are possible. Therefore V_2 in the second layer is given by

$$V_2 = \begin{vmatrix} e^{\gamma_2 z} & 0 \\ 0 & e^{\gamma_2 z} \end{vmatrix} \begin{vmatrix} a_3 \\ a_3' \end{vmatrix}$$

γ_2 being the propagation constant in layer 2.

From (A.1.4a) we get

$$[Z_2] I_2 = \frac{\partial V_2}{\partial z} = \gamma_2 \begin{vmatrix} e^{\gamma_2 z} & 0 \\ 0 & e^{\gamma_2 z} \end{vmatrix} \begin{vmatrix} a_3 \\ a_3' \end{vmatrix}$$

Z_2 being evaluated using (A.1.4c).

We want to find impedance Z_2^z at the top of layer 2 such that

$$[V_2]_{z=d} = [Z_2^z] [I_2]_{z=d}$$

Substituting for V_2 and I_2 from above, we get

$$\begin{vmatrix} e^{\gamma_2 d} & 0 \\ 0 & e^{\gamma_2 d} \end{vmatrix} \begin{vmatrix} a_3 \\ a_3' \end{vmatrix} = [Z_2^z] [K_2]^{-1} \begin{vmatrix} e^{\gamma_2 d} & 0 \\ 0 & e^{\gamma_2 d} \end{vmatrix} \begin{vmatrix} a_3 \\ a_3' \end{vmatrix}$$

where $[K_2]$ is the characteristic impedance of layer 2.

$$[Z_2^z] = \begin{vmatrix} e^{\gamma_2 d} & 0 \\ 0 & e^{\gamma_2 d} \end{vmatrix} \begin{vmatrix} e^{\gamma_2 d} & 0 \\ 0 & e^{\gamma_2 d} \end{vmatrix}^{-1} [K_2]$$

$$\left[Z_2^z\right] = \left[K_2\right]$$

That is, the impedance at the top of the bottom layer is equal to the characteristic impedance of that layer (because of the absence of reflection).

In the top layer there are waves travelling in both directions; therefore

$$V_1 = \begin{vmatrix} e^{\gamma_1 z} & 0 \\ 0 & e^{\gamma_1 z} \end{vmatrix} \begin{vmatrix} a_1 \\ a_1' \end{vmatrix} + \begin{vmatrix} e^{-\gamma_1 z} & 0 \\ 0 & e^{-\gamma_1 z} \end{vmatrix} \begin{vmatrix} a_2 \\ a_2' \end{vmatrix}$$

$$\left[K_1\right] I_1 = \left[e^{\gamma_1 z}\right] A_1 - \left[e^{-\gamma_1 z}\right] A_2$$

At the boundary z = d,

$$V_2 = V_1$$

$$I_2 = I_1$$

Also:

$$V_2 = \left[K_2\right] I_2$$

$$\left[K_2\right]\left[I_2\right]_{z=d} = \left[e^{\gamma_1 d}\right]\left[A_1\right] + \left[e^{-\gamma_1 d}\right]\left[A_2\right]$$

$$\left[K_1\right]\left[I_2\right]_{z=d} = \left[e^{\gamma_1 d}\right]\left[A_1\right] - \left[e^{-\gamma_1 d}\right]\left[A_2\right]$$

From these two equations we obtain:

$$\left[A_1\right] = \frac{1}{2}\left[e^{-\gamma_1 d}\right]\left[K_2 + K_1\right]\left[I_2\right]_{z=d}$$

$$\left[A_2\right] = \frac{1}{2}\left[e^{\gamma_1 d}\right]\left[K_2 - K_1\right]\left[I_2\right]_{z=d}$$

We want the impedance $[Z_1^z]$ at the top of layer 1 such that

$$\left[V_1\right]_{z=0} = \left[Z_1^z\right]\left[I_1\right]_{z=0}$$

Substitutin for V_1 and I_1 from above

$$\left[Z_1^z\right] = \left\{\left[e^{-\gamma_1 d}\right]\left[K_2 + K_1\right] + \left[e^{\gamma_1 d}\right]\left[K_2 - K_1\right]\right\}$$

$$\left\{\left[e^{-\gamma_1 d}\right]\left[K_2 + K_1\right] - \left[e^{\gamma_1 d}\right]\left[K_2 - K_1\right]\right\}^{-1}\left[K_1\right]$$

In general the impedance at the top of a layer (Z_{top}^z) can be calculated in terms of the impedance at the bottom (Z_{bot}^z) as follows:

$$\left[Z_{top}^z\right] = \left\{\left[e^{-\gamma d}\right]\left[Z_{bot}^z + K\right] + \left[e^{\gamma d}\right]\left[Z_{bot}^z - K\right]\right\}$$

$$\left\{\left[e^{-\gamma d}\right]\left[Z_{bot}^z + K\right] - \left[e^{\gamma d}\right]\left[Z_{bot}^z - K\right]\right\}^{-1}\left[K\right]$$

where γ is the propagation constant in the layer under consideration, d is the thickness of the layer and [K] is the characteristic impedance in the layer.

All matrices in the above expression are 2 by 2; hence computations involved in calculating the impedance of the layered medium are fast and straightforward.

REFERENCES

Brace, W., "Resistivity of saturated crustal rocks to 40 km based on laboratory measurements" in The Structure and Physical Properties of the Earth's Crust, Geophys. Monogr. Ser., Vol. 14, edited by J. G. Heacock, AGU, Washington D. C., 1971.

Bullard and Parker, "Electromagnetic induction in the ocean" in The Sea, Vol. 4, Pt. I, edited by A. E. Maxwell, Wiley Interscience, New York, pp. 695-1673, 1970.

Cox, C. S., "The electrical conductivity of the oceanic lithosphere", Geophys. Monogr. Ser., Vol. 14, 227-237, 1971.

Cox, C. S., J. H. Filloux and J. C. Larsen, "Electromagnetic studies of ocean currents and electrical conductivity below the ocean floor" in The Sea, Vol. 4, Pt. I, edited by A. E. Maxwell Wiley Interscience, New York, 1970.

Elsasser, W. M., "Thermal structure of the upper mantle and convection" in Advances in Earth Sciences, edited by P. M. Hurley, M. I. T. Press, Cambridge, Mass., 1965.

Filloux, J. H., "Ocean electric currents, geomagnetic variations and the deep electrical conductivity structure of the ocean-continent transition of central California", Ph. D. thesis, University of California, San Diego, 1967.

Hermance, J. F. and Grillot, L. R., "Correlation of magneto-telluric, seismic and temperature data from Southwest Iceland", J. Geophys. Res. 75, 6582-6591, 1970.

Honkura, Y., "Geomagnetic variation anomaly on Miyake-Jima Island", J. Geomag. Geoelec. 23, 307-333, 1971.

Honkura, Y., "Island effect and electrical conductivity structure beneath Miyake-Jima Island", J. Geomag. Geoelec. 25, 167-179, 1973.

Honkura, Y., S. Oshima and T. Kondo, "Geomagnetic variation anomaly on Hachijo-Jima Island", J. Geomag. Geoelec. 26, 23-37, 1974.

Kasameyer, P. W., "Low-Frequency Magnetotelluric Survey of New England", Ph. D. Thesis, Massachusetts Institute of Technology, Cambridge, Mass., 1974.

Keller, G. V., L. A. Anderson, and J. I. Pritchard, "Geological survey investigation of the electrical properties of the crust

and upper mantle", Geophys. 31, 1078-1087, 1966.

Klein, D. P., "Geomagnetic time-variations, the island effect and electromagnetic depth sounding on oceanic islands: results from the analysis of data obtained in the frequency range of 0.5 to 10 cph on Oahu, Hawaii", M.S. thesis, University of Hawaii, Honolulu, Hawaii, 1972.

Klein, D. P., "Magnetic variations (2 - 30 cpd) on Hawaii Island and mantle electrical conductivity", Ph.D. Thesis, University of Hawaii, Honolulu, Hawaii, 1976.

Larsen, J. C., "Electric and magnetic fields induced by deep sea tides", Geophys. J. R. Astr. Soc. 16, 47-70, 1968.

Larsen, J. C., "Low frequency (0.1 - 6.0 cpd) electromagnetic study of deep mantle electrical conductivity beneath the Hawaiian Islands", Geophys. J. Roy. Astr. Soc. 43, 17-46, 1975.

Mason, R. G., "Spatial dependence of time-variations of the geomagnetic field on Oahu, Hawaii" (abstr.), Trans. Am. Geophys. Un. 44, 40, 1963.

Madden, T. R., "The resolving power of geoelectric measurements for delineating resistive zones within the crust" in The Structure and Physical Properties of the Earth's Crust, Geophys. Monograph 14, edited by J. G. Heacock, Washington D.C., AGU, 1971.

Madden, T. R., "Transmission systems and network analogies to geophysical forward and inverse problems", ONR Technical Report, 72-3, Department of Earth and Planetary Sciences, M.I.T., 1972.

Madden, T. R., "Random Networks and Mixing Laws", Geophys. 41, 6A, 1104-1125, 1976.

Madden, T., T. Cantwell, D. Greenwalt, A. Kelly and A. Regier, "Progress report on geomagnetic studies and electrical conductivity in the earth's crust and upper mantle", Report of Project NR-371-401, Department of Geology and Geophysics, M.I.T., Cambridge, Mass., 1962.

Price, A. T., "The induction of electric currents in non-uniform thin sheets and shells", Quart. J. Mech. Appl. Math. 2, 263-310, 1949.

Richards, M. C., "Study of electrical conductivity in the earth near Peru", Ph.D. Thesis, University of California, San Diego, 1970.

Rikitake, T., Yokoyama, I, and Hishiyama, Y., "A preliminary study on the anomalous behaviour of geomagnetic variations of short period in Japan and its relation to subterranean structure", Bull. Earthquake Res. Inst., Tokyo Univ. 30, 207-221, 1952.

Rikitake, T., Yokoyama, I. and Hishiyama, Y., "The anomalous behaviour of geomagnetic variations of short period in Japan and its relation to subterranean structure", The 2nd report, Bull. Earthquake Res. Inst., Tokyo Univ. 31, 19-31, 1953.

Rikitake, T., Yokoyama, I., Uyeda, S., Yukutake, T. and Nakagawa, E., "The anomalous behaviour of geomagnetic variations of short period in Japan and its relation to the subterranean structure", The 7th Report, Bull. Earthquake Res. Inst., Tokyo Univ. 36, 1-26, 1958.

Rikitake, T., Uyeda, S., Yukutake, T., Tanaoka, I., and Nakagawa, E., "The anomalous behaviour of geomagnetic variations of short period in Japan and its relation to the subterranean structure", The 8th Report, Bull. Earthquake Res. Inst., Tokyo Univ. 37, 1-11, 1959.

Rikitake, T., Yaku, T. and Yamakawa, K., "The anomalous behaviour of geomagnetic variations of short period in Japan and its relation to the subterranean structure", The 10th Report, Bull. Earthquake Res. Inst., Tokyo Univ. 40, 693-717, 1962.

Roden, R. B., "Induction effects of geomagnetic time variations", Ph. D. Thesis, Churchill College, England, 1963.

Sasai, Y., "Spatial dependence of short period geomagnetic fluctuations on Oshima Island", Part 2, Bull. Earthquake Res. Inst., Tokyo Univ. 46, 907-926, 1968.

Schmucker, U., "Anomalies of geomagnetic variations in southwestern United States", J. Geomag. Geoelec. 15, 193-221, 1964.

Swift, C. M., "A magnetotelluric investigation of an electrical anomaly in the southwestern United States", Ph. D. Thesis, M. I. T., 1967.

Tozer, D. C., "The electrical properties of the earth's interior" in Physics and Chemistry of the Earth, eds.: L. Ahrens, F. Press, K. Rankama, and S. Runcorn, Pergamon Press, 414-436, 1959.

Waff, H. S., "Theoretical considerations of electrical conductivity in a partially molten mantle and implications for geothermometry", J. Geophys. Res. 79, 4003-4009, 1974.

Weidelt, P., "The inverse problem of geomagnetic induction", Z. Geophys. 38, 257-289, 1972.

Van Zijl, J. S. V. P., "A deep schlumberger sounding to investigate the electrical structure of the crust and upper mantle in South Africa", Geophysics 34, 450-462, 1969.

BIOGRAPHICAL NOTE

The author was born in Secunderabad, India. She received the B. Sc. degree in 1962 and the M. Sc. (Physics) degree in 1964 from Osmania University, Hyderabad, India. She held Government of India scholarships throughout her undergraduate and graduate work in India. She worked in the National Geophysical Research Institute, Hyderabad, India, from 1964 to 1970, first as Senior Scientific Assistant and then as Scientist. In 1970 she obtained the East West Center Grant to study for the M. S. (Geoscience) degree at the University of Hawaii, Honolulu. In 1972 she came to the Department of Earth and Planetary Sciences at M. I. T. to continue her graduate work. She held the position of Research Assistant during her stay at M. I. T. On the completion of her studies at M. I. T. she will join the Carnegie Institution of Washington, Washington D. C. as a Research Associate.